Iowa State University
Digital Repository

Graduate Theses and Dissertations

Iowa State University Capstones, Theses and Dissertations

2012

# Developing benzobisazole-containing conjugated polymers for semiconducting applications

Jeremy Joseph Intemann
*Iowa State University*

Follow this and additional works at: https://lib.dr.iastate.edu/etd

Part of the Organic Chemistry Commons, and the Polymer Chemistry Commons

Recommended Citation
Intemann, Jeremy Joseph, "Developing benzobisazole-containing conjugated polymers for semiconducting applications" (2012). *Graduate Theses and Dissertations*. 12350.
https://lib.dr.iastate.edu/etd/12350

This Dissertation is brought to you for free and open access by the Iowa State University Capstones, Theses and Dissertations at Iowa State University Digital Repository. It has been accepted for inclusion in Graduate Theses and Dissertations by an authorized administrator of Iowa State University Digital Repository. For more information, please contact digirep@iastate.edu.

المنارة للاستشارات

# Developing benzobisazole-containing conjugated polymers for organic semiconducting applications

By

Jeremy J. Intemann

A dissertation submitted to the graduate faculty

in partial fulfillment of the requirements for the degree of

DOCTOR OF PHILOSOPHY

Major: Organic Chemistry

Program of Study Committee:

Malika Jeffries-EL, Major Professor

Joseph Shinar

Jason Chen

William Jenks

Yan Zhao

Iowa State University

Ames, Iowa

2012

# TABLE OF CONTENTS

**CHAPTER 1.** General Introduction.................................................................1

**1.1** Introduction to This Dissertation.................................................1
**1.2** Introduction to Organic Semiconducting Polymers..................................3
**1.3** Benzobisazoles and Their Polymers...............................................10
**1.4** Organic Light-Emitting Diodes....................................................12
**1.5** Organic Photovoltaics............................................................20
**1.6** Conclusions......................................................................26
**1.7** References.......................................................................28

**CHAPTER 2.** Synthesis and Characterization of Poly(9,9-dialkylfluorenevinylene benzobisoxazoles): New Solution-Processable Electron-Accepting Conjugated Polymers..38

**2.1** Abstract..........................................................................38
**2.2** Introduction......................................................................39
**2.4** Results and Discussion...........................................................41
**2.4** Conclusions......................................................................51
**2.5** Experimental Methods.............................................................51
**2.6** Acknowledgements.................................................................57
**2.7** Supporting Information...........................................................58
**2.8** References.......................................................................72

**CHAPTER 3.** Benzobisthiazole-Fluorene Based Emissive Polymers for Guest-Host Polymer Light Emitting Diodes.........................................................76

**3.1** Abstract..........................................................................76
**3.2** Introduction......................................................................77
**3.3** Experimental Methods.............................................................78
**3.4** Results and Discussion...........................................................83
**3.5** Conclusions......................................................................91
**3.6** Acknowledgements.................................................................91
**3.7** Supporting Information...........................................................92
**3.8** References.......................................................................104

**CHAPTER 4.** Improving the Performance of Benzobisoxazole-Containing Polymers in Organic Light Emitting Diodes by Altering the Conjugation Pathway……… 107

**4.1** Abstract…………………………………………………………………………107
**4.2** Introduction……………………………………………………………………..108
**4.3** Results and Discussion……………………………………………………..... 109
**4.4** Conclusions……………………………………………………………………..123
**4.5** Experimental Methods………………………………………………………123
**4.6** Acknowledgements…………………………………………………………..128
**4.7** Supporting Information…………………………………………………....129
**4.8** References………………………………………………………………………147

**CHAPTER 5.** Changing the Conjugation Pathway in Benzobisoxazole-Containing Polymers: Effect on Physical and Electronic Properties……………………………………150

**5.1** Abstract…………………………………………………………………………150
**5.2** Introduction……………………………………………………………………..151
**5.3** Results and Discussion……………………………………………………… 155
**5.4** Conclusions……………………………………………………..……..…..163
**5.5** Experimental Methods…………………………………...………………..163
**5.6** Acknowledgements……………………………………………………...……168
**5.7** Supporting Information…………………………………………………....168
**5.8** References………………………………………………………………………185

**CHAPTER 6.** General Conclusions………………………………………………….189

**6.1** Future Research………………………………………………….……………….. 189
**6.2** Dissertation Conclusions…………………………………………….……… 192
**6.3** Acknowledgements……………………………………………………………..193
**6.4** References………………………………………………………………………194

**APPENDIX** List of Acronyms and Descriptions………………………………………..195

# Chapter 1

## General Introduction

### 1.1 INTRODUCTION TO THIS DISSERTATION

This dissertation follows the work performed by the author in the Jeffries-EL research group over the last six years. The focus of the work is on structure property relationships in organic semiconducting polymers and designing polymers with desirable physical and electronic properties for organic electronics with an emphasis on benzobisazole-containing emissive polymers for organic light-emitting diodes (OLEDs). Chapter 1 is a general introduction to organic semiconductors and how structural modifications result in different physical and electronic properties in these materials. An overview of organic based electronics and their engineering is also discussed including the rational design of organic semiconductors to obtain materials with ideal properties for optimum performance in organic electronic devices.

Chapter 2 is a paper that was published in *Macromolecules* in 2011 that describes the synthesis, characterization, and performance in OLEDs of four benzobisoxazole-fluorene containing copolymers. The bulk of the synthetic work was done by the author of this dissertation along with writing the experimental section of the paper and contributions to the supporting information. Dr. Jared Mike synthesized 2,6-dimethyl benzo[1,2-d;4,5-d´]bisoxazole-diethylphosphonate and 2,6-dimethyl benzo[1,2-d;5,4-d´]bisoxazole-diethylphosphonate. Device fabrication and characterization was performed by Dr. Min Cai and Dr. Teng Xiao under the guidance of Drs. Ruth and Joe Shinar while the thermal properties of the polymers were measured by Dr. Timothy Mauldin. X-ray data of the polymer films was collected by Robert Roggers and fluorescence decay lifetimes were measured by Dr. Sayantan Bose. Dr. Malika Jeffries-EL wrote the remainder of the paper.

Chapter 3 is a paper that has been submitted to *Journal of Polymer Science Part A: Polymer Chemistry* for publication and discusses the synthesis, characterization, and OLED performance of three benzobisthiazole-fluorene containing polymers. All of the synthetic work was performed by the author of this dissertation except the final step in the synthesis of 2,6-Dimethylbenzo[1,2-

d;4,5-d´]bisthiazolediethylphosphonate which was done by Dr. Jared Mike. Charles Barnes measured fluorescence decay lifetimes, Robert Roggers performed X-ray studies, and Dr. Min Cai and Dr. Teng Xiao fabricated and characterized the OLEDs under the guidance of Drs. Ruth and Joe Shinar. The majority of the paper was written by the author of this dissertation with significant contributions to the introduction section by Dr. Malika Jeffries-EL.

Chapter 4 is a paper that under review for publication in *Advanced Functional Materials* and reports a new approach to designing benzobisoxazole-containing polymers by changing the conjugation pathway through the benzobisoxazole moiety. Six benzobisoxazole copolymers were synthesized containing either N-alkylcarbazole, 9,9-dialkylfluorene, or 1,4-dialkoxyphenylene. Their physical, electronic, and device properties are reported. The new design strategy results in record efficiencies and brightness for benzobisoxazole-containing OLEDs, representing a significant breakthrough in this research. The bulk of the synthesis was performed by the author of this dissertation with contributions from Brian Tlach who made the 2,6-dihexyl-4,8-dibromobenzo[1,2-d;4,5-d']bisoxazole monomer. Charles Barnes performed fluorescence lifetime measurements, Brian Tlach performed fluorescence quantum yield measurements, and Emily Hellerich and Monique Ewan fabricated and characterized the OLEDs under the supervision of Drs. Ruth and Joe Shinar. The paper for this work was written entirely by the author of this dissertation.

Chapter 5 is a paper that will be submitted to *Macromolecules* for publication and is an extension of the work performed in the previous chapter. The implications of changing the conjugation pathway in benzobisoxazole-containing polymers are studied and its effects on the physical and electronic properties are examined. Six benzobisoxazole-containing polymers are reported where three possess the traditional conjugation pathway (through the oxazole rings) and three structurally analogous polymers that possess the new conjugation pathway (directly through the central benzene ring). The bulk of the synthetic work was done by the author of this dissertation with contributions from Achala Bhuwalka who made 4,4'-dioctyl-2,2'-bis(trimethylstannyl)-2,2'-bithiophene and Brian Tlach who made 2,6-dioctyl-4,8-dibromobenzo[1,2-d;4,5-d']bisoxazole, a precursor to one of the monomers used. X-ray diffraction analysis of the polymer films was performed by Robert Roggers. The paper for this work was written entirely by the author of this dissertation.

Finally, Chapter 6 draws some general conclusions of the work performed and discusses possible future research, including new synthetic design strategies. The possibilities for making semiconducting polymers based on two-dimensional π-systems are explored along with a discussion on recently reported work relating to this topic.

## 1.2 INTRODUCTION TO ORGANIC SEMICONDUCTING POLYMERS

Since the discovery of conductivity in doped polyacetylene in the 1970’s by Shirakawa et al.,[1, 2] conjugated polymers have become a subject of intense research. These materials have been adopted for use in a wide variety of applications such as organic photovoltaics (OPVs),[3-7] light-emitting diodes (OLEDs),[8-11] field-effect transistors (OFETs),[12-15] polymer batteries,[16-18] sensors,[19-21] and non-linear optics.[22, 23] Though organic semiconductors have not reached the same level of electrical performance as their inorganic counterparts, they do offer many advantages over inorganic materials. Inorganic semiconductors require an extremely high level of crystallinity and purity as defects result in poor devices.[24, 25] The need for materials such as ultra-high purity silicon increases the cost of materials and fabrication. Organic semiconductors, on the other hand, can be cheaply made from petroleum products and fabricated into devices using low cost techniques such as spin-coating[26], inkjet printing,[27] and screen printing.[28] Organic-based devices also offer the potential for applications beyond the capabilities of inorganic electronics such as flexible displays,[29] solar cells[30], and batteries[31]. One of the biggest advantages organic semiconductors have over inorganic materials is the ability to synthetically manipulate the physical and electronic properties of the materials whereas semiconductors like silicon have intrinsic properties, which devices must be engineered around. By changing the structure of organic molecules, organic semiconductors can be synthetically tuned to provide the material properties best suited for a particular application or device.[32]

The semiconducting properties of conjugated polymers arise from their extended π-system. As Figure 1.1 illustrates, increasing the conjugation of an organic molecule leads to an increased

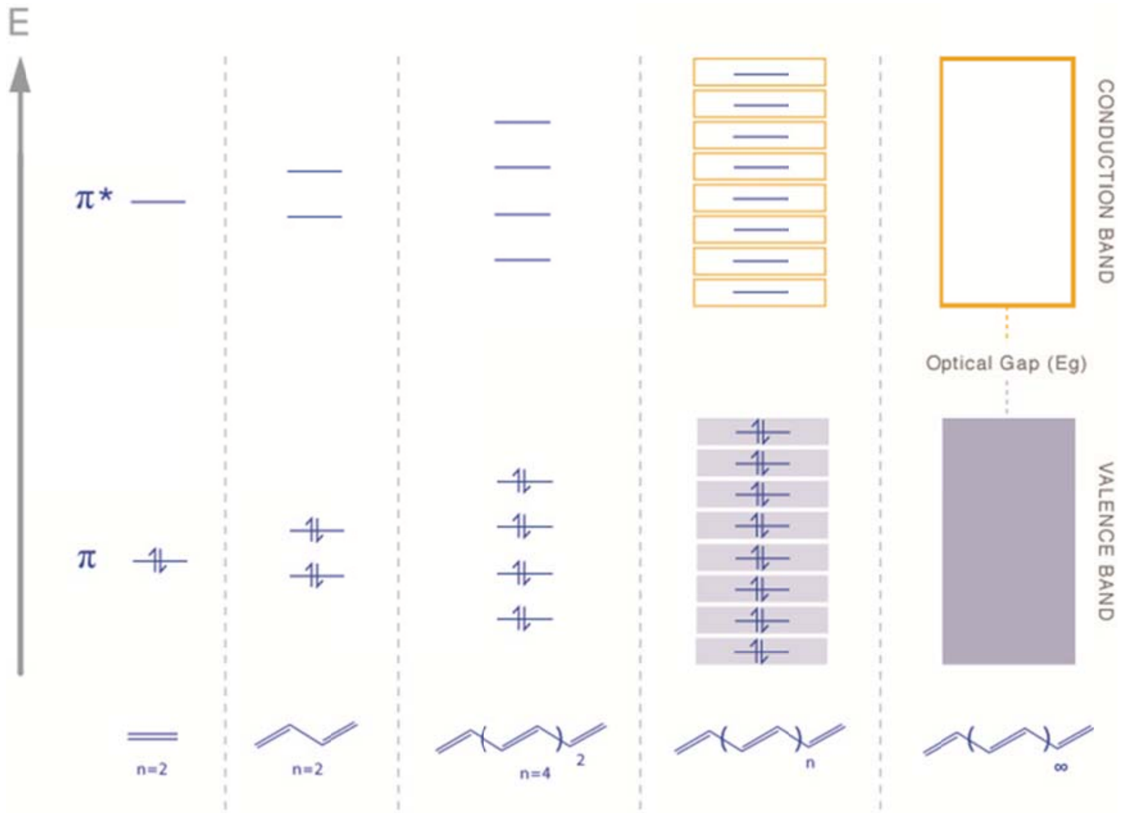

**Figure 1.1.** Effect of increased conjugation length on energy levels of conjugated polymers

number of π-molecular orbitals. As conjugation increases the highest occupied molecular orbital (HOMO) increases in energy while the lowest unoccupied molecular orbital (LUMO) decreases. The end result is a large number of filled π-orbitals that are very close in energy to each other along with a large number of unfilled antibonding π*-orbitals that are also close in energy with a gap separating the bonding and antibonding orbitals. The result is an electronic structure that is very similar to inorganic semiconductors with the π-orbitals constituting a valence band and the π*-orbitals making up the conduction band with a low energy bandgap separating them. The energy levels of the HOMO and LUMO as well as the bandgap are highly dependent on the structure of the polymer and being able to tune them for specific applications is of the upmost importance.

As a result of inherent defects in the polymer backbone and the tendency for the backbone to twist over larger distances, a conjugated polymer does not have complete electron delocalization

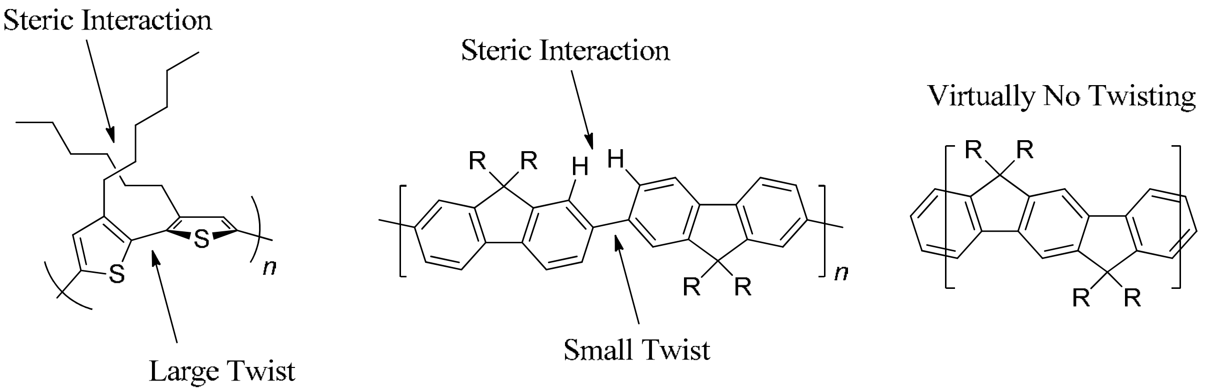

Regio-random
Poly(3-hexylthiophene)

Polyfluorene

Fused-ring Ladder Polymer

**Figure 1.2.** Structural effects on conjugation

over the entire π-system. Instead it has pockets of conjugation which is referred to as its effective conjugation length. The effective conjugation length is what gives rise to the material's electronic character, most notably the bandgap.[33] Although the bandgap generally decreases with increasing effective conjugation length, it should be noted that it will never reach zero and become a conductor due to Peierls distortions in the alternating bonds of the polymer.[34, 35] The effective conjugation length can be synthetically tuned to a certain extent by incorporating steric strain into the backbone, causing twisting of the backbone, decreasing π-orbital overlap and effective conjugation length. An example of this is shown below in Figure 1.2 which depicts the effects of steric interactions on the conjugated backbone. Regio-random poly(3-hexylthiophene) has strong alkyl-alkyl steric interactions that causes a high degree of twisting in the conjugated backbone while polyfluorene only has hydrogen-hydrogen interactions, which is a much weaker steric interaction, causing less twisting. Ladder polymers use fused rings to prevent twisting and are the most planar of all conjugated polymers.[36] In general, incorporation of fused rings (like that in polyfluorene) increases the effective conjugation length, narrowing the bandgap of the material. π-spacers such as vinylene and ethynylene can be incorporated into the backbone to reduce steric interactions between aromatic rings as well.

Conjugated polymers have two possible non-degenerate ground states. The aromatic benzoid form of the polymer is the lowest in energy but another possible resonance form is the

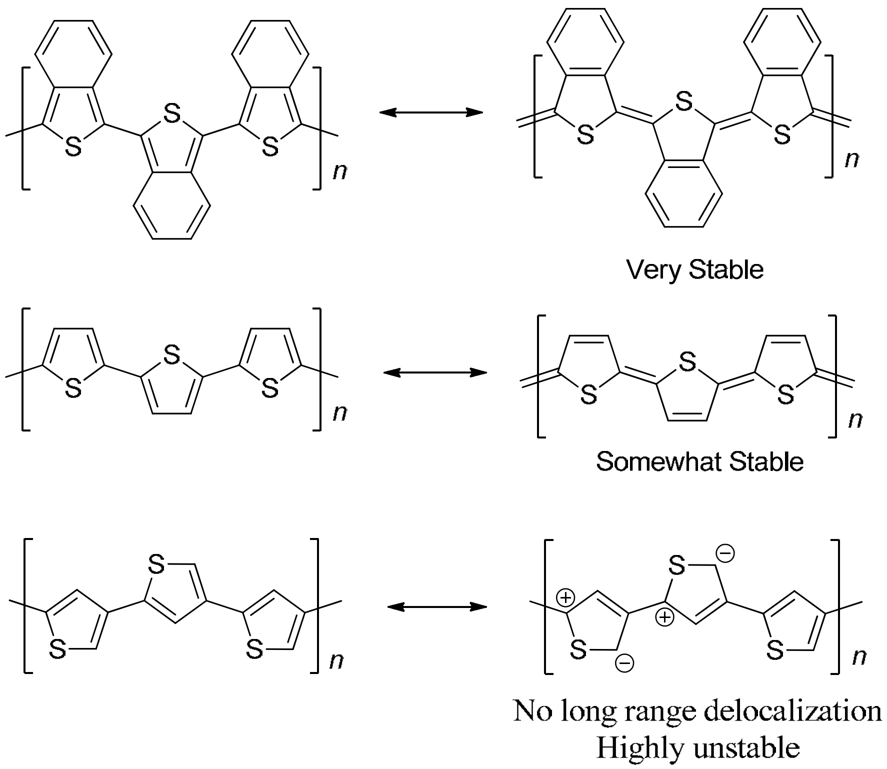

**Figure 1.3.** Benzoid and quinoid forms of various polythiophene derivatives with increasing band gap energy and decreasing quinoid character in the ground state from top to bottom.

quinoid form of the polymer. Because the quinoid form is no longer aromatic it is higher in energy than the benzoid form. In the quinoid form, the single bonds linking the ring systems together become double bonds and as a result the quinoid form is generally more planar than the benzoid with a longer effective conjugation length and therefor a narrower bandgap.[6] Structural changes that promote the quinoid form of the polymer will then necessarily decrease the band gap. This can be achieved by destabilizing the benzoid form of the polymer by decreasing its aromaticity (using thiophene or furan rings instead of benzene rings). The quinoid form can also be stabilized by adding conjugated groups to the backbone that stay aromatic in the quinoid resonance form. If the goal is a wider bandgap material, the quinoid resonance structure can be intentionally destabilized by incorporating groups that do not have a stable quinoidal form, such as meta-conjugated moieties, which makes it impossible to form a quinoidal structure over the length of the backbone (Figure 1.3).

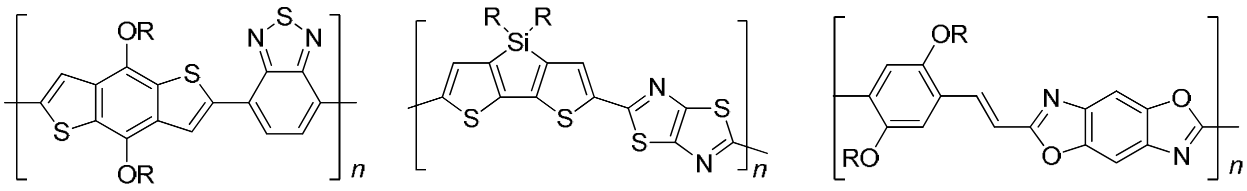

**Figure 1.4.** Some examples of donor-acceptor copolymers

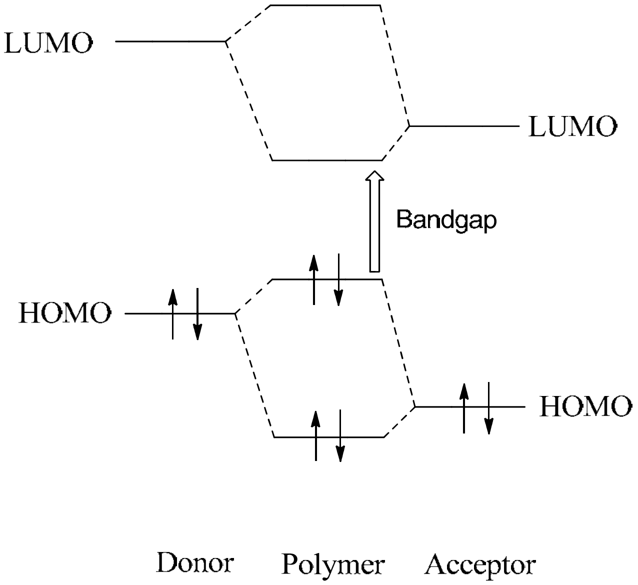

**Figure 1.5.** Molecular orbital diagram for donor-acceptor polymers.

Controlling the effective conjugation length is not the only way to synthetically tune polymers. Introduction of heteroatoms plays a key role in determining the electronic properties as well. Incorporation of electron withdrawing groups such as ketones, nitro groups, fluorines, nitriles, alkynes, and imines lead to increased electron affinities and lower lying LUMOs while adding electron donating groups like amines, alkoxyls, and thioalkyls reduce ionization potentials and raise HOMO levels.[37] Another strategy that has been adopted is copolymerizing electron rich monomers with electron deficient monomers to make donor-acceptor copolymers.[38] Some examples of donor-acceptor copolymers are shown in Figure 1.4. In these polymers, orbital mixing between the donor and acceptor leads to decreased band gaps. Figure 1.5

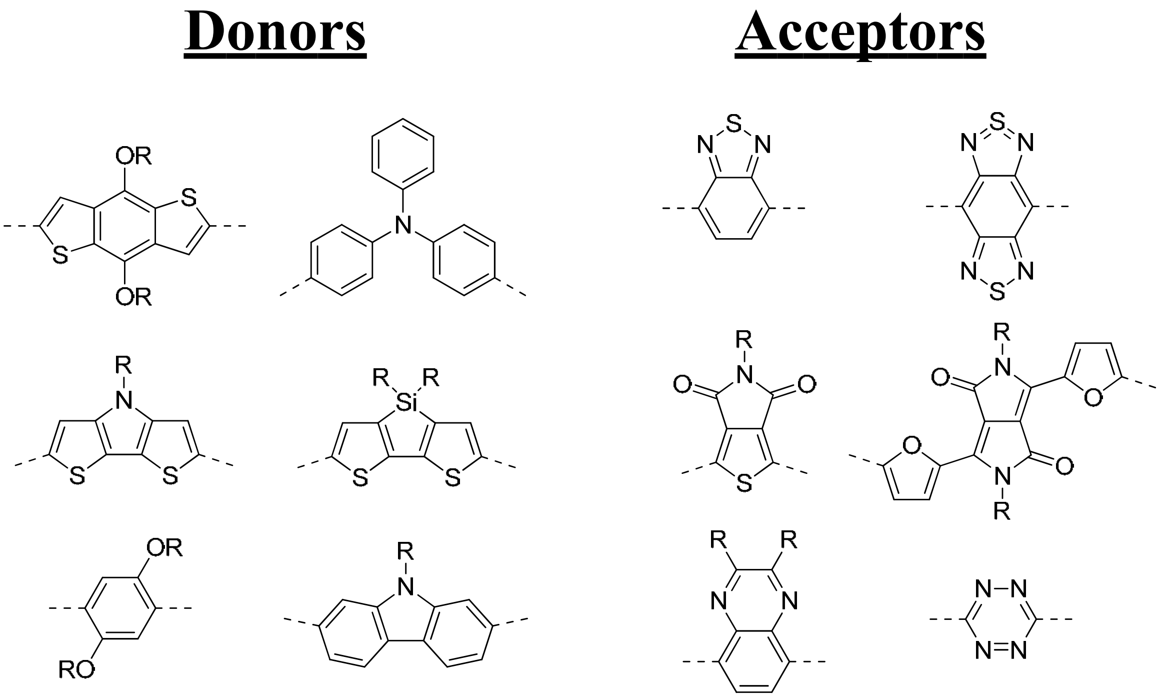

**Figure 1.6.** Examples of donor and acceptor units used in donor-acceptor copolymers.

illustrates how the HOMO of the donor heavily influences the resulting HOMO energy level of the polymer while the acceptor's LUMO energy level is primarily responsible for the energy level of the polymer's LUMO.[6] Some examples of donor and acceptor moieties are also shown in Figure 1.6. By using a donor that has a low lying HOMO, the resulting polymer will also have a low lying HOMO which improves the oxidative stability of the polymer. Electron-rich polymers can easily have an electron removed from the HOMO by oxygen, a common problem for homopolymers such as poly(3-hexylthiophene) which has a much higher HOMO than most donor-acceptor polymers and is notoriously oxidatively unstable.[39]

Another important aspect of designing polymers is incorporating flexible alkyl side chains. Alkyl side chains give the polymers solubility in organic solvents that they would otherwise lack. Alkyl chains disrupt crystallinity and influence polymer morphology in thin films.[40-42] Short linear (n-alkyl) chains typically lead to greater order in films[6, 43] which is desirable in OPVs and OFETs but also results in lower solubility of polymers. Short branched chains such as 2-ethylhexyl and 3,7-dimethyloctyl chains solves the solubility issues but disrupts solid state packing to a greater extent. Long alkyl chains such as hexadecyl or 2-octyldodecyl provide good solubilities while heavily disrupting $\pi$-stacking. This is undesirable for OPVs and OFETs but is very desirable for OLEDs as efficient $\pi$-stacking can lead to strong concentration quenching of fluorescence.[44, 45] Good solubility of semiconducting polymers is extremely important as they are generally processed by dissolving the polymers in organic solvents and then casting them on to substrates. Possessing good solubilities will also allow polymers to be made with high molecular weights, which is important for charge carrier mobilities (the ease with which electrons and holes can propagate through the polymer film) in devices. However, the addition of alkyl chains to a conjugated polymer does have the draw back that they generally reduce the polymer's thermal stability.[46] The decreased thermal stability is typically not significant enough, however, to cause the polymer's decomposition temperature to fall below the operating temperatures of most organic electronic devices.

Synthesizing semiconducting polymers with high electron and hole mobilities is very important for the performance of all organic electronic devices. The role mobilities play in devices will be discussed further later on but generally these devices perform better and are more efficient when current is able to flow through them more easily. The biggest problem currently with charge mobilities in conjugated polymers is that these materials generally have higher hole mobilities than electron mobilities.[47, 48] This is particularly problematic for OLEDs which require good mobilities of both charge carriers. Improving electron mobilities can be achieved by incorporation of electron deficient moieties into the conjugated backbone of a polymer. This decreases the energy of the LUMO, allowing the polymer to better stabilize a negative charge. Though several polymers have been made with high electron mobilities,[49-51] it is often difficult to achieve this while still maintaining the other desired electronic properties of the material.

Other major factors that effect mobilities in conjugated polymers are polymer chain length and the aforementioned solid state morphology.[15] When a hole or electron passes through a semiconducting polymer film, it moves from chain to chain using a charge-hoping mechanism where the charge carrier must "hop" over a potential barrier in order to reach the next polymer chain.[52, 53] This is an inefficient mechanism and the charge may fall into low energy traps that can result from polymer defects, phase segregation boundaries, functional endgroups, and impurities in the film.[54, 55] If a polymer chain is long, however, the charge may travel a longer distance without hopping to the next chain. This increases mobility as transport along the polymer backbone is much faster than charge hopping.[56]

## 1.3 BENZOBISAZOLES AND THEIR POLYMERS

A great deal of work has been done over the years in developing conjugated monomers with low ionization potentials as donors in donor-acceptor semiconducting materials,[57-59] leading toward a large library of extremely good donor moieties. Acceptor moieties, on the other hand, have not been nearly as well developed and new acceptor compounds are needed to obtain low band gap and high electron affinity materials for electronic applications. Acceptors such as isoindigo,[60-62] diketopyrolopyrole,[63-65] and thiazolothiazole,[66-68] have shown a great deal of promise but work remains to develop new electron deficient monomers for semiconducting polymers.

Benzobisazoles are a class of electron deficient conjugated moieties that have not been well developed for semiconducting applications. Figure 1.7 shows examples of benzobisazoles, two isomers of benzobisoxazole and one isomer of benzobisthiazole, which will be the focus of this dissertation. There currently is no known methodology for making the cis-isomer of benzobisthiazole which is why it has been omitted. These materials were first developed for dyes with much of the early work provided by Osman, et al.[69-71] Later on, rigid rod polymers of these materials were developed by Wolfe, et al., primarily as high performance materials for the air force.[72-74] These new benzobisazole-containing polymers exhibited very high mechanical

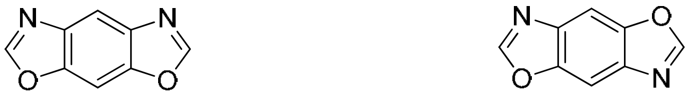

benzo[1,2-d;5,4-d']bisoxazole

benzo[1,2-d;4,5-d']bisoxazole

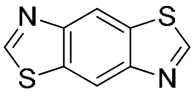

benzo[1,2-d;4,5-d']bisthiazole

**Figure 1.7.** Examples of benzobisazoles

strength, thermal stability, and oxidative stability. It was also found that polymers containing these moieties had interesting optical and electronic properties as well.[75, 76]

The polymers made by Wolfe are not well suited for organic electronic devices, however, because they lack solubilizing side chains. They are only soluble in strong protic solvents such as polyphosphoric acid (PPA) or methane sulfonic acid. Casting films from these types of solutions is extremely difficult and require several rinsing and drying cycles to remove residual acid. The polymers also end up being doped by protonation from residual acid resulting in undesirable electronic characteristics. Synthesizing polymers using Wolfe’s approach to benzobisoxazole polymerization is made difficult by the reaction conditions used (Figure 1.8). 2,5-diamino-1,4-benzenedithiol or 2,4-diaminoresorcinol is condensed with 1,4-benzenedicarboxylic acid using

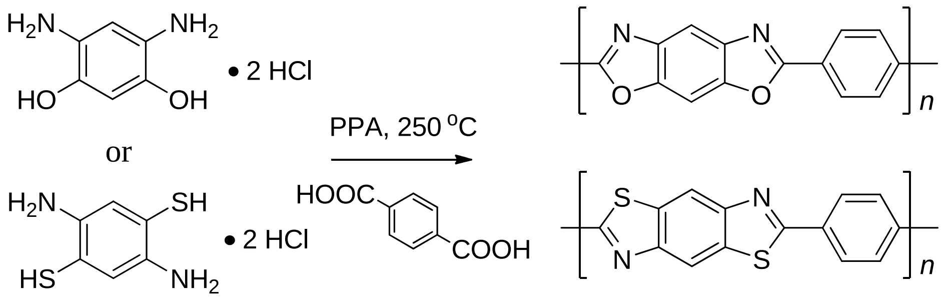

H2N
NH2
HO
OH
• 2 HCl
or
H2N
SH
HS
NH2
• 2 HCl
PPA, 250 °C
HOOC
COOH
N
O
S
n

**Wolfe Acid Condensation Method**

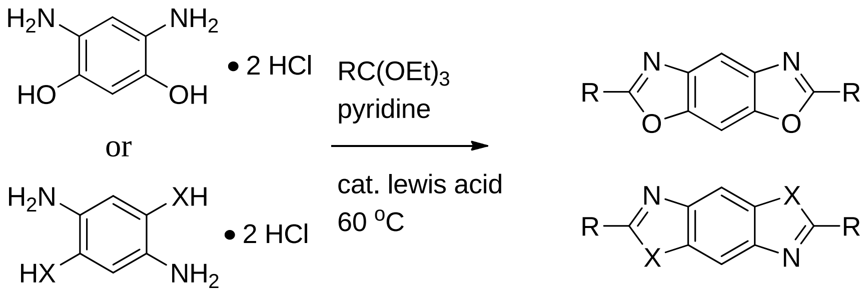

H2N
NH2
HO
OH
• 2 HCl
or
H2N
XH
HX
NH2
• 2 HCl
RC(OEt)3
pyridine
cat. lewis acid
60 °C
R
N
O
X

X = O or S

R = chloromethyl, bromomethyl,
trimethylsilylyethynyl,
5-bromo-4-octylthiophene,
methyl, or hydrogen

**Mike Orthoester Condensation Method**

**Figure 1.8.** Synthetic methods for synthesizing benzobisoxazole-containing polymers.

PPA at very high temperatures (~250 °C). These conditions do not tolerate many functional groups, including alkyl chains, which can become oxidized resulting in polymer defects. In addition to this, only the benzo[1,2-d;5,4-d']bisoxazole derivative can be made, as the other isomer's starting material, 2,5-diaminohydroquinone, is oxidized to the quinone under these conditions, preventing it's polymerization. It was not until 2008 when Mike, et al. reported a new method for preparing functionalized benzobisazole monomers that scientists were able to make solution soluble and relatively defect free benzobisazole containing polymers.[77, 78] This new approach, developed with assistance from the author of this dissertation, used rare earth metal catalyzed orthoester condensations under mild reaction conditions that gave functionalized benzobisazole monomers, including both benzobisoxazole isomers (Figure 1.8).

The newly found ability to make functionalized benzobisoxazole monomers has opened the door for the synthesis of a wide variety of copolymers designed for semiconducting applications, including the first reports of benzobisazole based polymers for use in OLEDs which is discussed in the following chapters. Though early results show only modest performance in organic electronic devices, as we continued to develop these materials, our results have steadily improved, demonstrating the potential these materials have in semiconducting applications.[7, 11, 46, 79]

## 1.4 ORGANIC LIGHT-EMITTING DIODES

Electroluminescence in polymer films was first observed in poly(N-vinylcarbazole) (PVK) by Roger Partridge at the National Physical Laboratory in the United Kingdom in the 1970s and consisted of a 2.2 µm think film of PVK between two injecting electrodes.[80-83] Tang et al. later developed the first true diode device at Eastman Kodak which consisted of a two layer structure with separate hole and electron transporting layers where light was emitted from recombining holes and electrons at the interface of the two organic layers. This resulted in a much lower drive voltage for the device and improved efficiency.[8] Since then researchers have developed a wide variety of OLEDs that cover the full spectrum of visible colors.[84-88] How the device functions is dependent on how it is engineered but the typical OLED will have a transparent electrode made of indium tinoxide (ITO) that exists as a thin film on a transparent glass substrate. A layer of

Poly(3,4-ethylenedioxythiophene) poly(styrenesulfonate) (PEDOT:PSS) is spin-coated on top of the ITO. PEDOT:PSS is an intrinsically doped conducting polymer that acts as a hole injection and transport layer. Next, a layer of light-emitting polymer is spin-cast onto the device using a solvent that will not dissolve the PEDOT:PSS layer. A layer of alkali fluoride (LiF for instance) is vapor deposited on top of the polymer layer. This layer helps facilitate electron injection and acts as a buffer between the polymer and the aluminum electrode that then gets vapor deposited on top of the LiF. If the aluminum is deposited directly on the polymer, plasmons on the surface of the electrode will quench excitons at the metal-polymer interface, decreasing device performance.[45] In this device, an electric field is applied which causes holes and electrons to be injected into the polymer film from opposite sides. As the charge carriers migrate through the film they begin to recombine to form excitons. The excitons then radiatively decay, giving off photons. The resulting light is omni-directional and unpolarized which means displays made from OLEDs have much wider viewing angles than liquid crystal displays (LCDs). Since all light generated by the OLED is used to make the displayed picture, OLED displays can obtain significantly higher contrast ratios than LCDs, which use a backlight and a liquid crystal pane that blocks most of the generated light and has light bleed through, causing brighter blacks.[89]

There have been many advances in OLED engineering since Kodak's first device, all of which are generally geared toward solving three major problems with their operation: inefficient hole-electron recombination, non-radiative decay of excitons, and charge carrier injection and transport. In order for an OLED to perform efficiently, a large number of photons must be emitted while applying only a small drive voltage. This requires that the polymer film be able to conduct holes and electrons well while possessing a low barrier to charge injection (the difference in energy between the Fermi level of the metal electrode and the HOMO energy level of the polymer for hole injection or the LUMO energy level for electron injection). Due to the tendency for conjugated polymers to have high-lying HOMOs, hole injection and transport is not typically a major problem, relatively speaking. But most conjugated polymers have high lying LUMOs as well. This creates a large barrier to electron injection that can be solved to some degree by using low work function electrodes.[48] Figure 1.9 illustrates the electronic inner-workings of an OLED and how the HOMO and LUMO energy levels effect charge injection.

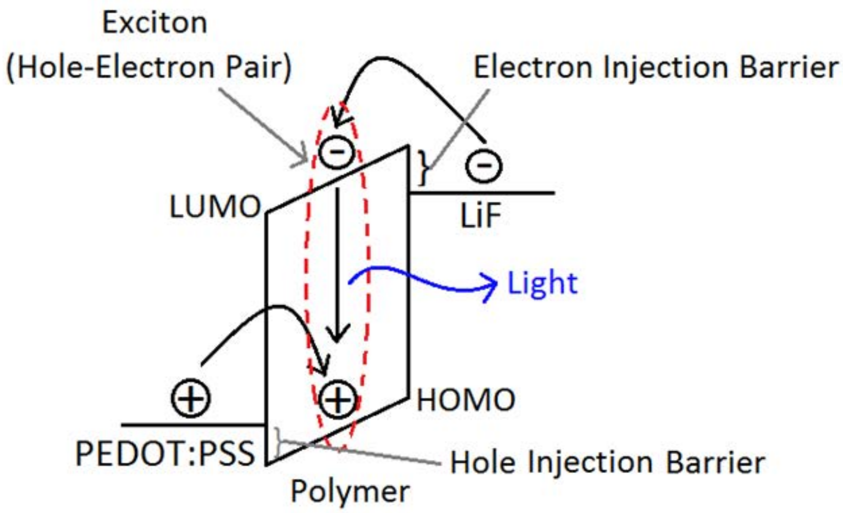

**Figure 1.9.** Energy level band diagram for a basic OLED

The slanted HOMO and LUMO levels represent and applied electric field and is referred to as band-bending.

The problem with this device architecture is that charge carriers can freely move through the polymer film without recombining before reaching the electrode. This is because there is no energy barrier preventing the charge carriers from leaving the polymer layer. To combat this problem a new layer of semiconducting polymer can be introduced that traps one type of charge carrier and blocks the other. Figure 1.10 shows the band diagram from a system such as this. In this system holes are injected into the semiconducting polymer with the higher HOMO (the hole transport layer) and electrons are injected into the semiconducting polymer with the lower LUMO (the electron transport layer). A large potential barrier prevents either carrier from migrating into the other film and instead holes and electrons recombine at the film interface. While this device architecture does improve brightness and efficiencies over the previously mentioned architecture, it has its own limitations. Recombination at the film interface results in exciplex formation which substantially reduces the external quantum efficiency of the device.[90] Also, the energy of the emitted photon is equal to the difference in energy between the HOMO of the hole transporting layer and the LUMO of the electron transporting layer. This produces a red-shifted emission and using this technique to obtain high energy photons, such as that needed for blue emission, becomes challenging.

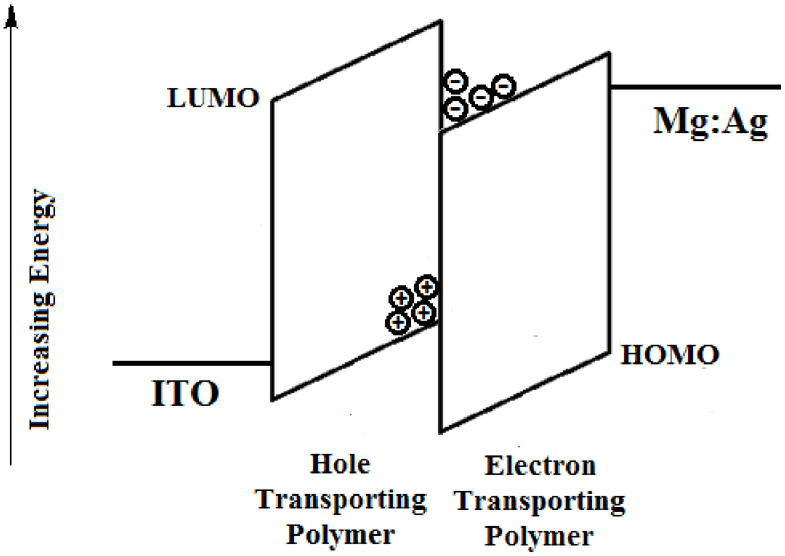

**Figure 1.10.** Energy level band diagram of a bilayer OLED.

In order to improve OLED performance a third layer can be introduced that has a HOMO higher than the hole transporting layer's and a LUMO lower than the electron transport layer's. In this device architecture the new layer is the emissive layer and the hole and electron transport layers funnel charge carriers to the emissive layer. Once charge carriers reach the emissive layer they are trapped there, guaranteeing hole-electron recombination, forming excitons, and emitting light possessing an energy similar to that of the emissive polymer's bandgap (Figure 1.11). This type of architecture, however, has some drawbacks as well. It requires spin-coating of multiple polymer layers on top of each other, each layer requiring an orthogonal solvent so as not to dissolve the previous layer. The added complexity of fabrication would also lead to increased manufacturing costs. This architecture relies on the emissive polymer to be a charge trap for carriers to ensure efficient charge recombination. Engineers have since found an alternative approach to do this that does not require the high complexity of device structure. These OLEDs are referred to as guest-host OLEDs.

In guest-host OLEDs a semiconducting small molecule or polymer "host" is doped with small amounts of an emitting material. Researchers have made guest-host OLEDs with a wide variety of emissive materials including small molecules,[91-94] and conjugated polymers.[11, 95-97] The inner-workings of a guest-host OLED is a bit more complicated than the devices previously

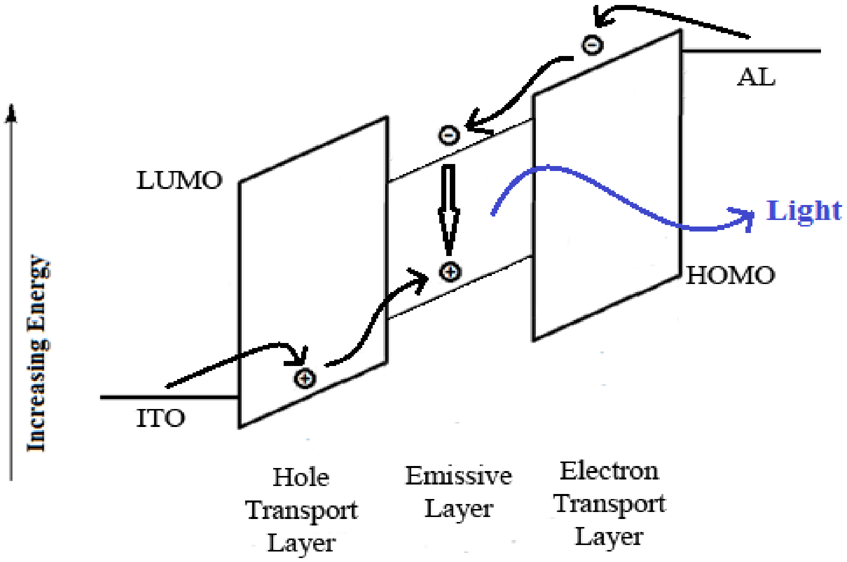

**Figure 1.11.** Energy level band diagram of a three layer OLED.

discussed. In a guest-host OLED a hole injection layer (generally PEDOT:PSS) is cast onto ITO followed by a layer of the host material already doped with the emissive guest. The host material can be either a small molecule or polymer but needs to be able to conduct holes and electrons. It also needs to be carefully chosen to meet the electronic criteria for the guest. A variety of hosts have been reported in the literature,[98-102] though PVK is the most widely used polymer host. On top of the guest-host layer is deposited a low work-function electron injection layer such as CsF or LiF followed by the metal cathode. If the host material is much better at conducting holes than electrons (which is often the case) a hole blocking layer (such as 4,7-Diphenyl-1,10-phenanthroline, also known as BPhen) can be added between the active layer and electron injection layer. Figure 1.12 illustrates the architecture of such a device.

When an electric field is applied to a guest-host OLED, charge carriers are injected into the host material in similar fashion to the neat layer device previously discussed. In this device though, charges are trapped on the guest molecules and cannot simply pass through the film without recombining. Excitons formed on the guest then radiatively decay, producing light. This, however, is only one mechanism by which light may be produced in this device. If hole-electron pairs recombine within the host material, forming a host

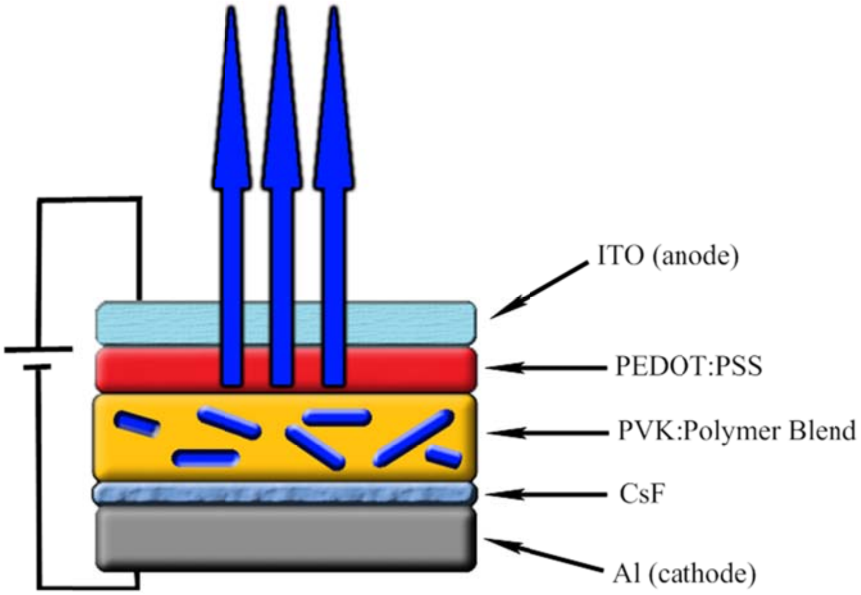

**Figure 1.12.** Schematic of a guest-host OLED (layers not to scale)

exciton, the excited state host can transfer its energy to the guest via Förster resonance energy transfer (FRET). FRET is a non-radiative energy transfer process that occurs when the excited state dipole of the host, caused by exciton formation, causes an induced excited state dipole on the guest. A "virtual photon" is transferred from the host to the guest causing exciton formation on the guest.[103] The guest then emits a photon as it returns to the ground state. The rate of energy transfer is dependent on overlap of the host's emission spectrum with the guest's absorption spectrum, even though this is a non-radiative energy transfer process. The exciton produced in the guest must also be lower in energy than the exciton from the host. Generally, if the guest's HOMO and LUMO both fall within the energy levels of the HOMO and LUMO of the host some overlap should occur and the guest's exciton will be lower in energy than the host's. These electronic requirements are why the host and guest selection need to be chosen carefully, in order to have the proper electronic states in each material. If FRET cannot efficiently or completely occur, the electroluminescence spectrum emitted by the device will show emission from both the host and the guest, altering the EL spectrum.[11] If the guest traps holes efficiently (the guest HOMO is >0.4 eV than the host[104]) but not electrons (or vice versa) holes will sit on the guest and recombination will not occur as readily. Also FRET cannot take place between an excited host molecule and a guest that has a charge carrier trapped on it. But if the guest doesn't

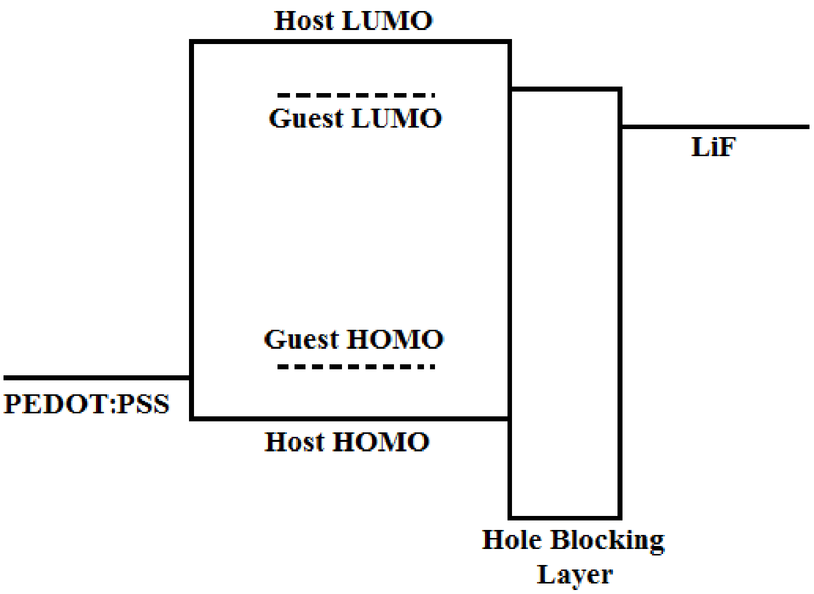

**Figure 1.13.** Energy level diagram for guest-host OLED

efficiently trap holes or electrons, FRET emission can still dominate even if hole-electron recombination directly on the guest is not occurring. This last scenario is particularly interesting, as it has been shown that if excitons form in the host material and can freely move around within the film, triplet-triplet annihilation can occur. This is a bimolecular process that results in two triplet excitons forming one singlet exciton on one molecule and a ground state in the other. [104]

The reason singlet excitons are important in fluorescent OLEDs is because only singlet excitons can fluoresce as triplet fluorescence is a spin forbidden transition. Unfortunately, when holes and electrons are injected and recombine there is only a 25% statistical chance that an exciton will be a singlet, with 3 triplets produced for every one singlet.[105, 106] This means that in fluorescent OLEDs like the devices described previously, internal quantum efficiencies of only 25% are theoretically possible. Devices utilizing Triplet-triplet annihilation exhibiting internal quantum efficiencies greater than 25% have been reported[107, 108] but even in these cases two triplet excitons are used to create just one singlet exciton. So 100% internal quantum efficiencies cannot be obtained even in these devices. In order to produce devices that approach 100% internal quantum efficiencies, phosphorescent OLEDs have been developed that take advantage of spin-orbit coupling between a conjugated organic ligand and a heavy metal, commonly iridium[109-112] or platinum[113-115]. This interaction causes intersystem crossing between the triplet and singlet states creating a state that is spin-allowed to radiatively relax to the ground state, taking advantage of both singlet and triplet excitons.[116, 117]

Another aspect of guest-host OLEDs that make them more efficient than neat-film devices is the fact that the host disrupts π-stacking induced aggregation of the guest. Aggregation causes concentration quenching in films and decreases the quantum yield of the emissive material.[118] Even in a host material, concentration quenching is a significant problem for emissive polymers. As mentioned previous, the addition of large flexible side chains to the polymer can help reduce this effect and is extremely important when designing conjugated polymers for OLEDs. Moieties such as fluorene, which has a $sp^3$ hybridized bridging carbon, that points the alkyl chains out of the plane of the π-system are also very effective at disrupting aggregation. Other common approaches are to use branched alkyl chains, such as 2-ethylhexyl, which disrupts packing to a greater extent than n-alkyl chains, or introducing a-symmetric moieties into the polymer backbone which prevents efficient π-stacking. In fact, 9,9-dialkylfluorene and 2-(2-ethylhexyloxy),5-methoxybenzene are among the two most studied moieties in OLED research.[119-123]

The biggest problem facing OLED research today is the development of high efficiency deep blue OLEDs. In order to make full color displays, red, green, and blue emitters are needed. Currently, green and red have been fairly well developed with high external quantum efficiencies and operational lifetimes.[124-126] Operational lifetime (the number of hours required to cause the original brightness at a set drive voltage to be reduced by 50%) is directly related to luminous efficiency, so improving efficiencies translates not only to lower power consumption with higher brightness, but also longer device lifetimes.[127] Unfortunately, it is much more difficult to obtain high efficiencies with shorter wavelength light, such as blue, because luminous efficiency is related to how sensitive the human eye is to light.[128] Figure 1.14 shows the photopic (light-adapted) luminous efficiency function of the human eye, which illustrates that in the blue region of the spectrum, the eye is not very sensitive to light. In a blue OLED, many more blue photons need to be emitted in order to produce the same apparent brightness as an OLED that emits light at 550 nm. This creates an inherent disadvantage for blue OLEDs, necessitating higher external quantum efficiencies than longer wavelength emitting devices.

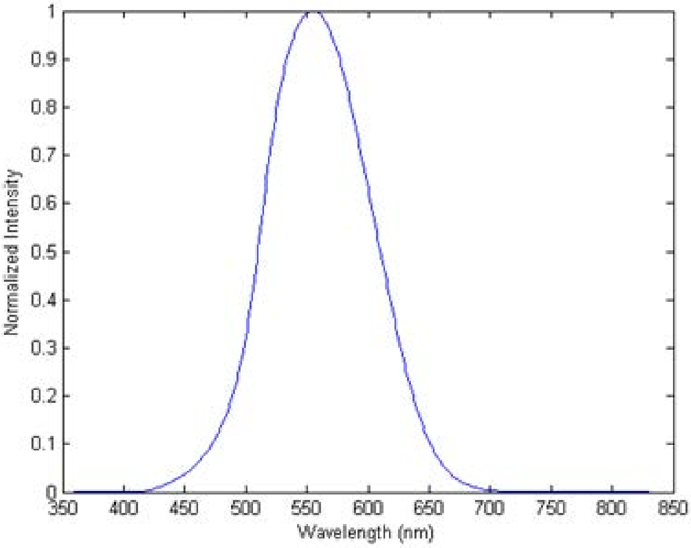

**Figure 1.14.** Photoptic luminous efficiency function plot representing the human eye's sensitivity to light at various wavelengths.

Research has been focused on developing blue OLEDs with high efficiencies but it has been challenging. Creating wide bandgap materials that emit blue, as previously mentioned, can be achieved by decreasing the quinoid resonance character of the polymer. An increased bandgap can also be achieved by twisting of the conjugated backbone of the material, though this typically decreases quantum yields of the materials, resulting in poor device efficiencies.[129, 130]. Large bandgap materials by nature often tend to have high lying LUMOs causing problems with electron injection and transport, decreasing device efficiencies. Attempts have been made to incorporate electron deficient moieties to improve electron injection and transport with some success.[11, 131-134]

## 1.5 ORGANIC PHOTOVOLTAICS

Renewable energy has become an extremely important area of research in order to meet the world's growing energy demands at a time when petroleum based resources are becoming increasingly scarce. Solar energy is a very important piece to that puzzle but current solar technology is very expensive. As previously discussed, inorganic solar cells require high purity silicon and high vacuum chemical vapor deposition in order to manufacture them. This high fabrication cost results in low kilowatt per dollar figures and limits the technology's application. The demand for low-cost high-efficiency solar cells has led the search for the next solar technology to organic photovoltaics. What makes this technology so appealing is their low cost of fabrication via spin-coating or inkjet printing, the low cost of materials, and the ability to make lightweight devices.[135, 136] The ability to make flexible solar cells on plastic substrates is also extremely appealing as it means literally any surface can be covered with OPVs, regardless of its shape.

The simplest OPV is a single layer device composed of a semiconducting polymer sandwiched between two electrodes. The anode is composed of a transparent high work function material, typically ITO. The cathode is made of a low work function metal such as aluminum, calcium, or magnesium. The difference in work functions between the electrodes results in the band bending seen in Figure 1.15 and creates an electric field in the polymer layer. As light is absorbed by the polymer, excitons form creating hole-electron pairs that are bound by a coulombic force. The electric field causes the holes and electrons to separate and travel to their

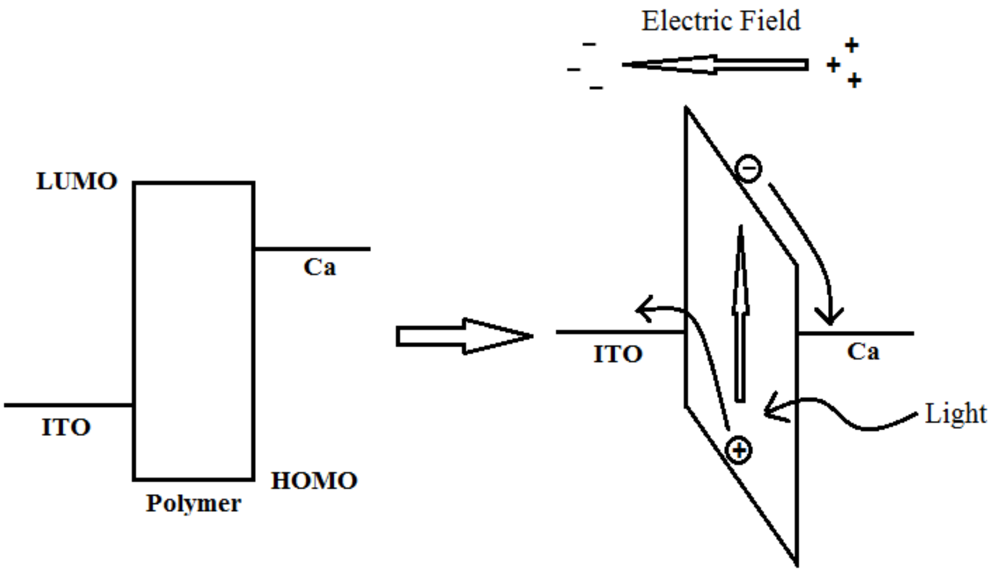

**Figure 1.15.** Energy level band diagram of a single layer OPV describing light induced exciton formation and dissociation.

respective electrode, creating a photocurrent. The created current and voltage can then be used to do work.[137, 138]

Single layer OPVs have many drawbacks and they do not generally perform well. They tend to have very low power conversion efficiencies (<0.1%) which is the result of poor exciton dissociation within the polymer film. The generated electric field is typically not strong enough to efficiently overcome the coulombic forces holding the exciton together so most holes and electrons simply recombine. To solve this problem a bilayer device can be made using two different semiconducting polymers. An electron rich (high lying HOMO) polymer is used as an electron donating layer and an electron deficient (low lying LUMO) polymer is used as an electron accepting layer. In this device, light is absorbed by one of the layers (for instance the donor layer), forming an exciton. The donor layer then transfers the electron from its LUMO to the LUMO of the acceptor. The difference in energy between donor and acceptor LUMOs needs to be greater than the exciton dissociation energy (~0.2 eV) or else exciton dissociation will not occur.[138, 139] Electrons then travel through the acceptor material while holes travel through the donor material to their respective electrodes, generating a photocurrent (Figure 1.16). This type of device shows an improved photocurrent over the previous architecture but is still plagued by low power conversion efficiencies.

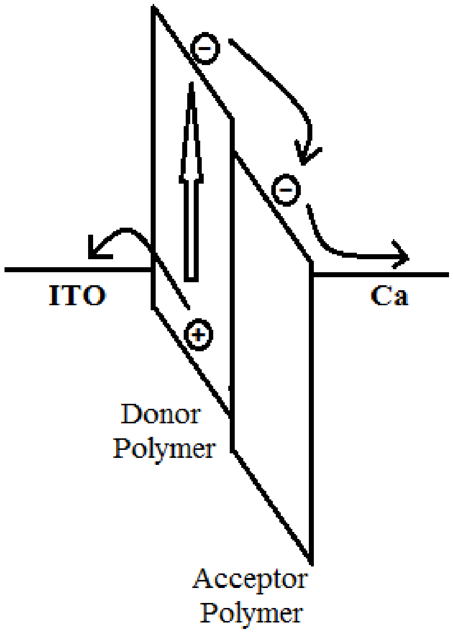

**Figure 1.16.** Energy level band diagram for a bilayer donor-acceptor OPV.

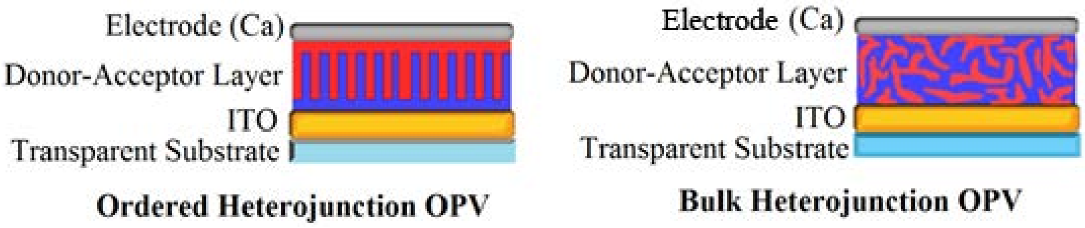

**Figure 1.17.** Illustration of ordered and bulk heterojunction solar cells (layers not to scale).

The problem with this device is that the active layers need to be fairly thick (~100 nm) in order to harvest as much of the incoming light as possible. This results in excitons being formed all throughout the film. But exciton dissociation can only happen at the donor-acceptor interface. In order for the exciton to reach the interface it must diffuse through the film, but because of the limited lifetime that excitons exist, they may only travel about ten nanometers before recombination occurs.[140] As a result, only excitons formed within 10 nm of the donor-acceptor interface are able to actually dissociate and produce the photocurrent. All other excitons are wasted, decreasing the quantum efficiency of the device. This is the biggest problem facing OPVs today and many different approaches have been made to overcome it. Dye sensitized solar cells have been developed which use small molecule dyes at the donor-acceptor interface. Excitons in the active layer can then transfer their energy to the dye molecules via FRET where they can then dissociate.[141-143] These devices, however, are much more difficult to fabricate with higher costs associated with their manufacturing.

The ideal alternative is an ordered heterojunction cell where donor and acceptor layers that are each 10-20 nm thick alternate side by side across the film (Figure 1.17). In this scenario, all formed excitons should be within 10 nm of a donor-acceptor interface. This structure also gives all dissociated holes and electrons percolation pathways through their transport material of choice to their respective electrodes. This type of ordered nano structure has currently not been obtained, however, and likely would have its own high level of difficulty in fabrication. Instead, what scientists have done is develop what is known as bulk heterojunction (BHJ) solar cells with the pioneering work done by Yu, et al.[144] In these cells, donor and acceptor materials are blended together in a solution and spin-cast as a single active layer. By controlling the film morphology through synthetic structural changes (such as polymer alkyl side chains)[145] and fabrication techniques such as film annealing,[146] donor-acceptor ratio,[5] casting temperature, [147] or additives,[148] efficiencies of BHJ solar cells have given superior results over bilayer devices with power conversion efficiencies greater than 7%.[149]

A major breakthrough occurred in BHJ solar cell development when Sariciftci, et al. observed efficient electron transfer in fullerene-polymer composites.[150] Since then, fullerenes have been the acceptor of choice for most researchers. Fullerenes are uniquely tailored to be acceptors in these devices and offer many advantages that electron accepting semiconducting polymers do not. The most common fullerene used, [6,6]-Phenyl $C_{61}$ butyric acid methyl ester (PCBM) has a very low lying LUMO which is triply degenerate, allowing for it to accept up to six electrons. Another major advantage it has is that electron transfer from a polymer to a fullerene is extremely fast (~45 fs) which is much faster than photoluminescence or back electron transfer.[6] This allows for excellent charge separation with a quantum yield approaching unity. One problem with BHJ solar cells is controlling phase segregation between the fullerene and polymer phases within the film. The BHJ shown in Figure 1.16 clearly shows areas where the red acceptor phase is isolated from the electrode. This means that charge carriers in this domain are trapped and have nowhere to go, reducing the efficiency of the device. Also, if large phase domain sizes result from casting films, there may be domains larger than 20 nm, meaning any excitons formed deep inside the domain may not be able to reach the donor-acceptor interface, preventing dissociation. The use of solvent additives such as 1,8-diiodooctane[151] and 1-chloronaphthalene[152] when casting films can help create smaller domain sizes and can impact the number of percolation pathways for charge carriers to reach the electrodes.

When designing conjugated polymers as donor materials a couple of key requirements need to be considered. The absorption spectrum of the polymer needs to overlap well with the solar spectrum which has a peak intensity around 700 nm at sea level (Figure 1.18). This corresponds to a band gap around 1.6-1.7 eV. The HOMO and LUMO of the polymer must also match up well with the acceptor. As mentioned previously, the LUMO of the donor must be greater than 0.2 eV higher than the LUMO of the acceptor for exciton dissociation to occur. The HOMO is also important in that it has been demonstrated that the difference in energy between the HOMO of the donor and the LUMO of the acceptor are directly proportional to the open

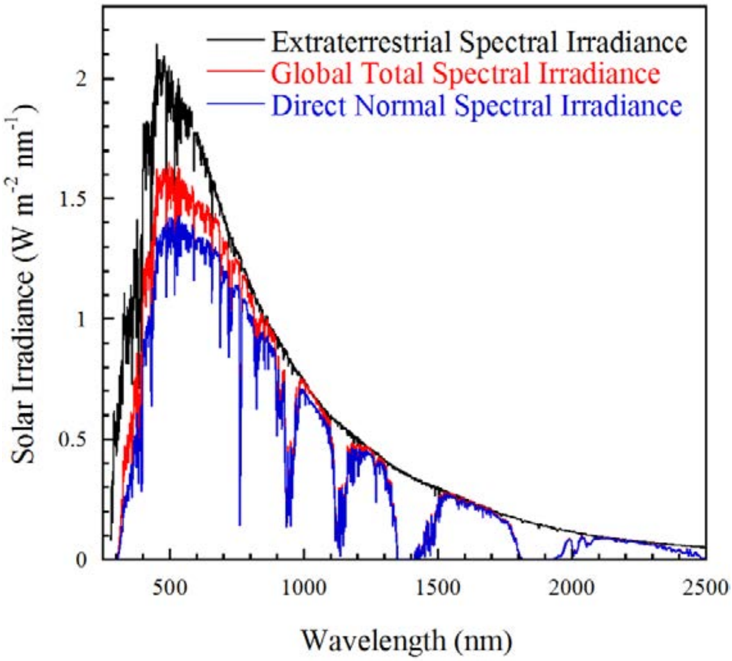

**Figure 1.18.** Solar irradiance spectrum for extraterrestrial spectral irradiance (outter atmosphere spectrum), the Global Total Spectral Irradiance on the 37° sun facing tilted surface, and the Direct Normal Spectral Irradiance (sea level spectrum).

circuit voltage of the cell.[153, 154] In order to obtain a high open circuit voltage, the polymer needs to have as low of a HOMO as possible while taking the aforementioned considerations into account. This necessitates a balanced tradeoff between good solar spectrum absorption, efficient electron transfer, and high open circuit voltages to make an optimum cell. In a BHJ solar cell using $PC_{60}BM$ as the acceptor, the ideal donor would have a LUMO between -3.7 and -4.0 eV and a HOMO between -5.2 and -5.8 eV.[155] Using donor-acceptor polymers has been the strategy of choice as the acceptors help generate lower LUMOs, narrowing the bandgap while maintaining a good open circuit voltage.

Proper HOMO and LUMO energy levels are not the only aspects of polymer design that are important in solar cells. The polymers need to have good film forming properties in order to obtain desirable film morphologies. This can be done by varying alkyl chain substitution on the polymer. Short linear chains that are spaced apart along the polymer backbone can result in

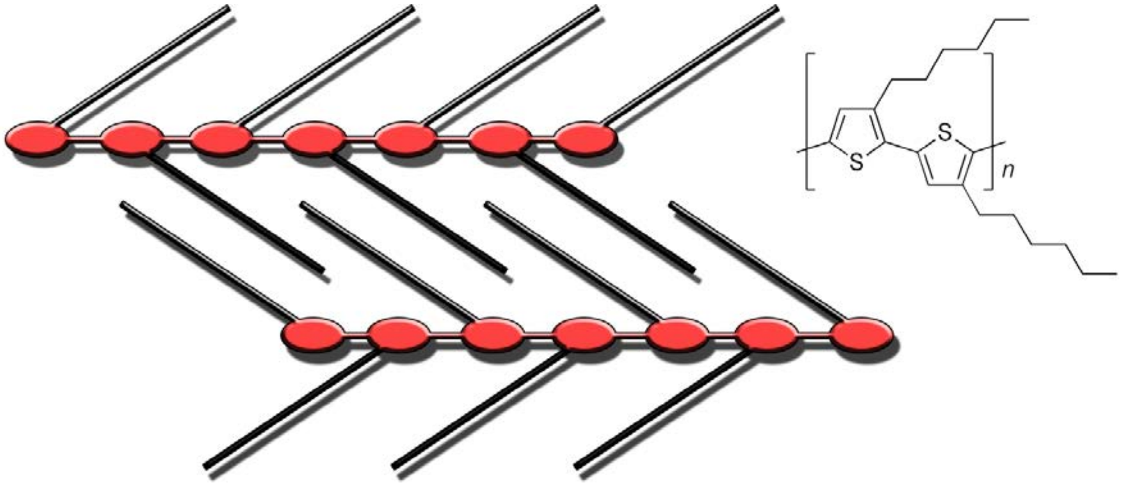

**Figure 1.19.** Illustration of interdigitation in poly(3-hexylthiophene) films.

interdigitation of side chains, improving crystallinity in films by introducing three-dimensional packing of the polymer chains (Figure 1.19).[156] Using longer branched alkyl chains improves the solubility of the polymer making it possible to achieve higher molecular weights during polymerization. Longer polymer chains leads to less electron hopping in films and improves the bulk charge carrier mobility of the film. Longer branched alkyl chains do tend to disrupt crystallinity in the BHJ film, however. Chain substitution can also influence phase segregation in the BHJ film by affecting how well it aggregates relative to PCBM.[157] If PCBM begins to crystallize out of the solution during spin-casting before the donor polymer, it can result in large acceptor domain sizes, decreasing cell efficiency.

## 1.6 CONCLUSIONS

In summation, the main factors that need to be taken into consideration when designing organic semiconductors is:

- Band Gap
    - Tuned by controlling the effective conjugation length.
        - Stabilizing the quinoid form or destabilizing the benzoid form of the polymer decreases the band gap.

    - Reducing steric effects that twist the backbone decreases the band gap.
  - Using donor-acceptor systems
    - HOMO is tuned by donor.
    - LUMO is tuned by acceptor.
- HOMO/LUMO Energy Levels
  - Tuned using electron donating or electron withdrawing groups or donor-acceptor systems.
  - Needs to be tuned based on desired device application.
    - HOMO needs to be low for high open circuit voltage in solar cells with high lying LUMO while balancing with narrow bandgap for good solar spectrum absorption.
    - HOMO needs to be high, LUMO needs to be low for balanced charge transport in OLEDs with band gap considerations depending on the desired color of the OLED.
- Oxidative and Thermal Stability
  - High lying HOMO and LUMO decreases oxidative stability
  - Alkyl chains reduce thermal stability
- Film Forming Properties
  - Long branched alkyl chains disrupt π-stacking and make amorphous films, desirable for OLEDs.
  - Short linear alkyl chains, spaced apart, increase crystallinity through interdigitation of alkyl chains, desirable for OPVs and OFETs.
  - Longer polymer chains and increased crystallinity leads to higher charger carrier mobilities in films.

Ultimately there are quite a number of factors that affect the performance of these materials in organic electronic devices. How each structural change affects a polymer is highly dependent on the system involved. Though many different semiconducting polymers have been reported in the literature there is still a great need to develop new materials with desirable electronic properties. It is particularly important to develop new electron deficient systems and to examine the structure-properties relationships they have in order to further our understanding of how best to go about rationally designing semiconducting polymers.

## 1.7 REFERENCES

1. Shirakawa, H.; Louis, E. J.; Macdiarmid, A. G.; Chiang, C. K.; Heeger, A. J. *Chemical Communications* **1977,** 16, 578-580.

2. Chiang, C. K.; Druy, M. A.; Gau, S. C.; Heeger, A. J.; Louis, E. J.; MacDiarmid, A. G.; Park, Y. W.; Shirakawa, H. *J. Am. Chem. Soc.* **1978,** 100, (3), 1013-1015.

3. Tang, C. W. *Appl. Phys. Lett.* **1986,** 48, (2), 183-185.

4. Scharber, M. C; Mühlbacher, D.; Koppe, M.; Denk, P.; Waldauf, C.; Heeger, A. J; Brabec, C. J. *Adv. Mater.* **2006,** 18, (6), 789-794.

5. Thompson, Barry C; Fréchet, Jean M J. *Angew. Chem., Int. Ed.* **2008,** 47, (1), 58-77.

6. Cheng, Yen-Ju; Yang, Sheng-Hsiung; Hsu, Chain-Shu. *Chem. Rev.* **2009,** 109, (11), 5868-5923.

7. Bhuwalka, Achala; Mike, Jared F.; He, Meng; Intemann, Jeremy J.; Nelson, Toby; Ewan, Monique D.; Roggers, Robert A.; Lin, Zhiqun; Jeffries-El, Malika. *Macromolecules* **2011**.

8. Tang, C. W.; Vanslyke, S. A. *Appl. Phys. Lett.* **1987,** 51, 913-915.

9. Burroughes, J. H.; Bradley, D. D. C.; Brown, A. R.; Marks, R. N.; Mackay, K.; Friend, R. H.; Burns, P. L.; Holmes, A. B. *Nature* **1990,** 347, (6293), 539-541.

10. Friend, R. H.; Gymer, R. W.; Holmes, A. B.; Burroughes, J. H.; Marks, R. N.; Taliani, C.; Bradley, D. D. C.; Santos, D. A. Dos; Bredas, J. L.; Logdlund, M.; Salaneck, W. R. *Nature* **1999,** 397, (6715), 121-128.

11. Mike, Jared F.; Intemann, Jeremy J.; Cai, Min; Xiao, Teng; Shinar, Ruth; Shinar, Joseph; Jeffries-El, Malika. *Polym. Chem.* **2011,** 2, (10), 2299-2305.

12. Dimitrakopoulos, C. D.; Malenfant, P. R. L. *Adv. Mater.* **2002,** 14, (2), 99-117.

13. Babel, A.; Jenekhe, S. A. *Adv. Mater.* **2002,** 14, (5), 371-374.

14. Babel, Amit; Jenekhe, Samson A. *J. Phys. Chem. B* **2002,** 106, (24), 6129-6132.

15. Tsao, Hoi Nok; Cho, Don M.; Park, Insun; Hansen, Michael Ryan; Mavrinskiy, Alexey; Yoon, Do Y.; Graf, Robert; Pisula, Wojciech; Spiess, Hans Wolfgang; Mullen, Klaus. *J. Am. Chem. Soc.* **2011,** 133, (8), 2605-2612.

16. Meyer, Wolfgang H. *Adv. Mater.* **1998,** 10, (6), 439-448.

17. Pan, L.; Qiu, H.; Dou, C.; Li, Y.; Pu, L.; Xu, J.; Shi, Y. *International journal of molecular sciences* **2010,** 11, (7), 2636-2657.

18. Murata, Kazuo; Izuchi, Shuichi; Yoshihisa, Youetsu. *Electrochimica Acta* **2000,** 45, (8–9), 1501-1508.

19. Zhou, Z.; Shinar, R.; Allison, A. J; Shinar, J. *Adv. Funct. Mater.* **2007,** 17, (17), 3530-3537.

20. McQuade, D. Tyler; Pullen, Anthony E.; Swager, Timothy M. *Chem. Rev.* **2000,** 100, (7), 2537-2574.

21. Li, Junfeng; Wu, Yuanzhao; Song, Fengyan; Wei, Guo; Cheng, Yixiang; Zhu, Chengjian. *J. Mater. Chem.* **2012,** 22, (2), 478-482.

22. Samyn, Celest; Verbiest, Thierry; Persoons, André. *Macromol. Rapid Commun.* **2000,** 21, (1), 1-15.

23. Nalwa, Hari Singh. *Adv. Mater.* **1993,** 5, (5), 341-358.

24. Gribov, B. G.; Zinov'ev, K. V. *Inorganic Materials* **2003,** 39, (7), 653-662.

25. Davis, J. R., Jr.; Rohatgi, A.; Hopkins, R. H.; Blais, P. D.; Rai-Choudhury, P.; McCormick, J. R.; Mollenkopf, H. C. *Electron Devices, IEEE Transactions on* **1980,** 27, (4), 677-687.

26. Chang, Jui-Fen; Sun, Baoquan; Breiby, Dag W.; Nielsen, Martin M.; Sölling, Theis I.; Giles, Mark; McCulloch, Iain; Sirringhaus, Henning. *Chem. Mater.* **2004,** 16, (23), 4772-4776.

27. Hebner, T. R.; Wu, C. C.; Marcy, D.; Lu, M. H.; Sturm, J. C. *Appl. Phys. Lett.* **1998,** 72, (5), 519-521.

28. Ling, Mang Mang; Bao, Zhenan. *Chem. Mater.* **2004,** 16, (23), 4824-4840.

29. He, Yi; Kanicki, Jerzy. *Appl. Phys. Lett.* **2000,** 76, (6), 661-663.

30. Al-Ibrahim, Maher; Roth, H. Klaus; Zhokhavets, Uladzimir; Gobsch, Gerhard; Sensfuss, Steffi. *Solar Energy Materials and Solar Cells* **2005,** 85, (1), 13-20.

31. Saunier, J.; Alloin, F.; Sanchez, J. Y.; Caillon, G. *Journal of Power Sources* **2003,** 119–121, (0), 454-459.

32. Kim, Young-Gi; Thompson, Barry C.; Ananthakrishnan, Nisha; Padmanaban, G.; Ramakrishnan, S.; Reynolds, John R. *Journal of Materials Research* **2011,** 20, (12), 3188-3198.

33. Bredas, J. L.; Silbey, R.; Boudreaux, D. S.; Chance, R. R. *J. Am. Chem. Soc.* **1983,** 105, (22), 6555-6559.

34. Jenekhe, Samson A. *Nature* **1986,** 322, (6077), 345-347.

35. Brédas, J. L.; Chance, R. R.; Silbey, R. *Phys. Rev. B: Condens. Matter Mater. Phys.* **1982,** 26, (10), 5843-5854.

36. Wohlgenannt, M.; Jiang, X. M.; Vardeny, Z. V. *Phys. Rev. B: Condens. Matter Mater. Phys.* **2004,** 69, (24), 241204.

37. van Mullekom, H. A. M.; Vekemans, J. A. J. M.; Havinga, E. E.; Meijer, E. W. *Materials Science and Engineering: R: Reports* **2001,** 32, (1), 1-40.

38. Yamamoto, Takakazu; Zhou, Zhen-hua; Kanbara, Takaki; Shimura, Masaki; Kizu, Kenichi; Maruyama, Tsukasa; Nakamura, Yoshiyuki; Fukuda, Takashi; Lee, Bang-Lin; Ooba, Naoki; Tomaru, Satoru; Kurihara, Takashi; Kaino, Toshikuni; Kubota, Kenji; Sasaki, Shintaro. *J. Am. Chem. Soc.* **1996,** 118, (43), 10389-10399.

39. Murphy, Amanda R.; Liu, Jinsong; Luscombe, Christine; Kavulak, David; Fréchet, Jean M. J.; Kline, R. Joseph; McGehee, Michael D. *Chem. Mater.* **2005,** 17, (20), 4892-4899.

40. Li, Yaowen; Chen, Yujin; Liu, Xing; Wang, Zhong; Yang, Xiaoming; Tu, Yingfeng; Zhu, Xiulin. *Macromolecules* **2011,** 44, (16), 6370-6381.

41. Friedel, Bettina; McNeill, Christopher R.; Greenham, Neil C. *Chem. Mater.* **2010,** 22, (11), 3389-3398.

42. Gadisa, Abay; Oosterbaan, Wibren D.; Vandewal, Koen; Bolsée, Jean-Christophe; Bertho, Sabine; D'Haen, Jan; Lutsen, Laurence; Vanderzande, Dirk; Manca, Jean V. *Adv. Funct. Mater.* **2009,** 19, (20), 3300-3306.

43. Chu, Chih-Wei; Yang, Hoichang; Hou, Wei-Jen; Huang, Jinsong; Li, Gang; Yang, Yang. *Appl. Phys. Lett.* **2008,** 92, (10), 103306.

44. Jenekhe, Samson A.; Osaheni, John A. *Science* **1994,** 265, (5173), 765-768.

45. Grimsdale, Andrew C.; Leok Chan, Khai; Martin, Rainer E.; Jokisz, Pawel G.; Holmes, Andrew B. *Chem. Rev.* **2009,** 109, (3), 897-1091.

46. Mike, Jared F.; Makowski, Andrew J.; Mauldin, Timothy C.; Jeffries-El, Malika. *J. Polym. Sci., Part A: Polym. Chem.* **2010,** 48, (6), 1456-1460.

47. Mihailetchi, V. D.; Wildeman, J.; Blom, P. W. M. *Phys. Rev. Lett.* **2005,** 94, (12), 126602.

48. Bernius, M. T.; Inbasekaran, M.; O'Brien, J.; Wu, W. *Adv. Mater.* **2000,** 12, (23), 1737-1750.

49. Zhan, Xiaowei; Tan, Zhan'ao; Domercq, Benoit; An, Zesheng; Zhang, Xuan; Barlow, Stephen; Li, Yongfang; Zhu, Daoben; Kippelen, Bernard; Marder, Seth R. *J. Am. Chem. Soc.* **2007,** 129, (23), 7246-7247.

50. Babel, Amit; Jenekhe, Samson A. *J. Am. Chem. Soc.* **2003,** 125, (45), 13656-13657.

51. Yan, He; Chen, Zhihua; Zheng, Yan; Newman, Christopher; Quinn, Jordan R.; Dotz, Florian; Kastler, Marcel; Facchetti, Antonio. *Nature* **2009,** 457, (7230), 679-686.

52. Rakhmanova, S. V.; Conwell, E. M. *Appl. Phys. Lett.* **2000,** 76, (25), 3822-3824.

53. Ballantyne, Amy M.; Chen, Lichun; Dane, Justin; Hammant, Thomas; Braun, Felix M.; Heeney, Martin; Duffy, Warren; McCulloch, Iain; Bradley, Donal D. C.; Nelson, Jenny. *Adv. Funct. Mater.* **2008,** 18, (16), 2373-2380.

54. Kline, R. J.; McGehee, M. D.; Kadnikova, E. N.; Liu, J.; Fréchet, J. M. J. *Adv. Mater.* **2003,** 15, (18), 1519-1522.

55. Cheng, Horng-Long; Lin, Wei-Qi; Wu, Fu-Chiao. *Appl. Phys. Lett.* **2009,** 94, (22), 223302.

56. Sirringhaus, H.; Wilson, R. J.; Friend, R. H.; Inbasekaran, M.; Wu, W.; Woo, E. P.; Grell, M.; Bradley, D. D. C. *Appl. Phys. Lett.* **2000,** 77, (3), 406-408.

57. Lim, Eunhee; Jung, Byung-Jun; Shim, Hong-Ku. *Macromolecules* **2003,** 36, (12), 4288-4293.

58. Ma, Zaifei; Wang, Ergang; Jarvid, Markus E.; Henriksson, Patrik; Inganas, Olle; Zhang, Fengling; Andersson, Mats R. *J. Mater. Chem.* **2012,** 22, (5), 2306-2314.

59. Liao, Liang; Dai, Liming; Smith, Adam; Durstock, Michael; Lu, Jianping; Ding, Jianfu; Tao, Ye. *Macromolecules* **2007,** 40, (26), 9406-9412.

60. Stalder, Romain; Grand, Caroline; Subbiah, Jegadesan; So, Franky; Reynolds, John R. *Polym. Chem.* **2012,** 3, (1), 89-92.

61. Liu, Bo; Zou, Yingping; Peng, Bo; Zhao, Bin; Huang, Kelong; He, Yuehui; Pan, Chunyue. *Polym. Chem.* **2011,** 2, (5), 1156-1162.

62. Wang, Ergang; Ma, Zaifei; Zhang, Zhen; Vandewal, Koen; Henriksson, Patrik; Ingana s, Olle; Zhang, Fengling; Andersson, Mats R. *J. Am. Chem. Soc.* **2011,** 133, (36), 14244-14247.

63. Tieke, Bernd; Rabindranath, A. Raman; Zhang, Kai; Zhu, Yu. *Beilstein Journal of Organic Chemistry* **2010,** 6, 830-845.

64. Wienk, Martijn M.; Turbiez, Mathieu; Gilot, Jan; Janssen, René A. J. *Adv. Mater.* **2008,** 20, (13), 2556-2560.

65. Zhou, Erjun; Wei, Qingshuo; Yamakawa, Shimpei; Zhang, Yue; Tajima, Keisuke; Yang, Chunhe; Hashimoto, Kazuhito. *Macromolecules* **2009,** 43, (2), 821-826.

66. Shi, Qinqin; Fan, Haijun; Liu, Yao; Hu, Wenping; Li, Yongfang; Zhan, Xiaowei. *J. Phys. Chem. C* **2010,** 114, (39), 16843-16848.

67. Osaka, Itaru; Zhang, Rui; Sauvé, Geneviève; Smilgies, Detlef- M.; Kowalewski, Tomasz; McCullough, Richard D. *J. Am. Chem. Soc.* **2009,** 131, (7), 2521-2529.

68. Osaka, Itaru; Zhang, Rui; Liu, Junying; Smilgies, Detlef- M.; Kowalewski, Tomasz; McCullough, Richard D. *Chem. Mater.* **2010,** 22, (14), 4191-4196.

69. Osman, A. M.; Mohamed, S. A. *Indian Journal of Chemistry* **1973,** 11, (9), 868-870.

70. Osman, A. M.; Mohamed, S. A. *United Arab Republic Journal of Chemistry* **1971,** 15, (5), 475-492.

71. Osman, Abdel-Megied; Khalil, Zarif H. *Journal of Applied Chemistry and Biotechnology* **1975,** 25, (9), 683-693.

72. Wolfe, James F.; Loo, Bock H.; Arnold, F. E. *Polymer Preprints* **1978,** 19, (2), 1-6.

73. Wolfe, James F.; Loo, Bock H.; Arnold, F. E. *Macromolecules* **1981,** 14, (4), 915-920.

74. Wolfe, James F.; Arnold, F. E. *Macromolecules* **1981,** 14, (4), 909-915.

75. Bhaumik, D.; Mark, J. E. *J. Polym. Sci., Part B: Polym. Phys.* **1983,** 21, (7), 1111-1118.

76. Osaheni, John A.; Jenekhe, Samson A. *Chem. Mater.* **1992,** 4, (6), 1282-1290.

77. Mike, Jared F.; Makowski, Andrew J.; Jeffries-El, Malika. *Org. Lett.* **2008,** 10, (21), 4915-4918.

78. Mike, Jared F.; Inteman, Jeremy J.; Ellern, Arkady; Jeffries-El, Malika. *J. Org. Chem.* **2009,** 75, (2), 495-497.

79. Mike, Jared F.; Nalwa, Kanwar; Makowski, Andrew J.; Putnam, Daniel; Tomlinson, Aimee L.; Chaudhary, Sumit; Jeffries-El, Malika. *Phys. Chem. Chem. Phys.* **2011,** 13, (4), 1338-1344.

80. Partridge, R.H. *Polymer* **1983,** 24, (6), 733-738.

81. Partridge, R.H. *Polymer* **1983,** 24, (6), 739-747.

82. Partridge, R.H. *Polymer* **1983,** 24, (6), 748-754.

83. Partridge, R.H. *Polymer* **1983,** 24, (6), 755-762.

84. Tasch, S.; List, E. J. W.; Hochfilzer, C.; Leising, G.; Schlichting, P.; Rohr, U.; Geerts, Y.; Scherf, U.; Müllen, K. *Phys. Rev. B: Condens. Matter Mater. Phys.* **1997,** 56, (8), 4479-4483.

85. Becker, H.; Spreitzer, H.; Kreuder, W.; Kluge, E.; Vestweber, H.; Schenk, H.; Treacher, K. *Synth. Met.* **2001,** 122, (1), 105-110.

86. Xu, Qianfei; Ouyang, Jianyong; Yang, Yang; Ito, Takayuki; Kido, Junji. *Appl. Phys. Lett.* **2003,** 83, (23), 4695-4697.

87. Huang, J.; Li, G.; Wu, E.; Xu, Q.; Yang, Y. *Adv. Mater.* **2006,** 18, (1), 114-117.

88. Huang, F.; Zhang, Y.; Liu, M. S; Cheng, Y. J.; Jen, A. K Y. *Adv. Funct. Mater.* **2007,** 17, (18), 3808-3815.

89. Xie, Z. Y.; Hung, L. S. *Appl. Phys. Lett.* **2004,** 84, (7), 1207-1209.

90. Zhu, Wen-qing; Jiang, Xue-yin; Zhang, Zhi-lin. *Journal of Shanghai University (English Edition)* **2006,** 10, (2), 156-160.

91. Lee, Chang-Lyoul; Lee, Kyung Bok; Kim, Jang-Joo. *Appl. Phys. Lett.* **2000,** 77, (15), 2280-2282.

92. Cai, Min; Xiao, Teng; Hellerich, Emily; Chen, Ying; Shinar, Ruth; Shinar, Joseph. *Adv. Mater.* **2011,** 23, (31), 3590-3596.

93. Chen, Fang-Chung; Yang, Yang; Thompson, Mark E.; Kido, Junji. *Appl. Phys. Lett.* **2002,** 80, (13), 2308-2310.

94. Lamansky, Sergey; Kwong, Raymond C.; Nugent, Matthew; Djurovich, Peter I.; Thompson, Mark E. *Organic Electronics* **2001,** 2, (1), 53-62.

95. Intemann, Jeremy J.; Mike, Jared F.; Cai, Min; Bose, Sayantan; Xiao, Teng; Mauldin, Timothy C.; Roggers, Robert A.; Shinar, Joseph; Shinar, Ruth; Jeffries-El, Malika. *Macromolecules* **2010,** 44, (2), 248-255.

96. Aharon, E.; Albo, A.; Kalina, M.; Frey, G. L. *Adv. Funct. Mater.* **2006,** 16, (7), 980-986.

97. Han, Yoon Soo; Kim, Hoyoung; Choi, Byeong Dae; Song, Jeong Han; Kwon, Younghwan; Hur, Youngjune; Kwak, Giseop; Kim, Soon Hak; Park, Lee Soon; Choi, Byeong-Dae. *Molecular Crystals and Liquid Crystals* **2007,** 470, (1), 329-340.

98. Yeh, S. J.; Wu, M. F.; Chen, C. T.; Song, Y. H.; Chi, Y.; Ho, M. H.; Hsu, S. F.; Chen, C. H. *Adv. Mater.* **2005,** 17, (3), 285-289.

99. Brunner, Klemens; van Dijken, Addy; Börner, Herbert; Bastiaansen, Jolanda J. A. M.; Kiggen, Nicole M. M.; Langeveld, Bea M. W. *J. Am. Chem. Soc.* **2004,** 126, (19), 6035-6042.

100. Su, Shi-Jian; Sasabe, Hisahiro; Takeda, Takashi; Kido, Junji. *Chem. Mater.* **2008,** 20, (5), 1691-1693.

101. Wong, Ken-Tsung; Chen, You-Ming; Lin, Yu-Ting; Su, Hai-Ching; Wu, Chung-chih. *Org. Lett.* **2005,** 7, (24), 5361-5364.

102. Balaganesan, Banumathy; Shen, Wen-Jian; Chen, Chin H. *Tetrahedron Letters* **2003,** 44, (30), 5747-5750.

103. Cheon, K. O.; Shinar, J. *Appl. Phys. Lett.* **2004,** 84, (7), 1201-1203.

104. Luo, Yichun; Aziz, Hany. *Adv. Funct. Mater.* **2010,** 20, (8), 1285-1293.

105. Brown, A. R.; Pichler, K.; Greenham, N. C.; Bradley, D. D. C.; Friend, R. H.; Holmes, A. B. *Chemical Physics Letters* **1993,** 210, (1–3), 61-66.

106. Baldo, M. A.; O'Brien, D. F.; Thompson, M. E.; Forrest, S. R. *Phys. Rev. B: Condens. Matter Mater. Phys.* **1999,** 60, (20), 14422-14428.

107. Okumoto, Kenji; Kanno, Hiroshi; Hamaa, Yuji; Takahashi, Hisakazu; Shibata, Kenichi. *Appl. Phys. Lett.* **2006,** 89, (6), 063504-063503.

108. Kido, Junji; Iizumi, Yasuhiro. *Appl. Phys. Lett.* **1998,** 73, (19), 2721-2723.

109. Zhou, Guijiang; Wong, Wai-Yeung; Yao, Bing; Xie, Zhiyuan; Wang, Lixiang. *Angew. Chem., Int. Ed.* **2007,** 46, (7), 1149-1151.

110. Tsuboyama, Akira; Iwawaki, Hironobu; Furugori, Manabu; Mukaide, Taihei; Kamatani, Jun; Igawa, Satoshi; Moriyama, Takashi; Miura, Seishi; Takiguchi, Takao; Okada, Shinjiro; Hoshino, Mikio; Ueno, Kazunori. *J. Am. Chem. Soc.* **2003,** 125, (42), 12971-12979.

111. Laskar, Inamur R.; Chen, Teng-Ming. *Chem. Mater.* **2003,** 16, (1), 111-117.

112. Lamansky, Sergey; Djurovich, Peter; Murphy, Drew; Abdel-Razzaq, Feras; Lee, Hae-Eun; Adachi, Chihaya; Burrows, Paul E.; Forrest, Stephen R.; Thompson, Mark E. *J. Am. Chem. Soc.* **2001,** 123, (18), 4304-4312.

113. Cocchi, M.; Virgili, D.; Fattori, V.; Rochester, D. L; Williams, J. A G. *Adv. Funct. Mater.* **2007,** 17, (2), 285-289.

114. Wong, Wai-Yeung; He, Ze; So, Shu-Kong; Tong, Ka-Lap; Lin, Zhenyang. *Organometallics* **2005,** 24, (16), 4079-4082.

115. Kwong, Raymond C.; Sibley, Scott; Dubovoy, Timur; Baldo, Marc; Forrest, Stephen R.; Thompson, Mark E. *Chem. Mater.* **1999,** 11, (12), 3709-3713.

116. Baldo, M. A.; Lamansky, S.; Burrows, P. E.; Thompson, M. E.; Forrest, S. R. *Appl. Phys. Lett.* **1999,** 75, (1), 4-6.

117. O'Brien, D. F.; Baldo, M. A.; Thompson, M. E.; Forrest, S. R. *Appl. Phys. Lett.* **1999,** 74, (3), 442-444.

118. Rothe, Carsten; Chiang, Chien-Jung; Jankus, Vygintas; Abdullah, Khalid; Zeng, Xianshun; Jitchati, Rukkiat; Batsanov, Andrei S.; Bryce, Martin R.; Monkman, Andrew P. *Adv. Funct. Mater.* **2009,** 19, (13), 2038-2044.

119. Mitschke, Ullrich; Bauerle, Peter. *J. Mater. Chem.* **2000,** 10, (7), 1471-1507.

120. Paik, Kyung Lim; Baek, Nam Seob; Kim, Hwan Kyu; Lee, Ji-Hoon; Lee, Youngil. *Optical Materials* **2003,** 21, (1–3), 135-142.

121. Barberis, Vasilis P.; Mikroyannidis, John A. *J. Polym. Sci., Part A: Polym. Chem.* **2006,** 44, (11), 3556-3566.

122. Grisorio, Roberto; Piliego, Claudia; Cosma, Pinalysa; Fini, Paola; Mastrorilli, Piero; Gigli, Giuseppe; Suranna, Gian Paolo; Nobile, Cosimo Francesco. *J. Polym. Sci., Part A: Polym. Chem.* **2009,** 47, (8), 2093-2104.

123. Lin, Ying; Chen, Zhi-Kuan; Ye, Teng-Ling; Dai, Yan-Feng; Ma, Dong-Ge; Ma, Zhun; Liu, Qin-De; Chen, Yu. *Polymer* **2010,** 51, (6), 1270-1278.

124. Kanno, H.; Hamada, Y.; Takahashi, H. *IEEE J. Sel. Top. Quantum Electron.* **2004,** 10, (1), 30-36.

125. Hamada, Yuji; Kanno, Hiroshi; Tsujioka, Tsuyoshi; Takahashi, Hisakazu; Usuki, Tatsuro. *Appl. Phys. Lett.* **1999,** 75, (12), 1682-1684.

126. Jarikov, Viktor V.; Kondakov, Denis Y.; Brown, Christopher T. *J. Appl. Phys.* **2007,** 102, (10), 104908-104908-104906.

127. Forrest, Stephen R. *Organic Electronics* **2003,** 4, (2–3), 45-48.

128. Forrest, S. R.; Bradley, D. D. C.; Thompson, M. E. *Adv. Mater.* **2003,** 15, (13), 1043-1048.

129. Grisorio, Roberto; Mastrorilli, Piero; Nobile, Cosimo F.; Romanazzi, Giuseppe; Suranna, Gian P.; Gigli, Giuseppe; Piliego, Claudia; Ciccarella, Giuseppe; Cosma, Pynalisa; Acierno, Domenico; Amendola, Eugenio. *Macromolecules* **2007,** 40, (14), 4865-4873.

130. Michinobu, Tsuyoshi; Osako, Haruka; Shigehara, Kiyotaka. *Macromolecules* **2009,** 42, (21), 8172-8180.

131. Hancock, Jessica M.; Gifford, Angela P.; Tonzola, Christopher J.; Jenekhe, Samson A. *J. Phys. Chem. C* **2007,** 111, (18), 6875-6882.

132. Lee, Yuh-Zheng; Chen, Xiwen; Chen, Show-An; Wei, Pei-Kuen; Fann, Wun-Shain. *J. Am. Chem. Soc.* **2001,** 123, (10), 2296-2307.

133. Paik, Kyung Lim; Baek, Nam Seob; Kim, Hwan Kyu; Lee, Youngil; Lee, Ki Jung. *Thin Solid Films* **2002,** 417, (1–2), 132-135.

134. Hung, Ming-Chin; Liao, Jin-Long; Chen, Show-An; Chen, Su-Hua; Su, An-Chung. *J. Am. Chem. Soc.* **2005,** 127, (42), 14576-14577.

135. Brabec, C. J.; Sariciftci, N. S.; Hummelen, J. C. *Adv. Funct. Mater.* **2001,** 11, (1), 15-26.

136. Günes, Serap; Neugebauer, Helmut; Sariciftci, Niyazi Serdar. *Chem. Rev.* **2007,** 107, (4), 1324-1338.

137. Jenny, Nelson. *Current Opinion in Solid State and Materials Science* **2002,** 6, (1), 87-95.

138. Hoppe, Harald; Sariciftci, Niyazi Serdar. *Journal of Materials Research* **2011,** 19, (07), 1924-1945.

139. Halls, J. J. M.; Cornil, J.; dos Santos, D. A.; Silbey, R.; Hwang, D. H.; Holmes, A. B.; Brédas, J. L.; Friend, R. H. *Phys. Rev. B: Condens. Matter Mater. Phys.* **1999,** 60, (8), 5721-5727.

140. Terao, Yuhki; Sasabe, Hiroyuki; Adachi, Chihaya. *Appl. Phys. Lett.* **2007,** 90, (10), 103515-103513.

141. Michael, Grätzel. *Journal of Photochemistry and Photobiology C: Photochemistry Reviews* **2003,** 4, (2), 145-153.

142. Law, Matt; Greene, Lori E.; Johnson, Justin C.; Saykally, Richard; Yang, Peidong. *Nat Mater* **2005,** 4, (6), 455-459.

143. Hagfeldt, Anders; Boschloo, Gerrit; Sun, Licheng; Kloo, Lars; Pettersson, Henrik. *Chem. Rev.* **2010,** 110, (11), 6595-6663.

144. Yu, G.; Gao, J.; Hummelen, J. C.; Wudl, F.; Heeger, A. J. *Science* **1995,** 270, (5243), 1789-1791.

145. Szarko, Jodi M.; Guo, Jianchang; Liang, Yongye; Lee, Byeongdu; Rolczynski, Brian S.; Strzalka, Joseph; Xu, Tao; Loser, Stephen; Marks, Tobin J.; Yu, Luping; Chen, Lin X. *Adv. Mater.* **2010,** 22, (48), 5468-5472.

146. Chen, Hsiang-Yu; Hou, Jianhui; Zhang, Shaoqing; Liang, Yongye; Yang, Guanwen; Yang, Yang; Yu, Luping; Wu, Yue; Li, Gang. *Nat Photon* **2009,** 3, (11), 649-653.

147. Oh, Jin Young; Lee, Tae Il; Myoung, Jae-Min; Jeong, Unyong; Baik, Hong Koo. *Macromol. Rapid Commun.* **2011,** 32, (14), 1066-1071.

148. Jo, Jang; Gendron, David; Najari, Ahmed; Moon, Ji Sun; Cho, Shinuk; Leclerc, Mario; Heeger, Alan J. *Appl. Phys. Lett.* **2010,** 97, (20), 203303-203303.

149. Liang, Yongye; Xu, Zheng; Xia, Jiangbin; Tsai, Szu-Ting; Wu, Yue; Li, Gang; Ray, Claire; Yu, Luping. *Adv. Mater.* **2010,** 22, (20), E135-E138.

150. Sariciftci, N. S.; Smilowitz, L.; Heeger, A. J.; Wudl, F. *Science* **1992,** 258, (5087), 1474-1476.

151. Lee, Jae Kwan; Ma, Wan Li; Brabec, Christoph J.; Yuen, Jonathan; Moon, Ji Sun; Kim, Jin Young; Lee, Kwanghee; Bazan, Guillermo C.; Heeger, Alan J. *J. Am. Chem. Soc.* **2008,** 130, (11), 3619-3623.

152. Hoven, Corey V.; Dang, Xuan-Dung; Coffin, Robert C.; Peet, Jeff; Nguyen, Thuc-Quyen; Bazan, Guillermo C. *Adv. Mater.* **2010,** 22, (8), E63-E66.

153. Brabec, C. J.; Cravino, A.; Meissner, D.; Sariciftci, N. S.; Fromherz, T.; Rispens, M. T.; Sanchez, L.; Hummelen, J. C. *Adv. Funct. Mater.* **2001,** 11, (5), 374-380.

154. Lenes, Martijn; Wetzelaer, Gert-Jan A. H.; Kooistra, Floris B.; Veenstra, Sjoerd C.; Hummelen, Jan C.; Blom, Paul W. M. *Adv. Mater.* **2008,** 20, (11), 2116-2119.

155. Blouin, Nicolas; Michaud, Alexandre; Gendron, David; Wakim, Salem; Blair, Emily; Neagu-Plesu, Rodica; Belletête, Michel; Durocher, Gilles; Tao, Ye; Leclerc, Mario. *J. Am. Chem. Soc.* **2007,** 130, (2), 732-742.

156. Kline, R. Joseph; DeLongchamp, Dean M.; Fischer, Daniel A.; Lin, Eric K.; Richter, Lee J.; Chabinyc, Michael L.; Toney, Michael F.; Heeney, Martin; McCulloch, Iain. *Macromolecules* **2007,** 40, (22), 7960-7965.

157. Thompson, Barry C.; Kim, Bumjoon J.; Kavulak, David F.; Sivula, Kevin; Mauldin, Clayton; Fréchet, Jean M. J. *Macromolecules* **2007,** 40, (21), 7425-7428.

# Chapter 2

## Synthesis and Characterization of Poly(9,9-dialkylfluorenevinylene benzobisoxazoles): New Solution-Processable Electron-Accepting Conjugated Polymers.

Reprinted with permission from *Macromolecules* **2011**, 44, 248.
Copyright © **2011**
American Chemical Society

*Jeremy J. Intemann,[1] Jared F. Mike[1], Min Cai,[2] Sayantan Bose[1], Teng Xiao,[2] Timothy C. Mauldin,[1] Robert A. Roggers,[1] Joseph Shinar,[2] Ruth Shinar,[3] and Malika Jeffries-EL.[1]**

[1]Department of Chemistry, Iowa State University, Ames IA 50011.
[2]Ames Laboratory-USDOE and Department of Physics and Astronomy,
Iowa State University, Ames, IA 50011
[3]Microelectronics Research Center and Department of Electrical and Computer Engineering,
Iowa State University Ames, IA 50011

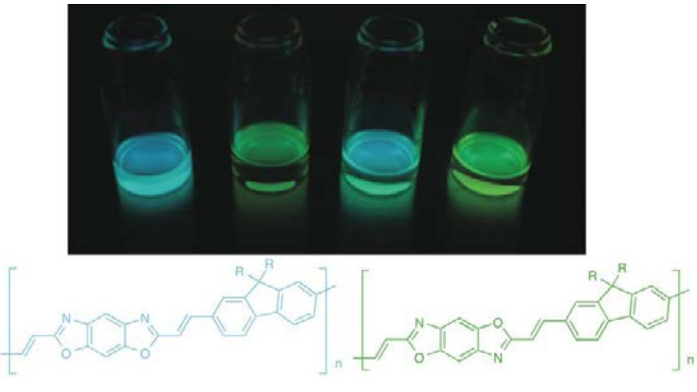

## 2.1 ABSTRACT

We present the synthesis of four new solution-processable, fluorescent poly(arylenevinylene)s containing benzobisoxazole and fluorene moieties. Two different moieties (*cis*- and *trans*-benzobisoxazole) and two different alkyl substituents (octyl and 3,7-dimethyloctyl) were used to study the impact of the structure on the electronic, optical, and

thermal properties of these polymers. The polymers were characterized using UV-visible and fluorescence spectroscopy, cyclic voltammetry, thermal gravimetric analysis (TGA), and differential scanning calorimetry (DSC). All of the polymers possess moderate molecular weights, good solubility in aprotic organic solvents, high fluorescence quantum efficiencies in dilute solutions, and high electron affinities. Cyclic voltammetry revealed quasi-reversible reduction for these polymers. Solution-processed light-emitting diodes using dilute blends of the polymer in a poly(*N*-vinyl carbazole) matrix gave blue emission with luminous efficiencies of up to 1 Cd/A at ~470 nm which is very promising for deep blue-emitting polymer LEDs.

## 2.2 INTRODUCTION

During the past three decades, conjugated polymers and the opportunities they provide for the development of organic-based electronic devices have stimulated the scientific community.[1, 2] The benefits of conjugated polymers include low-cost processing via solution-based techniques such as spin-coating or inkjet printing, and the ability to optimize the electronic, optical, and physical properties for various applications through chemical synthesis. Among the various classes of conjugated polymers, poly(9,9-dialkylfluorene)s (PDAF)s and substituted poly(phenylene vinylene)s (PPV)s are the most widely studied. PDAFs are popular due to their blue emission; high solid-state fluorescence efficiency; excellent chemical, thermal, and photo stability; good solubility; and ease of synthesis.[3] However, like most emissive conjugated polymers, PDAFs have low electron affinities and larger hole mobilities than electron mobilities; this difference in mobilities causes an imbalance in charge injection and transport. Collectively, these problems result in a decrease of external quantum efficiency (EQE) and ultimately diminish the performance of single-layer organic light emitting diodes (OLED)s.[4-6]

To improve device performance, low-work function cathodes such as calcium (Ca) have been utilized to improve electron injection, and multilayer devices have been fabricated using a separate electron-transport (n-type) material with an emissive p-type polymer.[7-9] Another approach for increasing EQE is to synthesize emissive copolymers containing both hole-transporting and electron-transporting moieties. This design strategy is expected to produce polymers with improved electron affinity and balanced charge transport, which would facilitate the fabrication of efficient single-layer OLEDs. In this regard, the synthesis of poly(arylenevinylene)s containing heterocyclic groups in the polymer backbone is a promising approach, since heteroatoms such as oxygen, nitrogen, and sulfur have higher electronegativities than carbon. Therefore, the incorporation of heterocycles can increase the electron affinity of π-conjugated polymers.[10-24]

Polybenzobisazoles such as poly(*p*-phenylene benzobisthiazole), and poly(*p*-phenylene benzobisoxazole) are known to have high electron affinities,[10] efficient electron transport,[7, 25-27] photoluminescence[13, 28-34] and thermal stability.[35-37] Although these properties make polybenzobisazoles promising materials, their development has been limited by two factors: 1) their poor solubility, requiring processing from harsh acidic solutions; and 2) their harsh reaction conditions, limiting the types of substituents that can be incorporated onto the polymer backbone.[38-41] To facilitate the synthesis of such polymers, we have developed new monomers based on 2,6-functionalized benzobisazoles.[42, 43] These monomers can be used to prepare a number of new benzobisazole containing polymers, such as poly(arylenevinylene-*co*-benzobisoxazole)s, bearing solubilizing side-chains using mild conditions.[44] This is beneficial since it is known that extending the conjugation of the polybenzobisazole backbone by adding double bonds increases the electron affinity of the resulting polymers.[25]

Previously, we synthesized poly(phenylene vinylene-*co*-benzobisoxazole)s which exhibited reversible reduction processes and were the first examples of benzobisoxazoles that were soluble in non-acidic organic solvents. Herein we describe the synthesis, characterization and electroluminescent properties of four poly(fluorene vinylene-*co*-benzobisoxazole)s, namely: poly[(9,9-dioctylfluorene-2,7-vinylene)-*alt*-benzo[1,2-*d*;5,4-*d*']bisoxazole-2,6-diyl] (**P43a**), poly[(9,9-bis(3,7-dimethyloctyl)fluorene-2,7-vinylene)-*alt*-benzo[1,2-*d*;5,4-*d*']bisoxazole-2,6-diyl] (**P43b**), poly[(9,9-dioctylfluorene-2,7-vinylene)-*alt*-benzo[1,2-*d*;4,5-*d*']bisoxazole-2,6-diyl] (**P53a**) and, poly[(9,9-bis(3,7-dimethyloctyl)fluorene-2,7-vinylene)-*alt*-benzo[1,2-*d*;4,5-*d*']bisoxazole-2,6-diyl] (**P53b**). The combination of the electron-transporting benzobisoxazole and 9,9-dialkylfluorene moieties into one polymer backbone results in new emissive, high electron-affinity polymers. Guest-host PLED devices fabricated from **P43a** and **P53a** in a poly(*N*-vinyl carbazole) matrix exhibited stable blue light emission with luminous efficiencies of up to 1 Cd/A at ~470 nm. These early results rival the performance of other known deep blue-emitting polymers, demonstrating the promise of these polymers for the development of blue PLEDs.[14, 24, 31, 45, 46]

## 2.3 RESULTS AND DISCUSSION

**2.3.1 Monomer Synthesis.** The 2,7-dibromo-9,9-dialkylfluorenes **1a**[47] and **1b**[48] and the isomeric benzobisoxazole monomers **4** and **5** were synthesized according to the literature procedures.[42, 44] These benzobisoxazole monomers differ in the arrangement of the oxygen atoms around the central benzene ring, which is known to give rise to different optical and electronic properties.[49-53] Whereas the fluorene monomers bore either linear octyl or branched 3,7-dimethyloctyl side chains, and were carefully purified via column chromatography to remove any monoalkylated side products.[54, 55] The synthetic routes for the fluorene monomers are outlined in Scheme 2.1. The direct synthesis of 9,9-dialkylfluorene-2,7-dicarboxaldehydes **3a** and **3b** from the corresponding 2,7-dibromo-9,9-dialkylfluorenes **1a** and **1b** resulted in mixtures of the mono and dicarboxaldehydes that were difficult to separate via column chromatography. For this reason we developed a two-step sequence to carry out the synthesis of the dicarboxaldehydes where the 2,7-dibromo-9,9-dialkylfluorenes **1a** and **1b** were reacted with *tert*-butyllithium and then paraformaldehyde to yield the 9,9-dialkylfluorenes-2,7-dimethanols **2a** and **2b**, which were readily separated from the mono-substituted side products. While the yield for this step is moderate, it is more efficient than the other reported methods for the synthesis of 9,9-dialkylfluorenes-2,7-dimethanols.[47, 56] Oxidation of **2a** and **2b** afforded the corresponding 9,9-dialkylfluorene-2,7-dicarboxaldehydes **3a** and **3b**, quantitatively.

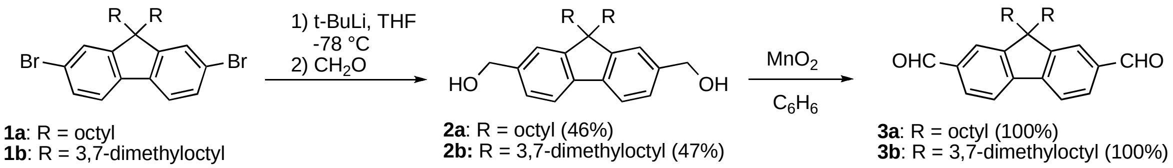

**Scheme 2.1.** Synthesis of 9,9-dialkylfluorene Monomers.

**2.3.2 Polymer Synthesis** The general synthetic route for the new benzobisoxazole copolymers is shown in Scheme 2.2. These polymers were synthesized using the Horner-Wadsworth-Emmons (HWE) polycondensation reaction between the 9,9-dialkylfluorene-2,7-dicarboxaldehydes **3a** and **3b** and the benzobisoxazole monomers **4** and **5** in anhydrous THF, and used a slight excess of potassium tert-butoxide. These reaction conditions were selected because the HWE reaction is known to produce polymers with all trans-double bonds. This method also prevents cross-linking, incomplete double bond formation, and other undesirable structural defects. Using these conditions, all four polymers were obtained with satisfactory yields (30-57%), after removing low molecular weight material via Soxhlet extraction. All of the polymers are soluble in common organic solvents, such as m-cresol, chloroform, *o*-dichlorobenzene, and THF. The $^1$H NMR spectra for polymers **P43a**, **P43b**, **P53a** and **P53b** were in agreement with the proposed polymer structures (see Supporting Information). All spectra showed signals in the range of 0.782-1.73 ppm, which can be assigned to the aliphatic protons on the side chains. The vinylic protons are doublets at approximately 7.3 and 8.0 ppm, while the aromatic protons are indistinguishable and exist together between 7.74 and 7.83 ppm.

**2.3.3 Polymer Characterization** We estimated the relative molecular weights of polymers **P43a**, **P43b**, **P53a** and **P53b** by gel permeation chromatography (GPC). The results are summarized in Table 2.1. **P43b** and **P53b**, bearing branched side chains, were obtained with higher yields, molecular weights, and PDI's than **P43a** and **P53a**, which bear linear side chains. This is due to the increased solubility of **P43b** and **P53b** in THF as a result of the branched alkyl chain. Conversely, the limited solubility of **P43a** and **P53a** in THF resulted in precipitation of these polymers at lower molecular weight and also reduced the amount of soluble material recovered. We evaluated the thermal properties of the polymers using thermogravimetric analysis and differential scanning calorimetry. The incorporation of flexible side chains to

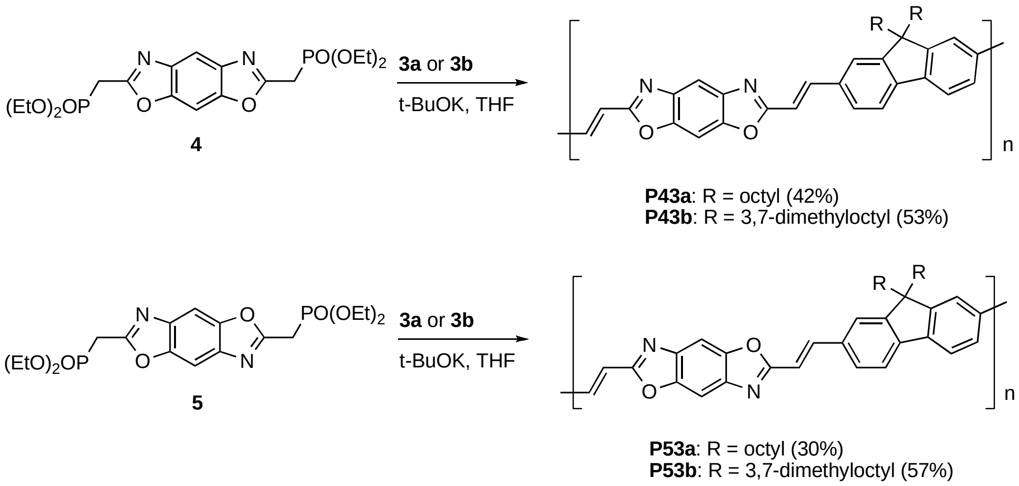

**Scheme 2.2.** Synthesis of Poly(fluorene vinylene-*co*-benzobisoxazole)s.

**Table 2.1.** Physical properties of Poly(fluorene vinylene-*co*-benzobisoxazole)s.

| Polymer | $M_n$[a] | $M_w$[a] | PDI | $T_d$ (ºC)[b] | $T_g$ (ºC)[c] |
|---|---|---|---|---|---|
| **P43a** | 6,900 | 11,100 | 1.59 | 342 | 177 |
| **P43b** | 8,300 | 18,100 | 2.18 | 332 | 170 |
| **P53a** | 9,700 | 20,200 | 2.08 | 332 | 182 |
| **P53b** | 13,900 | 46,500 | 3.35 | 303 | 186 |

[a] Determined by GPC in THF using polystyrene standards. [b] 5% weight loss temperature by TGA under $N_2$.[c] Data from second scan reported, heating rate 15 ºC/min under $N_2$.

improve the solubility of a conjugated polymer is only beneficial if the chains do not significantly diminish the thermal stability of the polymer. We found all of the polymers to be thermally stable with 5% weight loss onsets occurring in the range of 303-342 °C (Table 1). Typical second-heating differential scanning calorimetry (DSC) scans of all polymers showed weak glass transitions (Tg) for each polymer (Table 2.1). These values ranged from 170- 186 ºC and were similar to those obtained for poly(9,9-dioctylfluorene)-2,7-vinylene, and were higher than other known poly(fluorenevinylene) copolymers.[14, 21, 57] The presence of alkyl chains had a significant effect on the glass transition, as unsubstituted polybenzobisoxazoles did not show any observable transitions before their decomposition temperature. Varying the side chain length had little impact in the thermal properties of the polymers. In all cases the glass transition temperatures were sufficiently high enough to withstand the joule heating associated with the operation of organic electronic devices.[58]

**2.3.4 Optical Properties.** The photophysical characteristics of the polymers were evaluated by UV-vis absorption and fluorescence spectroscopy both as dilute solutions in THF and thin films. The normalized absorbance and emission spectra for all of the polymers are shown in Figure 2.1, and the data is summarized in Table 2.2. Regardless of the length of the side chains, the benzobisoxazole group determined the polymer’s optical properties in solution. The UV spectra of the polymers have two absorbance bands at approximately 424 nm and 450 nm for **P43a**, and

**P43b**, whereas the peaks are red-shifted to approximately 440 and 470 nm for **P53a**, and **P53b**. The thin film absorbance spectra for all of the polymers were broader than their solution spectra, and the vibronic coupling diminished giving rise to a maximum absorption at a shorter wavelength. The onsets of absorption for the polymers ranged from 497 to 516 nm, resulting in optical band gaps of 2.40-2.49 eV. **P53a**, and **P53b** had smaller bandgaps, indicating a higher degree of electron delocalization within these polymers in comparison to **P43a** and **P43b**. Furthermore, as thin films, the absorbance spectra for the **P43a** and **P53a**, which bear linear side chains is almost identical to the absorbance spectra for the **P43b** and **P53b**, with linear side

**Table 2.2.** Electronic and Optical Properties of PFVBBOs.

| **Polymer** | **Media** | **$\lambda^{abs}_{max}$(nm)** | **$\lambda^{em}_{max}$ (nm)** | **$E_g^{opt}$ (eV)[a]** | **EA (eV)[b]** | **IP (eV)[c]** | **$\Phi_{re}$** | **τ (ps)[f]** |
|---|---|---|---|---|---|---|---|---|
| **P43a** | THF | 451 | 460 | | | | 0.64[d] | 550±5 |
| | Film | 435 | 538 | 2.49 | 2.87 | 5.36 | 0.01[e] | 83±3 |
| **P43b** | THF | 450 | 460 | | | | 0.63[d] | 440±5 |
| | Film | 437 | 534 | 2.49 | 2.87 | 5.36 | 0.01[e] | 170±10 |
| **P53a** | THF | 469 | 479 | | | | 0.68[d] | 510±5 |
| | Film | 450 | 555 | 2.40 | 2.89 | 5.29 | 0.01[e] | 120±5 |
| **P53b** | THF | 470 | 480 | | | | 0.71[d] | 430±5 |
| | Film | 450 | 572 | 2.40 | 2.89 | 5.29 | 0.01[e] | 260±10 |

[a] Estimated from the optical absorption edge. [b] EA= -4.8-($E^{red}_{onset}$ – 0.44 V) (eV). [c] IP = EA + $E_g^{opt}$ (eV). Electrochemical properties were measured using a three-electrode cell (electrolyte: 0.1 mol/L $TBAPF_6$ in acetonitrile) with an $Ag/Ag^+$ reference electrode, a platinum auxiliary electrode, and a platinum button electrode as the working electrode. Reported values are referenced to Fc. Polymer films were made by drop coating a tetrahydrofuran solution of the polymers on to the working electrode. All cyclic voltammetry experiments were recorded at a scan rate of 50 mV/s. [d]Solution fluorescence quantum yield relative to Coumarin 6 in ethanol ($\Phi_f$ = 0.78, $\lambda_{ex}$ = 490 nm). [e] Solid-state quantum yield relative to perylene 10 wt% in PMMA ($\Phi_f$ = 0.87, $\lambda_{ex}$ = 520 nm). [f] Fluorescence lifetimes were obtained using a tri-exponential decay fit (see Supporting Information).[59, 60] The average lifetimes are given.

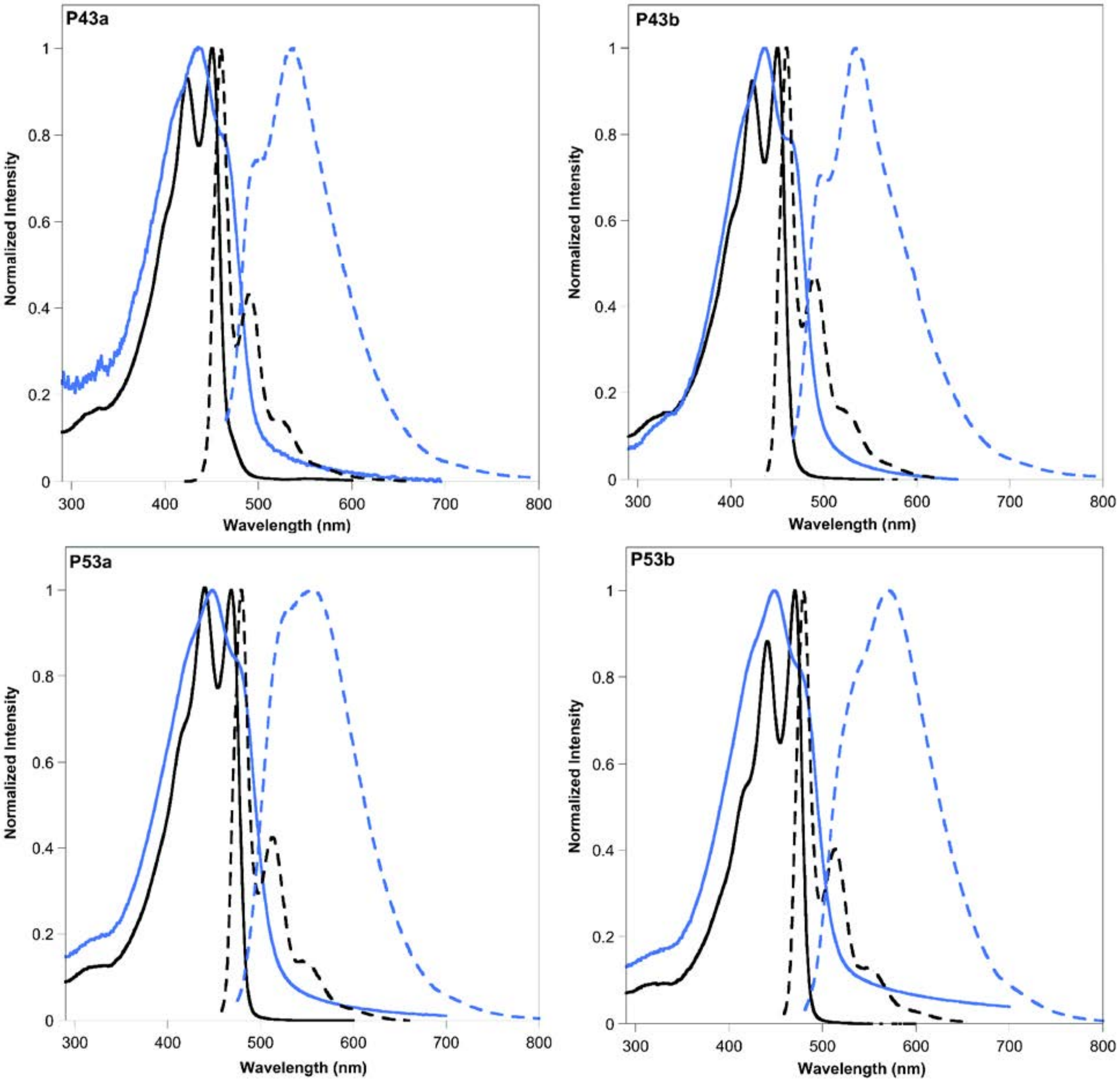

**Figure 2.1.** UV-vis (solid lines) and fluorescence (dashed lines) spectra **P43a**, **P43b**, **P53a** and **P53b** in solution THF (black) and as thin films (blue).

chains. This is an indication that the side chains do not affect the solid-state packing for these polymers. This assumption is supported by X-ray analysis, which shows that thin films of all polymers are amorphous.

In solution, all of the polymers are efficient fluorophores with fluorescence quantum yields of 0.64 - 0.71. The solution fluorescence spectra of the *cis*-PFVBBO polymers have $\lambda^{em}_{max}$ at 460 nm for **P43a** and **P43b** each with a shoulder at 491 nm, whereas the *trans*-PFVBBO polymers have $\lambda^{em}_{max}$ at 480 nm for **P53a** and **P53b** each with a shoulder at 514 nm. As neat films, **P43a** and **P43b** exhibit green emission while the emission of **P53a** and **P53b** is red-shifted resulting in yellow-green emission. The emission spectra of the polymer thin films were considerably red-shifted, relative to corresponding solution spectra and the fluorescence quantum yield is drastically diminished in the solid state with quantum yields of 0.01. This phenomenon is most likely caused by aggregation and excimer formation, and was generally independent of side chain structure. We performed fluorescence lifetime measurements for all of the polymers in both THF solution and thin films (cast from THF). In all cases the fluorescence decay curves were analyzed as the sum of three exponential decay curves; the average values are summarized in Table 2.2, and the details shown in Figures S2.13 and S2.14 (supporting material). The $\lambda^{abs}_{max}$ and $\lambda^{em}_{max}$ in solution of the poly(fluorene vinylene-*co*-benzobisoxazole)s are blue-shifted relative to those reported previously for the related poly(arylene vinylene-*co*-benzobisoxazole)s; poly(phenylene vinylene-*co*-benzobisoxazole)s ($\lambda^{abs}_{max}$ 405 - 450 nm and $\lambda^{em}_{max}$ 495-518 nm)[44] and poly(thiophene vinylene-*co*-benzobisoxazole) ($\lambda^{abs}_{max}$ 480 - 507 nm and $\lambda^{em}_{max}$ 635-653 nm).[61] The $\lambda^{abs}_{max}$ in solution of **P53a** and **P53b** is red-shifted relative to that of the homopolymer poly(fluorene vinylene) (414 - 458 nm) an blue-shifter relative to the $\lambda^{abs}_{max}$ **P43a** and **P43b**. The $\lambda^{em}_{max}$ of the homopolymers (453-496 nm) is within the same range as all of the poly(fluorene vinylene-*co*-benzobisoxazole)s.[47]

**2.3.5 Electrochemical Properties.** To evaluate the redox properties of the polymers, cyclic voltammetry measurements of polymer thin films were performed. The results are summarized in Table 2.2, and cyclic voltammograms for the polymer redox processes are presented in Figure 2.2. All polymers had quasi-reversible reduction waves with onsets at -1.53 V, versus SCE for both **P43a** and **P65** and onsets at -1.50 V versus SCE for both **P53a** and **P53b**. Using 4.8 eV as the SCE energy level relative to vacuum,[62] we estimated electron affinities (EA)s values of 3.27 eV for **P43a** and **P43b** and 3.30 eV for **P53a** and **P53b**. We only observed polymer degradation during oxidation cycle and no oxidation peak was seen. Since we could not

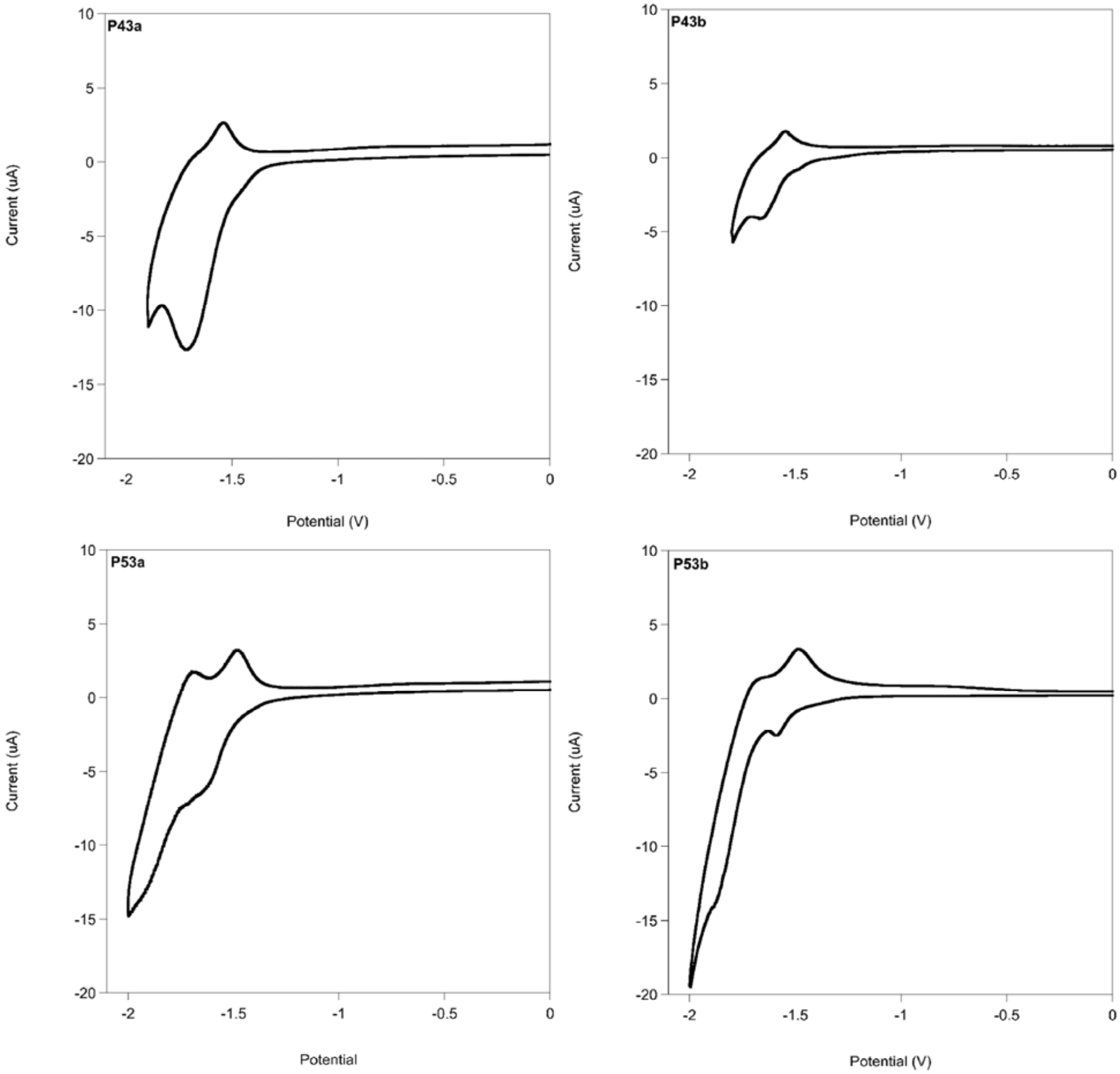

**Figure 2.2.** CV curves of **P43a**, **P43b**, **P53a** and **P53b**.

directly determine the ionization potential (IP) from the electrochemical spectra, we calculated the IP using the previously measured optical band gaps, EA values and the relation IP = EA + $E_g$ (eV).[63] Thus, we obtained IP values of 5.76 eV for **P43a** and **P43b** and 5.71 eV, for **P53a** and **P53b**. The optical band gaps for these poly(fluorene vinylene-*co*-benzobisoxazole)s are larger than those reported previously for the related polymers poly(phenylene vinylene-*co*-benzobisoxazole)s (2.2 - 2.4 eV)[21] and poly(thiophene vinylene-*co*-benzobisoxazole)s (2.04 -

2.17 eV),[61] as a result of the incorporation of the fluorene moiety. However, the EAs for these new polymers are higher than those obtained previously for poly(arylene vinylene-*co*-fluorene)s with electron withdrawing moieties in the backbone (2.83-3.17 eV).[57] This indicates that the electron-deficient benzobisoxazole moiety is beneficial for increasing the EA of conjugated polymers.

**2.3.6 Electroluminescent Devices.** The fluorescence quantum yields of the poly(arylenevinylene) copolymers in solution are 0.64 and 0.68 for **P43a** and **P53a**, respectively. In the solid state, however, they are only ~0.01 (see Table 2.2). Due to this apparently strong

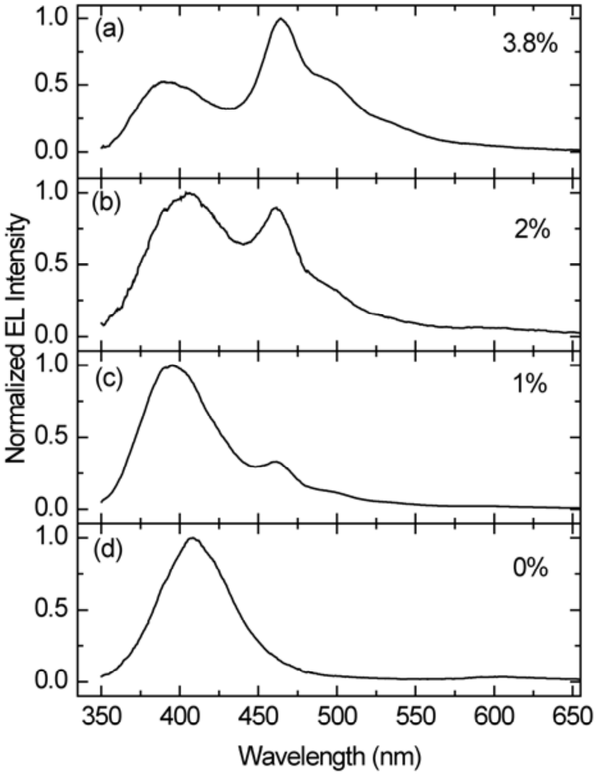

**Figure 2.3.** Normalized EL spectra of devices ITO/PEDOT:PSS(60 nm)/ **P43a**:PVK (55 nm)/CsF(1 nm)/Al(120 nm)(type I) with different concentrations (in wt. %) of **P43a**; the OLEDs were driven at 113 mA/cm$^2$.

concentration quenching in the films, the materials cannot be used as a neat emitting layer in OLEDs.[64, 65] These materials, however, show good solubility in organic solvents and high electron affinity, which makes them promising candidates for use in guest-host PLEDs. We therefore tested them as low levels dopants in PVK-based PLEDs.

Figure 2.3 shows the normalized EL spectra of OLEDs with the structure: ITO/PEDOT:PSS(60 nm)/PVK:**P43a**(55 nm)/CsF(1 nm)/Al(120 nm)(type I). In these devices the **P43a** was blended with PVK at different weight ratios. As seen, the intensity of the **P43a** emission at 460 nm increases relative to that of the PVK (peaks at ~410 nm) with increasing **P43a** level, and at ~4 wt. % the **P43a** emission surpasses that of the PVK, becoming the dominant emission peak. This behavior indicates energy transfer from the PVK to **P43a** or direct carrier trapping in the **P43a** guest. Further increasing the **P43a** concentration in the blend did not enhance the emission from **P43a**, and it decreased the overall performance of the devices, likely due to quenching of the **P43a** emission. The device with 1 wt. % **P43a** showed the highest brightness (350 Cd/m$^2$) and the highest luminous efficiency (0.19 Cd/A).

**Table 2.3**. Device Characteristics of OLEDs Based on Poly(arylenevinylene) Copolymers.

| **Polymer** | **Device**[a] | | **$V_{on}$**[b] **[V]** | **Drive Voltage [V]** | **Current Density [mA/cm$^2$]** | **Brightness [Cd/m$^2$]** | **Efficiency [Cd/A, (%EQE)**[c]**]** | **$\lambda_{max}^{EL}$ [nm] P43a, PVK** | **CIE 1931 [x,y]** |
|---|---|---|---|---|---|---|---|---|---|
| | Type | wt.% in PVK | | | | | | | |
| **P43a** | I | 0.0 | 6.2 | 8.8 | 116 | 45 | 0.06(0.18) | 409 | (0.18,0.06) |
| | | 1.0 | 6.4 | 8.2 | 253 | 350 | 0.19(0.43) | 460,395 | (0.17,0.09) |
| | | 2.0 | 6.0 | 7.8 | 504 | 240 | 0.07(0.10) | 462,404 | (0.17,0.11) |
| | | 3.8 | 8.0 | 12.8 | 493 | 177 | 0.06(0.05) | 464,395 | (0.16,0.17) |
| | II | 0.0 | 5.8 | 11.2 | 306 | 250 | 0.31(0.30) | 437 | (0.17,0.10) |
| | | 1.0 | 8.0 | 11.0 | 208 | 686 | 0.93(0.69) | 472,428 | (0.18,0.18) |
| | | 2.0 | 8.0 | 12.8 | 394 | 548 | 0.56(0.50) | 464,429 | (0.17,0.14) |
| **P53a** | II | 1.0 | 8.6 | 12.8 | 672 | 528 | 0.25(0.34) | 489,422 | (0.17,0.10) |
| | | 2.0 | 7.8 | 11.8 | 670 | 427 | 0.17(0.22) | 489,422 | (0.18,0.11) |
| | | 3.8 | 9.4 | 13.4 | 514 | 343 | 0.10(0.10) | 482,431 | (0.18,0.14) |

[a] Device type I: ITO/PEDOT:PSS/PVK: poly(arylenevinylene) copolymers/CsF/Al; device type II: ITO/PEDOT:PSS/PVK: poly(arylenevinylene) copolymers/BPhen/LiF/Al. [b] Turn-on voltage (at which EL is visible to the eyes). [c] EQE = external quantum efficiency.

To further improve the performance of the **P43a**:PVK-based diodes, we fabricated devices of the structure ITO/PEDOT:PSS(60 nm)/ **P43a**:PVK (55 nm)/BPhen(40 nm)/LiF(1 nm)/Al(120 nm)(type II). That is, a BPhen electron transporting/hole blocking layer was added by thermal vacuum evaporation of BPhen powder.[66] The normalized EL spectrum of the 1 wt. % type II device is shown in Figure 2.4 together with that of the type I device for comparison. In the type II device, the **P43a** emission at 460 nm is the main emission peak. This situation indicates that the BPhen enhances exciton formation on **P43a**. The LUMO levels of PVK, **P43a**, and BPhen are -2.2 eV, -2.9 eV, and -3.0 eV, respectively. Hence, the electrons injected through the BPhen layer are transported preferentially to the **P43a** molecules in comparison to the PVK molecules, leading to exciton formation on the previous. Thus the addition of the BPhen layer further enhances the device performance. A highest brightness of 686 Cd/m$^2$ and a maximal luminous efficiency of 0.93 Cd/A were obtained for 1 wt. % type II devices, which is 4 times more efficient than the 1 wt. % type I devices (see Table 2.3). We note that a luminous efficiency of ~1 Cd/A at ~470 nm is very promising for solution-processed deep blue-emitting polymer LEDs.

Type II diodes based on **P53a**:PVK at different weight ratios were also tested. The device with 1 wt. % showed the highest brightness (528 Cd/m$^2$) and the highest luminous efficiency (0.25 Cd/A); these values, however, are lower than those of the **P43a**:PVK-based devices. This

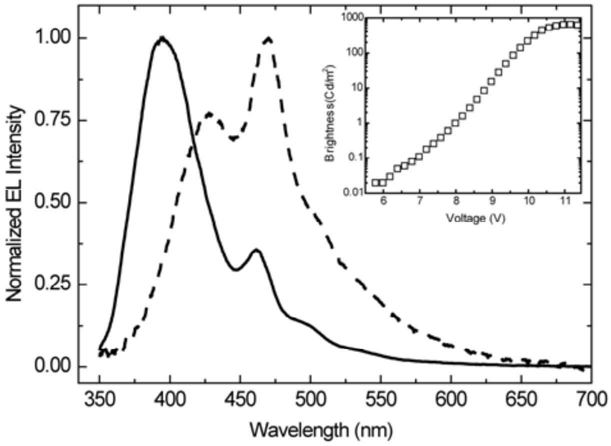

**Figure 2.4.** Comparison of the EL spectra of type I (solid line) and type II (dashed line) devices driven at 28 mA/cm$^2$. The inset shows the brightness as a function of bias voltage for the type II device with the BPhen layer. The **P43a** concentration was 1 wt %.

situation may be due to the higher molecular weight and PDI of the **P53a** (see Table. 1). It is suspected that the higher molecular weight increases aggregation of **P53a** in the **P53a**:PVK layer, which decreases the overall device performance due to increased **P53a**-induced concentration quenching of the emission. These initial results indicate that the poly(arylenevinylene)s copolymers can be used as dopants in other polymers used in PLEDs to control, following optimization, the emission wavelength and improve the overall device performance. Optimization of such PLEDs is ongoing.

## 2.4 CONCLUSIONS

In conclusion, four new benzobisoxazole containing polymers have been synthesized with good molecular weights and yields via the Horner-Wadsworth-Emmons coupling reaction. The optical and electronic properties of the polymers are determined by the type of benzobisoxazole monomer used and not impacted by the size of the side chain. The flexible side chains on the fluorene ring led to good solubility, while maintaining good thermal stability, whereas the incorporation of the electron-accepting benzobisoxazole moiety into the polymer chain led to high electron affinity. Preliminary electroluminescence studies showed that these polymers exhibit promising brightness in guest-host OLEDs. Collectively, these results suggest that poly(9,9-dialkylfluorene vinylene) benzobisoxazoles have great potential for use in organic semiconducting applications. The facile synthetic approach will enable the development of new derivatives of poly(arylenevinylene-*co*-benzobisoxazole)s with improved properties.

## 2.5 EXPERIMENTAL METHODS

**2.5.1 Materials and General Experimental Details.** Tetrahydrofuran was dried using an Innovative Technologies solvent purification system. 2,7-dibromo-9,9-dioctylfluorene (**1a**),[67] 2,7-dibromo-9,9-bis(3,7-dimethyloctyl)fluorene (**1b**),[48] 2,6-dimethylbenzo[1,2-d;5,4-d']bisoxazole-diethylphosphonate ester (**4**),[44] and 2,6-dimethylbenzo[1,2-d;4,5-d']bisoxazole-diethylphosphonate ester (**5**)[44] were prepared according to literature procedures. Chromatographic separation was performed using silica gel 60, using the eluents indicated. Poly(3,4-ethylenedioxy thiophene):poly(4-styrenesulfonate) (PEDOT:PSS) was purchased from H. C. Starck and used as the hole injection layer (HIL). Poly(N-vinyl carbazole) (PVK) and 4,7-

diphenyl-1,10-phenanthroline (BPhen) were purchased from Sigma-Aldrich. All other materials were purchased from commercial sources and used without further purification.

**2.5.2 Instrumentation.** Nuclear magnetic resonance spectra were obtained on a 400 MHz spectrometer ($^{1}$H at 400 MHz and $^{13}$C at 100 MHz). $^{1}$H NMR samples were referenced internally to residual protonated solvent $^{13}$C NMR were referenced to the middle carbon peak of $CDCl_3$. In both instances chemical shifts are given in δ relative to solvent. High-resolution mass spectra were recorded on a double focusing magnetic sector mass spectrometer using EI at 70 eV. Melting points were obtained using a melting point apparatus, upper temperature limit 260 ºC. Gel permeation chromatography (GPC) measurements were performed on a Viscotek GPC Max 280 separation module equipped with three 5μm I-gel columns connected in a series (guard, HMW, MMW and LMW) with a refractive index detector. Analyses were performed at 35 °C using THF as the eluent with the flow rate at 1.0 mL/min. Calibration was based on polystyrene standards. Fluorescence spectroscopy and UV-Visible spectroscopy were obtained using polymer solutions in THF, and thin films were spun from these solutions. The films were made by spin-coating 25x25x1mm glass slides, using a solution of 10 mg of polymer per 1 mL THF at a spin rate of 5000 rpms on a Spin-Coater. Thermal gravimetric analysis measurements were made within the temperature interval of 30 ºC - 900 ºC, with a heating rate of 20 ºC/minute, under ambient atmosphere. Differential scanning calorimetry was performed with a first scan at a heating rate of 15 ºC/min to erase thermal history and a second scan to measure transitions from 0 °C to 200 °C under nitrogen. Transitions were also measured with cooling at 15 ºC/min. Electrochemical properties were measured on an eDaq e-corder 410 potentiostat using a three-electrode cell (electrolyte: 0.1 mol/L $TBAPF_6$ in acetonitrile) with an $Ag/Ag^+$ reference electrode, a platinum auxiliary electrode, and a platinum button electrode as the working electrode. Polymer films were made by drop coating a tetrahydrofuran solution of the polymers on to the working electrode. All films were annealed at 200 ºC for 1 hour prior to use. All cyclic voltammetry experiments were carried out under argon atmosphere and were recorded at a scan rate of 50 mV/s. Excited-state lifetime measurements were performed using the TCSPC set-up described elsewhere.[59, 60] Briefly, a homebuilt mode-locked Ti: sapphire oscillator pumped by a Nd:VO4 laser (Millennia, Spectra Physics) producing femtosecond pulses tunable from 780 to

900 nm with a repetition rate of 82 MHz was used as the laser source. The fundamental wavelength at 814 nm from the Ti:sapphire oscillator was modulated by a Pockels cell (Model 350-160, Conoptics Inc.) to reduce the repetition rate to approximately 8.8 MHz and was subsequently frequency-doubled by using a harmonic generator (Model TP- 2000B, U-Oplaz Technologies). The resulting blue light, which had a central wavelength of 407 nm, provided the excitation source, and emission ($\lambda_{em} \geq$ 470 nm) was collected in front face geometry from solid films using appropriate filters to eliminate possible interference from scattered light. The full width at half-maximum (FWHM) of the instrument response function was ~40-45 ps. All of the measurements were made in a 3.5 ns time window with a total of 1024 channels. A total of 65530 counts were collected at the peak channel for all of the lifetime measurements. X-Ray diffraction patterns were obtained using Cu Kα radiation generated with a Rigaku Ultima IV x-ray diffractometer equipped with a multipurpose Eulerian cradle. The diffracted beam (40 kV, 44 mA) was passed through a 1/3 degree receiving slit and a 0.3 mm scattering slit.

### 2.5.3 Synthetic Procedures

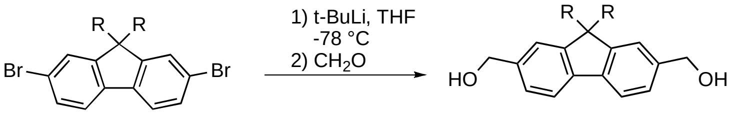

**1a**: R = octyl
**1b**: R = 3,7-dimethyloctyl

**2a**: R = octyl
**2b:** R = 3,7-dimethyloctyl

### 2,7-bis(hydroxymethyl)-9,9-dioctyl-fluorene (2a)

A dry round bottom flask was placed under an argon atmosphere and charged with 5.76g (10.5 mmol) 2,7-dibromo-9,9-dioctyl-9H-fluorene **1a**, dissolved in 90 mL of dry tetrahydrofuran. The mixture was cooled to -78 °C and stirred while 37.44 mL (63.6 mmol) of 1.7M tert-butyllithium in pentane was added drop wise. Once addition was complete the solution was stirred for 1 hour at which point 0.666g (22.2 mmol) of paraformaldehyde suspended in 30 mL of dry THF was added drop wise to the mixture. The reaction was then stirred for an additional 2 hours and then warmed to room temperature and stirred overnight. The reaction was then quenched in 100 mL of saturated ammonium chloride solution and extracted with (3x75 mL) diethyl ether. The organic extracts were combines, washed with water and brine, and then dried over magnesium sulfate. Solvent was evaporated and the resulting crude product was eluted through a silica gel column using 3:1 hexanes to ethyl acetate as the eluent. The resulting oil was crystallized in heptane to yield white crystals. (2.16g, 46% yield); Mp=127-128 °C, literature Mp =126-127 °C;[56] $^1$H NMR ($CDCl_3$) $\delta$: 7.66 (d, 2H), 7.33 (s, 2H), 7.31 (d, 2H), 4.76 (s, 4H), 1.92-1.96 (m, 4H), 1.86 (s, 2H), 1.03-1.27 (m, 20H), 0.81 (t, 6H), 0.58 (m, 4H).

**2,7-bis (hydroxymethyl) -9,9-bis(3,7-dimethyloctyl)-fluorene (2b)**

A dry round bottom flask was placed under an argon atmosphere and charged with 8.5 g (14 mmol) of 2,7-dibromo-9,9-bis(3,7-dimethyloctyl)-9H-fluorene (**1b**) dissolved in 120 mL of dry tetrahydrofuran. The mixture was cooled to -78 °C and stirred while 49.6 mL (84 mmol) of 1.7M tert-butyllithium in pentane was added drop wise. The mixture was then stirred for 1 hour before adding 0.901 g (30 mmol) of paraformaldehyde in small portions over 15 minutes. The mixture was stirred for 2 hours and then warmed to room temperature and stirred overnight. The reaction was quenched in 150 mL of saturated ammonium chloride solution and extracted with (3 x 75 mL) of ether. The organic extracts were combined, washed with water and brine, dried over magnesium sulfate, and the solvent evaporated. The residue was then purified on a silica gel column using 3:1 hexanes/ ethyl acetate as the eluent. Crystallization of the resulting oil in heptane yielded white crystals. (3.33 g, 47% yield); Mp= 64-65 °C; $^1$H NMR ($CDCl_3$) $\delta$: 7.67 (d, 2H), 7.33 (m, 4H), 4.76 (s, 4H), 1.92-2.00 (m, 4H), 1.67 (s, 2H), 1.40-1.44 (m, 2H), 0.92-1.07 (m, 12H), 0.88 (m, 2H), 0.80 (d, 12H), 0.67 (d, 6H), 0.58 (m, 2H), 0.45 (m, 2H); $^{13}$C NMR ($CDCl_3$) $\delta$: 151.5, 140.7, 140.0, 126.0, 121.7, 119.9, 66.1, 55.1, 39.4, 37.8, 36.9, 33.1, 30.8, 28.2, 24.9, 22.9, 19.7; HRMS (EI) Calcd. for $C_{35}H_{54}O_2$ 506.41236, found 506.41390, deviation 3 ppm.

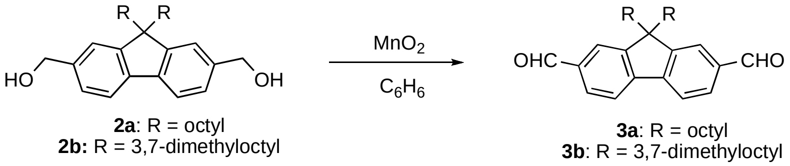

**2a**: R = octyl
**2b:** R = 3,7-dimethyloctyl

**3a**: R = octyl
**3b**: R = 3,7-dimethyloctyl

**9,9-dioctyl-fluorene-2,7-dicarboxaldehyde (3a)**

To a solution of 1.54 g (3.4 mmol) of 2,7-bis(hydroxymethyl)-9,9-dioctyl-9H-fluorene **2a** dissolved in 25 mL of benzene, was added 2.4 g (27.6 mmol) of activated manganese dioxide. The reaction flask was equipped with a dean-stark trap and condenser. The dean-stark trap was filled with additional benzene and the mixture was refluxed overnight. The mixture was then filtered to remove the remaining manganese dioxide and the solvent was evaporated to yield product as a yellow oil. The oil was crystallized by dissolving in methanol at room temperature and then cooling to -20 °C to yield yellow crystals. (1.53 g, 100% yield); Mp= 53-54 °C; $^1$H NMR ($CDCl_3$) δ: 10.09 (s, 2H), 7.88-7.94 (m, 6H), 2.03-2.08 (m, 4H), 0.90-1.20 (m, 20H), 0.77 (t, 6H), 0.47-0.58 (m, 4H).

**9,9-bis(3,7-dimethyloctyl)-9H-fluorene-2,7-dicarboxaldehyde (3b)**

To a solution of 3.01 g (5.9 mmol) of 2,7-bis(hydroxymethyl)-9,9-bis(3,7-dimethyloctyl)-9H-fluorene **2b** dissolved in 40 mL of benzene, was added 4.12 g (47.4 mmol) of activated manganese dioxide. The reaction flask was equipped with a dean-stark trap and condenser. The trap was filled with benzene and the reaction mixture was refluxed overnight. The mixture was then cooled to room temperature before filtering off the remaining manganese. The solvent was evaporated to yield the pure product as a yellow oil. (2.98 g, 100% yield); $^1$H NMR ($CDCl_3$, 400 MHz, ppm) δ: 10.09 (s, 2H), 7.89-7.95 (m, 6H), 2.08 (m, 4H), 1.39 (m, 2H), 0.90-1.16 (m, 12H), 0.71-0.90 (m, 14H), 0.65 (d, 6H), 0.50 (m, 2H), 0.36 (m, 2H); $^{13}$C NMR ($CDCl_3$) δ: 192.28, 153.0, 145.9, 136.7, 130.4, 123.6, 121.5, 55.7, 39.3, 37.6, 36.8, 33.0, 30.8, 28.1, 24.8, 22.9, 19.7; HRMS (EI) Calcd. for $C_{35}H_{50}O_2$ 502.38106, found 502.38217, deviation 2.2 ppm.

**2.5.4 General Polymerization Procedure.** A dry round bottom flask was placed under argon atmosphere and then charged with 1 mmol of fluorene monomer **3a** or **3b**, 1 mmol of benzobisoxazole monomer **4** or **5,** and 15 mL of dry THF. The mixture was stirred at room temperature while adding 2.5 mL of 1M solution of potassium tert-butoxide in THF drop-wise over 20 minutes. The mixture to was left to stir at room temperature for 2 days and then added another 15 mL of dry THF to the reaction flask. The reaction was then allowed to stir for another 3 days before quenching it by pouring the mixture into 100 mL of methanol. The precipitated polymer was filtered into a cellulose extraction thimble and then washed in a Soxhlet extractor with methanol, followed by hexane and lastly THF. The THF extract was poured into a crystallizing dish and the polymer recovered upon evaporation of the solvent

**Poly[(9,9-dioctylfluorene-2,7-vinylene)-*alt*-benzo[1,2-*d*;5,4-*d'*]bisoxazole-2,6-diyl] (P43a).** Polymer obtained as an orange solid (0.25 g, 42% yield); $^1$H NMR (THF-$d_8$)δ: 0.80 (br m, -$CH_2$-

), 0.89 (br m, $-CH_3$), 1.11 (br m, $-CH_2-$), 1.29 (m, $-CH_2-$), 2.20 (br m, homobenzylic $–CH_2-$), 7.28 (d, vinylic =CH-), 7.65-7.98 (br m, Ar-H and vinylic =CH-), 10.52 (terminal aldehyde peak), 10.69 (terminal $P(=O)(OH)_2$; GPC: $M_n$ = 6,941, $M_w$ = 11,067, PDI = 1.59.

**Poly[(9,9-bis(3,7-dimethyloctyl)fluorene-2,7-vinylene)-*alt*-benzo[1,2-*d*;5,4-*d'*]bisoxazole-2,6-diyl] (P43b).** Polymer obtained as an orange solid (0.35 g, 53% yield); $^1H$ NMR (THF-$d_8$) δ: 0.79 (br m, -CH2- and -CH3), 1.14 (br m, -CH2-), 2.18 (br m, homobenzylic -CH2-), 7.27 (d, vinylic =CH-), 7.62-7.98 (br m, Ar-H and vinylic =CH-), 10.70 (terminal $P(=O)(OH)_2$ peak); GPC: $M_n$ = 10,348, $M_w$ = 22,515, PDI = 2.18.

**Poly[(9,9-dioctylfluorene-2,7-vinylene)-*alt*-benzo[1,2-*d*;4,5-*d'*]bisoxazole-2,6-diyl] (P53a).** Polymer obtained as a red-orange solid (0.18 g, 30% yield); $^1H$ NMR (THF-$d_8$) δ: 0.80 (br m, $-CH_2-$ and $-CH_3$), 1.11 (br m, $-CH_2-$), 2.20 (br m, homobenzylic $-CH_2-$), 7.28 (d, vinylic =CH-), 7.64-7.98 (br m, Ar-H and vinylic =CH-), 10.51 (terminal aldehyde peak), 10.68 (terminal $P(=O)(OH)_2$ peak); GPC: $M_n$ = 9,739, $M_w$ = 20,242, PDI = 2.08.

**Poly[(9,9-bis(3,7-dimethyloctyl)fluorene-2,7-vinylene)-*alt*-benzo[1,2-d;4,5-d']bisoxazole-2,6-diyl] (P53b).** Polymer obtained as a red-orange solid (0.37 g, 57% yield); $^1H$ NMR (THF-$d_8$) δ: 0.79 (br m, -CH2- and -CH3), 1.10 (br m, -CH2-), 2.20 (br s, benzylic -CH2-), 7.28 (d, vinylic =CH-), 7.68-8.00 (br m, Ar-H and vinylic =CH-), 10.51 (terminal aldehyde peak), 10.69 (terminal $P(=O)(OH)_2$ peak); GPC: $M_n$ = 13,879, $M_w$ = 46,534, PDI = 3.35.

**2.5.5 Fabrication and Characterization of OLEDs.** OLEDs were fabricated on nominally 20 Ω/square, 140 nm-thick ITO-coated glass substrates (Colorado Concept Coatings). The substrates were first cleaned with a detergent and organic solvents; they were then treated in a UV/ozone oven to increase the work function of the ITO and hence facilitate hole injection, as described elsewhere.[68] A 60 nm PEDOT:PSS layer was spin-coated on the ITO and then baked in air at 250°C for 30 min. Blends of PVK and poly(arylenevinylene) copolymers in chlorobenzene solutions were spin-coated on top of the PEDOT:PSS layer in an Ar-filled glovebox. The combined concentration of the PVK and **P43a** was kept constant at 9 mg/mL; the **P43a** concentration varied in the range 0.09 to 0.36 mg/mL. The solution was spin coated at 1000 rpm for 60 s. Under these conditions the light-emitting layer was ~55 nm thick. The fabricated structure was then annealed at 60°C for 30 min. Following this annealing step, the samples were transferred into a thermal evaporator within the glovebox and the BPhen, LiF or CsF, and Al layers were deposited sequentially by thermal evaporation at a base pressure of ~$2\times10^{-6}$ Torr. The OLEDs were characterized by monitoring their electroluminescence (EL) spectra, brightness as a function of the applied voltage, and luminous efficiency.

## 2.6 ACKNOWLEDGMENTS

We thank the 3M Foundation, the National Science Foundation (DMR-0846607), and Iowa State University for financial support of this work. Partial support for this work was provided by the Director for Energy Research, Office of Basic Energy Sciences, USDOE. Ames Laboratory is operated by Iowa State University for the US Department of Energy (USDOE) under Contract No. DE-AC 02-07CH11358. The authors also thank Dr. Kamel Harrata and the Mass Spectroscopy Laboratory of Iowa State University for analysis of our compounds, Dr. Jacob Petrich for use of equipment for fluorescence lifetime measurements and Ms. Trisha Andrew (MIT) for PL spectra and PL quantum yield measurements.

## 2.7 SUPPORTING INFORMATION

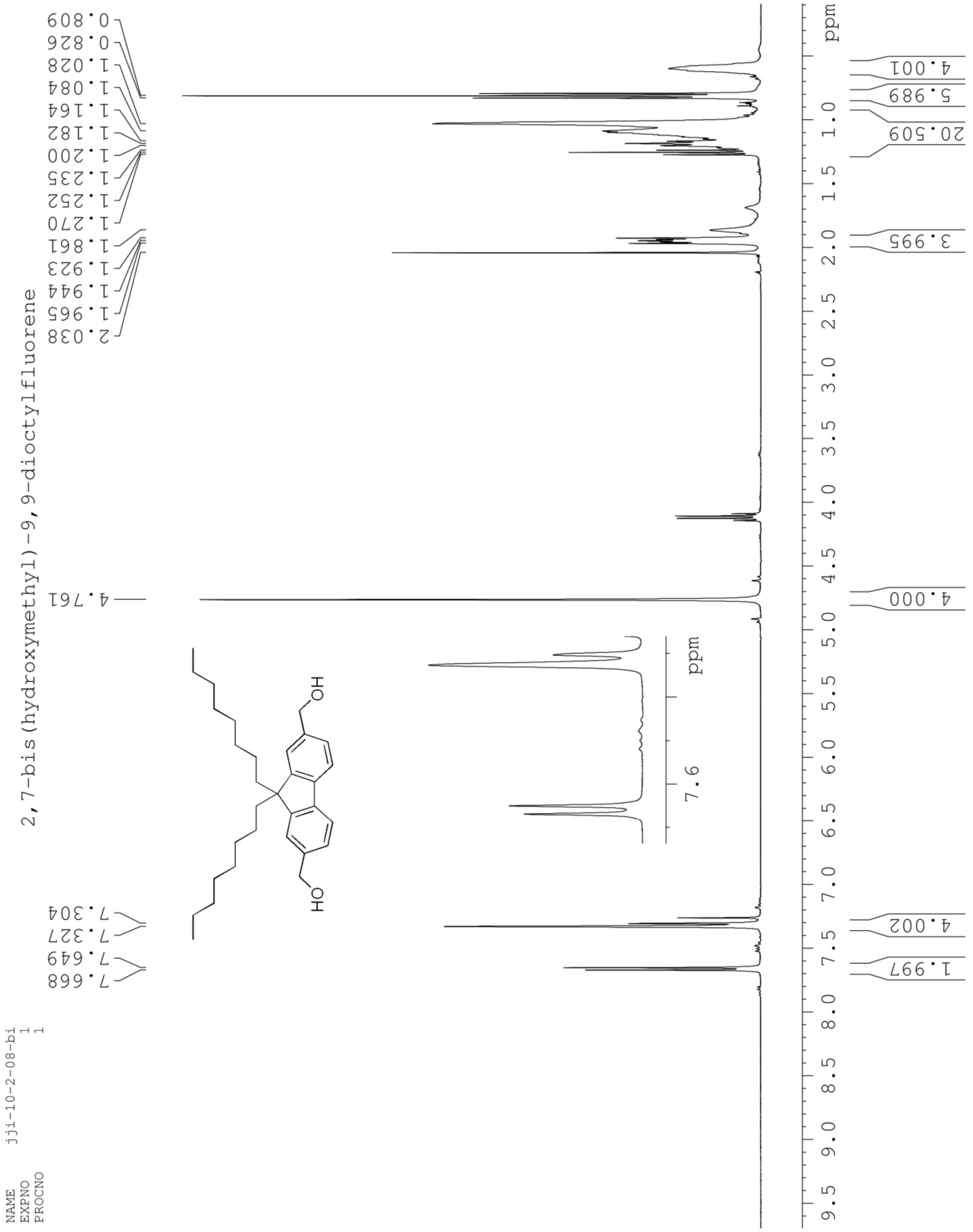

**Figure S2.1.** $^1$H NMR spectrum of **2a**

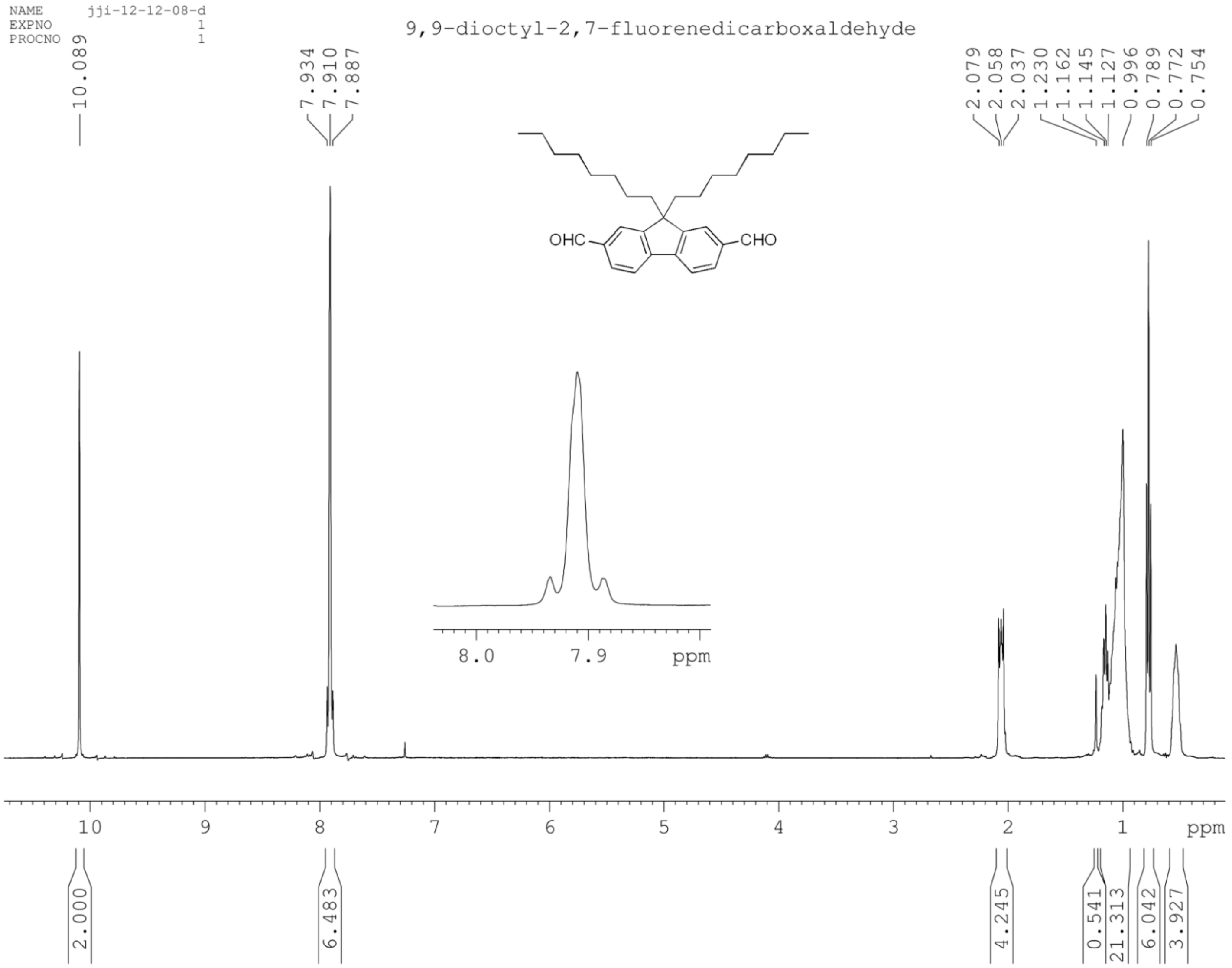

**Figure S2.2.** $^1$H NMR spectrum of **3a**

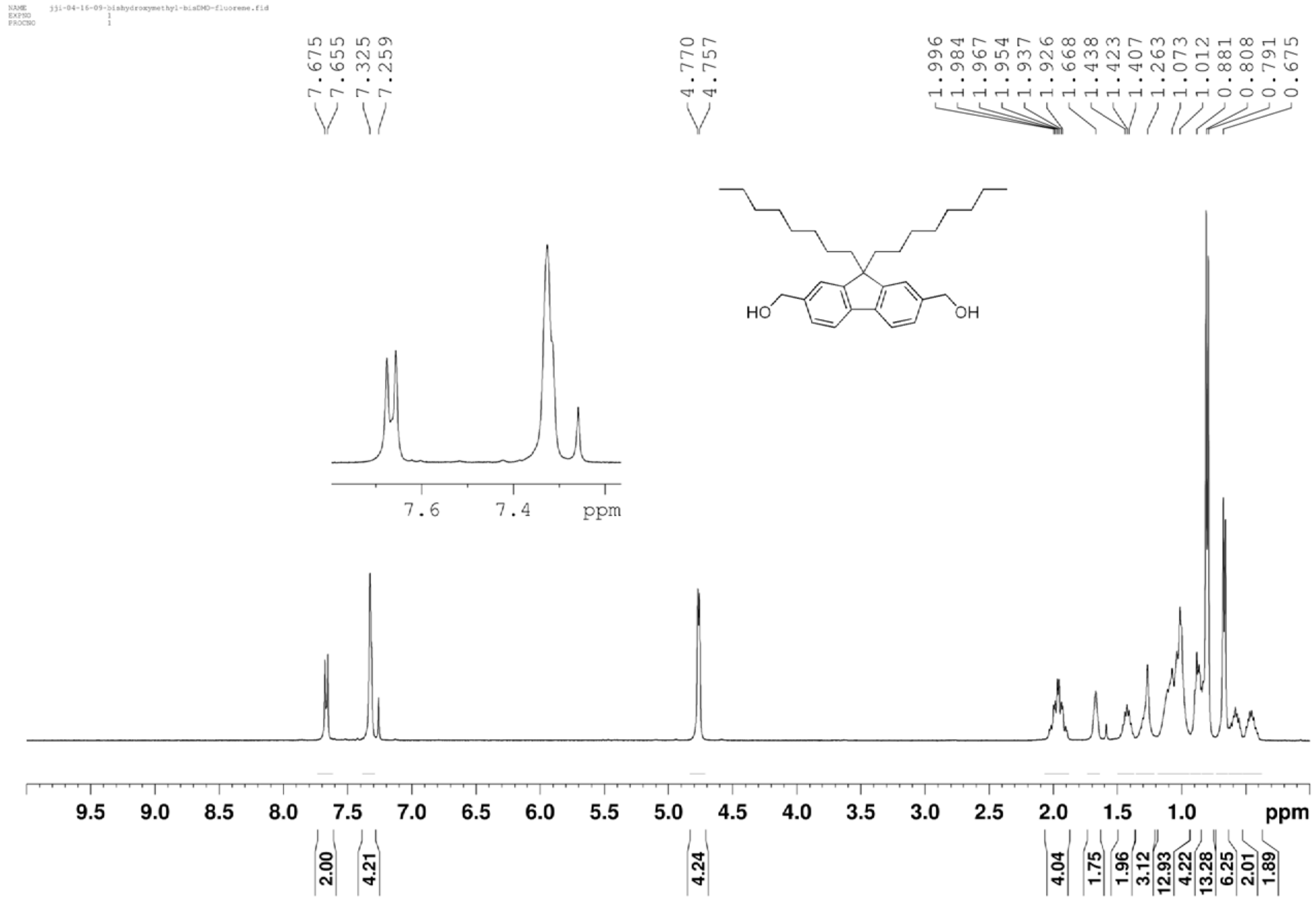

**Figure S2.3.** $^1$H NMR spectrum of **2b**

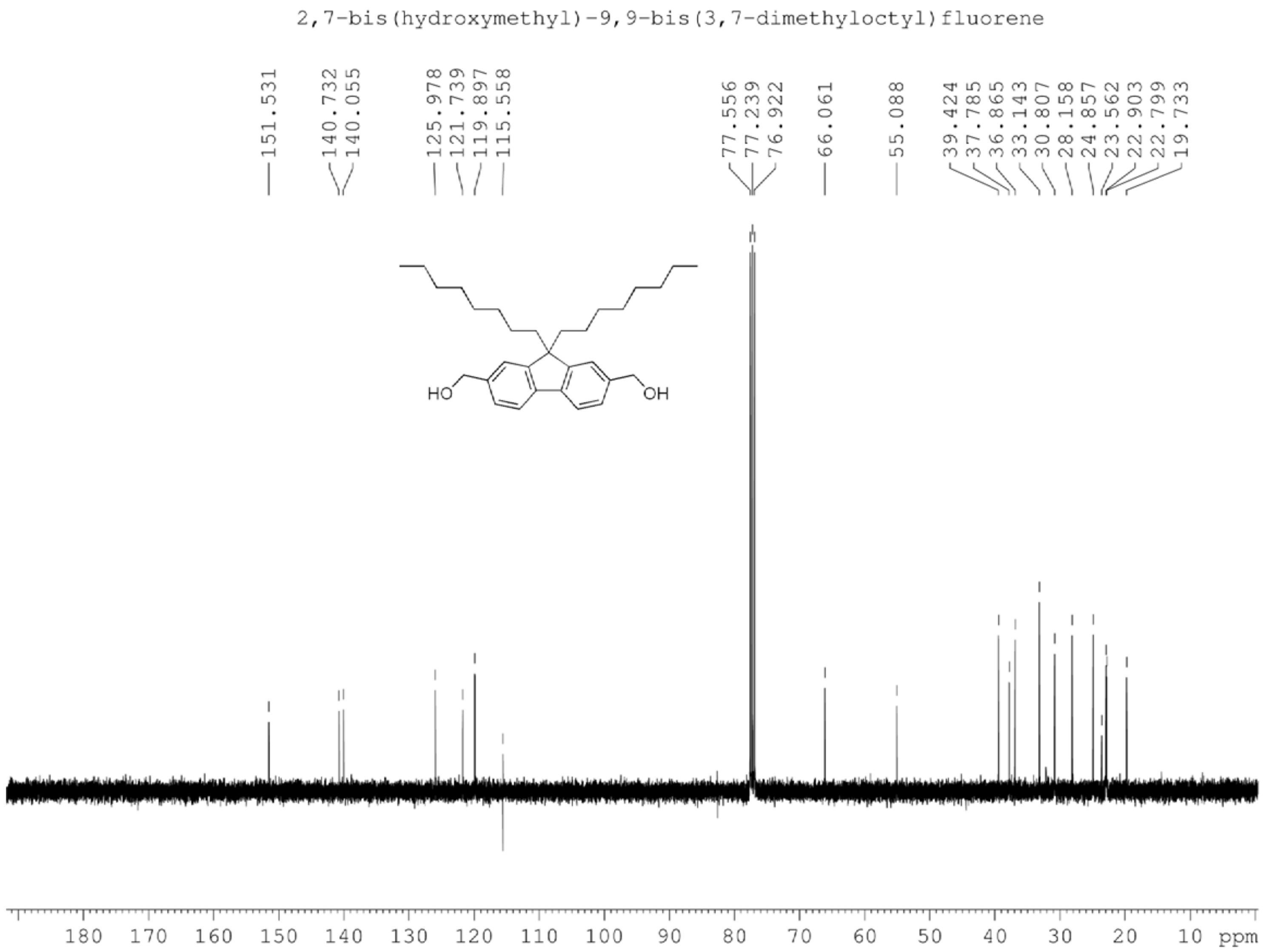

**Figure S2.4.** $^{13}$C NMR spectrum of **2b.**

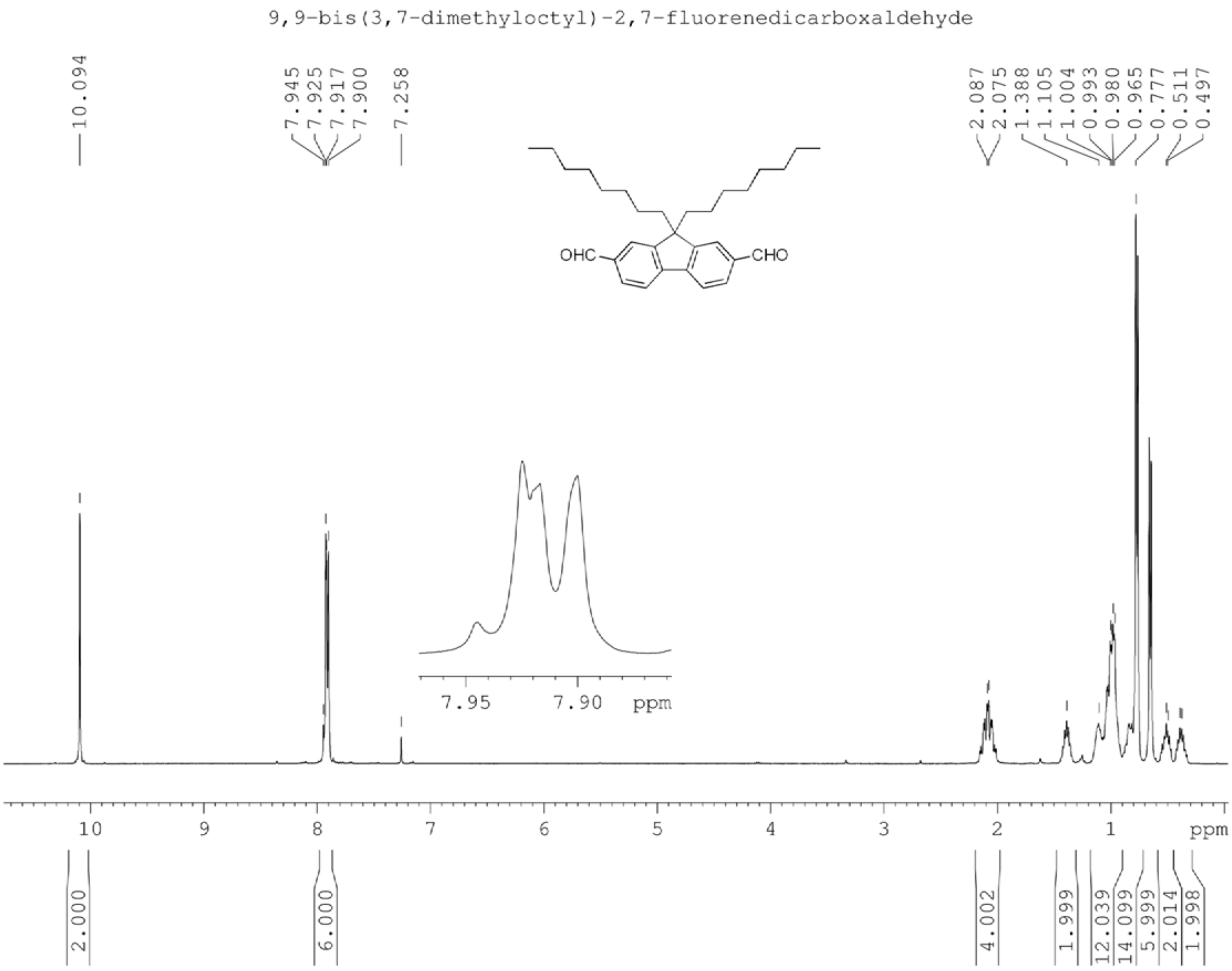

**Figure S2.5.** $^1$H NMR spectrum of **3b**

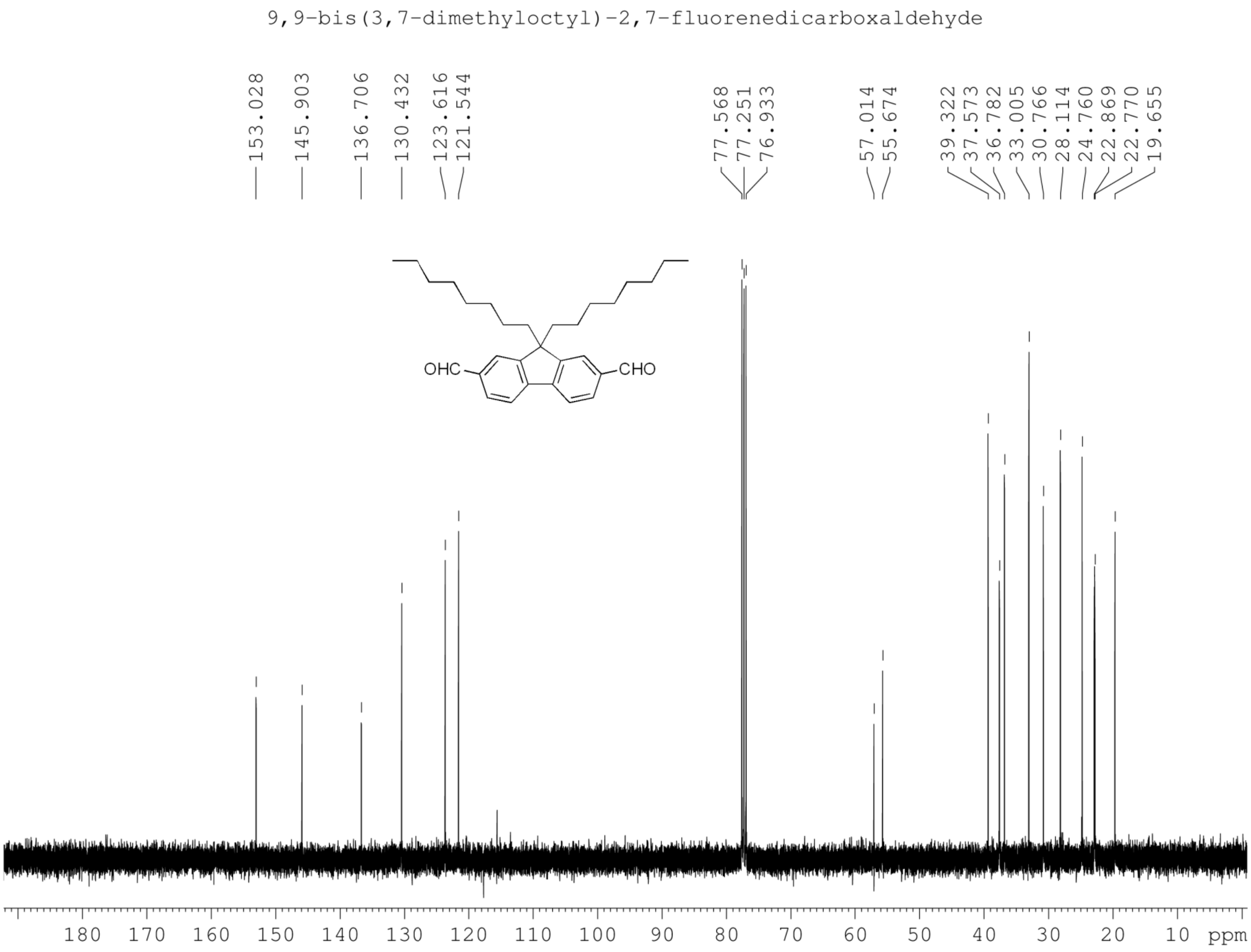

**Figure S2.6.** $^{13}$C NMR spectrum of **3b**

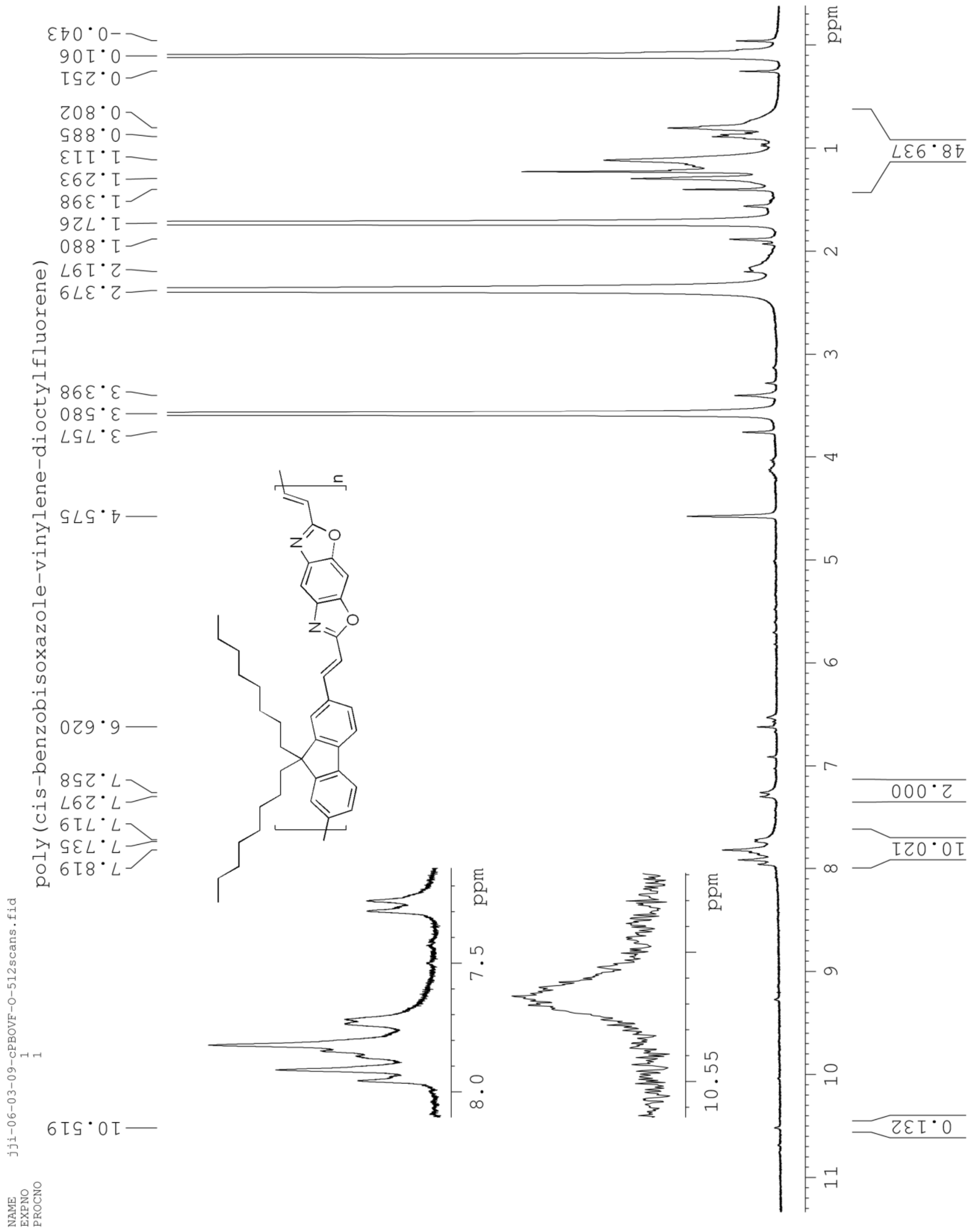

**Figure S2.7.** $^1$H NMR spectrum of **P43a** in THF-d$_8$.

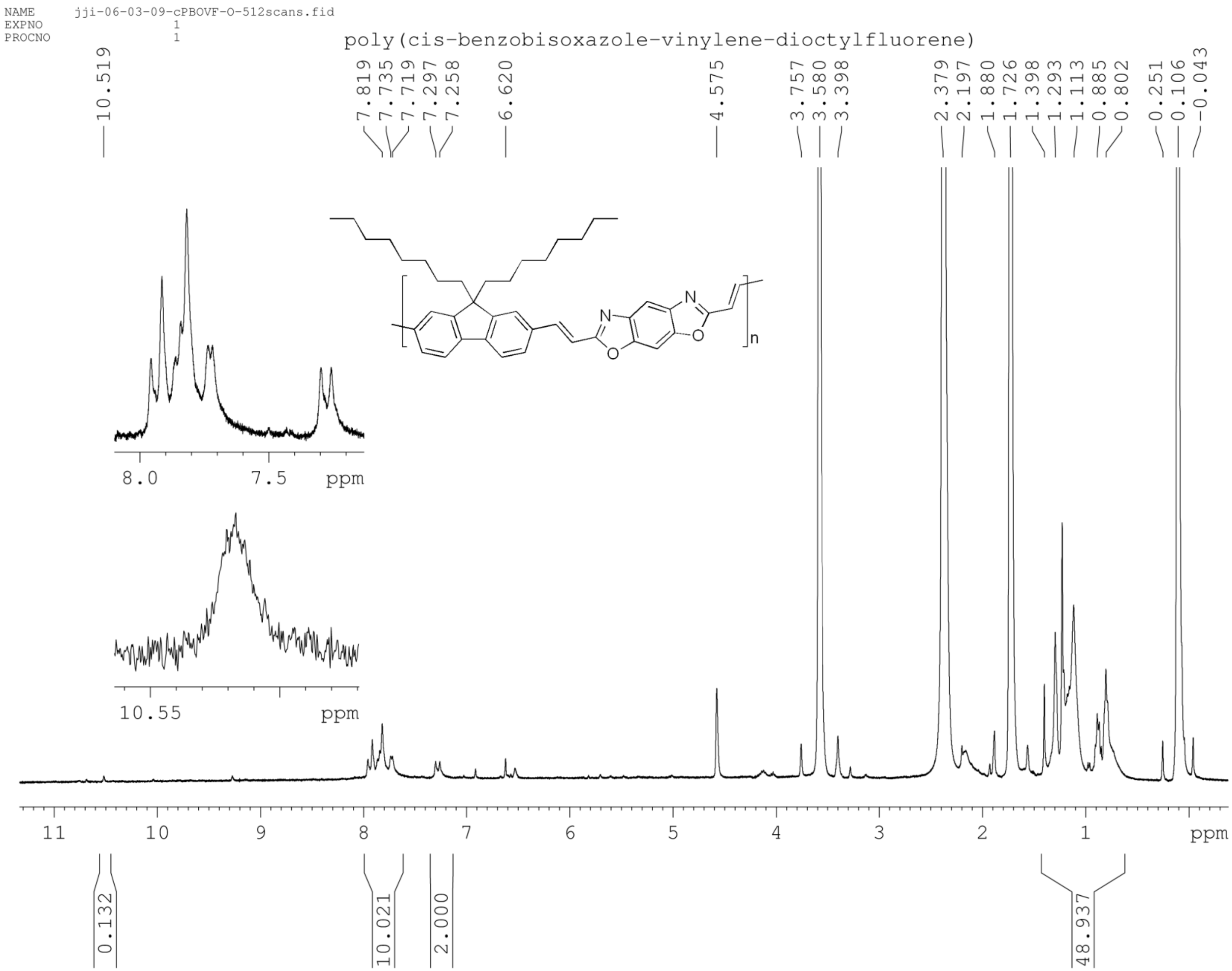

**Figure S2.8.** $^1$H NMR spectrum of **P43b** in THF-$d_8$.

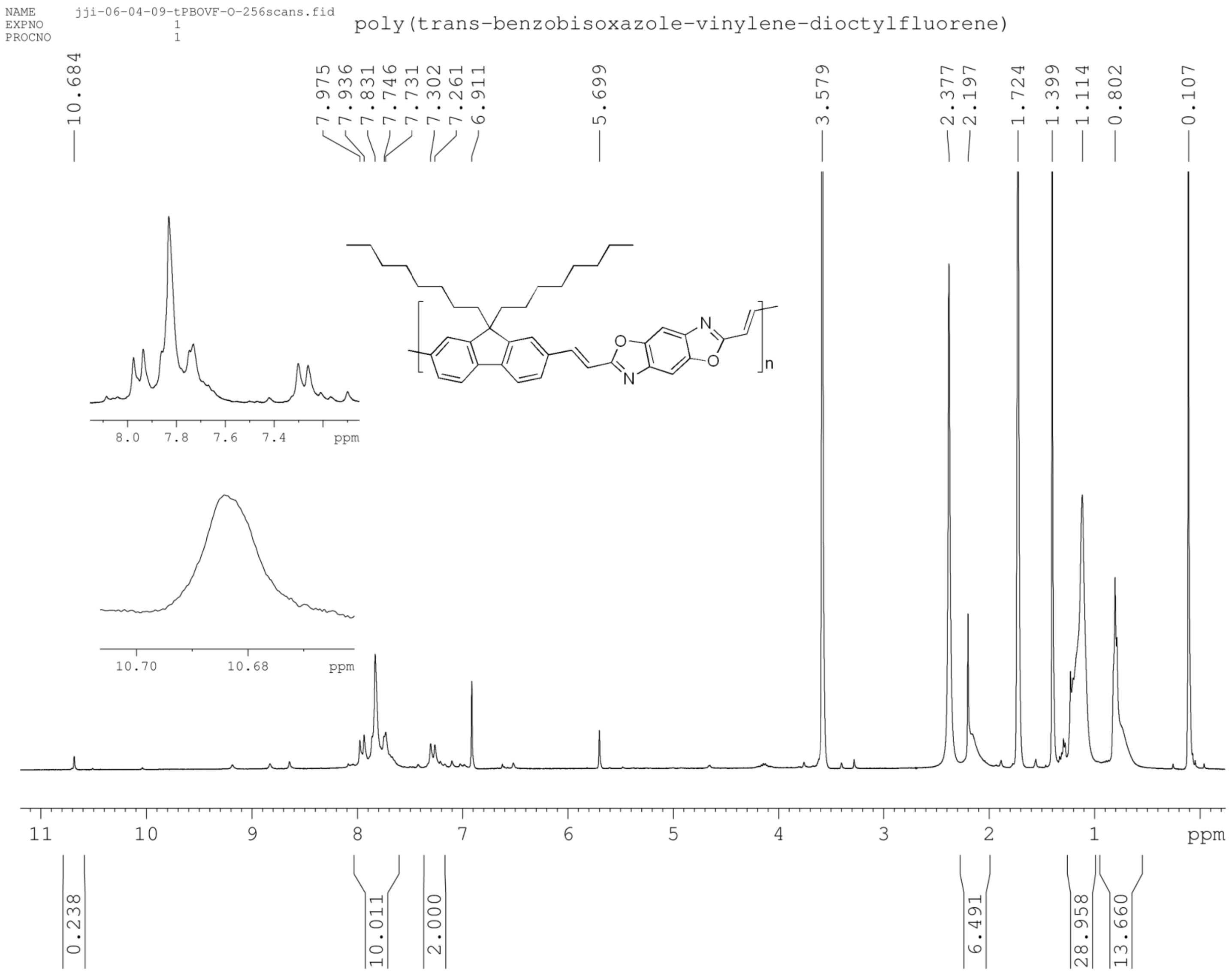

**Figure S2.9.** $^1$H NMR spectrum of **P53a** in THF-$d_8$

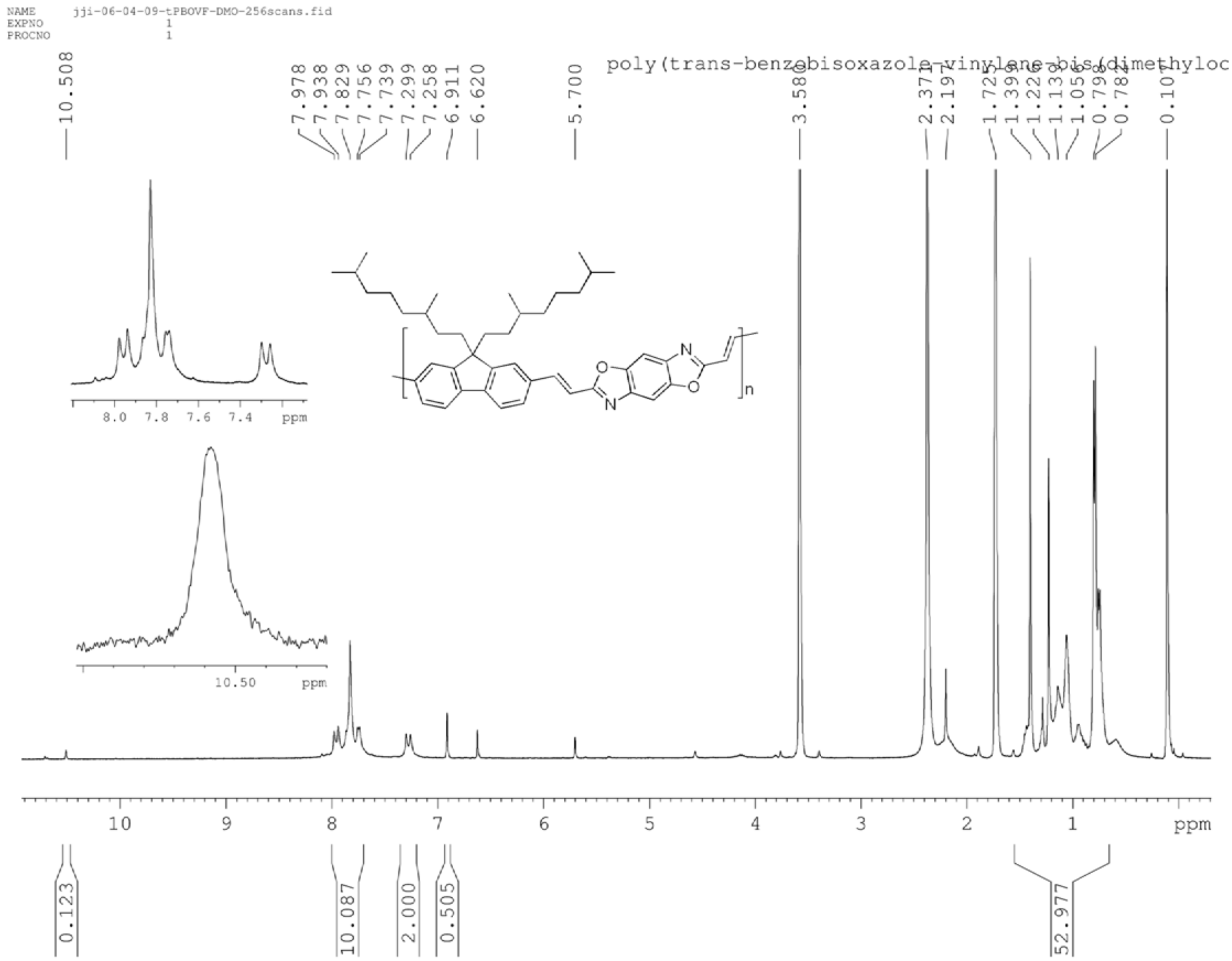

**Figure S2.10.** $^1$H NMR spectrum of **P53b** in THF-$d_8$

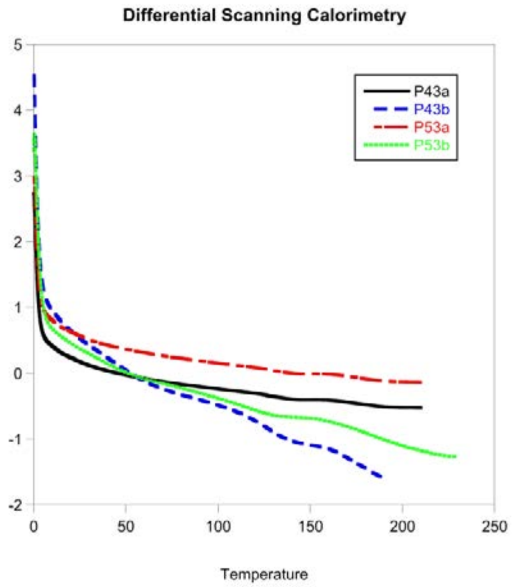

**Figure S2.11.** DSC curves **P43a**, **P643b**, **P53a** and **P53b**, (rate = 15 °C/min).

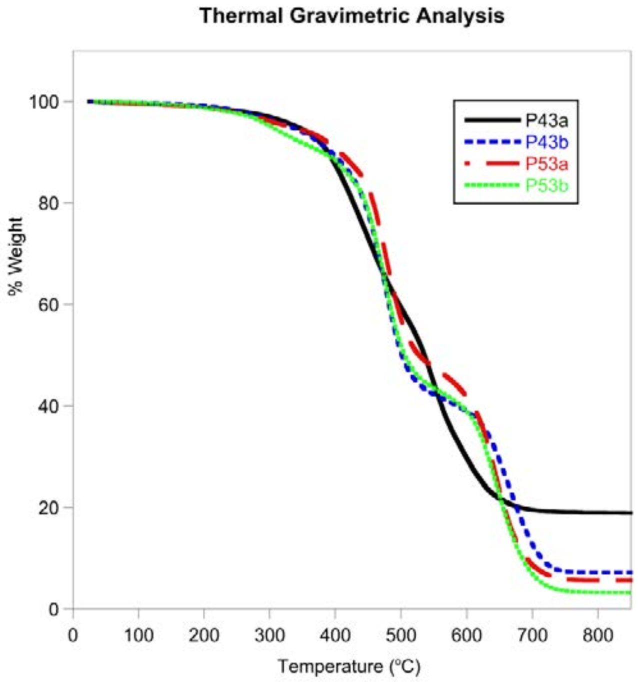

**Figure S2.12.** TGA curves of **P43a**, **P43b**, **P43a** and **P43b**.

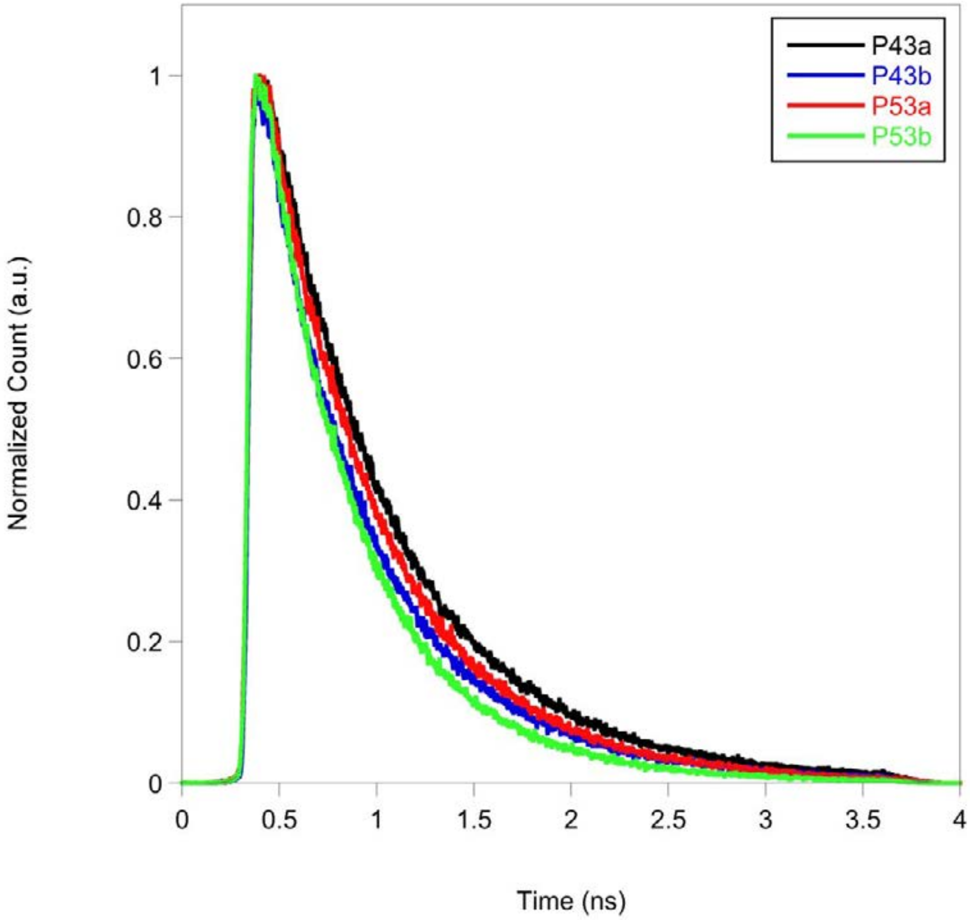

**Figure S2.13.** Fluorescence lifetimes of polymer solutions.

| **Polymer** | **$a_1$** | **$\tau_1$ (ps)** | **$a_2$** | **$\tau_2$ (ps)** | **$a_3$** | **$\tau_3$ (ps)** | **<τ>(ps)** |
|---|---|---|---|---|---|---|---|
| **P43a** | 0.72 | 700 | 0.16 | 280 | 0.12 | 48 | 550±5 |
| **P43a** | 0.70 | 650 | 0.22 | 270 | 0.08 | 43 | 510±5 |
| **P53b** | 0.25 | 860 | 0.54 | 400 | 0.21 | 58 | 440±5 |
| **P53b** | 0.52 | 580 | 0.38 | 270 | 0.07 | 46 | 430±5 |

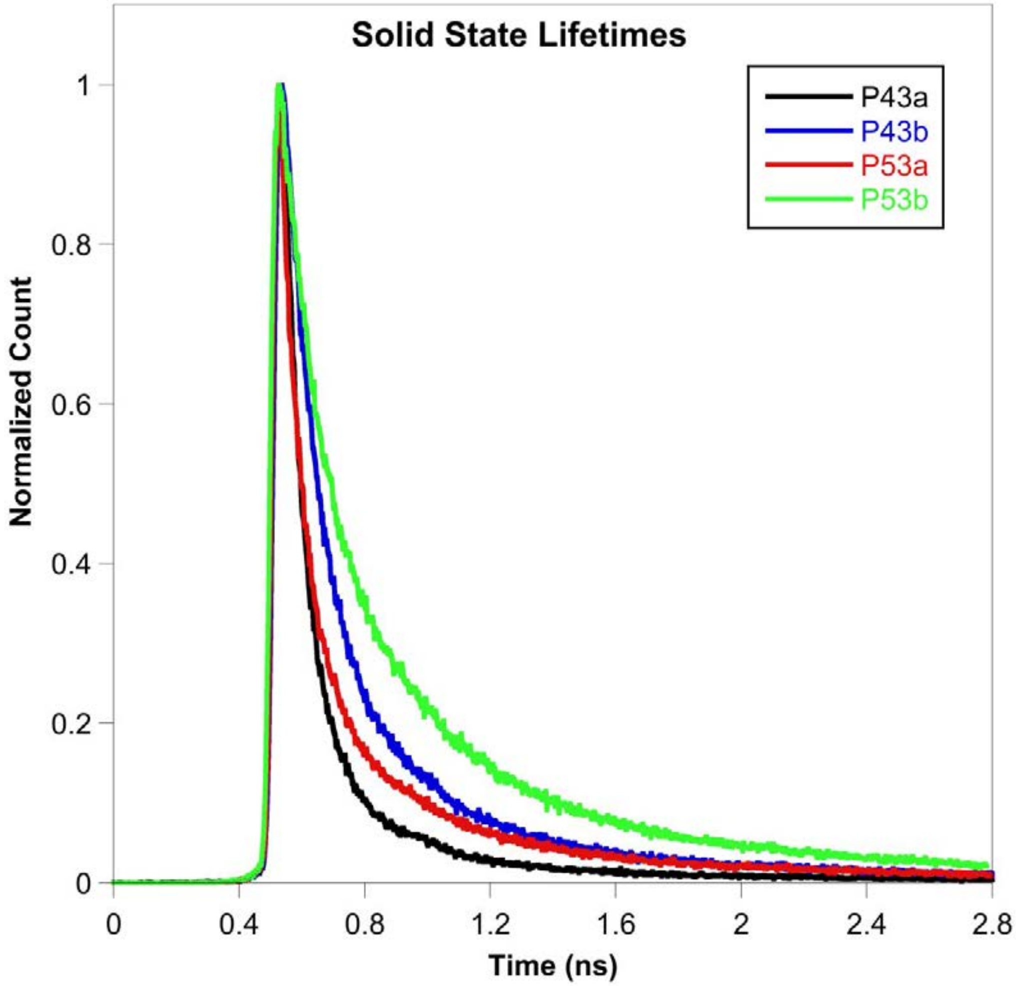

**Figure S14.** Fluorescence lifetimes of polymer films.

| **Polymer** | **$a_1$** | **$\tau_1$ (ps)** | **$a_2$** | **$\tau_2$ (ps)** | **$a_3$** | **$\tau_3$ (ps)** | **<$\tau$>(ps)** |
|---|---|---|---|---|---|---|---|
| **P43a** | 0.75 | 40 | 0.23 | 150 | 0.02 | 1000 | 85±3 |
| **P43a** | 0.72 | 40 | 0.23 | 200 | 0.05 | 900 | 120±5 |
| **P53b** | 0.59 | 62 | 0.36 | 200 | 0.06 | 1000 | 170±10 |
| **P53b** | 0.51 | 75 | 0.35 | 230 | 0.14 | 1000 | 260±10 |

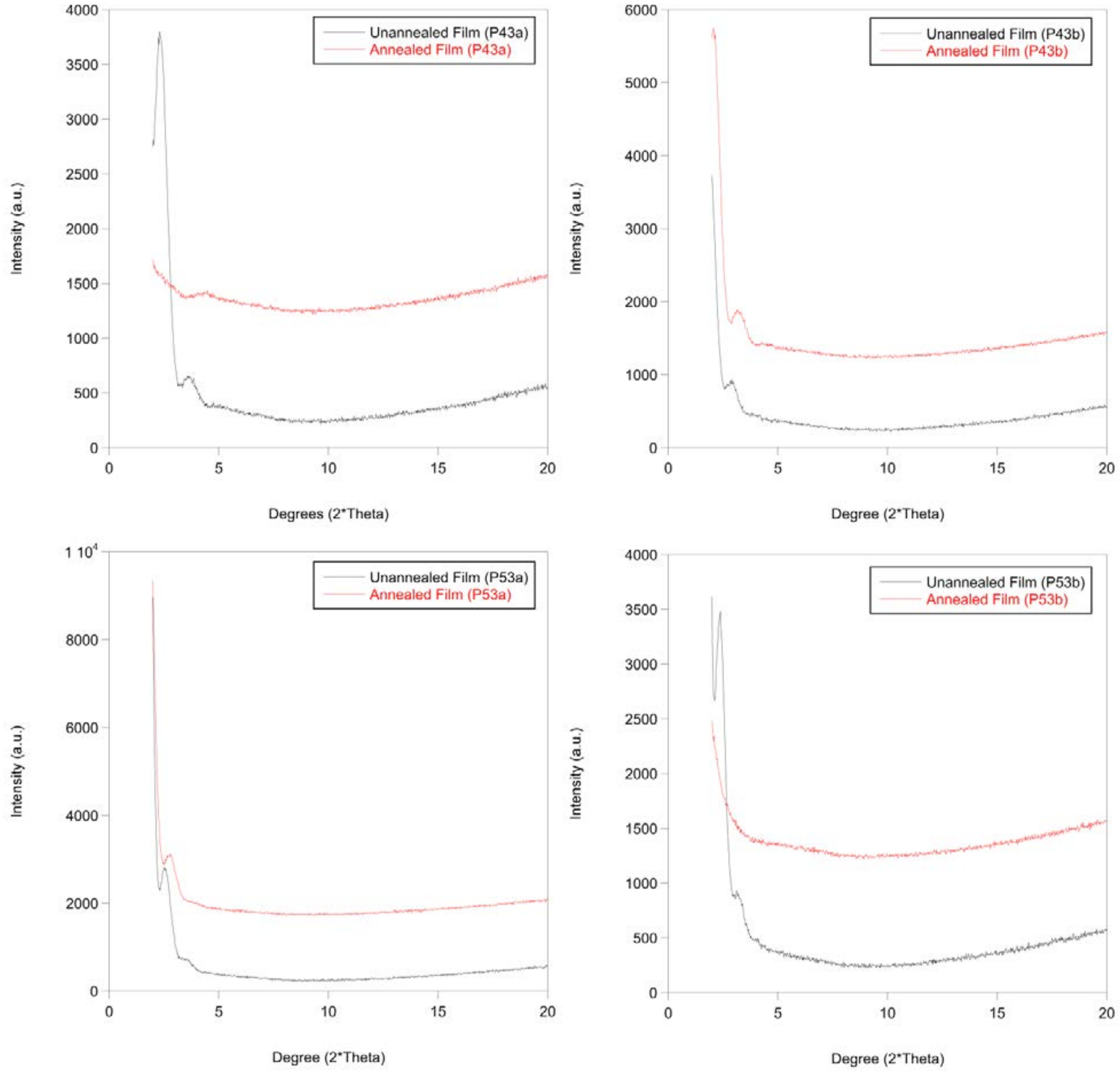

**Figure S15.** X-ray data of polymer films.

Analysis

Unannealed films: No periodicity of polymer chains observed. Peaks seen in XRD pattern are the result of the refractive properties of the thin film.

Annealed films: No periodicity of polymer chains observed in samples 2-4. Polymer film 1001a shows some degree of ordering as witnessed by the peak at approx 4.5 degrees (2*theta).

## 2.8 REFERENCES:

1. Forrest, Stephen R. *Nature* **2004,** 428, (6986), 911-918.

2. Kelley, Tommie W.; Baude, Paul F.; Gerlach, Chris; Ender, David E.; Muyres, Dawn; Haase, Michael A.; Vogel, Dennis E.; Theiss, Steven D. *Chem. Mater.* **2004,** 16, (23), 4413-4422.

3. Leclerc, Mario. *J. Polym. Sci., Part A: Polym. Chem.* **2001,** 39, (17), 2867-2873.

4. Kraft, Arno; Grimsdale, Andrew C.; Holmes, Andrew B. *Angew. Chem. Int. Ed. Eng.* **1998,** 37, (4), 403-428.

5. Friend, R. H.; Gymer, R. W.; Holmes, A. B.; Burroughes, J. H.; Marks, R. N.; Taliani, C.; Bradley, D. D. C.; Dos Santos, D. A.; Bredas, J. L.; Logdlund, M.; Salaneck, W. R. *Nature* **1999,** 397, (6715), 121-128.

6. Greenham, N.C.; Moratti, S.C.; Bradley, D.D.C.; Friend, R.H.; Holmes, A.B. *Nature* **1993,** 365, 628-630.

7. Jenekhe, Samson A.; de Paor, Liam R.; Chen, X. Linda; Tarkka, Richard M. *Chem. Mater.* **1996,** 8, (10), 2401-2404.

8. Kulkarni, Abhishek P.; Tonzola, Christopher J.; Babel, Amit; Jenekhe, Samson A. *Chem. Mater.* **2004,** 16, (23), 4556-4573.

9. Tonzola, C. J.; Alam, M. M.; Bean, B. A.; Jenekhe, S. A. *Macromolecules* **2004,** 37, (10), 3554-3563.

10. Ahmed, Eilaf; Kim, Felix S.; Xin, Hao; Jenekhe, Samson A. *Macromolecules* **2009,** 42, (22), 8615-8618.

11. Grimsdale, Andrew C.; Leok Chan, Khai; Martin, Rainer E.; Jokisz, Pawel G.; Holmes, Andrew B. *Chem. Rev.* **2009,** 109, (3), 897-1091.

12. Osaheni, John A.; Jenekhe, Samson A. *Chem. Mater.* **1992,** 4, (6), 1282-1290.

13. Osaheni, John A.; Jenekhe, Samson A. *Macromolecules* **1993,** 26, (17), 4726-4728.

14. Mikroyannidis, J. A.; Gibbons, K. M.; Kulkarni, A. P.; Jenekhe, S. A. *Macromolecules* **2008,** 41, (3), 663-674.

15. Mikroyannidis, John A.; Spiliopoulos, Ioakim K.; Kasimis, Theodoros S.; Kulkarni, Abhishek P.; Jenekhe, Samson A. *Macromolecules* **2003,** 36, (25), 9295-9302.

16. Lee, Yuh-Zheng; Chen, Xiwen; Chen, Show-An; Wei, Pei-Kuen; Fann, Wun-Shain. *J. Am. Chem. Soc.* **2001,** 123, (10), 2296-2307.

17. Barberis, Vasilis P.; Mikroyannidis, John A. . *J. Poly. Sci. A.* **2006,** 44, (11), 3556-3566.

18. Yang, Wei; Huang, Jian; Liu, Chuanzhen; Niu, Yuhua; Hou, Qiong; Yang, Renqiang; Cao, Yong. *Polymer* **2004,** 45, (3), 865-872.

19. Fu, Dian-Kui; Xu, Bing; Swager, Timothy M. *Tetrahedron* **1997,** 53, (45), 15487-15494.

20. Kim, Jong Lae; Kim, Jai Kyeong; Hong, Sung Il. *Polym. Bull.* **1999,** 42, (5), 511-517.

21. Mikroyannidis, John A. ; Fakis, Mihalis; Spiliopoulos, Ioakim K. . *J. Poly. Sci. A.* **2009,** 47, (13), 3370-3379.

22. Lee, Bum Hoon; Jaung, Jae Yun; Cho, Jae-whan; Yoon, Kee Jong. *Polym. Bull.* **2003,** 50, (1), 9-16.

23. Karastatiris, Panayiotis; Mikroyannidis, John A.; Spiliopoulos, Ioakim K.; Kulkarni, Abhishek P.; Jenekhe, Samson A. *Macromolecules* **2004,** 37, (21), 7867-7878.

24. Kulkarni, Abhishek P.; Zhu, Yan; Jenekhe, Samson A. *Macromolecules* **2005,** 38, (5), 1553-1563.

25. Alam, Maksudul M.; Jenekhe, Samson A. *Chem. Mater.* **2002,** 14, (11), 4775-4780.

26. Babel, Amit; Jenekhe, Samson A. *Adv. Mater.* **2002,** 14, (5), 371-374.

27. Babel, Amit; Jenekhe, Samson A. *J. Phys. Chem. B.* **2002,** 106, (24), 6129-6132.

28. Chen, Yan; Wang, Shanfeng; Zhuang, Qixin; Li, Xinxin; Wu, Pingping; Han, Zhewen. *Macromolecules* **2005,** 38, (23), 9873-9877.

29. Feng, Dongdong; Wang, Shanfeng; Zhuang, Qixin; Wu, Pingping; Han, Zhewen. *Polymer* **2004,** 45, (26), 8871-8879.

30. Jenekhe, Samson A.; Osaheni, John A. *Chem. Mater.* **1994,** 6, (11), 1906-1909.

31. Osaheni, John A.; Jenekhe, Samson A. *Macromolecules* **1994,** 27, (3), 739-742.

32. Osaheni, John A.; Jenekhe, Samson A. *Chem. Mater.* **1995,** 7, (4), 672-682.

33. Osaheni, John A.; Jenekhe, Samson A.; Burns, Andrew; Du, Gang; Joo, Jinsoo; Wang, Zhaohui; Epstein, Arthur J.; Wang, Chi Shun. *Macromolecules* **1992,** 25, (21), 5828-5835.

34. Zhang, Xuejun; Jenekhe, Samson A. *Macromolecules* **2000,** 33, (6), 2069-2082.

35. Wolfe, J.F., Polybenzothiazoles and Polybenzoxazoles. In *Encyclopedia of Polymer Science and Engineering*, John Wiley and Sons: New York, NY, 1988; Vol. 11, pp 601-635.

36. Wolfe, J.F.; Arnold, F.E. *Macromolecules* **1981,** 14, 909-915.

37. Wolfe, J.F.; Loo, B.H.; Arnold, F.E. *Macromolecules* **1981,** 14, 915-920.

المنـــارة للاستشارات

38. Guo, Peiying; Wang, Shanfeng; Wu, Pingping; Han, Zhewen. *Polymer* **2004,** 45, (6), 1885-1893.

39. Kricheldorf, Hans R.; Domschke, Angelika. *Polymer* **1994,** 35, (1), 198-203.

40. Liu, Xiaoyun; Xu, Xiaohui; Zhuang, Qixin; Han, Zhewen. *Polym. Bull.* **2008,** 60, (6), 765-774.

41. Wang, Shanfeng; Lei, Hui; Guo, Peiying; Wu, Pingping; Han, Zhewen. *Eur. Polym. J.* **2004,** 40, (6), 1163-1167.

42. Mike, Jared F.; Makowski, Andrew J.; Jeffries-El, Malika. *Org. Lett.* **2008,** 10, (21), 4915-4918.

43. Mike, Jared F.; Inteman, Jeremy J.; Ellern, Arkady; Jeffries-El, Malika. *J. Org. Chem.* **2010,** 75, (2), 495-497.

44. Mike, Jared F.; Makowski, Andrew J.; Mauldin, Timothy C.; Jeffries-El, Malika. *J. Poly. Sci. A.* **2010,** 48, (6), 1456-1460.

45. Hancock, Jessica M.; Gifford, Angela P.; Tonzola, Christopher J.; Jenekhe, Samson A. *J. Phys. Chem. C* **2007,** 111, (18), 6875-6882.

46. Huang, F.; Zhang, Y.; Liu, M.; Cheng, Y. J.; Jen, A. Y. *Adv. Fun. Mater.* **2007,** 17, (18), 3808-3815.

47. Anuragudom, Piched; Newaz, S. S.; Phanichphant, Sukon; Lee, T. Randall. *Macromolecules* **2006,** 39, (10), 3494-3499.

48. Kannan, Ramamurthi; He, Guang S.; Lin, Tzu-Chau; Prasad, Paras N.; Vaia, Richard A.; Tan, Loon-Seng. *Chem. Mater.* **2004,** 16, (1), 185-194.

49. Bhaumik, D.; Welsh, W. J.; Jaffe, H. H.; Mark, J. E. *Macromolecules* **1981,** 14, (4), 951-953.

50. Bhaumik, D.; Jaffe, H. H.; Mark, J. E. *Macromolecules* **1981,** 14, (4), 1125-1126.

51. Welsh, W. J.; Bhaumik, D.; Mark, J. E. *Macromolecules* **1981,** 14, (4), 947-950.

52. Bhaumik, D.; Mark, J. E. *J. Polym. Sci., Polym. Phys. Ed.* **1983,** 21, (Copyright (C) 2010 American Chemical Society (ACS). All Rights Reserved.), 1111-1118.

53. Welsh, W. J.; Mark, J. E. *Journal of Materials Science* **1983,** 18, (Copyright (C) 2010 American Chemical Society (ACS). All Rights Reserved.), 1119-1124.

54. Craig, Michael R.; Kok, Margreet M. de; Hofstraat, Johannes W.; Schenning, Albertus P. H. J.; Meijer, E. W. *J. Mater. Chem.* **2003,** 13, (12), 2861-2862.

55. Cho, Sung Yong; Grimsdale, Andrew C.; Jones, David J.; Watkins, Scott E.; Holmes, Andrew B. *J. Am. Chem. Soc.* **2007,** 129, (39), 11910-11911.

56. Liu, B.; Yu, W. L.; Pei, J.; Liu, S. Y.; Lai, Y. H.; Huang, W. *Macromolecules* **2001,** 34, (23), 7932-7940.

57. Grisorio, Roberto; Piliego, Claudia; Cosma, Pinalysa; Fini, Paola; Mastrorilli, Piero; Gigli, Giuseppe; Suranna, Gian Paolo; Nobile, Cosimo Francesco. *J. Poly. Sci. A.* **2009,** 47, (8), 2093-2104.

58. Tonzola, Christopher J.; Alam, Maksudul M.; Jenekhe, Samson A. *Macromolecules* **2005,** 38, (23), 9539-9547.

59. Bose, Sayantan; Adhikary, Ramkrishna; Mukherjee, Prasun; Song, Xueyu; Petrich, Jacob W. *J. Phys. Chem. B* **2009,** 113, (32), 11061-11068.

60. Chowdhury, P. K.; Halder, M.; Sanders, L.; Calhoun, T.; Anderson, J. L.; Armstrong, D. W.; Song, X.; Petrich, J. W. *The Journal of Physical Chemistry B* **2004,** 108, (29), 10245-10255.

61. Mike, Jared F.; Nalwa, Kanwar; Makowski, A. J.; Putnam, Daniel; Tomlinson, Aimee, L.; Chaudhary, Sumit; Jeffries-El, Malika. *Phys. Chem. Chem. Phys.* **2011**.

62. Agrawal, A. K.; Jenekhe, S. A. *Chem. Mater.* **1996,** 8, (2), 579-589.

63. Janietz, S.; Bradley, D. D. C.; Grell, M.; Giebeler, C.; Inbasekaran, M.; Woo, E. P. *Appl. Phys. Lett.* **1998,** 73, (17), 2453-2455.

64. Gontia, I.; Frolov, S. V.; Liess, M.; Ehrenfreund, E.; Vardeny, Z. V.; Tada, K.; Kajii, H.; Hidayat, R.; Fujii, A.; Yoshino, K.; Teraguchi, M.; Masuda, T. *Phys. Rev. Lett.* **1999,** 82, (20), 4058-4061.

65. Hidayat, Rahmat; Tatsuhara, Satoshi; Kim, Dong Wook; Ozaki, Masanori; Yoshino, Katsumi; Teraguchi, Masahiro; Masuda, Toshio. *Phys. Rev. B: Condens. Matter Mater. Phys.* **2000,** 61, (15), 10167-10173.

66. Wu, Jiun-Shian; Lu, Hsin-Hung; Hung, Wei-Chun; Lin, Guan-Hong; Chen, Show-An. *Appl. Phys. Lett.* **2010,** 97, (2), 023304-023303.

67. Ranger, M.; Rondeau, D.; Leclerc, M. *Macromolecules* **1997,** 30, (25), 7686-7691.

68. Zhou, Z.; Shinar, R.; Allison, A.†J.; Shinar, J. *Adv. Fun. Mater.* **2007,** 17, (17), 3530-3537.

# Chapter 3

## Benzobisthiazole-Fluorene Based Emissive Polymers for Guest-Host Polymer Light Emitting Diodes

*Jeremy J. Intemann,*[†] *Jared F. Mike,*[†] *Min Cai,*[‡] *Charles A. Barnes,*[†] *Teng Xiao,*[‡] *Robert A. Roggers,*[†] *Joseph Shinar,*[‡] *Ruth Shinar*[§] *and Malika Jeffries-EL**[†]

[†] Department of Chemistry, Iowa State University, Ames, Iowa 50011, United States

[‡] Ames Laboratory-USDOE and Department of Physics and Astronomy, Iowa State University, Ames, Iowa 50011, United States

[§] Microelectronics Research Center and Department of Electrical and Computer Engineering, Iowa State University, Ames, Iowa 50011, United States

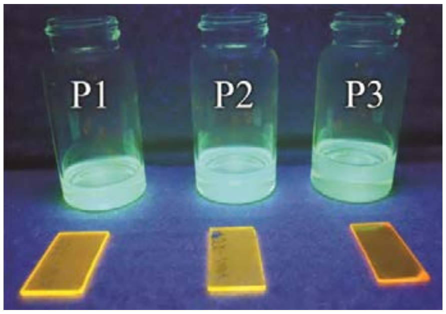

## 3.1 ABSTRACT

A series of vinylene-linked–donor-acceptor copolymers based on the electron-deficient benzobisthiazole and electron-rich fluorene moieties were synthesized via Horner-Wadsworth-Emmons polymerization. Three different polymers, **P1**, **P2**, and **P3,** were prepared bearing octyl, 3,7-dimethyloctyl, and 2-(2-ethoxy)ethoxyethyl side chains, respectively. All of the polymers possessed moderate molecular weights, good solubility in aprotic organic solvents, and high fluorescence quantum efficiencies in dilute solutions. **P2**, which bore branched 3,7-dimethyloctyl side chains, exhibited better solubility than the other polymers, but also exhibited the lowest

thermal decomposition temperature of all polymers. Overall, the impact of the side chains on the optical properties of the polymers in solution was negligible as all three polymers gave similar absorption and emission spectra in both solution and film. Guest-host light-emitting diodes using dilute blends of the polymers in a poly(*N*-vinylcarbazole) host gave blue-green emission with **P2** exhibiting the highest luminous efficiency, 0.63 Cd/A at ~500 nm.

## 3.2 INTRODUCTION

Conjugated polymers are currently of interest due to their potential impact on a diverse range of technologies, including polymer light-emitting diodes (PLED)s,[1, 2] photovoltaic cells (PVC)s[3, 4] and field-effect transistors (FET)s.[5, 6] Research in this area is motivated by the opportunity to fabricate large area displays via low-cost solution processing techniques and tuning of the optical properties of the polymers through chemical synthesis. Since the original report on conjugated polymer electroluminescence, scientists have been actively designing polymers with stable red, blue, or green emission for use in PLEDs.[7, 8] Conjugated polymer electroluminescence was first demonstrated in poly(phenylene vinylene). As a result, poly(arylene vinylene)s (PAVs) are the most widely studied class of electroluminescent polymers. Among aromatic building blocks, 9,9-dialkylfluorenes have been widely used in the synthesis of electroluminescent polymers. Poly(9,9-dialkylfluorene)s (PDAF)s are blue light-emitting polymers that have excellent solubility, high solid-state photoluminescence quantum yield and good charge carrier mobility. A number of copolymers containing 9,9-dialkylfluorene have been synthesized that give efficient emission across the entire visible spectrum.[9] Unfortunately, PDAFs have a low electron affinity, which makes the injection of electrons into the polymer difficult.[9-11] PDAFs also have high ionization potentials, which hinders the injection of holes into the polymer and increases the driving voltages of PLEDs based on them. The incorporation of vinylene linkages between aryl units has been shown to increase the effective conjugation length in PDAFs, resulting in lower IPs and hole injection barriers.[12] Since heteroatoms such as oxygen, nitrogen, and sulfur are more electronegative than carbon, the incorporation of heterocycles into poly(arylene vinylene)s can be used to improve the polymers' electron affinity.[13-17] Accordingly, the synthesis of PAVs composed of 9,9-dialkylfluorene and electron-deficient heterocycles has been investigated for the development of emissive materials with better charge injection and transport properties.[11, 16, 18, 19]

Among heterocycles, benzobisthiazole is unique as it contains two sulfur atoms and two nitrogen atoms within its fused three-ring system. Benzobisthiazole polymers and small molecules have been used as organic semiconductors in a variety of applications, including nonlinear optical materials,[20-22] field-effect transistors,[23-29] light-emitting diodes,[30, 31] and photovoltaic cells.[23-25, 32, 33] When used as electron-transport layers, polybenzobisthiazoles improved the performance of PAV based LEDs.[31] When used as emissive materials, thin films of poly(benzobisthiazo1e-1,4- phenylenebisvinylene) (PBTPV) emitted red light with an emission peak at 640 nm and an estimated quantum yield of 4-5%.[30] In spite of their many beneficial qualities, the development of benzobisthiazole-containing materials for PLEDs has been hindered by two factors: poor solubility, requiring processing from strongly acidic solutions; and harsh reaction conditions, which limit the types of substituents that can be incorporated into the polymer backbone. However, the recent development of monomers based on functional benzobisthiazoles has created the opportunity to develop new PAVs based on this moiety.[34]

Previously, we synthesized poly(fluorene vinylene-*alt*-benzobisoxazole)s, which exhibited reversible reduction processes and stable blue emission with luminous efficiencies of up to 1 Cd/A at ~470 nm in guest-host PLEDs using poly(*N*-vinyl carbazole) matrix. In this paper, we report the synthesis, characterization and electroluminescent properties of three new poly(fluorene vinylene-*alt*-benzobisthiazole)s. Since benzobisthiazole is a stronger electron-accepting moiety than benzobisoxazoles, we anticipated that the resulting polymers would have lower LUMOs than the oxygen-containing analogs.

## 3.3 EXPERIMENTAL METHODS

**3.3.1 Materials.** All chemicals were purchased from commercial sources and used without further purification unless otherwise noted. Tetrahydrofuran (THF) was dried using an Innovative Technologies solvent purification system. 9,9-dioctylfluorene-2,7-dicarbaldehyde,[35] 9,9-bis(3,7-dimethyloctyl)fluorene-2,7-dicarbaldehyde,[35] and 2,7-dibromofluorene,[36] 2,6-dimethylbenzo[1,2-d;4,5-d']bisthiazolediethylphosphonate ester,[34] and 2-(2-ethoxy)ethoxyethyl bromide[37] were synthesized according to literature procedures. Chromatograhic separations were performed using silica gel 60, using eluents as indicated**.**

**3.3.2 Instrumentation.** Nuclear magnetic resonance spectra were obtained on a 400 MHz spectrometer ($^1$H at 400 MHz and $^{13}$C at 100 MHz). $^1$H NMR samples were referenced internally to residual protonated solvent. $^{13}$C NMR spectra were referenced to the middle carbon peak of $CDCl_3$. In both instances, chemical shifts are given in $\delta$ relative to solvent. High-resolution mass spectra were recorded on a double focusing magnetic sector mass spectrometer using EI at 70 eV. Melting points were obtained using a melting point apparatus, upper temperature limit 260 ºC. Gel permeation chromatography (GPC) measurements were performed on a Viscotek GPC Max 280 separation module equipped with three 5µm I-gel columns connected in a series (guard, HMW, MMW and LMW) with a refractive index detector. Analyses were performed at 35 °C using THF as the eluent with the flow rate at 1.0 mL/min. Calibration was based on polystyrene standards. Fluorescence spectroscopy and UV-Visible spectroscopy were obtained using polymer solutions in chloroform and as thin films. The films were made by spin-coating 25x25x1mm glass slides, using a solution of 10 mg of polymer per 1 mL chloroform at a spin rate of 2000 rpm. Thermal gravimetric analysis measurements were made within the temperature interval of 25 ºC - 850 ºC, with a heating rate of 20 ºC/minute, under ambient atmosphere. Differential scanning calorimetry was performed with a first scan at a heating rate of 15 ºC/min to erase thermal history and a second scan to measure transitions from 0 °C to 200 °C under nitrogen. Electrochemical properties were measured on an eDaq e-corder 410 potentiostat using a three-electrode cell (electrolyte: 0.1 mol/L $TBAPF_6$ in acetonitrile) with an $Ag/AgNO_3$ reference electrode, a platinum auxiliary electrode, and a platinum button electrode as the working electrode. Polymer films were drop-cast from a chloroform solution on to the working electrode. All films were annealed at 160 ºC for one hour prior to use. All cyclic voltammetry experiments were carried out under argon atmosphere and were recorded at a scan rate of 100 mV/s and referenced to ferrocene/ferrocenium. Powder diffraction patterns of thin films were obtained using a Riguku Ultima IV X-Ray diffractometer equipped with an MPA-U4 multipurpose Eulerian cradle and 1.76 kW Cu Kα radiation. Samples were first scanned from 0.05 to 0.501 degrees 2θ using parallel-beam optics to determine the critical angle of the films.[38] The incident angles of the X-ray beam for the diffraction studies were chosen to be at a value slightly above the external critical reflection for the polymer films. Fluorescence lifetime measurements were performed using the time-correlated–single-photon counting (TCSPC) method. Pulses tunable from ~780-880 nm were produced from a homebuilt 82-MHz mode-locked Ti:sapphire oscillator pumped by a 5-W Nd:$VO_4$ laser (Millennia, Spectra Physics). The resulting fundamental wavelength at ~814 nm was modulated by a Pockels cell (Model 350-160, Conoptics Inc.) to reduce the repetition rate to ~8.8 MHz. The frequency-doubling of this laser source by a harmonic generator (Model TP-2000B, U-Oplaz Technologies) provided the excitation wavelength at ~407 nm. A half-wave plate and polarizer placed before the sample chamber ensured vertically polarized excitation. Emission (≥500 nm) was collected in a perpendicular geometry and passed through a polarizer set at the magic angle (54.7°) for solutions and 90° for solid films, with respect to the excitation polarization. For polymer solution lifetime measurements, dilute solutions of each were prepared in chloroform and placed in a 1 cm path-length cuvette. Notably, a front-faced geometry was also used for solid films. The placement of appropriate filters before the microchannel plate, MCP (Hamamatsu, R3809U-50) eliminated the excitation light and allowed selection of emission from the sample. The full width at half-maximum (FWHM) of the instrument response function was ∼37-40 ps. All measurements were made in a 3-5 ns time window with a total of 4096 channels. A total of 65536 counts were collected at the peak channel for all lifetime measurements. The fluorescence quantum yield measurements were conducted by using an $Ar^+$ laser as excitation source and a homebuilt integrating sphere connected to a calibrated Ocean Optics spectrometer through an optical fiber, as described elsewhere.[39, 40]

### 3.3.3 Monomer Synthesis

***2,7-dibromo-9,9-bis(2-(2-ethoxy)ethoxyethyl)fluorene***

A round-bottom flask was charged with 2,7-dibromofluorene (27.05 g, 83.5 mmol) and potassium iodide (1.39 g, 8.35 mmol) in dimethyl sulfoxide (70 mL). The mixture was cooled in a cold-water bath and stirred as potassium hydroxide power (23.45 g, 418 mmol) was added in a single portion. 2-(2-Ethoxy)ethoxyethyl bromide (36.0 g, 184 mmol) was added dropwise while keeping the pot temperature between 0 and 20 °C. The reaction was stirred at room temperature for 24 hours and then poured into water. The mixture was extracted with chloroform (3 x 125 mL) and the organic extracts were combined, washed with brine, dried over $MgSO_4$, and the solvent evaporated. The excess alkyl bromide was removed by distillation under reduced pressure and the remaining residue was purified by column chromatography using silica gel and a 5:1 mixture of chloroform : ethyl acetate as the eluent to yield a white solid (28.80 g, 62% yield). Mp = 88-89 °C; $^1$H NMR ($CDCl_3$) δ: 7.53 (s, 2H), 7.51 (d, 2H), 7.46 (d, 2H), 3.42 (q, 4H), 3.33 (t, 4H), 3.20 (t, 4H), 2.78 (t, 4H), 2.35 (t, 4H), 1.15 (t, 6H); $^{13}$C NMR ($CDCl_3$) δ: 151.0, 138.5, 130.8, 126.8, 121.8, 121.3, 70.3, 69.8, 66.9, 66.8, 52.0, 39.6, 15.2; HRMS (EI) Calcd. for $C_{25}H_{33}Br_2O_4$ ($MH^+$) 555.074, found 555.0744, deviation -0.7 ppm.

### *2,7-bis(hydroxymethyl)-9,9-bis(2-(2-ethoxy)ethoxyethyl)fluorene*

A flame-dried three-neck round-bottom flask was placed under argon and charged with 2,7-dibromo-9,9-bis(2-(2-ethoxy)ethoxyethyl)fluorene (15.75 g, 28.3 mmol) and dry THF (270 mL). The mixture was cooled to -78 °C and stirred as *tert*-butyllithium (1.7 M in pentane, 100 mL) was added dropwise via an addition funnel. It was then stirred an additional 1 hour at -78 °C before adding paraformaldehyde (2.55 g, 85 mmol) in small portions over 15 minutes. The reaction was then stirred for another 2 hours after which it was warmed to room temperature and stirred overnight. The reaction was then quenched by adding saturated aqueous ammonium chloride solution and the mixture was extracted with diethyl ether (3 x 100 mL). The organic extracts were combined, washed with water and brine, and dried over $MgSO_4$. After evaporation of the solvent, the crude oil was purified by column chromatography on a silica gel column using a gradient of 10:1 to 2:1 of diethyl ether : isopropyl alcohol to yield a yellow oil (8.22 g, 63% yield). $^1$H NMR ($CDCl_3$) δ: 7.63 (d, 2H), 7.42 (s, 2H), 7.32 (d, 2H), 4.72 (s, 4H), 3.39 (q, 4H), 3.30 (t, 4H), 3.15 (t, 4H), 2.75 (t, 4H), 2.38 (t, 4H), 2.32 (s, 2H), 1.12 (t, 6H); $^{13}$C NMR ($CDCl_3$) δ: 149.5, 140.3, 139.7, 126.3, 122.0, 119.8, 69.8, 69.7, 67.1, 66.5, 65.5, 51.2, 39.6, 15.0; HRMS (EI) Calcd. for $C_{27}H_{38}O_6Na$ ($MNa^+$) 481.2561, found 481.2558, deviation 0.57 ppm.

### *9,9-bis(2-(2-ethoxy)ethoxyethyl)fluorene-2,7-dicarboxaldehyde (2c)*

A round-bottom flask was charged with 9,9-bis(2-(2-ethoxy)ethoxyethyl)fluorene-2,7-dicarboxaldehyde (4.62g, 10 mmol) and activated manganese dioxide (6.96 g, 80 mmol) in benzene (70 mL). A Dean-Stark trap with a condenser was attached to the flask and the reaction was refluxed overnight. The mixture was then cooled to room temperature and passed through a short silica gel plug using benzene as the eluent. The solvent was evaporated yielding a yellow oil (4.56 g, 100% yield). $^1$H NMR ($CDCl_3$) δ: 10.08 (s, 2H), 7.99 (s, 2H), 7.92 (m, 4H), 3.35 (q, 4), 3.24 (t, 4H), 3.12 (t, 4H), 2.78 (t, 4H), 2.49 (t, 4H), 1.09 (t, 6H); $^{13}$C NMR ($CDCl_3$) δ: 192.1, 151.6, 145.1, 136.7, 130.3, 124.7, 121.6, 70.3, 69.8, 67.1, 66.8, 52.1, 39.5, 15.3; HRMS (EI) Calcd. for $C_{27}H_{35}O_6$ ($MH^+$) 455.2428, found 455.2434, deviation -1.29 ppm.

**3.3.4 General Procedure For Polymerization.** A flame-dried Schlenk flask was placed under an argon atmosphere and charged with compounds 1 (1 mmol) and 2(a-c) (1 mmol) followed by addition of THF (30 mL). The mixture was stirred while potassium *tert*-butoxide (1.0M in THF, 2.2 mL) was added dropwise over 20 minutes. The reaction was then stirred for 24 hours followed by precipitation of the polymer in methanol (~100 mL). The solid was filtered and washed in a Soxhlet extractor with methanol, followed by hexanes, and then extracted with THF. The THF fraction was evaporated to yield the solid polymer.

### *Poly[(9,9-dioctylfluorene-2,7-vinylene)-alt-benzo[1,2-d;4,5-d']bisthiazole-2,6-diyl] (P1)*

The polymer was obtained as an orange solid (510 mg, 81% yield). $^1$H NMR ($CDCl_3$) δ: 8.44 (s, Ar-H), 7.38-7.86 (br m, Ar-H and vinylic =C-H), 2.05 (s, $-CH_2-$), 1.02-1.28 (br m, $-CH_2-$), 0.59-0.92 (br m, $-CH_2-$ and $CH_3$); GPC: $M_n$ = 11,500, $M_w$ = 32,900, PDI = 2.9.

### *Poly[(9,9-bis(3,7-dimethyloctyl)fluorene-2,7-vinylene)-alt-benzo[1,2-d;4,5-d']bisthiazole-2,6-diyl] (P2)*

The polymer was obtained as an orange solid (427 mg, 62% yield). $^1$H NMR ($CDCl_3$) δ: 8.37 (s, Ar-H), 7.38-7.74 (br m, Ar-H and vinylic =C-H), 1.98 (br m, $-CH_2-$), 0.38-1.40 (br m, $-CH_2-$ and $–CH_3$); GPC: $M_n$ = 13,000, $M_w$ = 38,000, PDI = 2.9.

### *Poly[(9,9-bis(2-(2-ethoxy)ethoxyethyl))fluorene-2,7-vinylene)-alt-benzo[1,2-d;4,5-d']bisthiazole-2,6-diyl] (P3)*

The polymer was obtained as an orange solid (386 mg, 60% yield). $^1$H NMR ($CDCl_3$) δ: 8.47 (s, Ar-H), 7.41-7.82 (br m, Ar-H and vinylic =C-H), 3.16-3.45 (br m, $-O-CH_2-$), 2.92 (br s, $-O-CH_2-$), 2.49 (br s, $-O-CH_2-$), 1.27 (s, $-CH_2-$), 0.89 (s, $-CH_3$); GPC: $M_n$ = 7 349, $M_w$ = 15,300, PDI = 2.1.

## 3.4 RESULTS AND DISCUSSION

**3.4.1 Synthesis and Characterization.** The benzobisthiazole monomer **1**[34] and the 2,7-dibromo-9,9-dialkylfluorenes **2a**[41] and **2b**[42] were synthesized according to the literature procedures. 9,9-Bis(2-(2-ethoxy)ethoxyethylfluorene-2,7-dicarboxaldehyde **2c** was synthesized in three steps starting from 2,7-dibromofluorene using methods analogous to those for the synthesis of **2a** and **2b**. All fluorene monomers were carefully purified via column chromatography to remove any monoalkylated side products that could lead to defects in the polymer.[43, 44] The base-catalyzed Horner-Wadsworth-Emmons (HWE) polycondensation reaction between the benzobisthiazole monomer **1** and fluorene monomers **3a**, **3b** and **3c** in anhydrous THF afforded the polymers **P1**, **P2** and **P3** respectively (Scheme 3.1). The HWE reaction is preferable because it is known to produce polymers with all *trans*-double bonds while preventing cross-linking, incomplete double bond formation, and other undesirable structural defects.[45] All polymers were obtained in 60 – 81% yields after purification by Soxhlet extraction with methanol to remove residual salts, followed by hexanes to remove the lower molecular weight material, and finally THF to recover the soluble polymer. The THF was evaporated to yield solid polymer. All of the polymers were

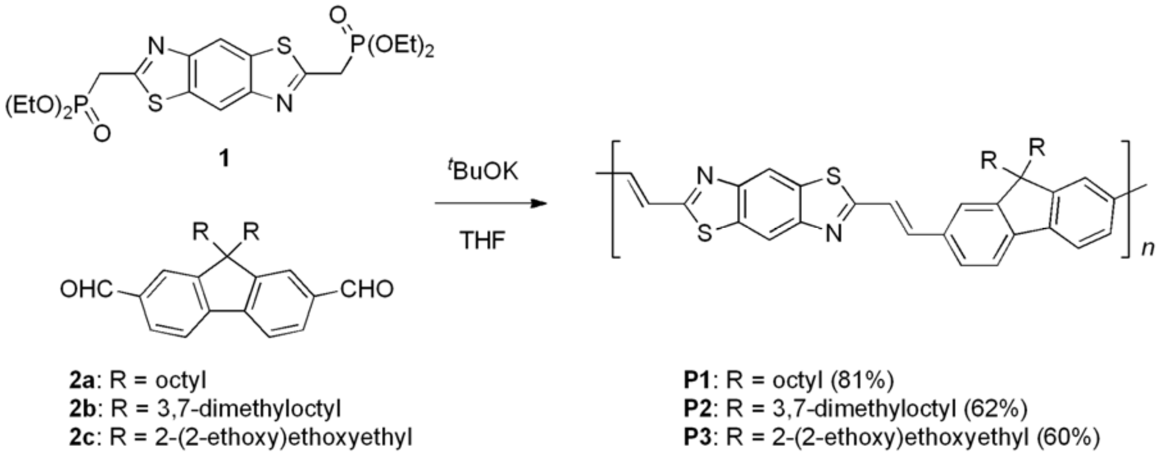
1
$^t$BuOK
THF
n
2a: R = octyl
2b: R = 3,7-dimethyloctyl
2c: R = 2-(2-ethoxy)ethoxyethyl
P1: R = octyl (81%)
P2: R = 3,7-dimethyloctyl (62%)
P3: R = 2-(2-ethoxy)ethoxyethyl (60%)

**Scheme 3.1. Synthesis of poly(fluorene vinylene-*alt*-benzobisthiazole)s.**

**Table 3.1. Physical properties of poly(fluorene vinylene-*alt*-benzobisthiazole)s.**

| Polymer | $M_n$[a] | $M_w$[a] | PDI | $T_d$[b] (°C) |
|---|---|---|---|---|
| P1 | 11,500 | 32,900 | 2.9 | 361 |
| P2 | 13,000 | 38,200 | 2.9 | 258 |
| P3 | 7,350 | 15,280 | 2.1 | 276 |

[a] Determined by GPC in THF using polystyrene standards. [b] 5% weight loss temperature by TGA.

soluble in common organic solvents, such as *m*-cresol, chloroform, *o*-dichlorobenzene, and THF. The $^1$H NMR spectra for polymers **P1**, **P2**, and **P3** were in agreement with the proposed polymer structures (see Figures S3.10 – S3.12 Supporting Information). The number-averaged degree of polymerization ($DP_n$) as determined by gel permeation chromatography (GPC) ranged from 11 – 18.

The thermal stability of the benzobisthiazole polymers were evaluated using thermal gravimetric analysis (TGA) and differential scanning calorimetry (DSC). The TGA curves are shown in Figure 3.1 and the data is summarized in Table 3.1. All of the polymers were found to

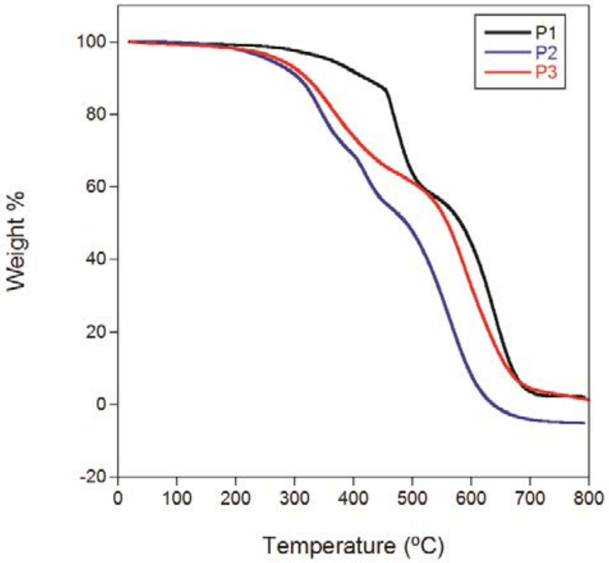

**Figure 1.** TGA plot of poly(fluorene vinylene-*alt*-benzobisthiazole)s.

be thermally stable with weight loss onsets occurring above 250 °C. As expected, the introduction of flexible side chains onto the polymer backbone results in significantly lower decomposition temperatures in comparison to related poly(phenylenevinylene benzobisthiazole), which does not possess side chains and exhibits 5% weight loss at 560 ºC.[30] However, the decomposition temperatures of these polymers are all high enough to be useful in semiconducting applications. Additionally, DSC indicated that none of the polymers had glass transition temperatures, which is desirable for good color purity in PLEDs.[46]

**3.4.2 Optical and Electrochemical Properties.** The UV-Vis absorption and photoluminescence (PL) spectra of the polymers, both as dilute solutions in chloroform and as thin solid films, were evaluated. The normalized absorption and PL spectra for all of the polymers in solution and films are shown in Figure 3.2 and the data is summarized in Table 3.2. In solution, it is apparent that the alkyl chains have no impact on the optical properties of the polymers as the UV spectra for all of the polymers are virtually identical and possess two absorption bands, due to vibronic coupling. In thin films, the absorption spectra for all of the polymers exhibit significant broadening of the absorption band and the relative magnitudes of the absorbances of each peak

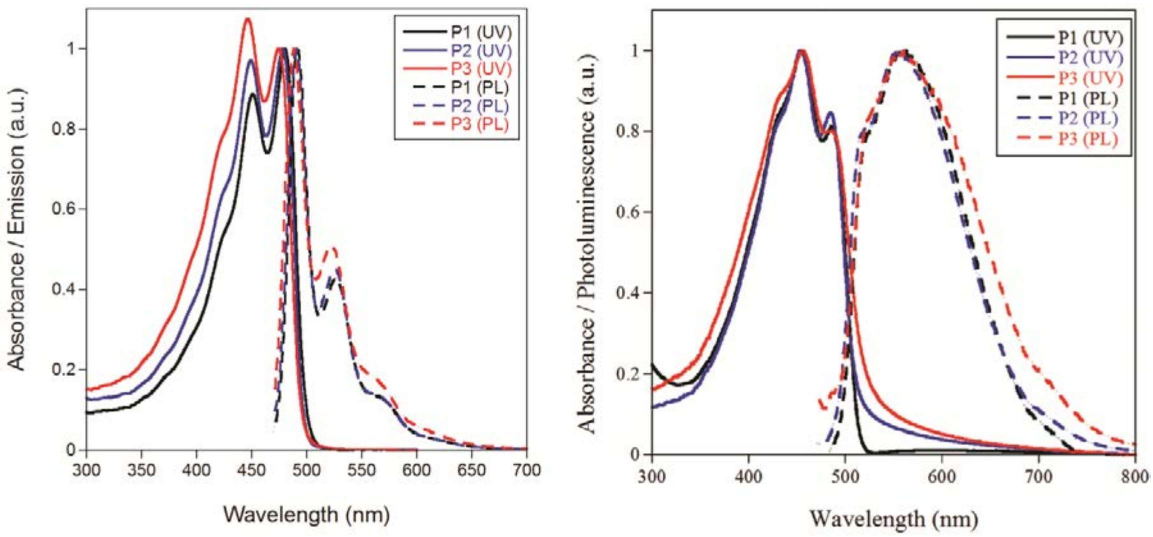

**Figure 3.2.** UV-Vis absorption (solid lines) and photoluminescence (dashed lines) of P1, P2, and P3 in chloroform solutions (left) and thin films (right).

**Table 3.2. Electronic and Optical Properties of Benzobisthiazole Polymers.**

| | Solution | | Thin Film | | | | | |
|---|---|---|---|---|---|---|---|---|
| Polymer | $\lambda_{max}$ (nm) | $\lambda_{em}$ (nm) | $\lambda_{max}$ (nm) | $\lambda_{em}$ (nm) | $E_g^{opt}$ (eV)[a] | $E_g^{ec}$ (eV) | EA (eV)[b] | IP (eV)[c] |
| P1 | 480*, 451 | 492 | 486, 455* | 559 | 2.4 | 2.6 | 2.9 | 5.5 |
| P2 | 478*, 449 | 491 | 485, 454* | 558 | 2.4 | 2.6 | 3.0 | 5.6 |
| P3 | 475, 446* | 488 | 486, 456* | 560 | 2.4 | 2.5 | 3.0 | 5.5 |

*Denotes actual $\lambda_{max}$. [a]Optical band gap measured from the onset of absorption in films. [b]Electron affinity calculated from reduction onset ($E_{red}$) in CV trace using EA = -($E_{red}$ + 4.8). [c]Ionization potential calculated from oxidation onsent ($E_{ox}$) in CV trace using IP = -($E_{ox}$ + 4.8).

changes. This results in a new $\lambda_{max}$ at a lower wavelength without any of the peaks actually blue-shifting. In fact, there is actually a slight red-shift in the absorption of the polymers (6-11 nm), which is a consequence of aggregation of the polymers in the films. As seen with the solution absorption spectra, the film spectra are the same for all of the polymers. This is an indication that the side chains do not affect the solid-state packing for any of these polymers. This is supported by X-ray analysis, which shows that thin films of all polymers are completely amorphous with no observable periodicity (see supporting information). The optical band gap ($E_g^{opt}$) was determined from the absorption onset of the polymer films and was 2.4 eV for all of the polymers, further evidence that alkyl chain substitution has no effect on the electronic properties of these materials.

The photoluminescence of the polymers in solution shows a narrow blue-green emission at ~490 nm which is independent of alkyl chain substitution as the emission spectra are essentially the same for all of them. All of the polymers show a significant red-shift in their film PL spectra into the orange region of the visible spectrum relative to their emissions in solution which indicates exciplex formation within the films.[47] The wavelength of emitted light is similar for all three polymer films (558-560 nm) and is also independent of alkyl chain substitution. **P3** exhibits a broader emission band than **P1** and **P2** which is the result of increased aggregation in the **P3** film relative to **P1** and **P2**. This is an effect of the 2-(2-ethoxy)ethoxyethyl chains of **P3** disrupting $\pi$-stacking to a lesser extent than the alkyl chains on **P1** and **P2** which is evident from its reduced solubility and molecular weight.

The redox properties of the polymers were evaluated using cyclic voltammetry (CV). The calculated electron affinities (EA) and ionization potentials (IP) are listed in Table 3.2. All of the polymers had partially reversible reduction waves with reduction onsets at -1.9 V, -1.8 V, and -1.8 V for **P1**, **P2**, and **P3** respectively. These reduction potentials translate to EAs of 2.9 eV, 3.0 eV, and 3.0 eV which are lower than the homopolymer poly(9,9-dihexylfluorene-2,7-vinylene), which has an EA of 2.7 eV,[12] a consequence of incorporating the benzobisthiazole moiety into the conjugated backbone. The polymers did not show oxidative reversibility but gave onsets of 0.7 V, 0.8 V, and 0.7 V for **P1**, **P2**, and **P3,** which corresponds to IPs of 5.5 eV, 5.6 eV, and 5.5 eV, respectively. Both the EAs and IPs of these polymers are higher than the structurally analogous poly[(9,9-dioctylfluorene-2,7-vinylene)-*alt*-benzo[1,2-*d*;4,5-*d'*]bisoxazole-2,6-diyl] (PFVBBO) (EA = 2.87 eV, IP = 5.36 eV) which has oxygen atoms in place of sulfur in the backbone.[35] The higher EAs are the result of increased acceptor strength of benzobisthiazole due to d-orbital contributions. The higher IPs are a consequence of the increased aromaticity of the thiazole ring over the oxazole, which stabilizes the HOMOs of **P1-3**.[33] The resulting electrochemical band gaps are in close agreement with the optical band gaps and these results are

**Table 3.3.** Photoluminescence Decay Lifetimes (τ) and Quantum Yields (Φ).

| | Solution[a] | | Thin Film | |
|---|---|---|---|---|
| Polymer | τ (ns)[b] | Φ | τ (ns)[b] | Φ |
| P1 | 0.47 | 0.54 | 0.12 | < 0.01 |
| P2 | 0.46 | 0.62 | 0.15 | < 0.01 |
| P3 | 0.60 | 0.56 | 0.07 | < 0.01 |

[a]Taken in dilute chloroform solutions. [b]Photoluminescence decay lifetimes were obtained using a triexponential decay fit.

further evidence that the alkyl chain substitution has no impact on the electronic properties of these polymers.

The photoluminescence decay lifetimes of the polymers were measured both in dilute solutions and thin films and results summarized in Table 3.3. In solution, the polymers show relatively short lifetimes of 0.46-0.60 ns but are comparable to the previously mentioned PFVBBO polymer which had a PL decay lifetime of 0.51 ns.[35] In films, the lifetimes for PL decay were even shorter (0.07-0.15 ns) due to excimer formation within the film creating non-radiative decay pathways, thus quenching film fluorescence. **P3** showed a much larger drop off in decay lifetimes than **P1** and **P2**, which can be attributed to the greater extent of aggregation in the **P3** film. The decay rate for **P1** in film is identical to that of the structurally analogous PFVBBO (also 0.12 ns), which suggests replacing the oxygen atoms in PFVBBO with sulfur atoms does not affect PL decay.

Photoluminescence quantum yields were measured for all three polymers and it was found that in solution all of the polymers were efficient fluorophores with yields between 0.54-0.62. In solution the alkyl chain substitution did not have a significant impact on quantum yield and all three polymers had yields similar to that of PFVBBO (Φ = 0.68). In thin films, as seen with the PL decay lifetimes, the quantum yield fell to near zero. This is an effect of concentration quenching of the polymers in film and has also been reported for PFVBBO.

**3.4.3 Electroluminescent Devices.** We first examined the use of the polymers as neat emitting layers in PLEDs with the structure ITO/PEDOT:PSS (60 nm)/**P1-P3**/BPhen (40 nm)/LiF (1 nm)/Al (100 nm), where ITO is indium tin oxide, PEDOT:PSS is poly(3,4-ethylenedioxythiophene):poly(4-styrenesulfonate), and BPhen is 4,7-diphenyl-1,10-phenanthroline. However, due to low solid-state quantum yields, electroluminescence was not observed. Due to their high quantum yield in solution, these polymers are good candidates for guest-host PLEDs. We therefore fabricated PLEDs where the polymers were used as low level dopants in poly(*N*-vinylcarbazole) (PVK) matrix. The device architecture was ITO/PEDOT:PSS (60 nm)/PVK:**P1-P3**/BPhen (40 nm)/LiF (1 nm)/Al (100 nm), and the PVK had an average molecular weight 50,000-100,000 g/mol). The devices were optimized by varying the weight percentage (wt%) of **P1**, **P2**, or **P3** in PVK and the properties of the resulting devices are shown in Table 3.4. As the concentration of guest polymer in PVK was increased, overall performance

**Table 3.4.** Device Characteristics of PLEDs Made From Benzobisthiazole Polymers

| Device[a] | | $V_{on}$[b] [V] | Drive Voltage [V] | Current Density [mA/cm$^2$] | Brightness [Cd/m$^2$] | Efficiency [Cd/A, %EQE[c]] | $\lambda_{max}^{EL}$ [nm] | CIE 1931 [x,y] |
|---|---|---|---|---|---|---|---|---|
| Polymer | wt. % | | | | | | | |
| PVK | 0.0 | 4.4 | 9.2 | 303 | 296 | 0.44, 0.76 | 423 | (0.17, 0.07) |
| P1 | 1.0 | 7.3 | 10.8 | 753 | 478 | 0.30, 0.25 | 499, 428 | (0.18, 0.15) |
| | 2.0 | 8.3 | 13.0 | 770 | 289 | 0.24, 0.17 | 499, 425 | (0.19, 0.20) |
| | 4.0 | 9.4 | 17.6 | 543 | 195 | 0.14, 0.08 | 499, 427 | (0.20, 0.25) |
| P2 | 1.0 | 7.4 | 11.2 | 392 | 478 | 0.61, 0.45 | 502, 429 | (0.19, 0.18) |
| | 2.0 | 8.7 | 13.4 | 377 | 452 | 0.35, 0.20 | 504, 428 | (0.22, 0.27) |
| | 4.0 | 7.8 | 12.8 | 377 | 323 | 0.21, 0.12 | 505, 429 | (0.24, 0.31) |
| P3 | 1.0 | 6.6 | 9.8 | 358 | 199 | 0.25, 0.35 | ---, 429 | (0.17, 0.08) |
| | 2.0 | 6.4 | 10.2 | 240 | 208 | 0.22, 0.29 | ---, 429 | (0.17, 0.09) |
| | 4.0 | 7.0 | 10.8 | 311 | 213 | 0.19, 0.22 | 495, 427 | (0.17, 0.11) |

[a] Device structure: ITO/PEDOT:PSS/PVK:(**P1**, **P2**, or **P3**)/BPhen/LiF/Al. Wt% is weight percent of polymer in PVK. [b] Turn-on voltage (at which EL is visible to the eyes). [c] EQE = external quantum efficiency.

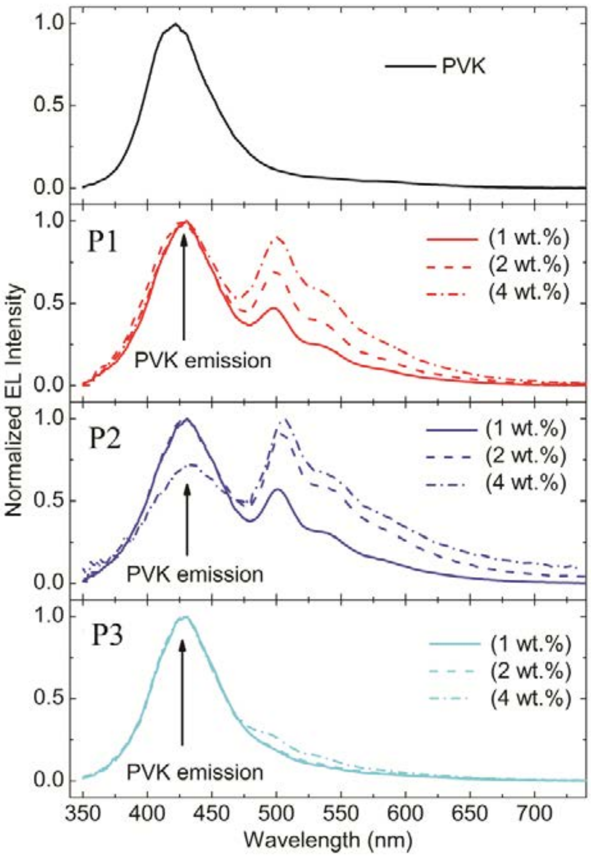

**Figure 3.2.** Electroluminescent spectra of the benzobisthiazole polymers in PLEDs.

decreased with the most efficient devices made from 1 wt% polymer guest in PVK. Concentration quenching was particularly evident in the devices containing **P3**, which didn't show significant emission from the guest at any concentration. The device containing 1 wt% of **P2** in PVK exhibited the best efficiency at 0.61 Cd/A with a brightness of 478 Cd/m$^2$. This efficiency is higher than the 0.25 Cd/A obtained from a similar device containing PFVBBO.[35] The improved efficiency over PFVBBO can be attributed to the higher EA of **P2**, which may improve the electron injection and transport, leading to a higher population of electron charge carriers in the device.

Still, the overall efficiencies of these devices are low and the electroluminescence spectra of the polymers (Figure 3.2) suggest a possible reason for this. In all of the devices, PVK emission at ~425 nm dominates the spectrum, overshadowing the guest emission at ~500 nm, which implies inefficient Förster resonance energy transfer between the host and guest. The degree of energy transfer depends on the overlap of the host's emission spectrum with the guest's absorption band.[48] Because these polymers have absorptions much more red-shifted (~480 nm) than PVK emission (~425 nm), there is poor spectral overlap between the two. This results in a decrease in guest emission and a reduction in overall device performance. These materials could benefit from using a host with a narrower band gap that would give better spectral overlap, improving the energy transfer.

## 3.5 CONCLUSIONS

In summary, three new solution-processible benzobisthiazole-fluorene–containing polymers were synthesized via Horner-Wadsworth-Emmons condensation polymerization. The optical and electrochemical properties of the polymers showed that incorporation of the benzobisthiazole moiety increased their electron affinities relative to fluorene homopolymers. Changing the alkyl chains on the fluorene units did not lead to a change in the electronic properties of the materials but did improve the solubility of the polymers in organic solvents while maintaining high thermal stabilities. Preliminary electroluminescent devices made from these polymers showed promising brightness with modest efficiencies. These results demonstrate the potential benzobisthiazoles have for designing electron deficient emissive materials for PLEDs.

## 3.6 ACKNOWLEDGEMENTS

We thank the 3M Foundation, the National Science Foundation (DMR-0846607), and Iowa State University for financial support of this work. Partial support for this work was provided by the Director for Energy Research, Office of Basic Energy Sciences, USDOE. Ames Laboratory is operated by Iowa State University for the US Department of Energy (USDOE) under Contract No. DE-AC 02-07CH11358. The authors also thank Dr. Kamel Harrata and the Mass Spectroscopy Laboratory of Iowa State University for analysis of our compounds and Dr. Jacob Petrich for use of equipment for fluorescence lifetime measurements.

## 3.7 SUPPORTING INFORMATION

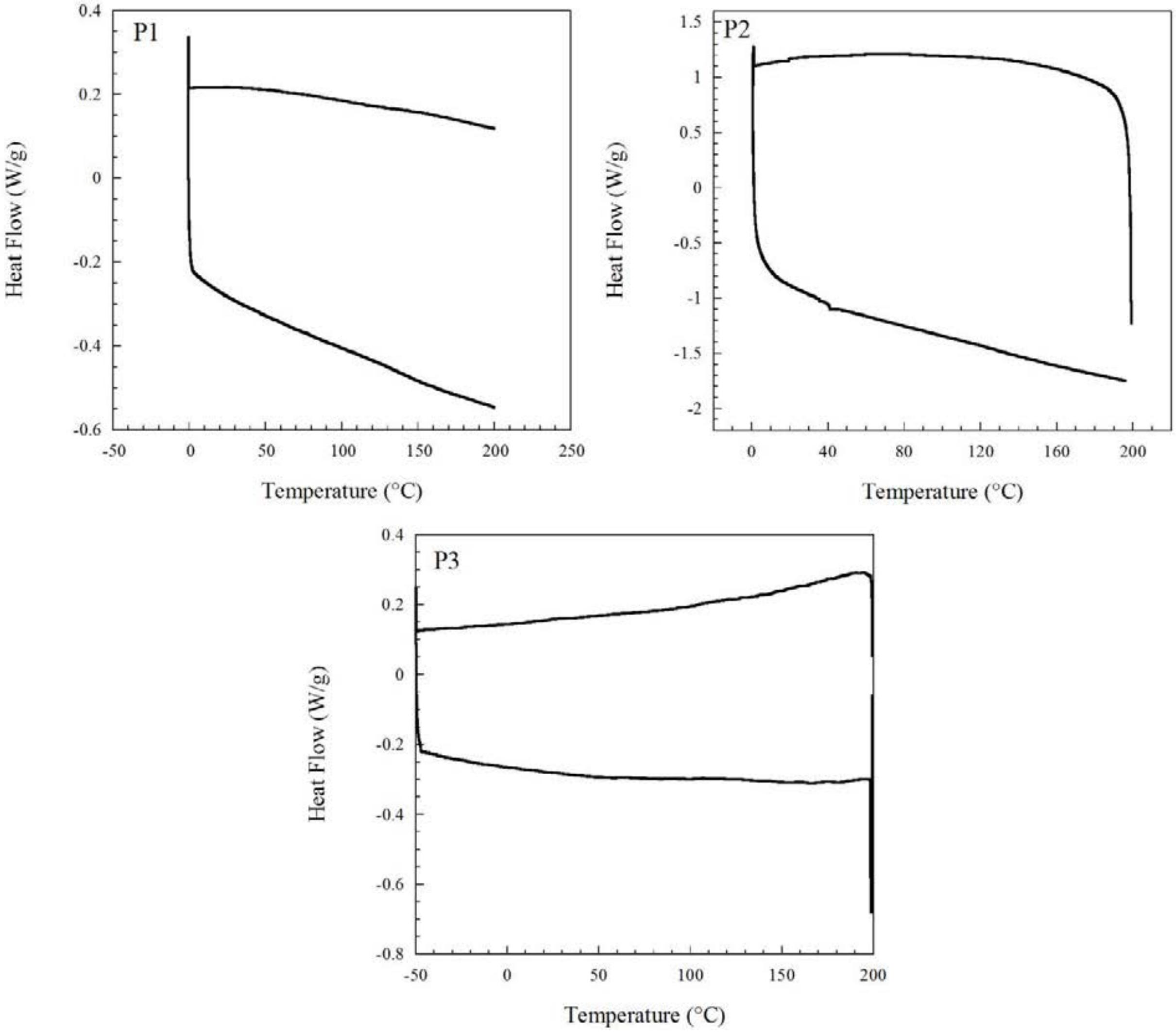

**Figure S3.1.** Differential scanning calorimetry plots of polymers P1, P2, and P3.

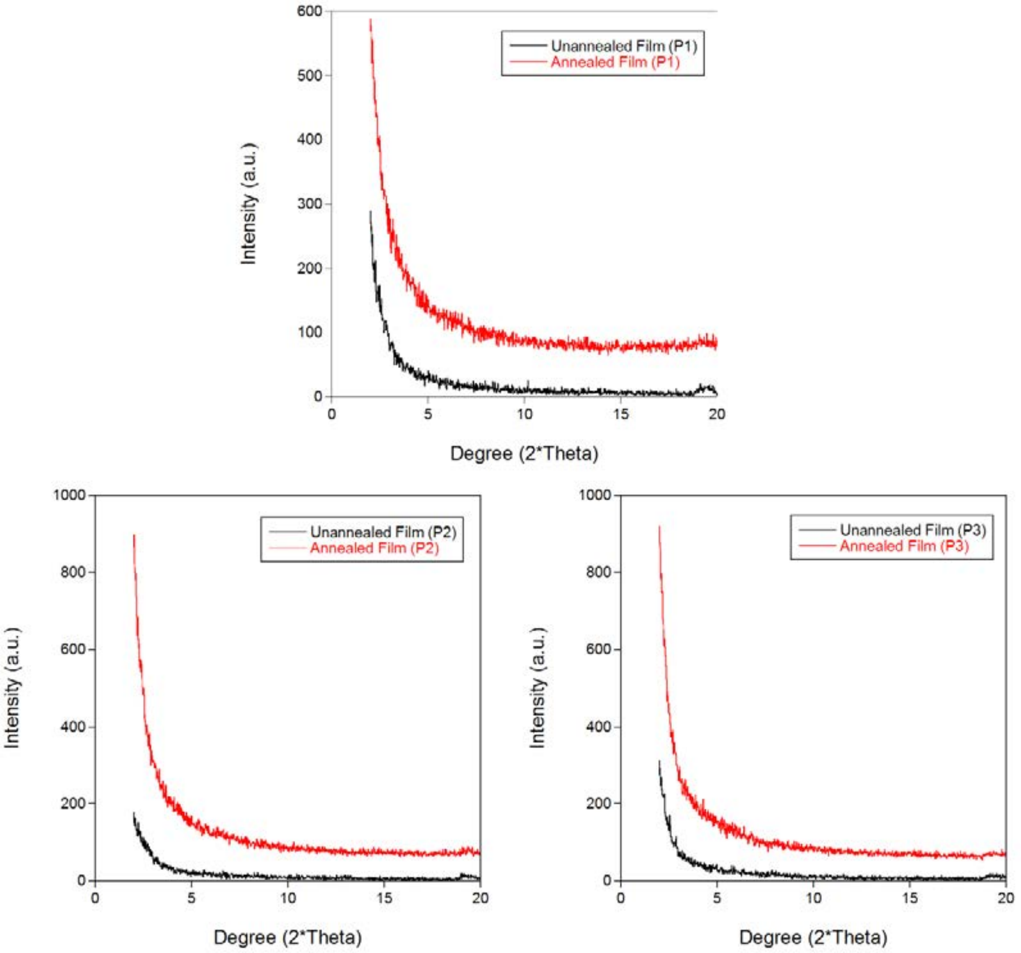

**Figure S3.2.** X-ray defraction plots for P1 (top), P2 (bottom left), and P3 (bottom right).

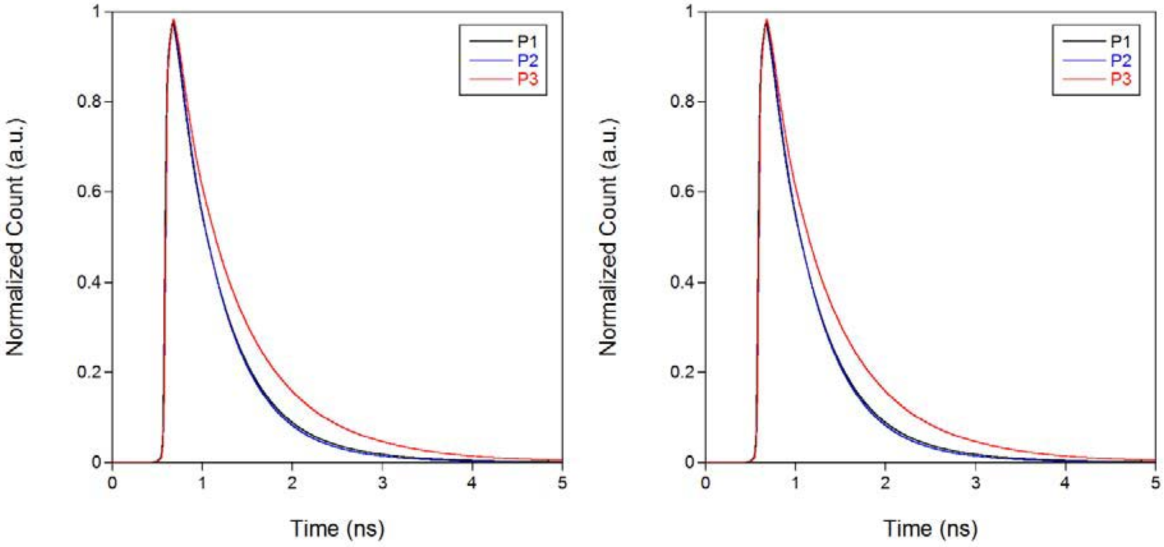

**Figure S3.3.** Photoluminescence decay lifetime plots for polymers in solution (left) and film (right).

للاستشارات المنارة

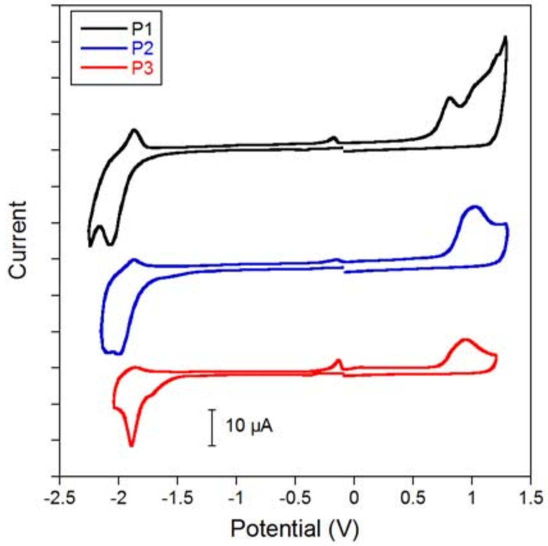

**Firgure S3.4.** Cyclic Voltammetry traces of **P1**, **P2**, and **P3** films cast on platinum electrodes using a Ag/Ag$^+$ reference electrode, platinum counter electrode, and 0.1M $Bu_4NPF_6$ electrolyte in acetonitrile under an argon atmosphere. Readings taken with a 100 mV/s scan rate and referenced to Fc/Fc$^+$.

**Table S3.1.** Photoluminescence decay lifetime data for polymers in solution and film.

| Solution | | | | |
|---|---|---|---|---|
| Polymer | $\tau_1$ (ps), [$A_1$][a] | $\tau_1$ (ps), [$A_1$][a] | $\tau_1$ (ps), [$A_1$][a] | $\tau$ (ps)[b] |
| P1 | 100 [12%] | 486 [80%] | 967 [8%] | 470 |
| P2 | 110 [13%] | 470 [69%] | 680 [18%] | 460 |
| P3 | 170 [27%] | 700 [67%] | 1300 [6%] | 600 |
| Thin Film | | | | |
| P1 | 37 [77%] | 220 [18%] | 1100 [5%] | 120 |
| P2 | 46 [75%] | 280 [19%] | 1100 [6%] | 150 |
| P3 | 27 [90%] | 280 [7%] | 960 [3%] | 70 |

[a] A1, A2, and A3 represent the % applitude of the lifetime. [b] Average PL decay lifetime determined by full width at half max.

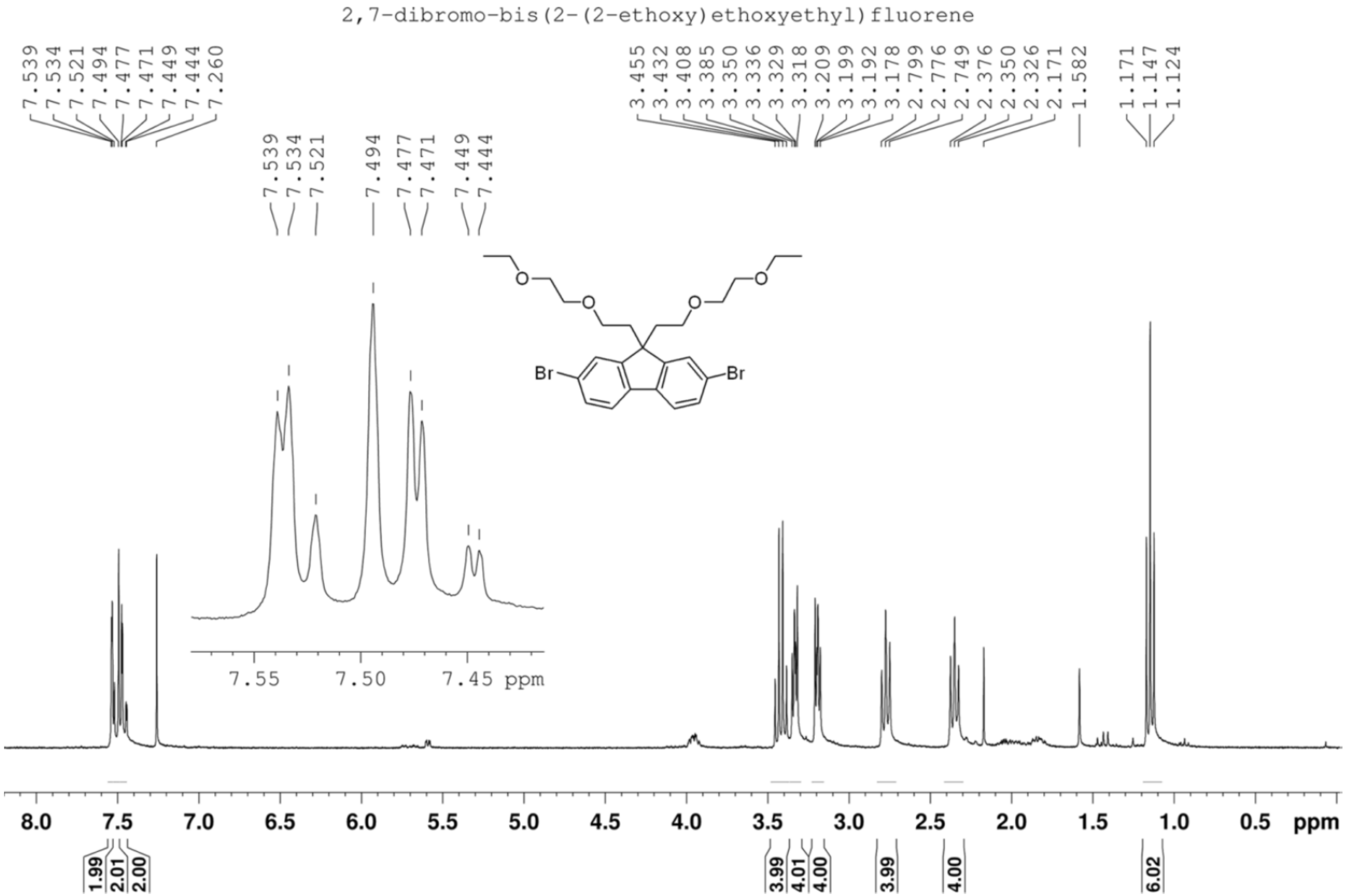

**Figure S3.5.** $^1$H NMR Spectrum of 2,7-dibromo-9,9-bis(2-(2-ethoxy)ethoxyethyl)fluorene

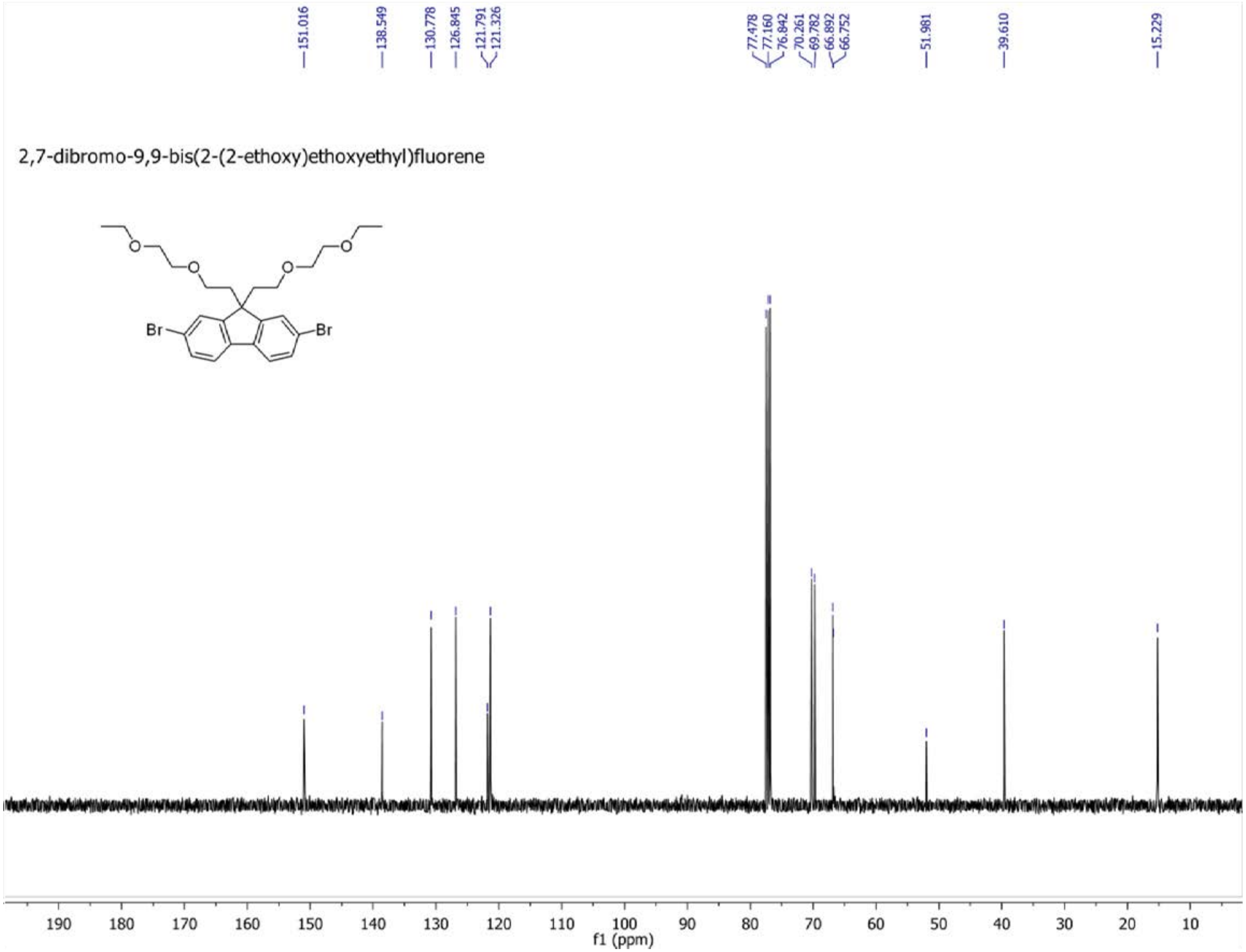

**Figure S3.6.** $^{13}$C NMR spectrum of 2,7-dibromo-9,9-bis(2-(2-ethoxy)ethoxyethyl)fluorene.

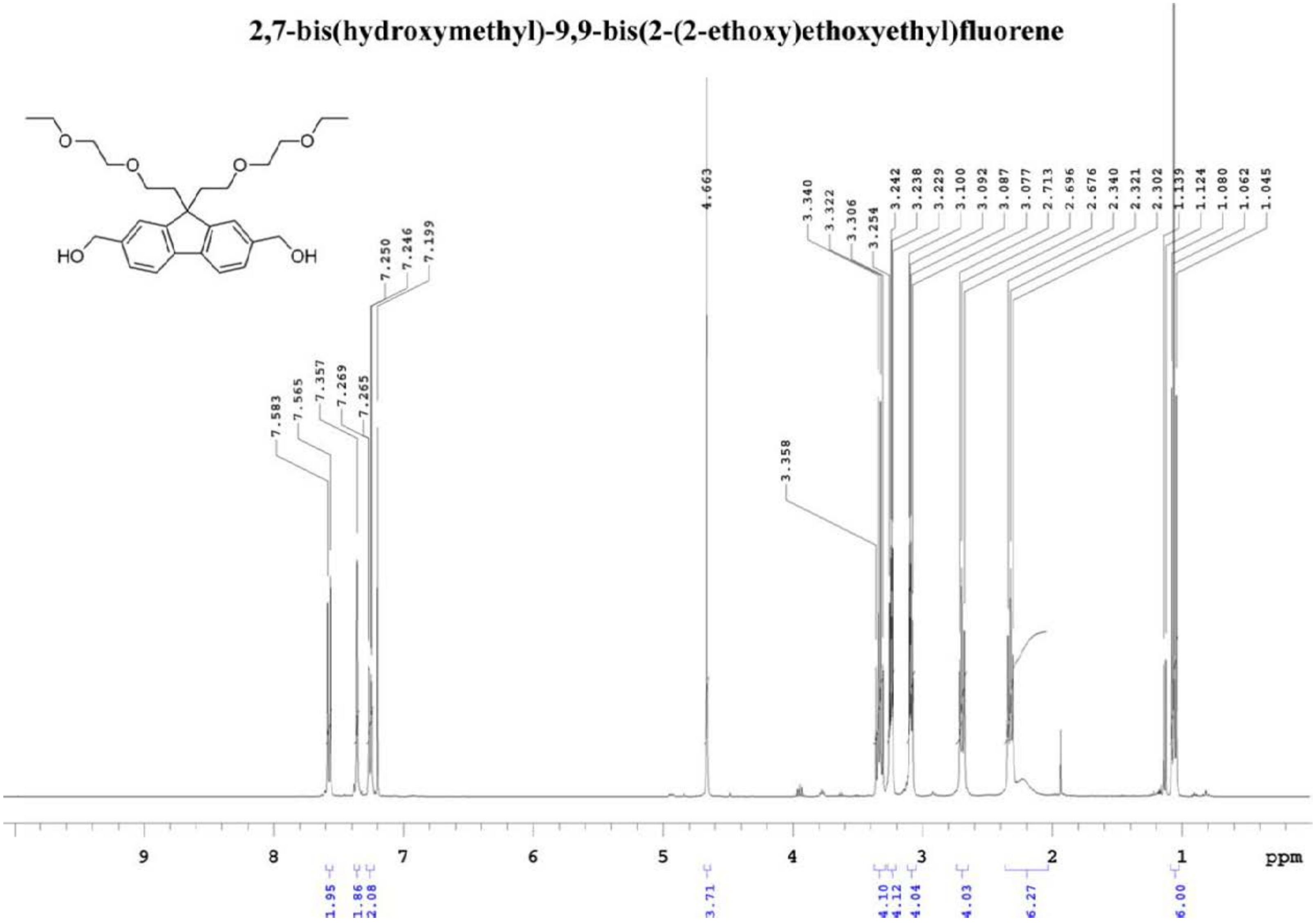

2,7-bis(hydroxymethyl)-9,9-bis(2-(2-ethoxy)ethoxyethyl)fluorene

**Figure S3.7.** $^1$H NMR spectrum of 2,7-bis(hydroxymethyl)-9,9-bis(2-(2-ethoxy)ethoxyethyl)fluorene.

**2,7-bis(hydroxymethyl)-9,9-bis(2-(2-ethoxy)rthoxyethyl)fluorene**

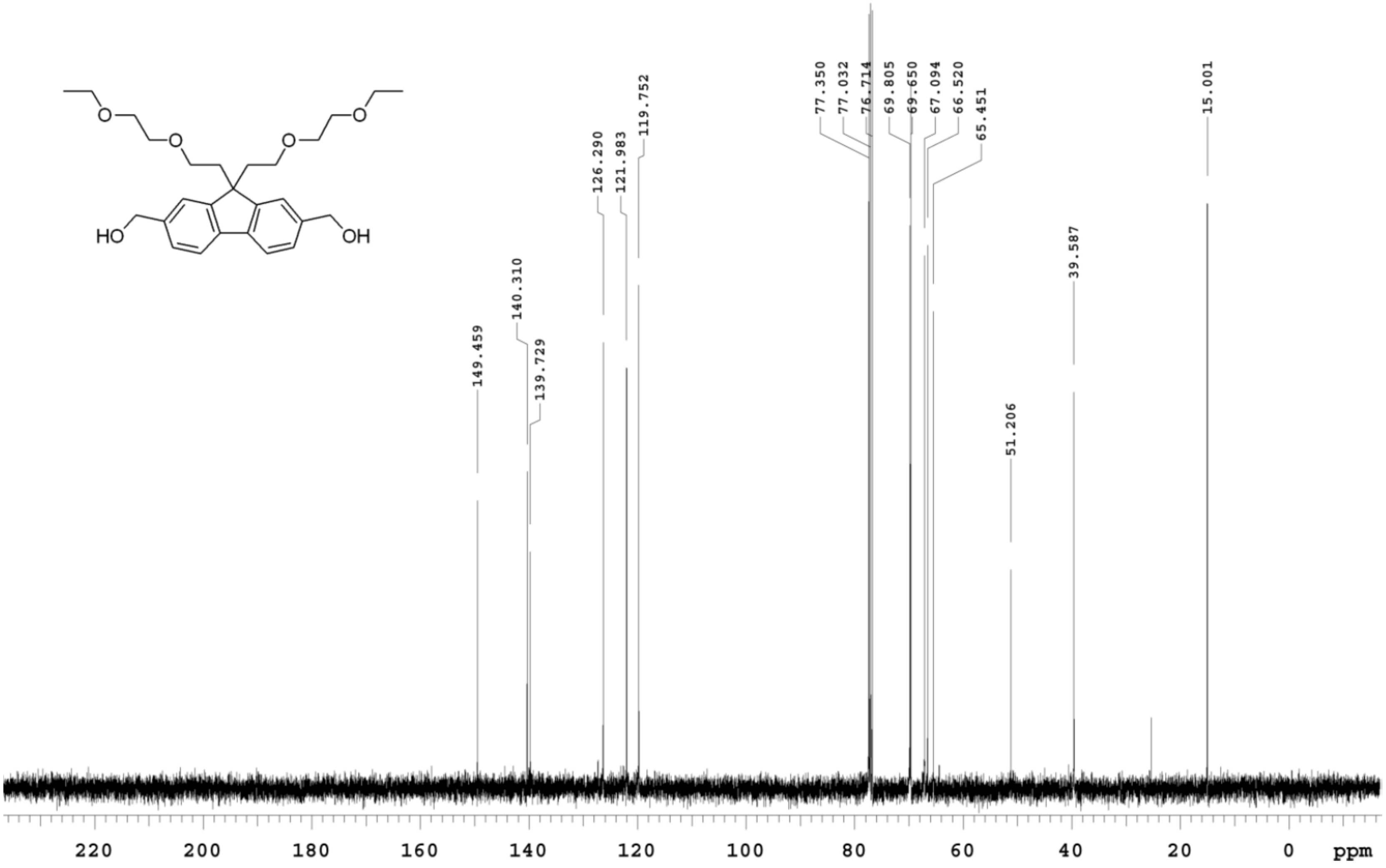

**Figure S3.8.** $^{13}$C NMR spectrum of 2,7-bis(hydroxymethyl)-9,9-bis(2-(2-ethoxy)ethoxyethyl)fluorene.

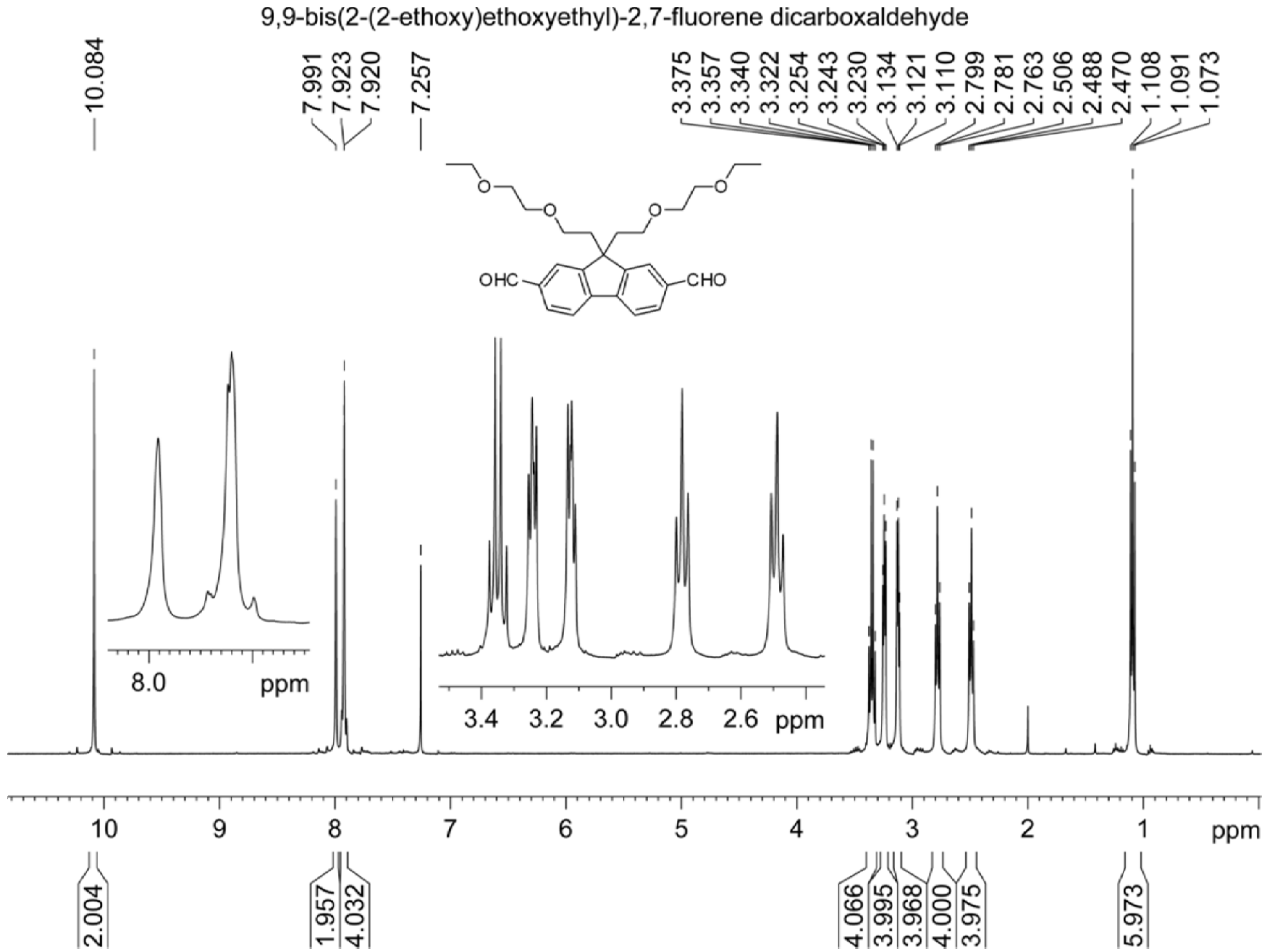

**Figure S3.9.** $^1$H NMR spectrum of 2c.

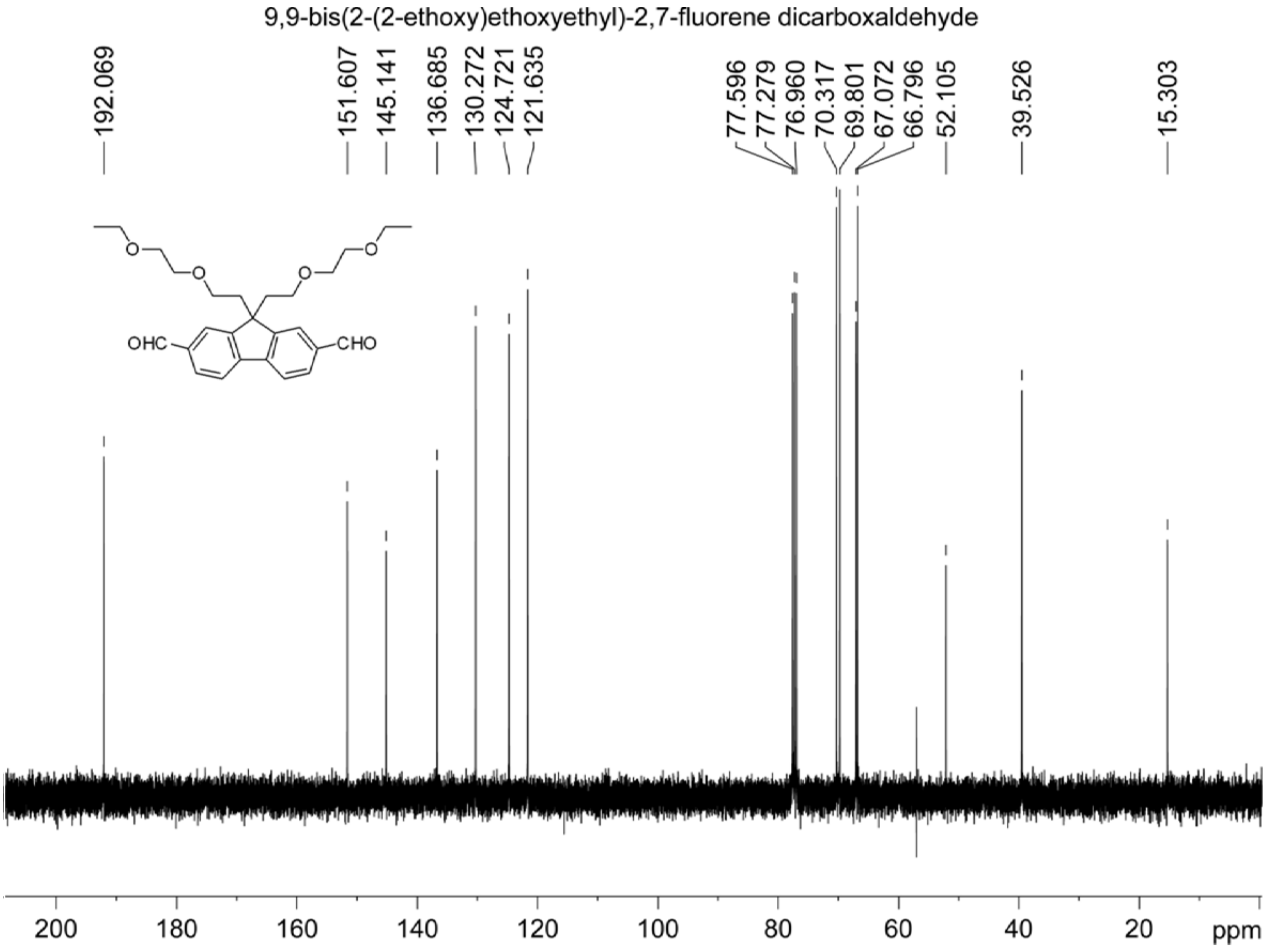

**Figure S3.10.** $^{13}$C NMR spectrum of 2c.

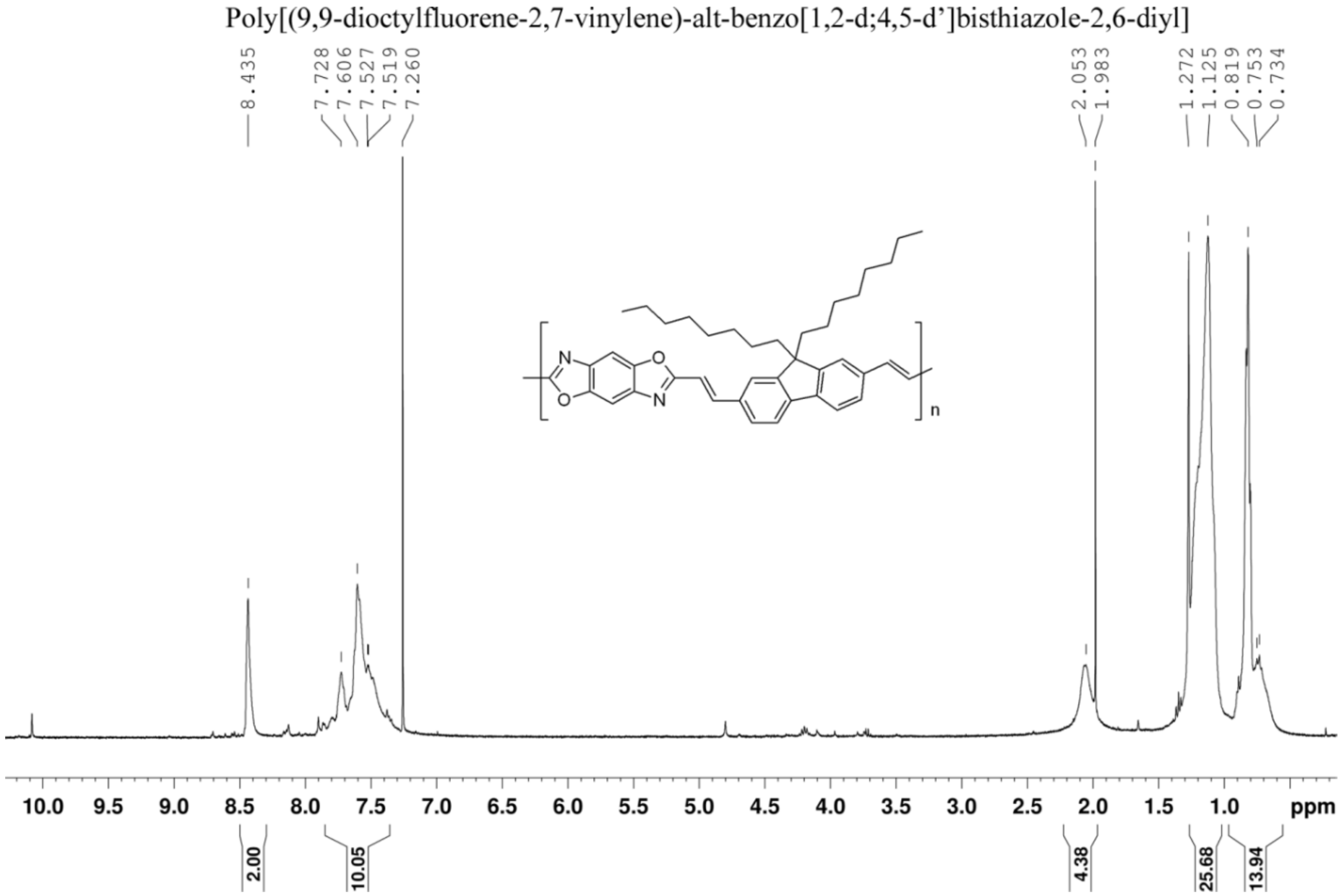

**Figure S3.11.** $^1$H NMR spectrum of P1.

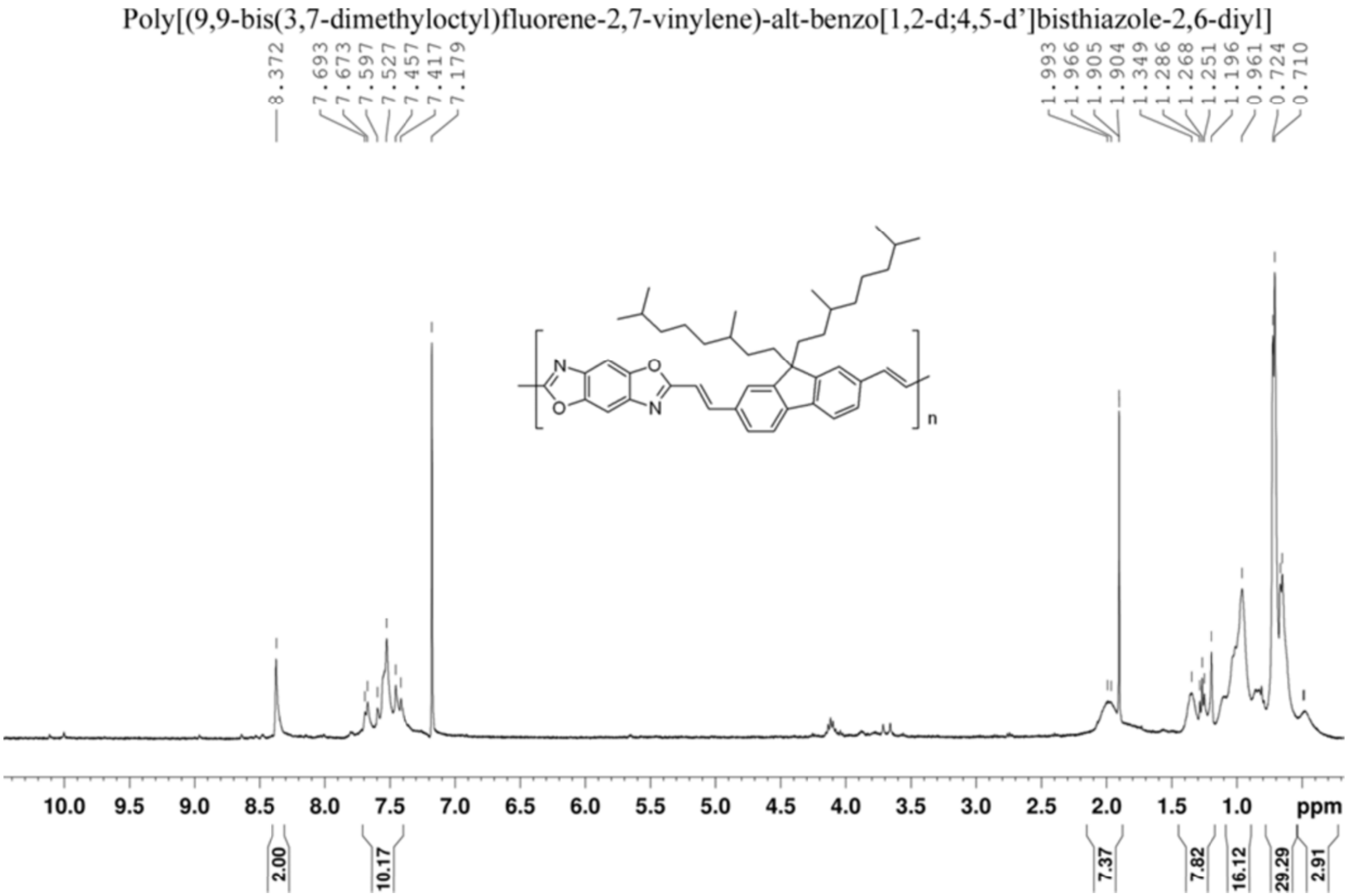

**Figure S3.12.** $^1$H NMR spectrum of P2.

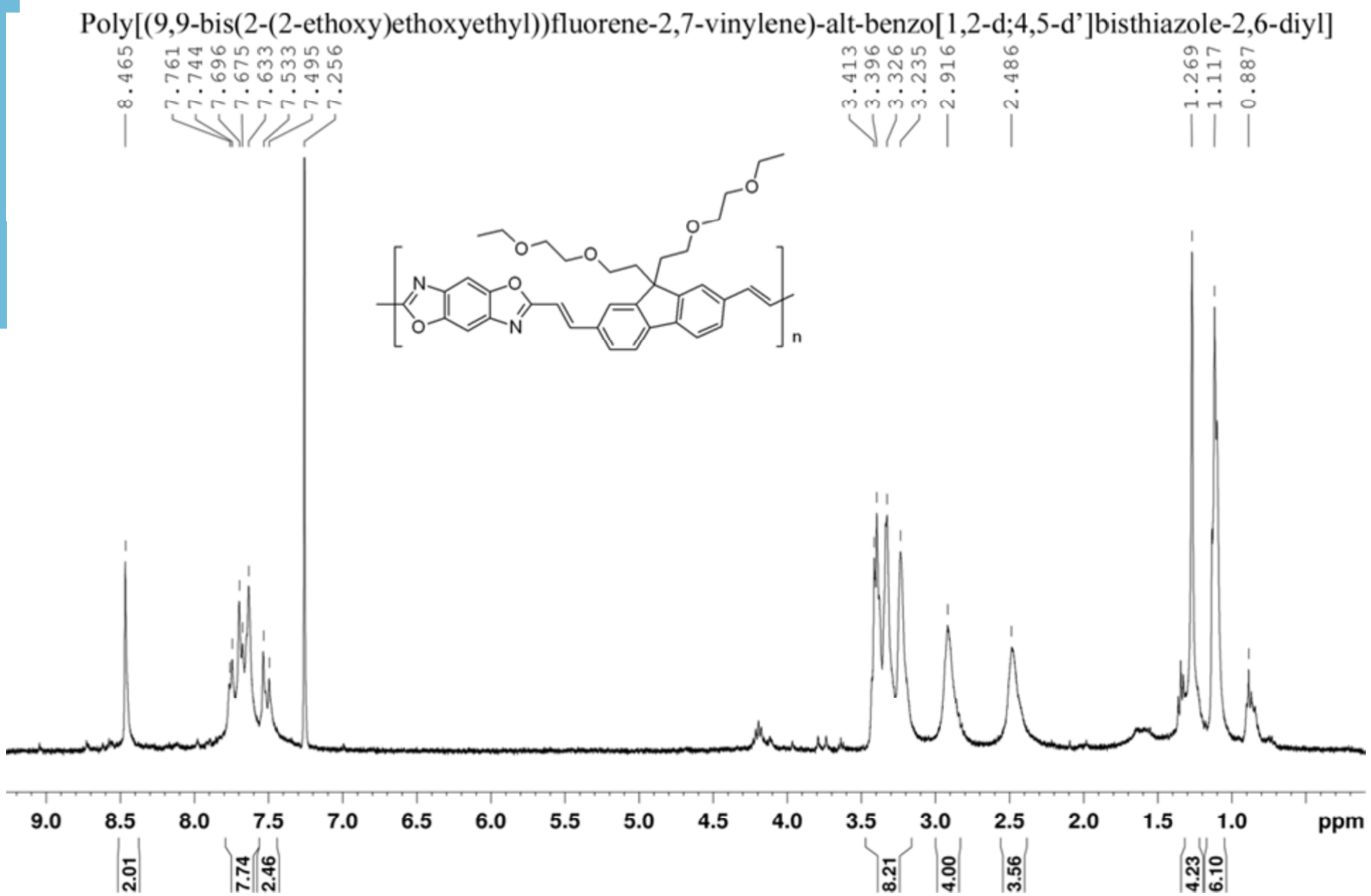

**Figure S3.13.** $^1$H NMR spectrum of P3.

## 3.8 REFERENCES

1. Friend, R. H.; Gymer, R. W.; Holmes, A. B.; Burroughes, J. H.; Marks, R. N.; Taliani, C.; Bradley, D. D. C.; Dos Santos, D. A.; Bredas, J. L.; Logdlund, M.; Salaneck, W. R. *Nature* **1999,** 397, (6715), 121-128.

2. Tang, C.W.; VanSlyke, S.A. *Appl. Phys. Lett.* **1987,** 51, (12), 913-915.

3. Scharber, Markus C.; Muehlbacher, David; Koppe, Markus; Denk, Patrick; Waldauf, Christoph; Heeger, Alan J.; Brabec, Christoph J. *Adv. Mater.* **2006,** 18, (6), 789-794.

4. Thompson, Barry C.; Frechet, Jean M. J. *Angew, Chem. Int. Ed.* **2008,** 47, (1), 58-77.

5. Dimitrakopoulos, C.D.; Malenfant, P.R.L. *Adv. Mater.* **2002,** 14, (2), 99-117.

6. Osaka, Itaru; Zhang, Rui; Sauve, Genevieve; Smilgies, Detlef- M.; Kowalewski, Tomasz; McCullough, Richard D. *J. Am. Chem. Soc.* **2009,** 131, (7), 2521-2529.

7. Burroughes, J. H.; Bradley, D. D. C.; Brown, A. R.; Marks, R. N.; Mackay, K.; Friend, R. H.; Burns, P. L.; Holmes, A. B. *Nature* **1990,** 347, (6293), 539-541.

8. Grimsdale, Andrew C.; Leok Chan, Khai; Martin, Rainer E.; Jokisz, Pawel G.; Holmes, Andrew B. *Chem. Rev.* **2009,** 109, (3), 897-1091.

9. Leclerc, Mario. *J. Polym. Sci., Part A: Polym. Chem.* **2001,** 39, (17), 2867-2873.

10. Kulkarni, Abhishek P.; Kong, Xiangxing; Jenekhe, Samson A. *Macromolecules* **2006,** 39, (25), 8699-8711.

11. Kulkarni, Abhishek P.; Zhu, Yan; Jenekhe, Samson A. *Macromolecules* **2005,** 38, (5), 1553-1563.

12. Jin, Sung-Ho; Park, Hye-Jin; Kim, Jin Young; Lee, Kwanghee; Lee, Sang-Phil; Moon, Doo-Kyung; Lee, Hyung-Jong; Gal, Yeong-Soon. *Macromolecules* **2002,** 35, (20), 7532-7534.

13. Fu, Dian-Kui; Xu, Bing; Swager, Timothy M. *Tetrahedron* **1997,** 53, (45), 15487-15494.

14. Gebler, D. D.; Wang, Y. Z.; Jessen, S. W.; Blatchford, J. W.; MacDiarmid, A. G.; Swager, T. M.; Fu, D. K.; Epstein, A. J. *Synth. Met.* **1997,** 85, (1-3), 1205-1208.

15. Mikroyannidis, John A. ; Fakis, Mihalis; Spiliopoulos, Ioakim K. . *J. Poly. Sci. A.* **2009,** 47, (13), 3370-3379.

16. Mikroyannidis, J. A.; Gibbons, K. M.; Kulkarni, A. P.; Jenekhe, S. A. *Macromolecules* **2008,** 41, (3), 663-674.

17. Mikroyannidis, John A.; Spiliopoulos, Ioakim K.; Kasimis, Theodoros S.; Kulkarni, Abhishek P.; Jenekhe, Samson A. *Macromolecules* **2003,** 36, (25), 9295-9302.

18. Zhan, Xiaowei; Liu, Yunqi; Wu, Xia; Wang, Shuai; Zhu, Daoben. *Macromolecules* **2002,** 35, (7), 2529-2537.

19. Grisorio, Roberto; Piliego, Claudia; Cosma, Pinalysa; Fini, Paola; Mastrorilli, Piero; Gigli, Giuseppe; Suranna, Gian Paolo; Nobile, Cosimo Francesco. *J. Poly. Sci. A.* **2009,** 47, (8), 2093-2104.

20. Osaheni, John A.; Jenekhe, Samson A. *Chem. Mater.* **1992,** 4, (6), 1282-1290.

21. Reinhardt, B.A.; Unroe, M.R.; Evers, R.C. *Chem. Mater.* **1991,** 3, 864-871.

22. Belfield, Kevin D.; Yao, Sheng; Morales, Alma R.; Hales, Joel M.; Hagan, David J.; Van Stryland, Eric W.; Chapela, Victor M.; Percino, Judith. *Polym. Adv. Technol.* **2005,** 16, (2-3), 150-155.

23. Ahmed, Eilaf; Kim, Felix S.; Xin, Hao; Jenekhe, Samson A. *Macromolecules* **2009,** 42, (22), 8615-8618.

24. Ahmed, Eilaf; Subramaniyan, Selvam; Kim, Felix S.; Xin, Hao; Jenekhe, Samson A. *Macromolecules* **2011,** 44, (18), 7207-7219.

25. Osaka, Itaru; Takimiya, Kazuo; McCullough, Richard D. *Adv. Mater.* **2010,** 22, (44), 4993-4997.

26. Pang, Hao; Vilela, Filipe; Skabara, Peter J.; McDouall, Joseph J. W.; Crouch, David J.; Anthopoulos, Thomas D.; Bradley, Donal D. C.; de Leeuw, Dago M.; Horton, Peter N.; Hursthouse, Michael B. *Adv. Mater.* **2007,** 19, (24), 4438-4442.

27. McEntee, Greg J.; Vilela, Filipe; Skabara, Peter J.; Anthopoulos, Thomas D.; Labram, John G.; Tierney, Steve; Harrington, Ross W.; Clegg, William. *J. Mater. Chem.* **2011,** 21, (7), 2091-2097.

28. Mamada, Masashi; Nishida, Jun-ichi; Tokito, Shizuo; Yamashita, Yoshiro. *Chem. Lett.* **2008,** 37, (7), 766-767.

29. Babel, Amit; Jenekhe, Samson A. *J. Phys. Chem. B.* **2002,** 106, (24), 6129-6132.

30. Osaheni, John A.; Jenekhe, Samson A. *Macromolecules* **1993,** 26, (17), 4726-4728.

31. Alam, Maksudul M.; Jenekhe, Samson A. *Chem. Mater.* **2002,** 14, (11), 4775-4780.

32. Jenekhe, Samson A.; Yi, Shujian. *Appl. Phys. Lett.* **2000,** 77, (17), 2635-2637.

33. Bhuwalka, Achala; Mike, Jared F.; He, Meng; Intemann, Jeremy J.; Nelson, Toby; Ewan, Monique D.; Roggers, Robert A.; Lin, Zhiqun; Jeffries-El, Malika. *Macromolecules* **2011**.

34. Mike, Jared F.; Inteman, Jeremy J.; Ellern, Arkady; Jeffries-El, Malika. *J. Org. Chem.* **2010,** 75, (2), 495-497.

35. Intemann, Jeremy J.; Mike, Jared F.; Cai, Min; Bose, Sayantan; Xiao, Teng; Mauldin, Timothy C.; Roggers, Robert A.; Shinar, Joseph; Shinar, Ruth; Jeffries-El, Malika. *Macromolecules* **2011,** 44, (2), 248-255.

36. Hung, Ming-Chin; Liao, Jin-Long; Chen, Show-An; Chen, Su-Hua; Su, An-Chung. *J. Am. Chem. Soc.* **2005,** 127, (42), 14576-14577.

37. Kim, In-Hae; Tsai, Hsing-Ju; Nishi, Kosuke; Kasagami, Takeo; Morisseau, Christophe; Hammock, Bruce D. *J. Med. Chem.* **2007,** 50, (21), 5217-5226.

38. Potemkin, Igor I.; Busch, Peter; Smilgies, Detlef- M.; Posselt, Dorthe; Papadakis, Christine M. *Macromol. Rapid Commun.* **2007,** 28, (5), 579-584.

39. de Mello, John C.; Wittmann, H. Felix; Friend, Richard H. *Adv. Mater.* **1997,** 9, (3), 230-232.

40. Marchioni, F.; Chiechi, R.; Patil, S.; Wudl, F.; Chen, Y.; Shinar, J. *Appl. Phys. Lett.* **2006,** 89, (6), 061101-061103.

41. Anuragudom, Piched; Newaz, S. S.; Phanichphant, Sukon; Lee, T. Randall. *Macromolecules* **2006,** 39, (10), 3494-3499.

42. Kannan, Ramamurthi; He, Guang S.; Lin, Tzu-Chau; Prasad, Paras N.; Vaia, Richard A.; Tan, Loon-Seng. *Chem. Mater.* **2004,** 16, (1), 185-194.

43. Craig, Michael R.; Kok, Margreet M. de; Hofstraat, Johannes W.; Schenning, Albertus P. H. J.; Meijer, E. W. *J. Mater. Chem.* **2003,** 13, (12), 2861-2862.

44. Cho, Sung Yong; Grimsdale, Andrew C.; Jones, David J.; Watkins, Scott E.; Holmes, Andrew B. *J. Am. Chem. Soc.* **2007,** 129, (39), 11910-11911.

45. Anuragudom, Piched; Newaz, S. S.; Phanichphant, Sukon; Lee, T. Randall. *Macromolecules* **2006,** 39, (10), 3494-3499.

46. Tonzola, Christopher J.; Alam, Maksudul M.; Jenekhe, Samson A. *Macromolecules* **2005,** 38, (23), 9539-9547.

47. Jenekhe, Samson A.; Osaheni, John A. *Science* **1994,** 265, (5173), 765-768.

48. Cheon, K. O.; Shinar, J. *Appl. Phys. Lett.* **2004,** 84, (7), 1201-1203.

# Chapter 4

## Improving the Performance of Benzobisoxazole-Containing Polymers in Organic Light Emitting Diodes by Altering the Conjugation Pathway

*Jeremy J. Intemann*[1], *Emily S. Hellerich*[2], *Brian C. Tlach*[1], *Monique D. Ewan*[1], *Charles A. Barnes*[1], *Joseph Shinar*[2], *Ruth Shinar*[3], and *Malika Jeffries-EL*[1]*

[1]Department of Chemistry, Iowa State University, Ames, IA 50011 (USA)
[2]Ames Laboratory-USDOE and Department of Physics and Astronomy, Iowa State University, Ames, IA 50011 (USA)
[3]Microelectronics Research Center and Department of Electrical and Computer Engineering, Iowa State University, Ames, IA 5011 (USA)

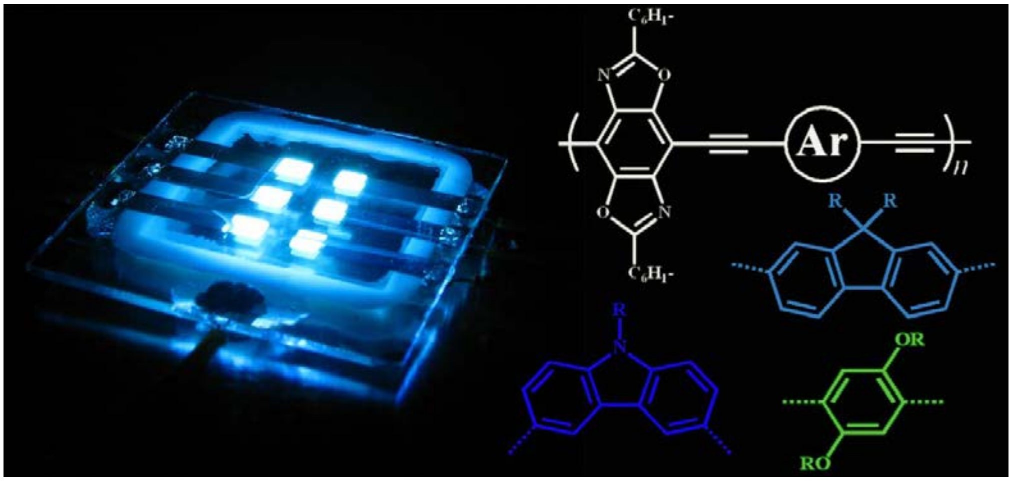

## 4.1 ABSTRACT

We report the synthesis and electroluminescent properties of a new class of poly(benzobisoxazoles) (PBOs) in which the conjugation pathway is directly through the central benzene ring. Like traditional PBOs, where the conjugation pathway is through the oxazole rings, these materials also possess high electron affinities. However, these new PBOs exhibit superior Förster resonance energy transfer in guest-host organic light emitting diodes (OLEDs), resulting in much higher efficiencies than previously seen in any PBOs. Six PBO copolymers

containing N-alkylcarbazole, 9,9-dialkylfluorene, and 2,5-dialkoxyphenylene were synthesized and their properties investigated. The resulting materials were also used as guests in guest-host OLEDs. Devices containing carbazole or fluorene polymers gave rise to blue emission (446-463 nm) with brightness as high as 2020 Cd $m^{-2}$ and luminous efficiencies as high as 3.43 Cd $A^{-1}$. Devices made with the phenylene polymers provide green emission (491-519 nm) and displayed brightness of nearly 3400 Cd $m^{-2}$ and efficiencies as high as 5.7 Cd $A^{-1}$ These results represent a significant improvement over the performance of previously reported PBOs indicating that the conjugation pathway plays a critical role in designing emissive materials for guest-host OLEDs.

## 4.2 INTRODUCTION

Organic light-emitting diodes (OLEDs) are an evolving technology for use in solid state lighting and flat panel display applications.[1-3] Polymer OLEDs (PLEDs) have several advantages over other OLED-based display technologies such as low cost processing via solution based inkjet printing.[4, 5] In the two decades since PLEDs were first reported,[6] research has been aimed at developing polymers with efficient and stable red, green, and blue emission required for displays.[7] Unfortunately, most emissive conjugated polymers have low electron affinities that diminish the electron mobilities in films. Because these materials also have higher hole mobilities, an imbalance in charge injection and carrier mobilities occurs within the device, reducing efficiencies and overall performance.[8, 9]

Various strategies have been developed to overcome these limitations including the fabrication of multilayer devices containing an electron transport layer and the use of low-work function electrodes, such as calcium[10], and alkali fluoride buffer layers to improve electron injection.[11] Alternatively, electron deficient moieties can be incorporated into the backbone of the emissive polymer resulting in increased electron affinities, potentially improving electron injection and transport.[12-17] For these reasons benzobisoxazoles (BBOs) are promising building blocks in semiconducting polymers as they increase the electron affinities,[16] electron transport,[10, 18-20] photoluminescence (PL),[21, 22] and thermal stability[23, 24] of materials containing them. We recently reported several poly(9,9-dialkylfluorenevinylenes) containing benzobisoxazole[25, 26] which exhibited reversible reduction processes and stable blue electroluminescence (EL) at 470 nm with luminous efficiencies up to 0.93 Cd $A^{-1}$ when used as a guest in a host matrix of poly(N-vinylcarbazole) (PVK). We believe that the performance of these materials in OLEDs was limited due largely to fluorescence quenching caused by aggregation of the polymer in the PVK matrix. The aggregation may be the result of the large extended π-system of the BBO moiety and a limited number of side chains per repeat unit to disrupt π-stacking. The devices were also plagued by incomplete Förster resonance energy transfer (FRET) between the PVK host and the poly(benzobisoxazole) (PBO) guest, giving rise to substantial host contributions to the emission spectrum.

In order to overcome the limitations of our previous PBOs we developed new PBOs with a conjugation pathway directly through the central benzene ring. This modification resulted in materials that incorporated the beneficial properties of BBOs while allowing for alkyl substitution at the 2 and 6 positions, which can disrupt π-stacking between polymer chains. Herein we report the synthesis, characterization, and PLED performance of six new PBOs, namely poly[(N-octylcarbazole-3,6-ethynylene)-alt-(2,6-dihexylbenzo[1,2-d;4,5-d']bisoxazole-4,8-diyl)] (PBOCz-O), poly[(N-(2-ethylhexyl)carbazole-3,6-ethynylene)-alt-(2,6-dihexylbenzo[1,2-d;4,5-d']bisoxazole-4,8-diyl)] (PBOCz-EH), poly[(9,9-dioctylfluorene-2,7-ethynylene)-alt-(2,6-dihexylbenzo[1,2-d;4,5-d']bisoxazole-4,8-diyl)] (PBOTF-O), poly[(9,9-bis(3,7-dimethyloctyl)fluorene-2,7-ethynylene)-alt-(2,6-dihexylbenzo[1,2-d;4,5-d']bisoxazole-4,8-diyl)] (PBOTF-DMO), poly[(2,5-didodecyloxybenzene-1,4-ethynylene)-alt-(2,6-dihexylbenzo[1,2-d;4,5-d']bisoxazole-4,8-diyl)] (PBOP-D), and poly[(2-(2-ethylhexyloxy)-5-methoxybenzene-1,4-ethynylene)-alt-(2,6-dihexylbenzo[1,2-d;4,5-d']bisoxazole-4,8-diyl)] (PBOP-MEH). The guest-host OLEDs made using these polymers as guests in either a PVK or 4,4'-Bis(N-carbazolyl)-1,1'-biphenyl (CBP) host displayed blue and green EL emission with efficient FRET from host to guest resulting in an emission profile that was virtually free of host contribution. As a result, luminous efficiencies as high as 5.7 Cd $A^{-1}$ were obtained, which is more than a six-fold improvement over our previously reported materials, demonstrating the potential these new PBOs have as emissive materials in guest-host OLEDs.

## 4.3. RESULTS AND DISCUSSION

**4.3.1. Synthesis and Characterization.** The monomer 2,6-dihexyl-4,8-dibromobenzobisoxazole (2) was prepared by the condensation of dibromodiaminohydroquinone (1) with heptanoyl chloride in the presence of poly(trimethylsilylphosphate) (PPSE). This method of BBO synthesis, while less efficient than our previously reported route utilizing orthoesters,[27-29] was necessary due to the unavailability of suitable alkylorthoesters. The synthetic routes to the monomer (2) and corresponding copolymers are outlined in Scheme 4.1. The six new copolymers were made via Sonogashira cross-coupling of monomer (2) with the corresponding dialkynyl comonomer using palladium and copper catalysts in a mixture of diisopropylamine and toluene. These conditions yielded polymers in good yields after removal of lower molecular weight material. All of the polymers were soluble in common organic solvents such as chloroform, THF, and chlorobenzene and the $^1$H NMR spectra were in agreement with the proposed structures for each polymer (see supporting information).

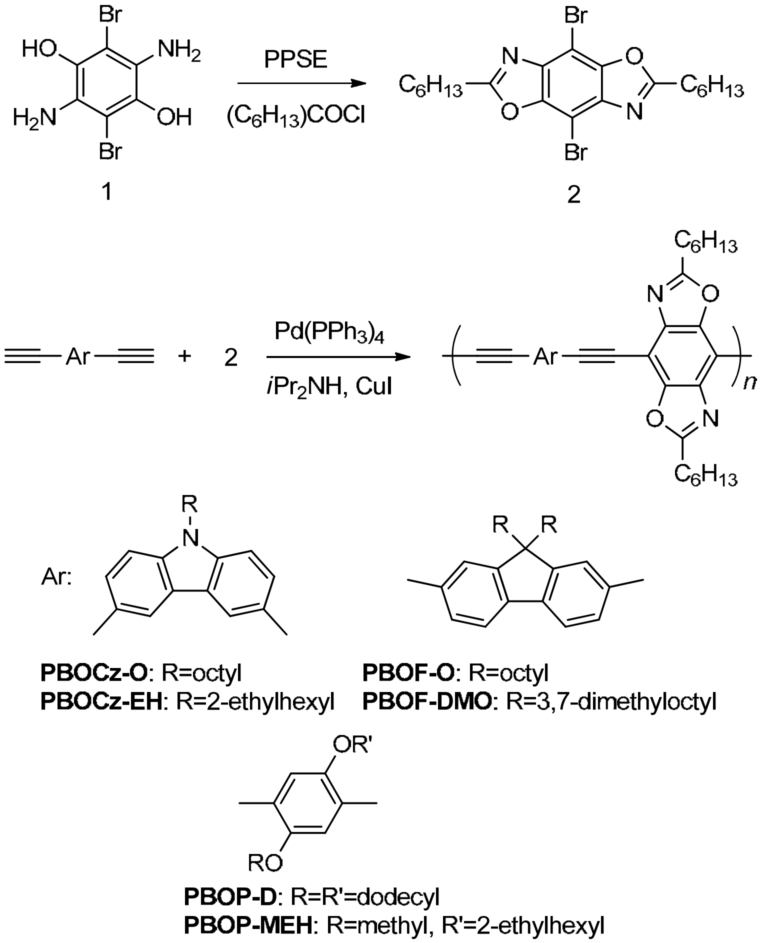
Br
HO
NH2
H2N
OH
Br
1
PPSE
(C6H13)COCl
Br
N
O
C6H13
C6H13
O
N
Br
2
Ar
+
2
Pd(PPh3)4
iPr2NH, CuI
C6H13
N
O
Ar
n
O
N
C6H13
Ar:
R
N
R
R
PBOCz-O: R=octyl
PBOCz-EH: R=2-ethylhexyl
PBOF-O: R=octyl
PBOF-DMO: R=3,7-dimethyloctyl
OR'
RO
PBOP-D: R=R'=dodecyl
PBOP-MEH: R=methyl, R'=2-ethylhexyl

**Scheme 4.1.** Synthesis of benzobisoxazole monomer and poly(aryleneethynylene benzobisoxazoles)

**Table 4.1.** Physical Properties of Benzobisoxazole Polymers

| Polymer | Yield [%] | $M_n$ [kDa][a] | $M_w$ [kDa][a] | PDI | $T_d$ [°C][b] | $T_g$ [°C][c] |
|---|---|---|---|---|---|---|
| **PBOCz-O** | 74 | 13.0 | 23.8 | 1.8 | 354 | 139 |
| **PBOCz-EH** | 95 | 47.9 | 74.9 | 1.6 | 353 | 140 |
| **PBOF-O** | 73 | 38.2 | 145.0 | 3.8 | 352 | 123 |
| **PBOF-DMO** | 49 | 51.9 | 188.3 | 3.6 | 298 | 110 |
| **PBOP-D** | 59 | 33.1 | 45.8 | 1.4 | 320 | n.o. |
| **PBOP-MEH** | 51 | 26.2 | 87.2 | 3.3 | 310 | n.o. |

[a] Determined by GPC in chloroform using polystyrene standards. [b] 5% weight loss temperature by TGA in air. [c] Data from second scan reported, heating rate 15 °C $min^{-1}$ under $N_2$.

The molecular weights of the polymers were estimated using gel permeation chromatography measured in chloroform relative to polystyrene standards. The results are summarized in Table 4.1. Polymers bearing branched side chains were obtained with higher molecular weights than the polymers with linear side chains, reflecting their improved solubilities. The thermal properties of the polymers were evaluated using thermal gravimetric analysis (TGA) and differential scanning calorimetry (DSC). TGA indicates that 5% weight loss onsets occur between 298-354 °C (Table 1), while typical second heating DSC showed glass transition temperatures ($T_g$) for the carbazole and fluorene containing polymers. PBOCz-O and PBOCz-EH displayed endotherms at 139 and 140 °C respectively while PBOF-O and PBOF-DMO had much lower $T_g$s at 123 and 110 °C. The lower $T_g$s of the fluorene polymers can be attributed to the $sp^3$ hybridization of the C-9 carbon causing the alkyl chains to point out of the plane of the π-system, further disrupting π-stacking. $T_g$s were not observed for PBOP-D and PBOP-MEH and none of the polymers exhibited endotherms corresponding to melting points. The $T_g$s were all above typical joule heating temperatures seen in electroluminescent devices, which is a necessity in order to obtain stable color emission.[30]

**4.3.2. Optical Properties.** The photophysical characteristics of the polymers both in dilute solutions and thin films were examined using UV-vis absorption and fluorescence spectroscopy. The normalized absorbance spectra of the polymers in solution and films are shown in Figure 4.1 and the data is summarized in Table 4.2. The absorption profiles of PBOCz-O and PBOCz-EH were virtually identical both in solutions and films, regardless of side chain structure. In solution, these polymers had absorption maxima at 392 and 394 nm respectively, which were the shortest wavelengths of the six polymers. The absorption spectra of the carbazole polymer films showed a bathochromic shift of ~35 nm relative to the solution spectra, which is a consequence of π-stacking between polymers in the solid state. The similarities between the PBOCz-O and PBOCz-EH spectra indicate that the branched side chain does not disrupt π-stacking any more than the linear chain. The carbazole polymers have among the largest optical band gaps among the six polymers, which can be attributed to a decrease in effective conjugation length arising from the 3,6-substitution on the carbazole. This arrangement leads to unfavorable steric interactions by the alkyl chains on flanking BBO units, twisting the polymer backbone.

In contrast to the carbazole polymers, the absorption spectra of the fluorene polymers did vary as a function of alkyl chain substitution. PBOF-O showed absorption maxima of 433 nm in solution and 440 nm as a film, while PBOF-DMO had absorption maxima of 399 nm in solution and 404 nm as a film. The ipsochromic shift seen between the absorptions of PBOF-O and PBOF-DMO in both solution and film may be the result of a larger distribution of highest occupied molecular orbitals (HOMOs) within the PBOF-DMO material. This is further supported be the fact that both PBOF-O and PBOF-DMO have similar band gaps of 2.72 and 2.76 eV. The large bathochromic shift seen between solutions and films of the carbazole

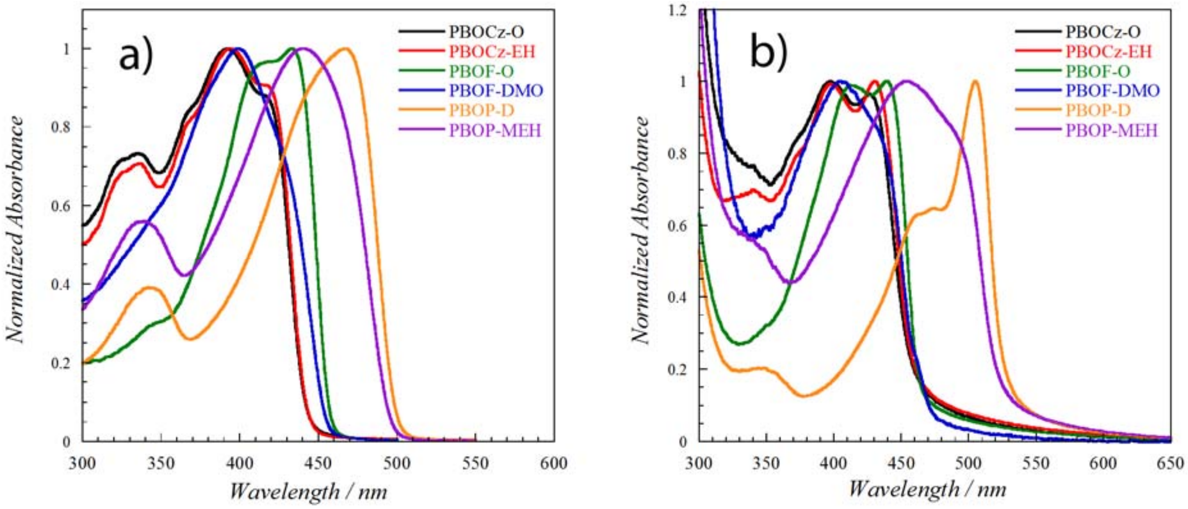

**Figure 4.1.** UV-vis spectra of benzobisoxazole polymers a) in chloroform solutions and b) as thin films.

**Table 4.2.** Optical and Electronic Properties of Benzobisoxazole Polymers

| | Solution | | Thin Film | | | | |
|---|---|---|---|---|---|---|---|
| Polymer | $\lambda_{max}^{abs}$ [nm] | $\lambda_{max}^{PL}$ [nm] | $\lambda_{max}^{abs}$ [nm] | $\lambda_{max}^{PL}$ [nm] | $E_g^{opt}$ [eV][a] | EA [eV][b] | IP [eV][c] |
| PBOCz-O | 392 | 440 | 427 | 517 | 2.72 | 2.78 | 5.50 |
| PBOCz-EH | 394 | 439 | 430 | 515 | 2.69 | 2.83 | 5.52 |
| PBOF-O | 433 | 453 | 440 | 495 | 2.72 | 3.19 | 5.91 |
| PBOF-DMO | 399 | 451 | 404 | 466 | 2.76 | 3.12 | 5.88 |
| PBOP-D | 467 | 494 | 505 | 566 | 2.36 | 2.93 | 5.29 |
| PBOP-MEH | 440 | 491 | 454 | 525 | 2.44 | 3.05 | 5.49 |

[a]Optical band gap measured from the onset of absorption in films. [b]electron affinity calculated from the optical band gap: EA = IP - $E_g^{opt}$. [c]ionization potential determined by ultraviolet photoelectron spectroscopy.

polymers are not seen with PBOF-O and PBOF-DMO. Instead they exhibit only a small shift of 7 nm for PBOF-O and 5 nm for PBOF-DMO which may be attributed to decreased excimer formation caused by the $sp^3$ C-9 carbon on the fluorene, which reduces the π-stacking between polymer chains.

The phenylene containing polymers also showed differences in absorption between the straight and branched chain derivatives. PBOP-D absorbed at 467 nm in solution and 505 nm as a film, while PBOP-MEH absorbed at 440 nm in solution and 454 as a film. These are the longest wavelengths of the six polymers, which is a product of the long linear and rigid structure of these polymers combined with the electron donating nature of the comonomer. As with the fluorene polymers, the difference in absorption spectra between PBOP-D and PBOP-MEH is probably the result of a larger HOMO distribution in PBOP-MEH than in PBOP-D. The difference between the absorption maxima in solution and in film is greater in the phenylene polymers than in the fluorene polymers. The larger difference in absorption maxima is a consequence of increased aggregation in PBOP-D. The branched side chain in PBOP-MEH better disrupts aggregation decreasing the red-shift between solution and film. The slight difference in optical band gaps for PBOP-D (2.36 eV) and PBOP-MEH (2.44 eV) may be the result of a slightly shorter effective conjugation length of the branched chain derivative.

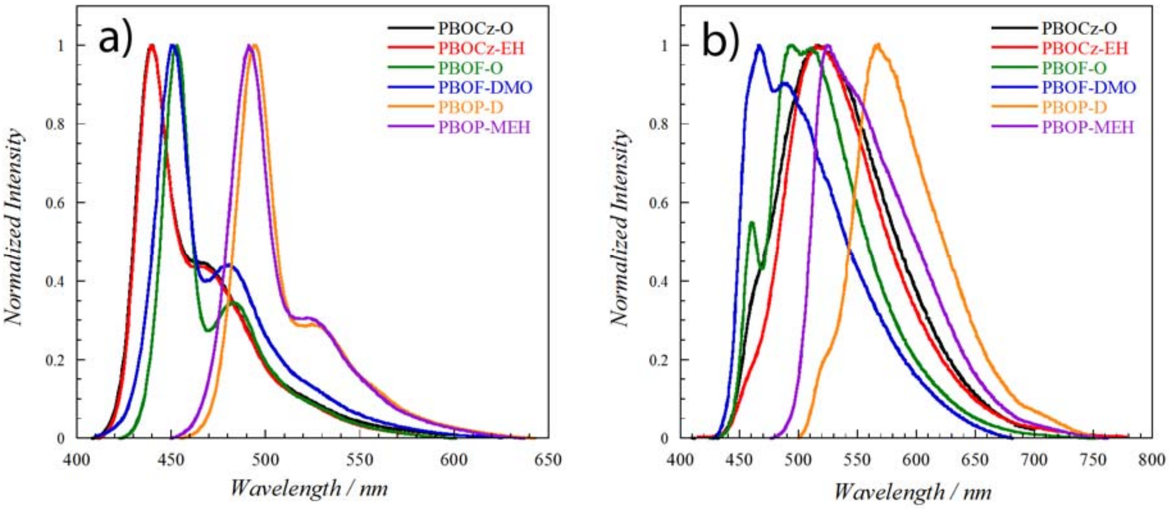

**Figure 4.2.** Photoluminescence spectra of benzobisoxazole polymers a) in chloroform solutions and b) as thin films.

The fluorescence spectra for the polymers in both dilute solutions and as thin films are shown in Figure 4.2. In solution emission is generally independent of side chain substitution. PBOCz-O and PBOCz-EH have the deepest blue emission at 440 and 439 nm while PBOF-O and PBOF-DMO display blue emission at 453 and 451 nm, respectively. PBOP-D and PBOP-MEH fluoresce in the green region of the visible spectrum at 494 and 491 nm in solution.

The PL of the polymers in thin films shows significant broadening of the emission peaks accompanied by bathochromic shifts of varying degrees. The carbazole polymers both redshift ~76 nm, again indicating that alkyl substitution has little impact on the electronic properties of the carbazole polymers, even in thin films. The fluorene and phenylene polymers exhibit a strong dependence of the emission wavelength on alkyl chain subsititution as the polymers with branched side chains are shifted more to the blue end of the spectrum in comparison to polymers with linear side chains. The emission profile of PBOF-DMO peaks at 466 nm. A peak is seen at the same wavelength in the spectrum of PBOF-O, though it is far less intense. Although PBOF-O and PBOF-DMO seem to have similar fluorescent transitions, the relative intensities of the transitions are different, resulting in a deeper blue emission from PBOF-DMO. As a film, PBOP-MEH shows a bathochromic shift of 34 nm between solution and film, giving yellow emission at 525 nm. The film emission of PBOP-D shows an even greater bathochromic shift of 72 nm causing orange emission at 566 nm. The red-shifted emission of PBOP-D relative to PBOP-MEH is the result of increased π-stacking of the polymer.

**4.3.3. Ultraviolet Photoelectron Spectroscopy.** The ionization potentials of the polymers were measured using ultraviolet photoelectron spectroscopy. This technique determines the HOMO energy level in organic thin films by bombarding the sample with UV photons and measuring the kinetic energies of the ejected valence electrons.[31] Thus, the HOMO values obtained by this technique are very precise as opposed to the more commonly used technique of cyclic voltammetry, which requires the use of approximations and has a high degree of error associated with the measurements (> 0.1 eV).[32] The electron affinities (EAs) were calculated from the measured IPs using the optical band gap. These values are summarized in Table 4.2.

The fluorene polymers were the most electron deficient with EAs of 3.19 and 3.12 eV for PBOF-O and PBOF-DMO, respectively. The phenylene polymers were slightly more electron rich with EAs of 2.93 and 3.05 eV for PBOP-D and PBOP-MEH, respectively. The carbazoles had the lowest EAs at 2.78 and 2.83 eV for PBOCz-O and PBOCz-EH. Interestingly, the side chain substitution had a significant impact on the IPs of the phenylene polymers, which may be a consequence of the a-symmetry of the phenylene unit in PBOP-MEH and the regio-random nature of the polymer. Due to the random position of its side chains, PBOP-MEH cannot pack as efficiently as PBOP-D and is less planar in films resulting in a shorter effective conjugation length and an increased IP.

**Table 4.3.** Photoluminescence Lifetimes and Quatum Yields

| Polymer | $\tau$ [ns] in $CHCl_3$[a] | $\tau$ [ns] as Film[a] | $\Phi_{re}$[b] |
|---|---|---|---|
| PBOCz-O | 1.00 | 0.46 | 0.33 |
| PBOCz-EH | 1.00 | 0.45 | 0.43 |
| PBOF-O | 0.49 | 0.36 | 0.68 |
| PBOF-DMO | 0.43 | 0.24 | 0.35 |
| PBOP-D | 0.59 | 0.17 | 0.57 |
| PBOP-MEH | 0.63 | 0.32 | 0.47 |

[a] Average PL lifetime. [b] PL Quantum yields measured in dilute chloroform solutions relative to Coumarin 152.

**4.3.4. PL Lifetimes and Quantum Yields.** To explore the excited state characteristics of the polymers the PL lifetimes were measured both in dilute chloroform solutions and as neat films, the results of which are summarized in Table 4.3. Fairly short lifetimes were observed in the range of 0.43 to 1.00 ns in dilute solutions of chloroform. PL lifetimes were considerably shorter (0.17-0.46 ns) in the thin films of the polymers. This is likely the result of exciplex formation in polymer aggregates fostering non-radiative decay pathways for excitons.[33] The solution PL lifetimes for PBOF-O (0.49 ns) and PBOF-DMO (0.43 ns) are virtually identical to the previously reported values[25] for the related poly[(9,9-dioctylfluorene-2,7-vinylene)-alt-benzo[1,2-d;4,5-d']bisoxazole-2,6-diyl] (PFVBBO-O) and poly[(9,9-bis(3,7-dimethyloctyl)fluorene-2,7-vinylene)-alt-benzo[1,2-d;4,5-d']bisoxazole-2,6-diyl] (PFVBBO-DMO) which are 0.51 and 0.43 ns respectively in solution.[25] The film measurements in PBOF-O and PBOF-DMO do show a small increase in PL lifetimes relative to PFVBBO-O and PFVBBO-DMO that is likely the result of the BBO alkyl chains, which are not present in the previously reported PBOs, disrupting π-stacking and decreasing non-radiative decay pathways. Though it is a small sample size to draw from and the structures are not completely analogous (vinylene instead of ethynylene), the similar solution PL lifetimes suggest that changing the polymerization substitution on the BBO from the 2,6-position to the 4,8-position does not have a significant impact on PL lifetime.

The quantum yields of the polymers in dilute solutions of chloroform were taken relative to Coumarin 152, the results of which are listed in Table 4.3. PBOF-O and PBOP-D had the highest quantum yields at 0.68 and 0.57, respectively. Interestingly, the branched alkyl derivatives PBOF-DMO and PBOP-MEH had much lower quantum yields (0.35 and 0.47 respectively) than their linear chain counterparts despite having similar PL lifetimes. A drop off in quantum yield, however, is expected to a certain degree as the branching of the side chains introduces additional degrees of freedom resulting in added non-radiative decay pathways. Overall, the carbazole polymers PBOCz-O and PBOCz-EH have lower quantum yields than the fluorene and phenylene polymers. This can be attributed to the twisted backbone of the carbazole polymers resulting in a less rigid polymer that can vibrationally relax more effectively.

**4.3.5. Electroluminescent Devices.** The polymers were first evaluated as neat emissive layers in PLEDs, however, these devices either did not emit light or failed to provide a useful brightness (< 100 Cd $m^{-2}$) due to strong concentration quenching in the neat film. We then fabricated guest-host PLEDs using the polymers as low level dopants in PVK. A device architecture of ITO/PEDOT:PSS/Host:Guest/BPhen/LiF/Al was adopted where PEDOT:PSS (poly(3,4-ethylenedioxy thiophene):poly(4-styrenesulfonate)) is a hole transporting layer and BPhen (4,7-diphenyl-1,10-phenanthroline) is a hole blocking/electron transporting layer, which also prevents exciton quenching at the metal cathode. There was concern that the low lying HOMOs of PBOF-O and PBOF-DMO relative to the HOMO of PVK, would prevent hole trapping on the guest while allowing efficient electron trapping on the it. This would inhibit FRET between the host and guest and could lead to lower energy exciplex formation between the host and guest, decreasing device performance.[34] To improve hole trapping on the guest, OLEDs using PBOF-O and PBOF-DMO were also made using a 4,4'-bis(N-carbazolyl)-1,1'-biphenyl (CBP) host, which has a lower lying HOMO than PVK and has recently been shown to produce spin-coated devices with high efficiencies.[35] To evaluate whether any improvements in PBOF-O or PBOF-DMO device performance were the result of improved hole trapping on the guest, PBOP-D was also made into a device with a CBP host in addition to a PVK based device. The energy level diagram in Figure 4.3 illustrates the various energy levels of the different devices

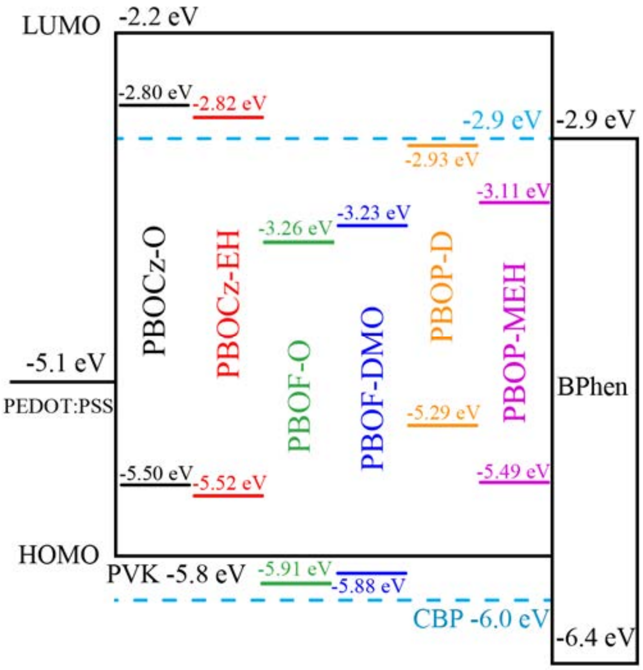
LUMO
-2.2 eV
-2.80 eV
-2.82 eV
-2.9 eV
-2.9 eV
-2.93 eV
-3.11 eV
-3.23 eV
-3.26 eV
PBOCz-O
PBOCz-EH
PBOF-O
PBOF-DMO
PBOP-D
PBOP-MEH
-5.1 eV
PEDOT:PSS
BPhen
-5.29 eV
-5.50 eV
-5.52 eV
-5.49 eV
HOMO
PVK -5.8 eV
-5.91 eV
-5.88 eV
CBP -6.0 eV
-6.4 eV

**Figure 4.3.** Energy level diagram of the materials used in the guest-host OLEDs.

**Table 4.4.** Device Characteristics of OLEDs Based on Benzobisoxazole Polymers

| Device[a] | | $V_{on}$[b] [V] | Drive voltage[c] [V] | Current Density[d] [mA cm$^{-2}$] | Brightness[e] [Cd m$^{-2}$] | Efficiency[f] [Cd A$^{-1}$, %EQE [g], lm W$^{-1}$] | $\lambda_{max}$ EL [nm] | CIE 1931 (x, y) |
|---|---|---|---|---|---|---|---|---|
| Polymer / **Host** | Wt [%] | | | | | | | |
| PBOCz-O | 0.5 | 5.2 | 9.4 | 250 | 210 | 0.50, 0.48, 0.27 | 449 | (0.17, 0.11) |
| **PVK** | 1.0 | 5.2 | 9.8 | 260 | 210 | 0.72, 0.68, 0.36 | 451 | (0.17, 0.12) |
| | 2.0 | 6.6 | 10.8 | 100 | 190 | 0.50, 0.57, 0.20 | 449 | (0.18, 0.14) |
| | 4.0 | 5.8 | 8.8 | 50 | 44 | 0.18, -----, 0.08 | ---- | ------ |
| PBOCz-EH | 0.5 | 6.0 | 10.8 | 380 | 310 | 0.53, 0.58, 0.25 | 446 | (0.17, 0.10) |
| **PVK** | 1.0 | 5.2 | 9.2 | 340 | 330 | 0.59, 0.51, 0.28 | 451 | (0.17, 0.12) |
| | 2.0 | 5.0 | 9.6 | 300 | 330 | 0.53, 0.46, 0.28 | 452 | (0.17, 0.12) |
| | 4.0 | 6.0 | 10.8 | 230 | 310 | 0.63, 0.40, 0.27 | 452 | (0.18, 0.21) |
| PBOF-O | 0.5 | 5.0 | 10.8 | 370 | 840 | 1.7, 1.10, 0.86 | 462 | (0.14, 0.12) |
| **PVK** | 1.0 | 5.4 | 11.6 | 430 | 1250 | 1.7, 1.20, 0.72 | 462 | (0.14, 0.13) |
| | 2.0 | 5.2 | 11.4 | 510 | 960 | 1.1, 0.92, 0.47 | 462 | (0.15, 0.17) |
| | 4.0 | 6.0 | 10.8 | 850 | 510 | 0.07, 0.05, 0.03 | 462 | (0.15, 0.15) |
| PBOF-O | 0.5 | 5.4 | 10.2 | 5000 | 2010 | 2.5, 1.9, 1.1 | 462 | (0.14, 0.14) |
| **CBP** | 1.0 | 4.4 | 10.2 | 570 | 1720 | 3.4, 2.4, 1.7 | 463 | (0.14, 0.16) |
| | 2.0 | 4.4 | 10.2 | 760 | 1300 | 1.5, 0.80, 0.76 | 463 | (0.16, 0.21) |
| | 4.0 | 3.6 | 10.4 | 610 | 2020 | 0.86, 0.53, 0.54 | 463 | (0.15, 0.19) |
| PBOF-DMO | 0.5 | 5.6 | 8.8 | 150 | 570 | 1.2, 1.2, 0.57 | 458 | (0.15, 0.11) |
| **PVK** | 1.0 | 6.0 | 9.2 | 150 | 660 | 1.2, 1.1, 0.49 | 458 | (0.15, 0.11) |
| | 2.0 | 6.5 | 9.6 | 74 | 230 | 0.56, 0.59, 0.22 | 459 | (0.15, 0.09) |
| | 4.0 | 8.0 | 11.0 | 30 | 58 | 0.22, 0.14, 0.07 | 460 | (0.16, 0.16) |
| PBOF-DMO | 0.5 | 4.9 | 8.2 | 320 | 1860 | 1.6, 1.5, 0.77 | 458 | (0.15, 0.12) |
| **CBP** | 1.0 | 5.4 | 9.0 | 440 | 2020 | 1.2, 1.1, 0.51 | 459 | (0.15, 0.11) |
| | 2.0 | 4.8 | 8.8 | 470 | 670 | 0.35, 0.24, 0.19 | 459 | (0.17, 0.19) |
| | 4.0 | 4.8 | 10.2 | 390 | 750 | 0.19, 0.12, 0.10 | 460 | (0.16, 0.17) |
| PBOP-D | 0.5 | 4.0 | 10.0 | 280 | 1150 | 3.1, 1.1, 1.6 | 501 | (0.18, 0.50) |
| **PVK** | 1.0 | 4.4 | 10.6 | 300 | 890 | 2.4, 0.88, 1.2 | 500 | (0.21, 0.51) |
| | 2.0 | 4.7 | 10.0 | 540 | 710 | 0.25, 0.07, 0.10 | 519 | (0.35, 0.61) |
| | 4.0 | 4.3 | 10.4 | 560 | 860 | 0.81, 0.28, 0.36 | 517 | (0.25, 0.54) |
| PBOP-D | 0.5 | 5.2 | 9.0 | 230 | 1620 | 5.7, 2.1, 2.8 | 506 | (0.20, 0.55) |
| **CBP** | 1.0 | 5.3 | 10.2 | 630 | 3380 | 4.3, 1.3, 1.8 | 507 | (0.22, 0.62) |
| | 2.0 | 4.6 | 10.2 | 660 | 2360 | 1.5, 0.49, 0.63 | 517 | (0.26, 0.60) |
| | 4.0 | 3.1 | 6.8 | 470 | 1460 | 0.51, 0.16, 0.40 | 519 | (0.35, 0.56) |
| PBOP-MEH | 0.5 | 5.4 | 8.6 | 240 | 1380 | 2.3, 1.1, 1.1 | 491 | (0.16, 0.36) |
| **PVK** | 1.0 | 5.5 | 9.6 | 280 | 1300 | 1.9, 0.73, 0.86 | 500 | (0.17, 0.49) |
| | 2.0 | 6.0 | 9.4 | 500 | 1340 | 0.40, 0.14, 0.15 | 502 | (0.21, 0.53) |
| | 4.0 | 6.0 | 9.6 | 480 | 910 | 0.28, 0.09, 0.13 | 511 | (0.27, 0.54) |

[a]Device architecture: ITO/PEDOT:PSS/Host:Polymer/BPhen/LiF/Al. Wt% is the weight percent of the polymer in the host. [b]Turn-on voltage, voltage applied to produce 1 Cd m$^{-2}$ brightness. [c]Voltage at peak brightness. [d]Current density at peak brightness. [e]Peak brightness. [f]Peak efficiencies. [g]EQE = external quantum efficiency.

materials.[36-38] All the devices were optimized by varying the weight percent of the guest in the host material using 0.5, 1.0, 2.0, and 4.0 weight percent (wt%) of guest polymer in the PVK or CBP hosts. The device characteristics are summarized in Table 4.4.

The carbazole polymers provided the deepest blue OLEDs but gave the poorest overall performance. Of the PBOCz-O-based devices , 1 wt% PBOCz-O in PVK gave the best performance but with a maximum brightness of only 210 Cd m$^{-2}$ and a maximum luminous efficiency of 0.72 Cd A$^{-1}$. The PBOCz-EH devices were slightly brighter but had worse efficiencies with the best results obtained from 1 wt% PBOCz-EH in PVK, giving a maximum brightness of 330 Cd m$^{-2}$ and a maximum luminous efficiency of 0.59 Cd A$^{-1}$. The poor efficiencies of the carbazole polymer-containing devices is a consequence of the low quantum

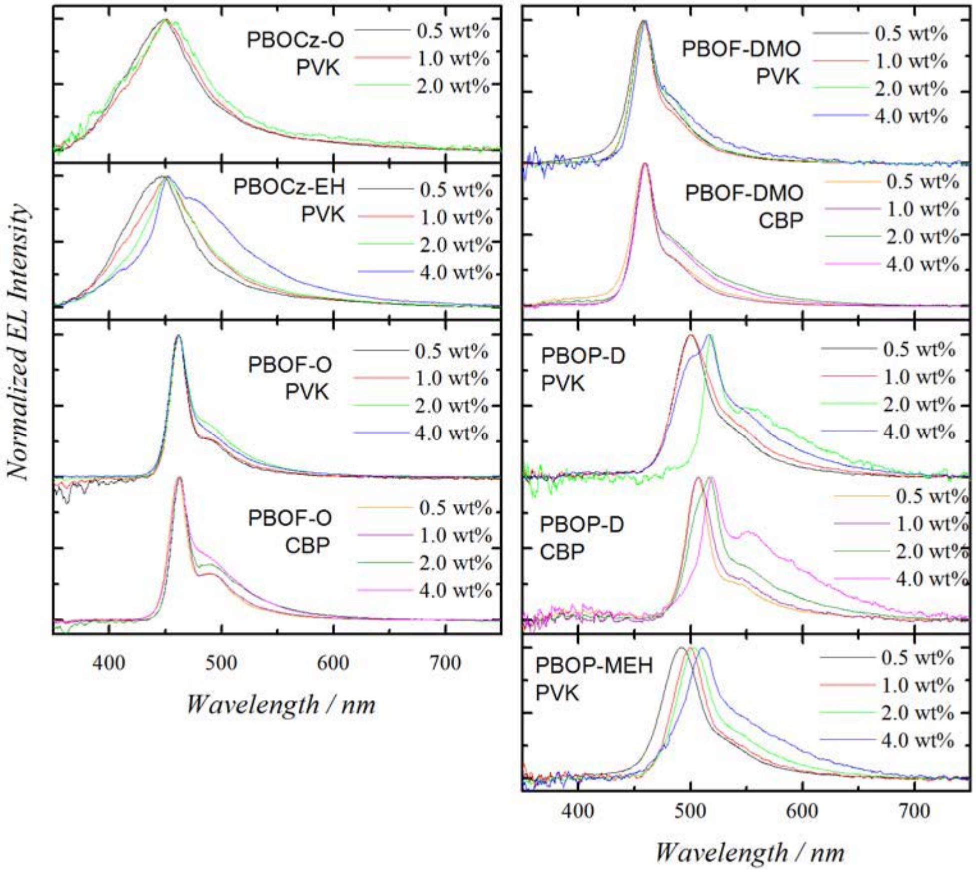

**Figure 4.4.** Normalized electroluminescent spectra of devices with different weight % concentrations of the benzobisoxazole polymers in CBP or PVK. Devices using a CBP host are off-set vertically from the devices using a PVK host.

yields in the polymers which results in energy loss to heat. As seen from the EL spectra (Figure 4.4), devices based on the carbazole polymers display a broad emission between ~400-500 nm with EL maxima in the range of 452-462 nm. The PBOCz-O devices also show little variation in their emission profile as the concentration of the guest is increased.

The EL maximum for PBOCz-EH does not change noticeably as the guest concentration increases but the band narrows and a shoulder at ~480 nm appears for 4 wt% of the guest. This narrowing of the EL emission is the result of a decreased emission in the ~400-430 nm range and while this may be a decrease in the host emission (PVK emits at ~410 nm) as the guest concentration increases, the change in the emission is small and is not seen in the PBOCz-O containing devices. This suggests the change in emission is due to aggregation of the polymers in the host with the increased aggregation caused by the much higher molecular weight of PBOCz-EH relative to PBOCz-O.

Devices based on the fluorene polymers also gave stable blue emission with the best device performance resulting from 1 wt% of PBOF-O in the CBP host. This gave a maximum brightness of 1720 Cd m$^{-2}$ with a maximum luminous efficiency of 3.4 Cd A$^{-1}$ at an emission wavelength of 463 nm. The efficiency for both this device and the identical PVK based device as a function of brightness is shown in Figure 4.5. Interestingly, there is a large improvement in device efficiency when CBP is used as the host instead of PVK. We had previously speculated that PVK may decrease hole trapping in the guest resulting from the fluorene polymer’s lower HOMO relative to PVK. The large increase in efficiency in CBP based devices may be indicative

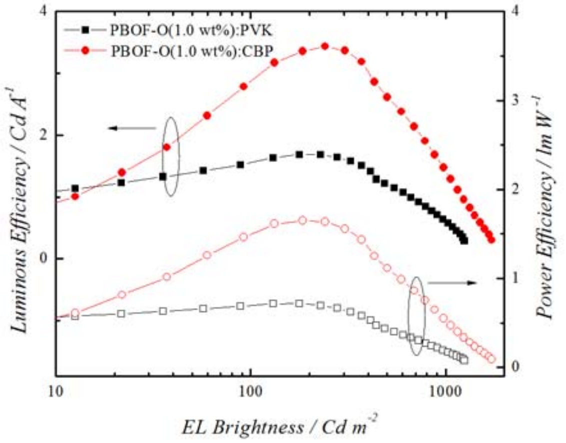

**Figure 4.5.** Luminous and power efficiency as a function of OLED brightness for devices using PBOF-O in a PVK or CBP host.

of improved hole trapping on the guest, though the increased efficiencies may also be attributed to the higher EA and extended conjugation of CBP compared to PVK, which yields a lower electron injection barrier and increased charge carrier mobilities. This is reflected in the generally lower turn on voltages of the CBP-based devices. Additionally, it has been shown that replacing PVK with CBP in spin-coated small molecule guest-host OLEDs results in smoother films with less phase separation,[35] therefore CBP may be providing better film morphologies, resulting in higher efficiencies. The values from the PBOF-O/CBP containing devices in fact, represent the highest efficiencies for a blue emitting benzobisoxazole-based OLED to date.

The PBOF-DMO devices did not perform as well with the best device made with 0.5 wt% polymer in CBP. This device displayed a brightness of 1860 Cd m$^{-2}$ with a luminous efficiency of 1.6 Cd A$^{-1}$. The improvement in efficiency between PVK and CBP is also seen in the devices containing PBOF-DMO, though the improvement is not as substantial. OLEDs made with PBOF-O generally had higher efficiencies and brightness than PBOF-DMO-containing devices, a consequence of PBOF-DMO's reduced quantum yield relative to PBOF-O. The EL spectra for the fluorene polymer based devices showed only guest emission with no contribution from the host. Both PBOF-O and PBOF-DMO displayed emission bands at 463 and 459 nm, respectively. These bands were extremely narrow with full widths at half maxima (FWHM) of ~22 nm. A weak peak at ~490 nm is also seen making the EL spectra virtually identical to the solution PL spectra of the polymers. This suggests that the fluorene polymers are not aggregating, even at

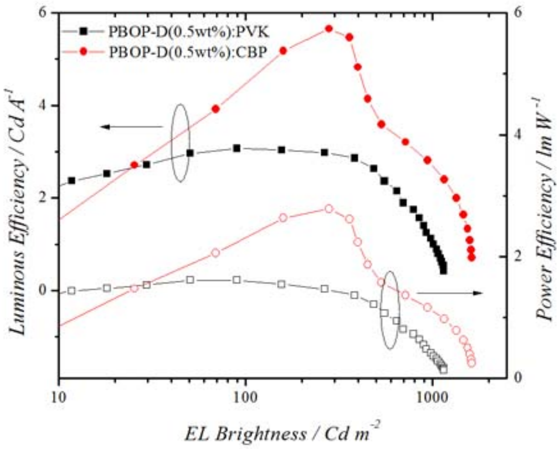

**Figure 4.6.** Luminous and power efficiency as a function of OLED brightness for devices using PBOP-D in a PVK or CBP host.

higher concentrations, within the host matrix.

Devices made from the phenylene polymers gave green emission with the best PBOP-D device made from 0.5 wt% in CBP displaying a maximum brightness of 1620 Cd $m^{-2}$ and a maximum efficiency of 5.7 Cd $A^{-1}$. This represents the highest efficiency to date for any OLED using a PBO irrespective of the BBO isomer or emission color. The efficiency as a function of brightness is plotted for both this device and the identical PVK device in Figure 4.6. It shows that just as with the PBOF-O and PBOF-DMO devices, there is a large increase in efficiency for the CBP based devices compared to the PVK based devices. Because PBOP-D should efficiently trap holes and electrons in PVK, these results show that the improvement in device efficiencies is not simply related the guest's ability to trap charge carriers but also the result of differences in the electronic characteristics of PVK and CBP. Devices made from PBOP-MEH did not perform quite as well as PBOP-D, though the difference in efficiencies between them was not as extreme as the difference in the fluorene polymer based devices. The best PBOP-MEH containing OLED was made with 0.5 wt% guest in PVK and exhibited a maximum brightness of 1380 Cd $m^{-2}$ with a maximum luminous efficiency of 2.3 Cd $A^{-1}$. The lower efficiencies of the PBOP-MEH devices relative to the PBOP-D devices are likely the consequence of PBOP-MEH's lower quantum yield. The EL spectra for the phenylene polymers are much broader than the fluorene polymer's with emission coming exclusively from the guest. The EL emission maxima are also heavily dependent on guest concentration, with an increasing red-shift seen as the guest concentration is increased. This EL dependence on concentration is the result of efficient π-stacking by the guest in the host material likely leading to excimer formation, which is not surprising given the flat rigid nature of the phenylene polymer's structure.

The most surprising aspect of these devices is the efficient FRET from host to guest, which resulted in no observable host emission. Our previous reports of PBOs used as guests in PVK showed very poor guest emission with host emission dominating the EL spectrum. In a device made with 1 wt% PFVBBO-O, emission from the PVK was four times more intense than emission from the guest.[25] The previously reported PFTBBO showed an intensity ratio of host emission to guest emission of 4:3 for 1 wt % guest in a PVK host with similar device architecture.[26] The rate of energy transfer is generally dependent on the overlap of the host emission spectrum and the guest absorption spectrum.[39] The carbazole and fluorene polymers do have slightly better spectral overlap with PVK than the previously reported materials, which would lead to the conclusion that the wider bandgap of these materials lead to the improved energy transfer. But the phenylene polymers have worse spectral overlap than PFVBBO and PFTBBO yet do not show any of the problems with FRET between host and guest and in fact have significantly improved efficiencies in PVK-based devices despite this disadvantage in overlap. This suggests that the improved FRET is not from increased spectral overlap, but is the result of other factors. We speculate that by changing the orientation of the BBO moiety within the conjugated structure of the polymer, so that the electron withdrawing oxazole rings are now perpendicular to the backbone, a change in the excited state dipole of the polymer occurs. This change in the dipole leads to increased coupling between the host and guest excited state dipoles, improving the FRET between host and guest.[34] Further studies are currently underway to better understand this phenomenon.

## 4.4. CONCLUSIONS

In conclusion, six new PBOs containing N-alkylcarbazole, 9,9-dialkylfluorene, and 2,5-dialkoxybenzene were synthesized with high molecular weights, high electron affinities, and in good yields. These polymers differed from previously reported PBOs in that the conjugation pathway was directly through the central benzene ring instead of through the oxazole rings. The electroluminescent properties of OLEDs with these materials as guests in PVK or CBP were studied in guest-host structures and the devices exhibited substantially higher brightness and efficiencies than any previously reported PBO-containing OLED. We attribute these higher efficiencies to improved FRET between the host and guest, which we believe is the direct result of changing the orientation of the BBO moiety within the polymer backbone so that the oxazole rings are perpendicular to the conjugated backbone. This discovery will greatly benefit the future development of PBOs as emissive materials for high efficiency guest-host OLEDs and work is currently underway to better understand the nature of this improved energy transfer.

## 4.5. EXPERIMENTAL METHODS

**4.5.1. Materials.** 3,6-diethynyl-N-octylcarbazole,[40] 3,6-diethynyl-N-(2-ethylhexyl)carbazole[41], 2,7-diethynyl-9,9-dioctylfluorene[42], 1,4-diethynyl-2,5-dodecyloxybenzne[43], 1,4-diethynyl-2-(2-ethylhexyloxy)-5-methoxybenzne[44], 3,6-diamino-2,5-dibromo-1,4-hydroquinone,[45] and 2,7-dibromo-9,9-bis(3,7-dimethyloctyl)fluorene[46] were prepared according to literature procedures.

Tetrahydrofuran and toluene were dried using an Innovative Technologies solvent purification system. Tetrakis(triphenylphosphine)palladium(0) was purchased from Strem Chemicals, Inc. Trimethylactylene was purchased from GFS Chemicals. Spectral grade coumrain-152 was purchased from Exciton. Poly(3,4-ethylenedioxy thiophene):poly(4-styrenesulfonate) (PEDOT:PSS) was purchased from H. C. Starck. All other chemicals were purchased from Sigma-Aldrich and used without further purification.

**4.5.2. Monomer Synthesis.** *4,8-Dibromo-2,6-dihexylbenzo[1,2-d;4,5-d']bisoxazole* (2): A dry 250 mL flask was placed under an argon atmosphere and charged with poly(trimethylsilylphosphate) (16.0 g, 118 mmol) dissolved in dry/degassed *o*-dichlorobenzene (60 mL). To the solution was added 3,6-diamino-2,5-dibromo-1,4-hydroquinone (1) (5.87 g, 19.7 mmol) and heptanoyl chloride (7.32 g, 49.3 mmol). The mixture was heated to 90 °C and stirred for 96 hours under argon. It was then cooled to room temperature and poured into 300 mL of methanol and cooled to -40 °C. The precipitated product is filtered and washed with methanol. The crude product was then recrystallized from hexanes by dissolving the solid in boiling hexanes and hot filtering the solution before allowing it to recrystallize to afford an off-white solid (6.03 g, 63% yield). mp 108-110 °C; $^1$H NMR (400 MHz, $CDCl_3$, δ): 0.89 (t, $J$ = 8 Hz, 6H), 1.31-1.39 (m, 8H), 1.45 (m, 4H), 1.93 (quintet, $J$ = 8 Hz, 4H), 3.01 (t, $J$ = 8 Hz, 4H); $^{13}$C NMR (400 MHz, CDCl3, δ): 22.7, 27.1, 29.1, 29.2, 31.5, 91.4, 138.5, 146.6, 169.4; HRMS (ESI, *m/z*): $[M + H]^+$ Calcd for $C_{20}H_{27}Br_2N_2O_2$, 485.0434; found, 485.0445.

*2,7-bis(trimethylsilylethynyl)-9,9-bis(3,7-dimethyloctyl)fluorene*: A flame-dried 250 mL flask was charged with 2,7-dibromo-9,9-bis(3,7-dimethyloctyl)fluorene (6.05 g, 10 mmol), N,N-diisopropylamine (14.2 mL, 100 mmol), and triphenylphosphine (131.5 mg, 0.5 mmol) dissolved in THF (75 mL). The mixture was then degassed by bubbling argon through it for 30 minutes followed by addition of trimethylsilylacetylene (2.95 g, 30 mmol) and an additional 5 minutes of degassing. Tetrakis(triphenylphosphine)palladium(0) (351 mg, 5 mol %) and copper iodide (95.2 mg, 5 mol %) was then added and the reaction was refluxed under argon for 2 days. The mixture was then cooled to room temperature and filtered. The filtrate was diluted with saturated aqueous ammonium chloride solution (100 mL) and extracted with ether (3 x 75 mL). The organic extracts were combined and washed with water and brine before drying it over magnesium sulfate and then concentrated under reduced pressure. The crude residue was then purified using silica gel column chromatography with a eluent gradient starting with hexane and going to 5:1 hexane:chloroform. Evaporation of the solvent gave a yellow oil (5.56 g, 87% yield). 1H NMR (400 MHz, CDCl3, δ): 0.28 (s, 18H), 0.40 (m, *J* = 6 Hz, 2H), 0.50 (m, *J* = 6 Hz, 2H), 0.68 (d, *J* = 6 Hz, 6H), 0.82 (d, *J* = 7 Hz, 12H), 0.89 (m, 2H), 0.95-1.16 (m, 12H), 1.44 (m, *J* = 6 Hz, 2H), 1.94 (m, 4H), 7.40 (s, 2H), 7.45 (d of d, $^3J$ = 8 Hz, $^4J$ = 1 Hz, 2H), 7.59 (d, *J* = 8 Hz, 2H); $^{13}C$ NMR (400 MHz, $CDCl_3$, δ): 0.3, 19.7, 22.8, 22.9, 24.7, 28.1, 30.5, 33.1, 36.7, 37.8, 39.4, 55.3, 94.4, 106.3, 120.0, 122.0, 126.3, 131.5, 141.1, 151.1; HRMS (ESI, *m/z*): $[M + H]^+$ Calcd for $C_{43}H_{67}Si_2$, 639.4776; found, 639.4772.

*2,7-diethyny)-9,9-(3,7-dimethyloctyl)fluorene*: A 250 mL flask was charged with 2,7-bis(trimethylsilylethynyl)-9,9-(3,7-dimethyloctyl)fluorene (5.21 g, 8.15 mmol) and potassium carbonate (1.69 g, 12 mmol) dissolved in methanol (57 mL) and THF (11 mL). The mixture was then stirred overnight and then poured into water and extracted with ether (3 x 75 mL). The organic extracts were combined, washed with brine, dried over magnesium sulfate, and solvent evaporated under reduced pressure. The crude residue was purified using silica gel column chromatography with 10:1 hexane:dichloromethane as eluent. Evaporation of the solvent under reduced pressure yielded a yellow oil (3.45 g, 86% yield). 1H NMR (400 MHz, $CDCl_3$, δ): 0.42 (m, J = 6 Hz, 2H), 0.54 (m, *J* = 6 Hz, 2H), 0.68 (d, *J* = 6 Hz, 6H), 0.81 (d, *J* = 7 Hz, 12H), 0.88 (m, 2H), 1.02 (m, 12H), 1.44 (m, 2H), 1.95 (m, 4H), 7.45 (s, 2H), 7.48 (d of d, $^3J$ = 8 Hz, $^4J$ = 2 Hz, 2H); $^{13}C$ NMR (400 MHz, $CDCl_3$, δ): 19.4, 22.6, 22.7, 24.5, 27.9, 30.3, 32.8, 36.0, 37.5, 39.2, 55.0, 77.3, 84.5, 119.9, 120.9, 126.5, 131.2, 141.0, 151.0; HRMS (ESI, *m/z*): $[M + H]^+$ Calcd for $C_{37}H_{51}$, 495.3985; found, 495.3992.

**4.5.3. General Procedure for Polymer Synthesis.** A flame dried 50 mL Schlenk flask was charged with 4,8-Dibromo-2,6-dihexylbenzo[1,2-d;4,5-d']bisoxazole (2) (243.1 mg, 0.5 mmol) and diethynyl-comonomer (0.5 mmol) dissolved in N,N-diisopropylamine (6 mL) and toluene (12 mL). The mixture was degassed by bubbling argon through it for 30 minutes followed by addition of tetrakis(triphenylphosphine)palladium(0) (11.6 mg, 2 mol %) and copper iodide (4.8 mg, 5 mol %). The reaction was heated to 70 °C and stirred under argon for 24 hours. The polymer was then precipitated out in methanol and the solid was filtered and washed in a Soxhlet with methanol followed by acetone and then extracted with THF. Evaporation of the THF yielded the polymers as solids of varying color.

*PBOCz-O*: Yield was 74% as a yellow solid. $^1$H NMR (400 MHz, CDCl3, δ): 0.91 (9H), 1.27-1.49 (22H), 1.92-2.05 (6H), 3.10 (4H), 4.34 (2H), 7.42 (2H), 7.85 (2H), 8.49 (2H); UV/Vis ($CHCl_3$): $\lambda_{max}$ = 392 nm; UV/Vis (film): $\lambda_{max}$ = 427 nm; GPC ($CHCl_3$): $M_n$ = 13,000, $M_w$ = 23,800, PDI = 1.8.

*PBOCz-EH*: Yield was 95% as a yellow solid. $^1$H NMR (400 MHz, CDCl3, δ): 0.86-0.92 (12H), 1.27-1.54 (20H), 2.00-2.11 (5H), 3.10 (4H), 4.21 (2H), 7.42 (2H), 7.85 (2H), 8.49 (2H); UV/Vis ($CHCl_3$): $\lambda_{max}$ = 394 nm; UV/Vis (film): $\lambda_{max}$ = 430 nm; GPC ($CHCl_3$): $M_n$ = 47,900, $M_w$ = 74,900, PDI = 1.6.

*PBOF-O*: Yield was 73% as a yellow solid. $^1$H NMR (400 MHz, CDCl3, δ): 0.68 (4H), 0.84 (6H), 0.95 (6H), 1.11-1.27 (20H), 1.41 (8H), 1.53 (4H), 2.01 (8H), 3.09 (4H), 7.68-7.78 (6H); UV/Vis ($CHCl_3$): $\lambda_{max}$ = 433 nm; UV/Vis (film): $\lambda_{max}$ = 440 nm; GPC ($CHCl_3$): $M_n$ = 38,200, $M_w$ = 145,000, PDI = 3.8.

*PBOF-DMO*: Yield was 49% as a yellow solid. $^1$H NMR (400 MHz, CDCl3, δ): 0.51-1.44 (56H), 1.92 (8H), 3.00 (4H), 7.62-7.66 (6H); UV/Vis ($CHCl_3$): $\lambda_{max}$ = 399 nm; UV/Vis (film): $\lambda_{max}$ = 404 nm; GPC ($CHCl_3$): $M_n$ = 51,900, $M_w$ = 188,300, PDI = 3.6.

*PBOP-D*: Yield was 59% as an orange solid. $^1$H NMR (400 MHz, CDCl3, δ): 0.86-0.95 (12H), 1.23-1.28 (32H), 1.39 (8H), 1.48-1.59 (8H), 1.98 (8H), 3.05 (4H), 4.16 (4H), 7.24 (2H). UV/Vis ($CHCl_3$): $\lambda_{max}$ = 467 nm; UV/Vis (film): $\lambda_{max}$ = 505 nm; GPC ($CHCl_3$): $M_n$ = 33,100, $M_w$ = 45,800, PDI = 1.4.

*PBOP-MEH*: Yield was 51% as an orange solid. $^1$H NMR (400 MHz, CDCl3, δ): 0.81-0.98 (12H), 1.27-1.52 (20H), 1.99 (5H), 3.04 (4H), 4.02 (5H), 7.25 (2H). UV/Vis ($CHCl_3$): $\lambda_{max}$ = 440 nm; UV/Vis (film): $\lambda_{max}$ = 454 nm; GPC ($CHCl_3$): $M_n$ = 26,200, $M_w$ = 87,200, PDI = 3.3.

**4.5.4. Characterization.** NMR spectra were obtained on a Varian MR-400 at 400 MHz using $CDCl_3$ as the solvent and all samples were referenced to their internal protonated solvent. Gel permeation chromatography (GPC) measurements were performed on a GPC separation module equipped with four columns connected in a series (gaurd, 10,000 Å, 1,000 Å, and 100 Å from American Polymer Services Corporation), a refractive index detector and a UV-Vis detector. Analysis was performed at 35 °C using chloroform as the eluent with a flow rate of 1.0 mL min$^{-1}$. Calibration was based on polystyrene standards. Fluorescence spectroscopy and UV-Visible spectroscopy were performed using polymer solution in chloroform and as thin films spun from

10 mg mL$^{-1}$ solutions on to glass slides with a spin rate of 2,000 rpm. Photoluminescence spectra were obtained using an excitation wavelength equal to the wavelength of maximum absorption for the UV spectra. Thermal gravimetric analysis was taken in the temperature range of 30-850 °C using a heating rate of 20 °C min$^{-1}$ under ambient atmosphere. Differential scanning calorimetry was performed with a first scan heating rate of 15 °C min$^{-1}$ to erase thermal history and a second scan to measure transitions between 0-250 °C under nitrogen. Transitions were also measured with cooling at 15 °C min$^{-1}$. Ultraviolet photoelectron spectroscopy measurements were performed on polymer films using a RKI Instruments Model AC-2 instrument. Quantum yield measurements were taken of the polymers in dilute solutions of chloroform relative to Coumarin-152 in acetonitrile.[47] Fluorescence lifetime measurements were performed using the time-correlated single-photon counting (TCSPC) method. Pulses tunable from ~780-880 nm were produced from a homebuilt 82-MHz mode-locked Ti:sapphire oscillator pumped by a 5-W Nd:VO4 laser (Millennia, Spectra Physics). The resulting fundamental wavelength at ~814 nm was modulated by a Pockels cell (Model 350-160, Conoptics Inc.) to reduce the repetition rate to ~8.8 MHz. The frequency-doubling of this laser source by a harmonic generator (Model TP-2000B, U-Oplaz Technologies) provided the excitation wavelength at ~407 nm. A half wave plate and polarizer before the sample chamber ensured vertically polarized excitation. Emission (≥500 nm) was collected in a perpendicular geometry and passed through a polarizer set at the magic angle (54.70) for solutions and 900 for solid films, with respect to the excitation polarization. Notably, a front faced geometry was also used for solid films. The placement of appropriate filters before the microchannel plate, MCP (Hamamatsu, R3809U-50) eliminated the excitation light and allowed selection of emission from the sample. The full width at half-maximum (FWHM) of the instrument response function was ∼37-40 ps. All measurements were made in a 5 ns time window with a total of 4096 channels. A total of 65530 counts were collected at the peak channel for all lifetime measurements.

**4.5.5. OLED Fabrication and Characterization.** OLEDs were fabricated on nominally 20 Ω/square, 140 nm-thick ITO-coated glass substrates (Colorado Conecpt Coatings). The substrates were first cleaned with a detergent and organic solvents and then treated in a UV/ozone oven to increase the work function of the ITO and hence facilitate hole injection, as described elsewhere.[48] A 60 nm PEDOT:PSS layer was spin-coated onto the ITO and then baked in air at 120 °C for 1 hour and then in an argon filled glovebox at 120 °C for another 30 minutes. Blends of PVK or CBP and PBO copolymers in chlorobenzene solutions were spin-coated on top of the PEDOT:PSS layer in an argon filled glovebox. The combined concentration of host and guest material was kept constant at 9 mg $mL^{-1}$. The solution was spin-coated at 4,000 rpm for 60 seconds. The fabricated structure was then annealed at 60 °C for 30 minutes. Following this annealing step, the samples were transfered to a thermal evaporator within the golvebox and the Bphen, LiF, and Al layers were deposited sequentially by thermal evaporation at a base pressure of ~1 x $10^{-6}$ Torr. The OLEDs were characterized by monitoring their EL spectra, brightness as a function of the applied voltage, and luminous efficiency.

## 4.6 ACKNOWLEDGEMENTS

We would like to thank Dr. Elena Sheina of Plextronics for providing UPS measurements, Dr. Kamel Harrata and the Mass Spectrometry Laboratory of Iowa State University (ISU) for compound analysis, Ms. Achala Bhuwalka for assisting in the collection of thermal data, Dr. Min Cai for the fabrication of single layer OLEDs, Dr. Jacob Petrich for use of equipment for fluorescence lifetime measurements, and Mr. Michael Zenner for taking the OLED photograph seen in the table of contents graphic. We also thank the 3M Foundation and the National Science Foundation (DMR-0846607) for financial support of this work. Partial support for this work was provided by the Director of Energy Research, Office of Basic Energy Sciences, USDOE. Ames Laboratory is operated by Iowa State University for the US Department of Energy (USDOE) under Contract No. DE-AC 02-07CH11358.

## 4.7 SUPPORTING INFORMATION

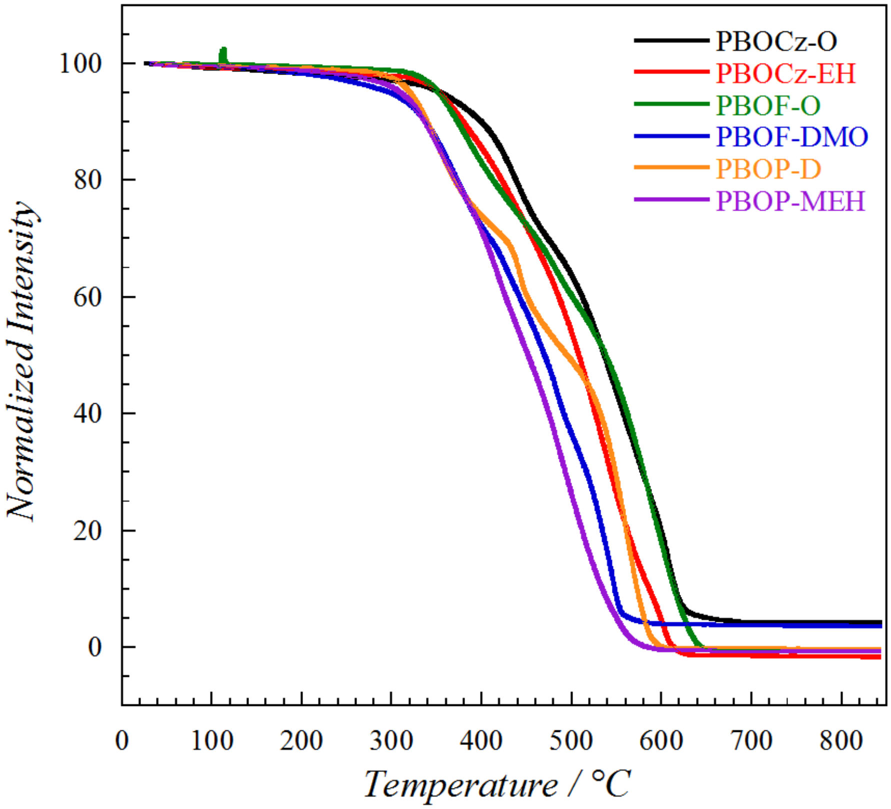

**Figure S4.1.** Thermal gravimetric analysis of benzobisoxazole polymers.

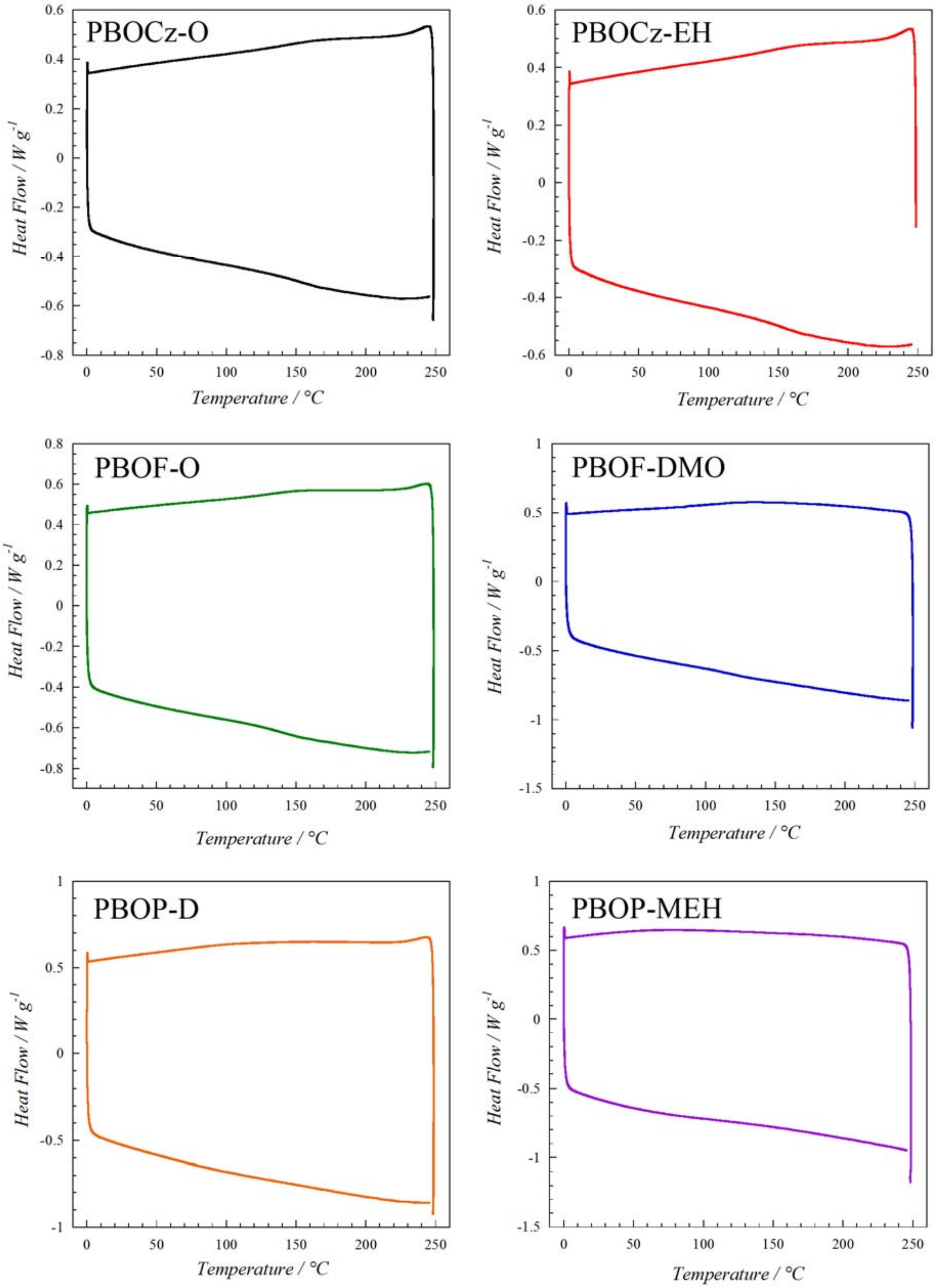

**Figure S4.2.** Differential scanning calorimetry plots of benzobisoxazole polymers.

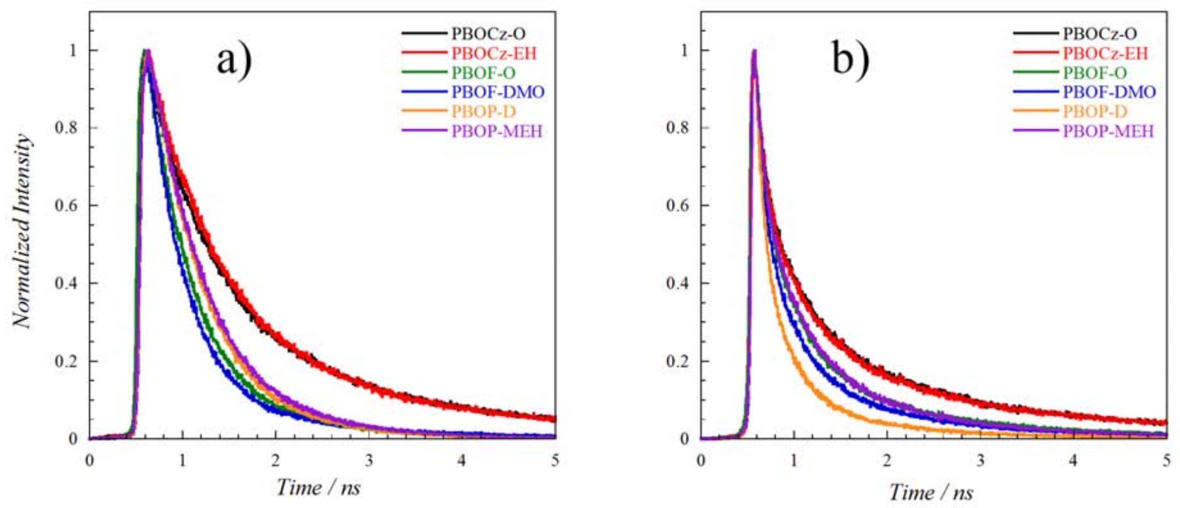

**Figure S4.3.** Photoluminescence lifetime plots of polymers a) in dilute chloroform solutions and b) as thin films.

**Table S4.1.** Photoluminescence Lifetimes of the Polymers

| Polymer | $\tau_1$ [ns], ($A_1$) [%] [a] | $\tau_2$ [ns], ($A_2$) [%] [a] | $\tau_3$ [ns], ($A_3$) [%] [a] | $\tau$ [ns] [b] |
|---|---|---|---|---|
| **Solution** | | | | |
| PBOCz-O | 0.33 (26) | 0.77 (48) | 2.10 (26) | 1.00 |
| PBOCz-EH | 0.32 (30) | 0.86 (45) | 2.10 (25) | 1.00 |
| PBOF-O | 0.25 (31) | 0.75 (28) | 0.50 (41) | 0.49 |
| PBOF-DMO | 0.27 (71) | 0.71 (24) | 1.40 (5) | 0.43 |
| PBOP-D | 0.53 (88) | 0.75 (10) | 2.20 (2) | 0.59 |
| PBOP-MEH | 0.49 (51) | 0.71 (47) | 2.20 (2) | 0.63 |
| **Thin Film** | | | | |
| PBOCz-O | 0.05 (57) | 0.41 (26) | 2.00 (16) | 0.46 |
| PBOCz-EH | 0.06 (58) | 0.42 (27) | 2.00 (15) | 0.45 |
| PBOF-O | 0.08 (59) | 0.46 (30) | 1.60 (11) | 0.36 |
| PBOF-DMO | 0.05 (64) | 0.35 (28) | 1.40 (8) | 0.24 |
| PBOP-D | 0.05 (69) | 0.29 (25) | 1.10 (6) | 0.17 |
| PBOP-MEH | 0.06 (60) | 0.43 (29) | 1.50 (11) | 0.32 |

[a] A1, A2, and A3 represent the preexponentials of the three difference decay terms. [b] Average PL lifetime determined by full width at half max.

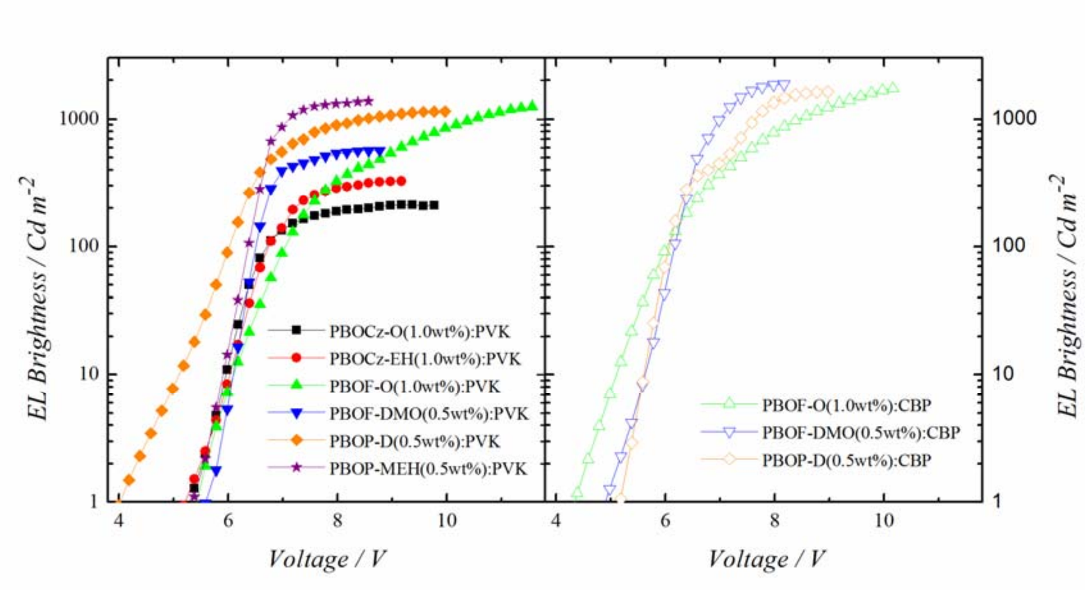

**Figure S4.4.** Brightness as a function of applied voltage for the best performing devices with a PVK host (left) or CBP host (right)

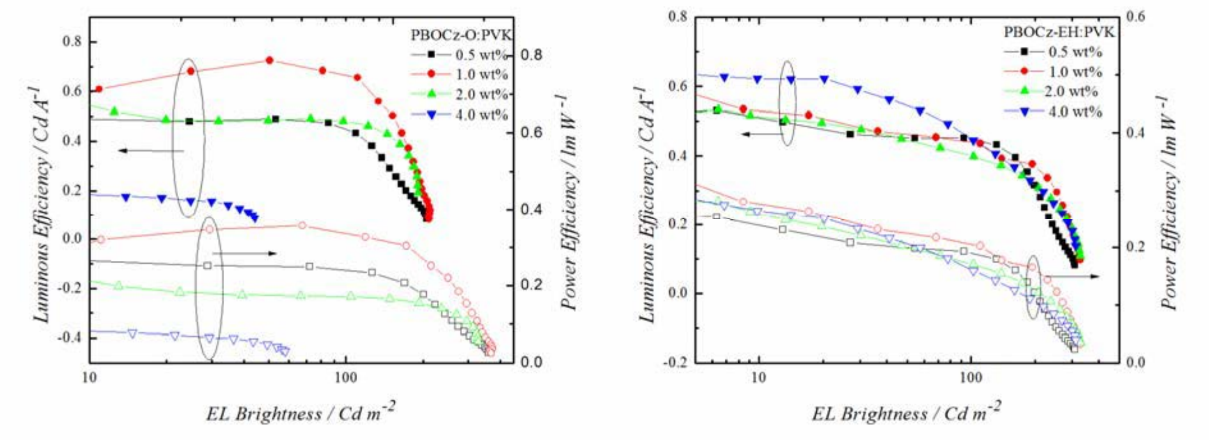

**Figure S4.5.** Efficiency as a function of brightness for all PBOCz-O devices (left) and PBOCz-EH devices (right).

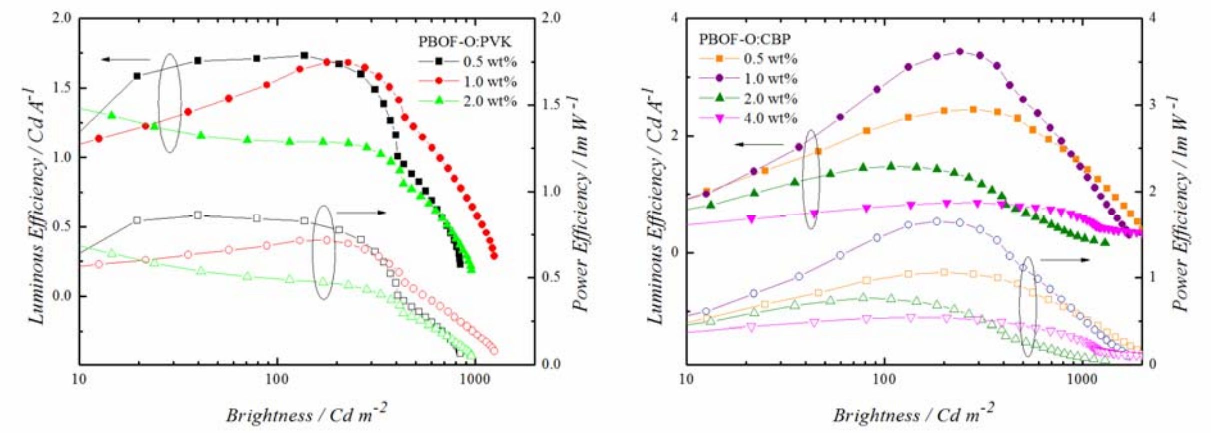

**Figure S4.6.** Efficiency as a function of brightness for all PBOF-O devices using a PVK host (left) or CBP host (right).

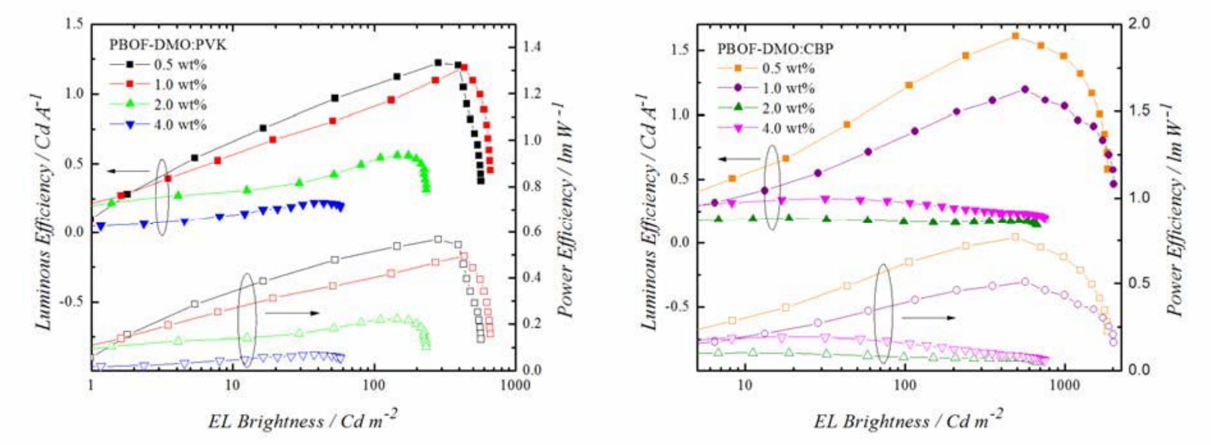

**Figure S4.7.** Efficiency as a function of brightness for all PBOF-DMO devices using a PVK host (left) or a CBP host (right).

للاستشارات المنارة

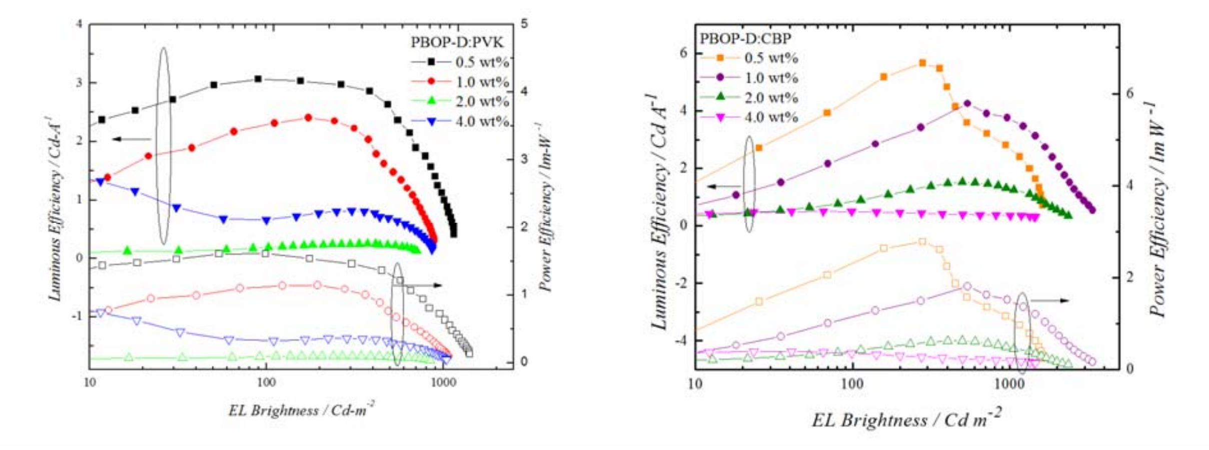

**Figure S4.8.** Efficiency as a function of brightness for all PBOP-D devices using a PVK host (left) or CBP host (right).

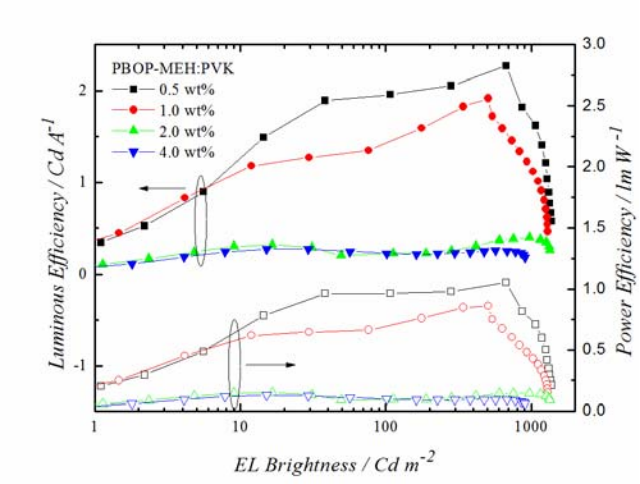

**Figure S4.9.** Efficiency as a function of brightness for all PBOP-MEH devices.

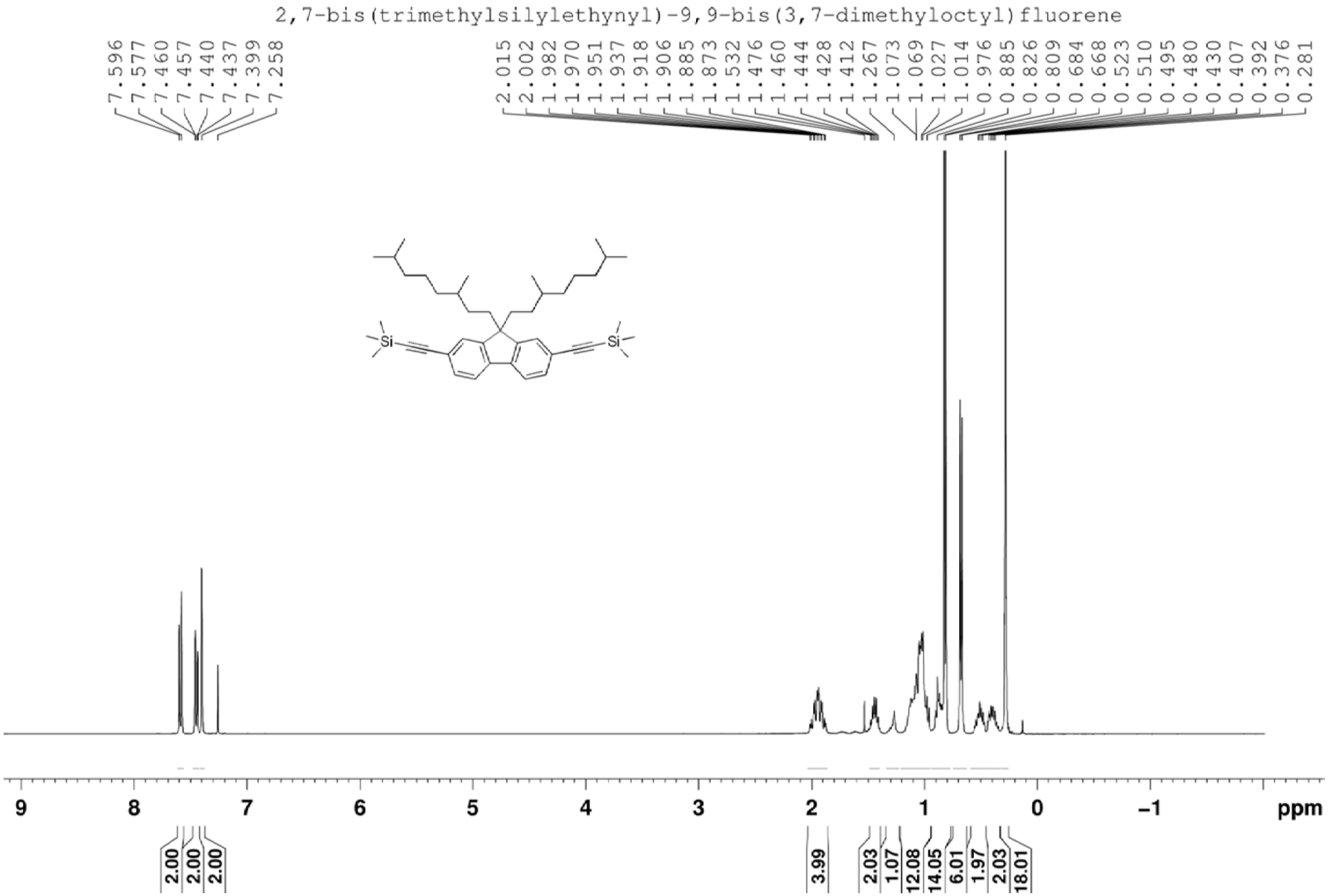

**Figure S4.10.** $^{1}$H NMR of 2,7-bis(trimethylsilylethynyl)-9,9-bis(3,7-dimethyloctyl)fluorene.

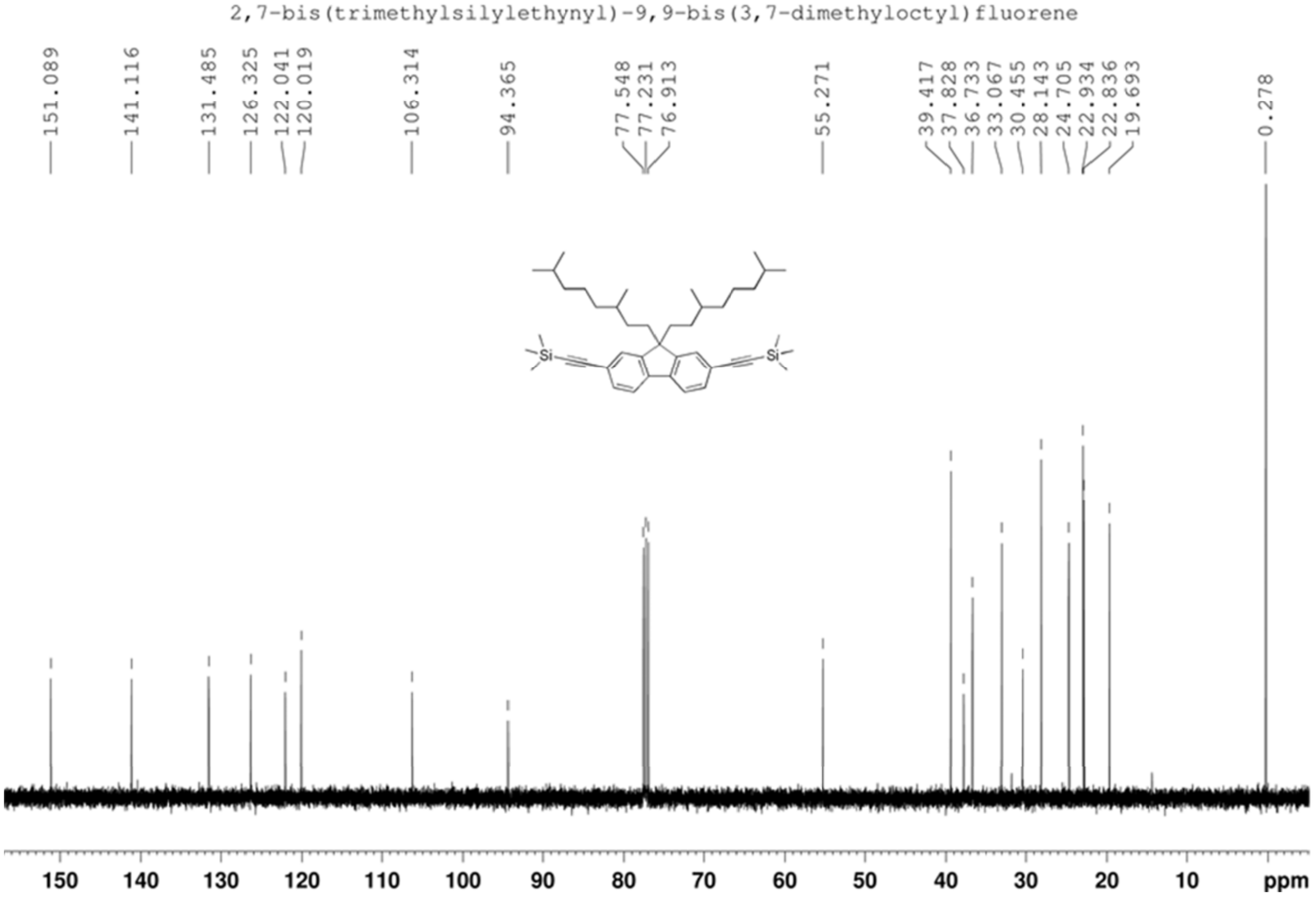

**Figure S4.11.** $^{13}$C NMR of 2,7-bis(trimethylsilylethynyl)-9,9-bis(3,7-dimethyloctyl)fluorene.

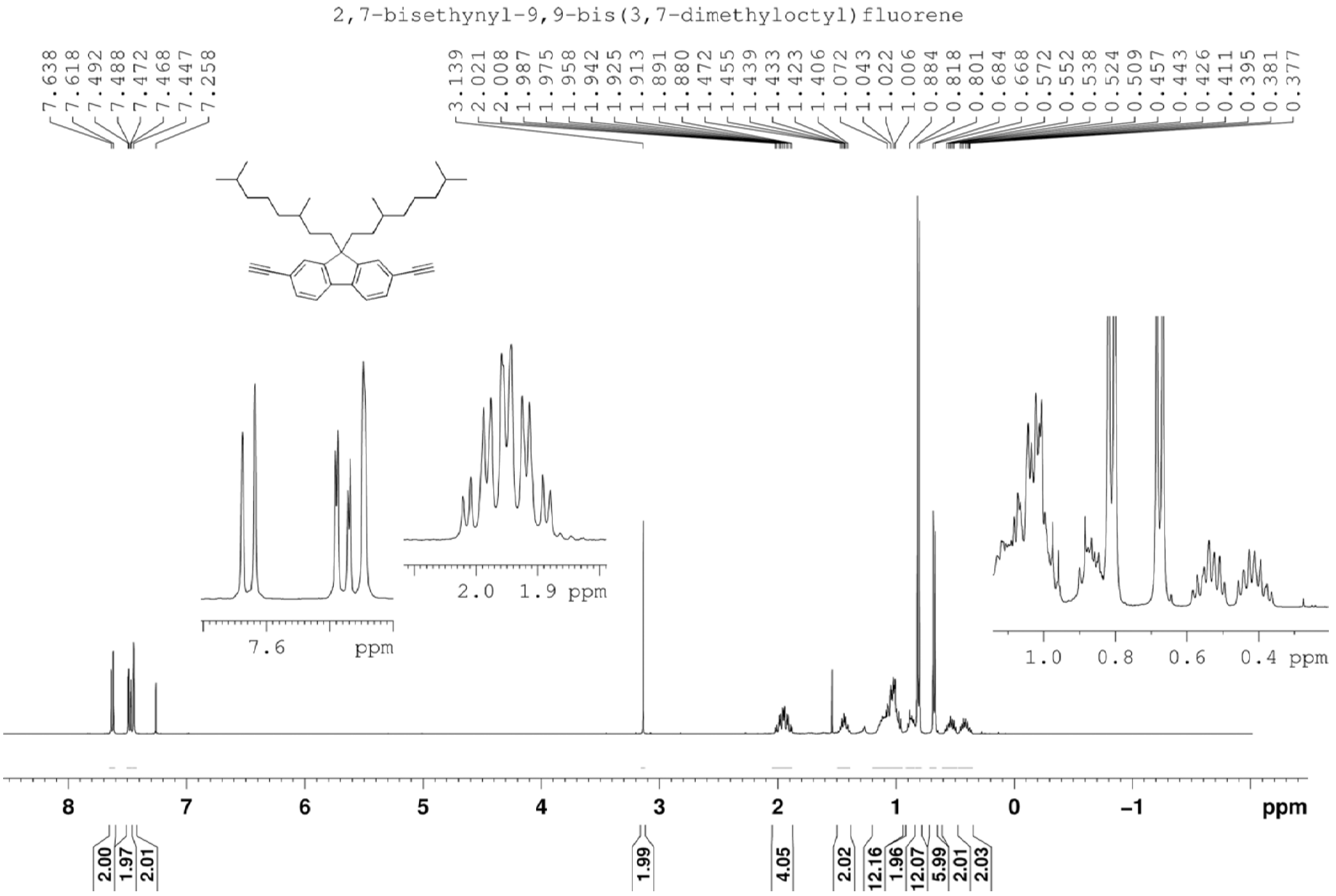

**Figure S4.12.** $^1$H NMR of 2,7-diethynyl-9,9-bis(3,7-dimethyloctyl)fluorene.

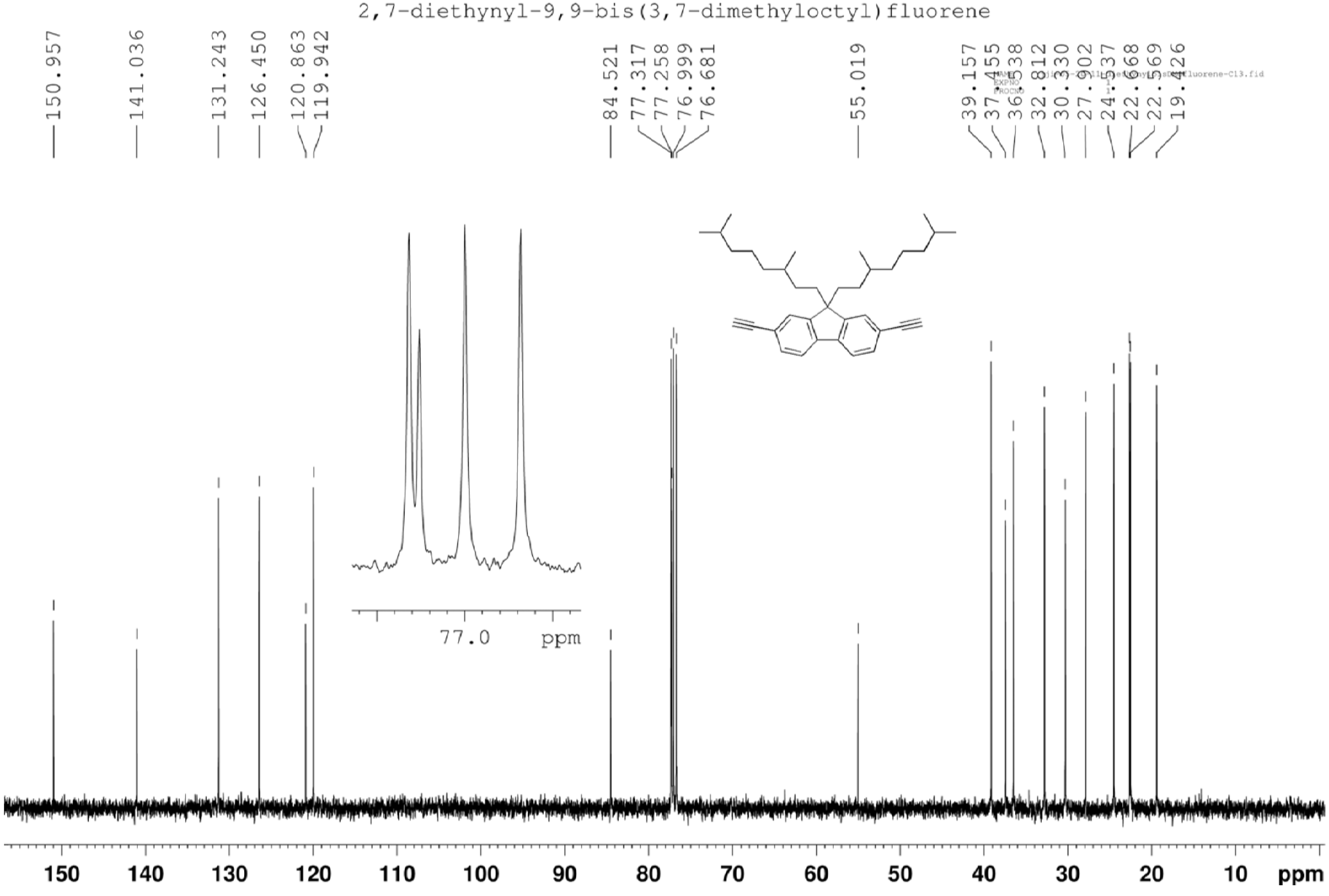

**Figure S4.13.** $^{13}$C NMR of 2,7-diethynyl-9,9-bis(3,7-dimethyloctyl)fluorene.

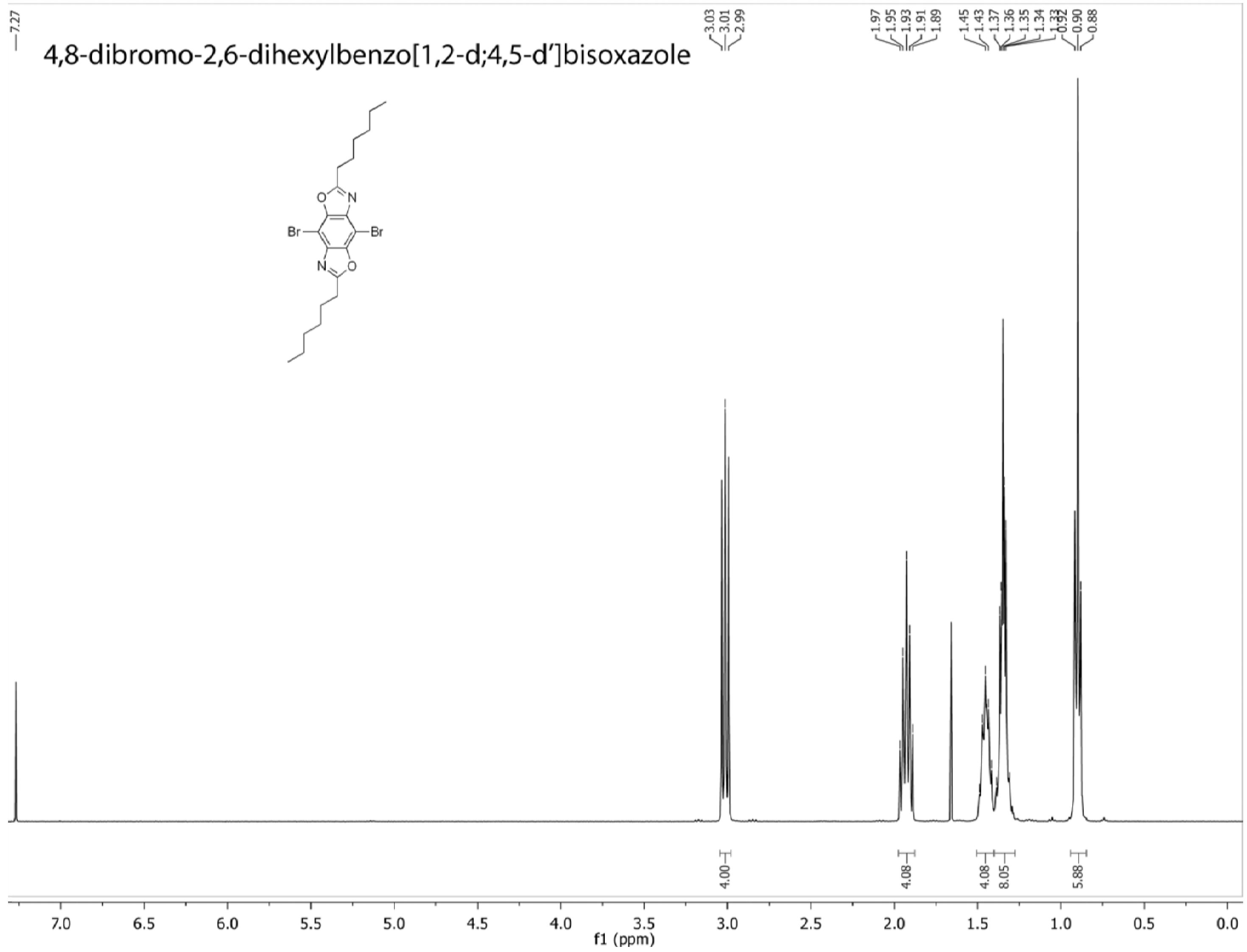

**Figure S4.14.** $^1$H NMR of 4,8-dibromo-2,6-dihexylbenzo[1,2-d;4,5-d']bisoxazole.

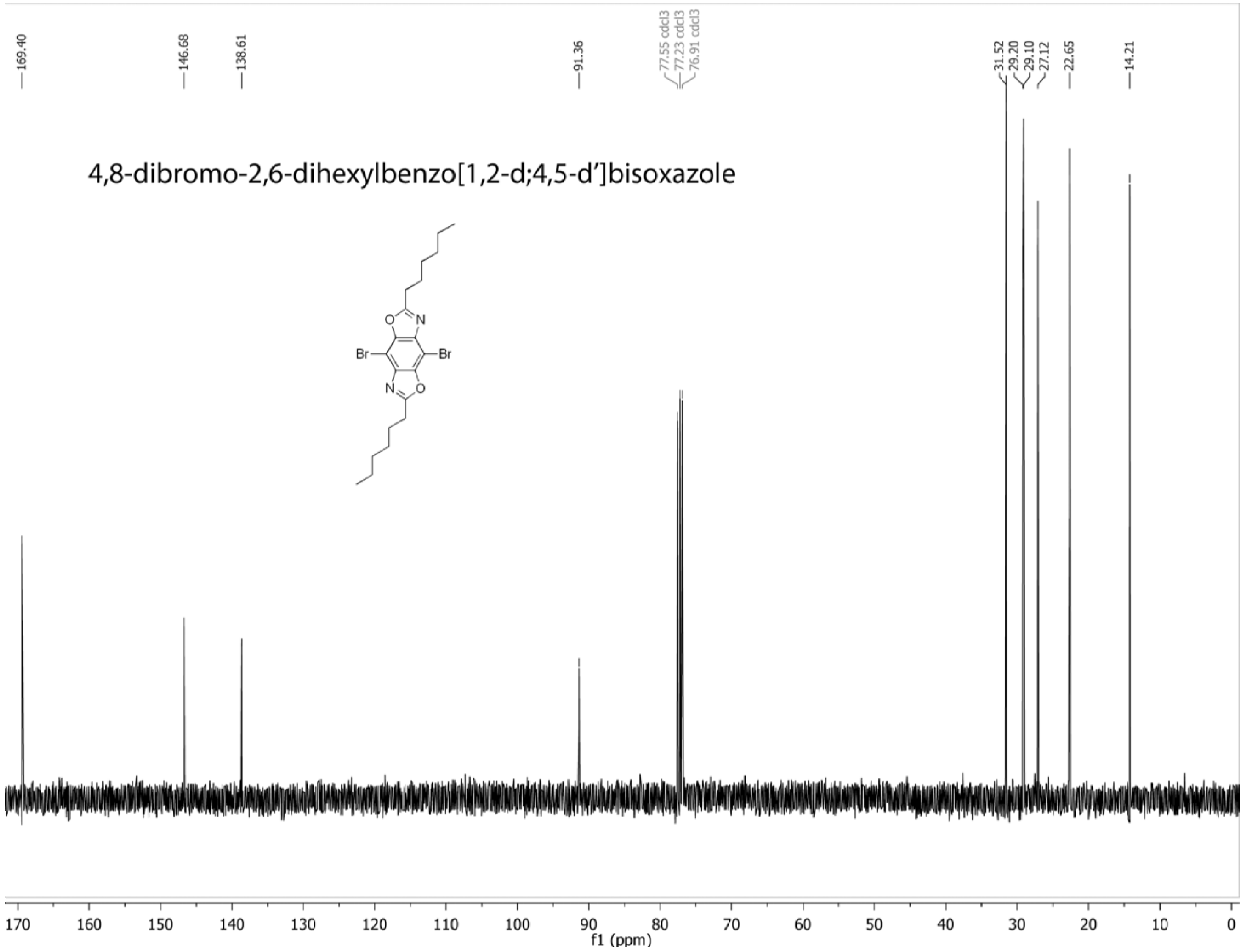

**Figure S4.15.** $^{13}$C NMR of 4,8-dibromo-2,6-dihexylbenzo[1,2-d;4,5-d’]bisoxazole.

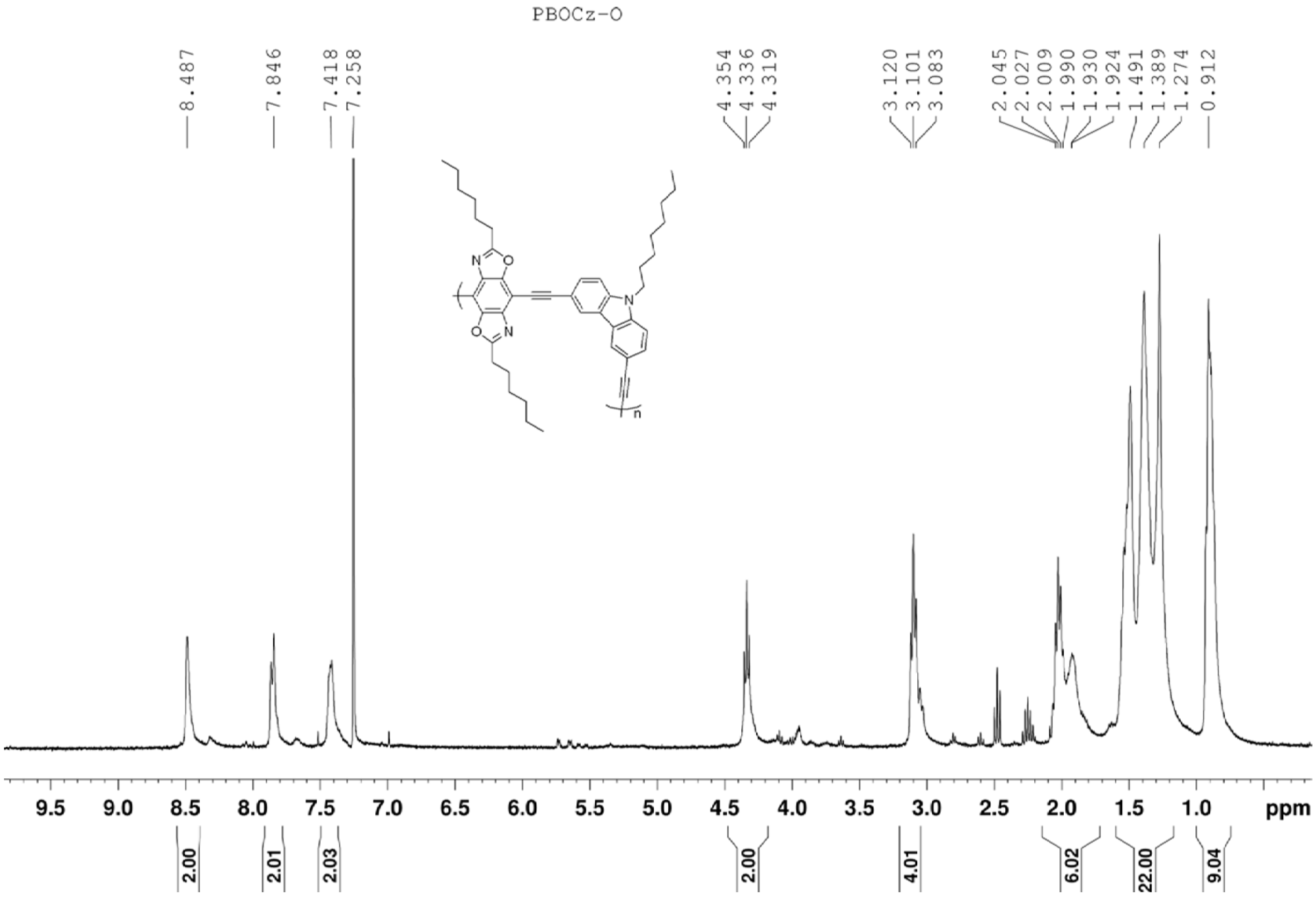

**Figure S4.16.** $^1$H NMR of PBOCz-O.

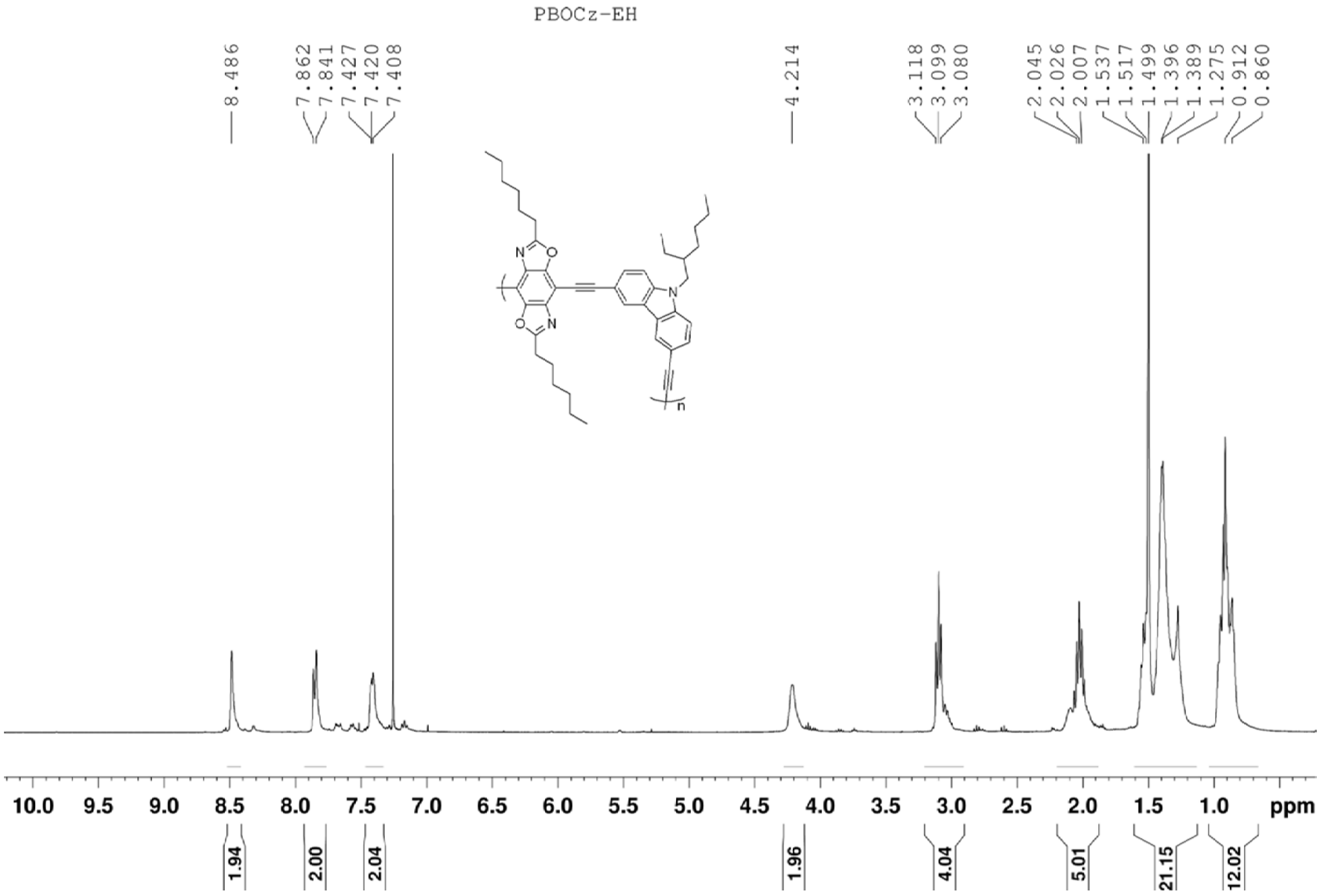

**Figure S4.17.** $^1$H NMR of PBOCz-EH.

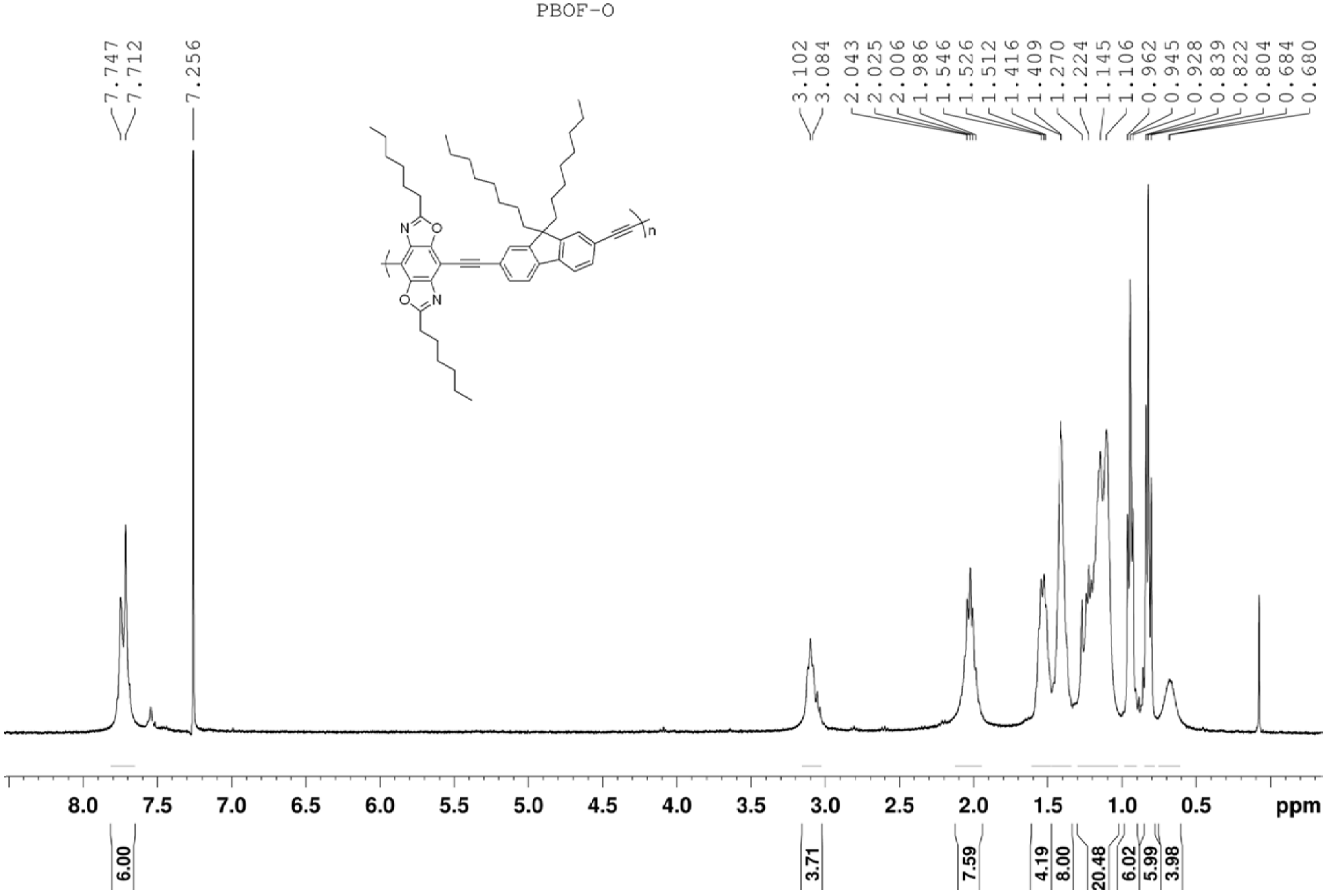

**Figure S4.18.** $^{1}$H NMR of PBOF-O.

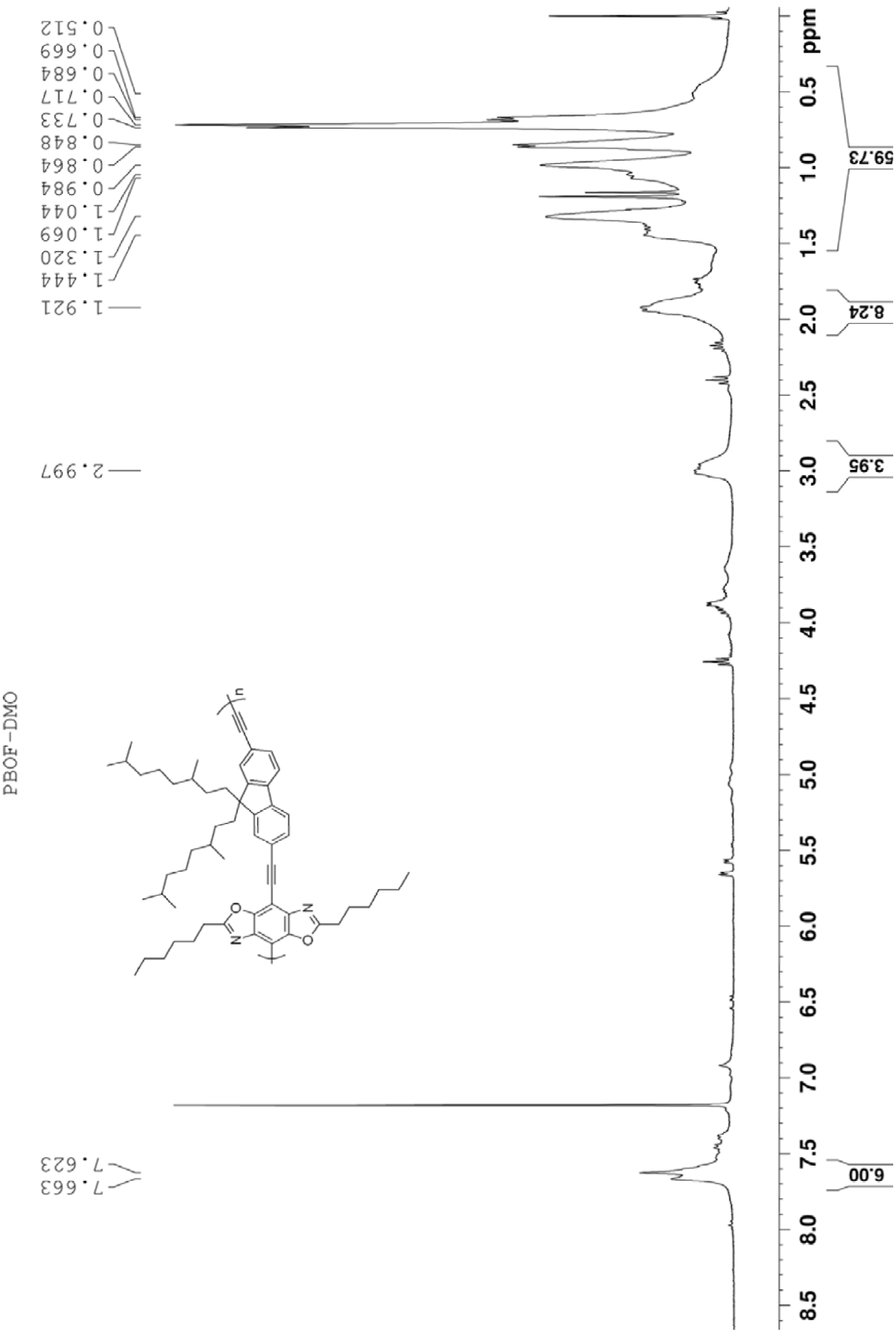

**Figure S4.19.** $^1$H NMR of PBOF-DMO.

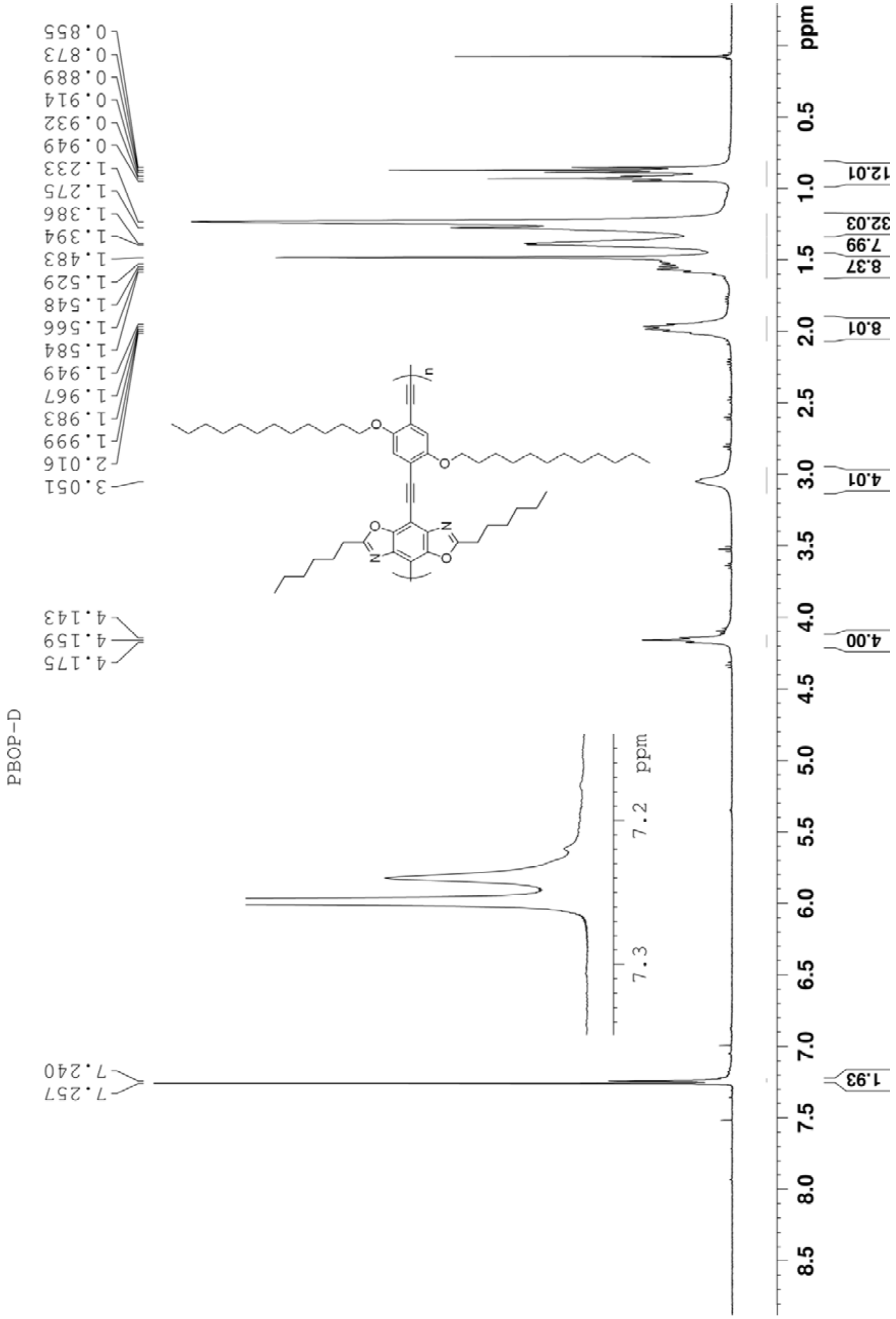

**Figure S4.20.** $^1$H NMR of PBOP-D.

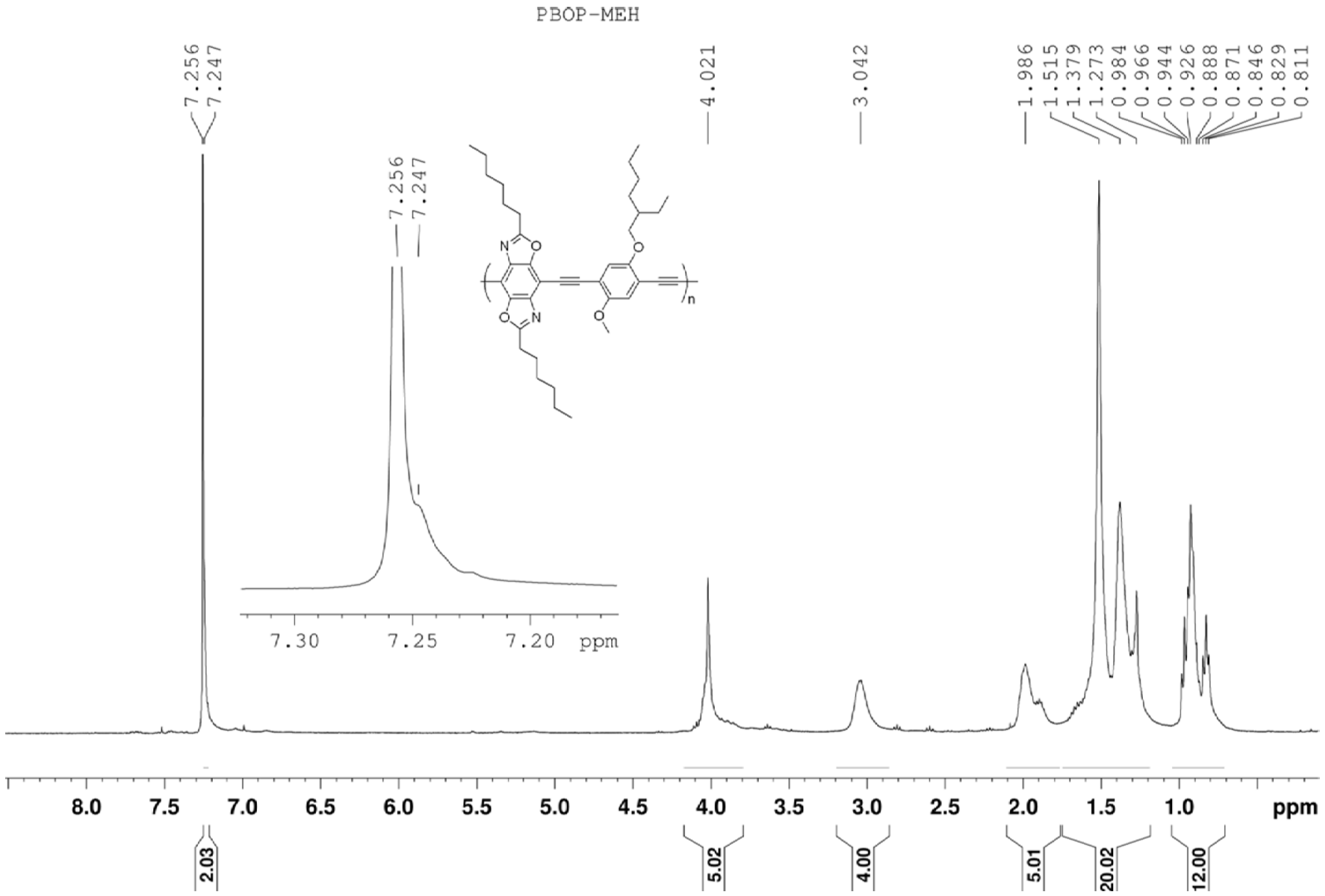

**Figure S4.21.** $^1$H NMR of PBOP-MEH.

## 4.8 REFERENCES

1. Tang, C. W.; Vanslyke, S. A. *Appl. Phys. Lett.* **1987,** 51, 913-915.
2. Friend, R. H.; Gymer, R. W.; Holmes, A. B.; Burroughes, J. H.; Marks, R. N.; Taliani, C.; Bradley, D. D. C.; Santos, D. A. Dos; Bredas, J. L.; Logdlund, M.; Salaneck, W. R. *Nature* **1999,** 397, (6715), 121-128.
3. Reineke, Sebastian; Lindner, Frank; Schwartz, Gregor; Seidler, Nico; Walzer, Karsten; Lussem, Bjorn; Leo, Karl. *Nature* **2009,** 459, (7244), 234-238.
4. Bernius, M. T.; Inbasekaran, M.; O'Brien, J.; Wu, W. *Adv. Mater.* **2000,** 12, (23), 1737-1750.
5. I.S, Millard. *Synth. Met.* **2000,** 111-112, (0), 119-123.
6. Burroughes, J. H.; Bradley, D. D. C.; Brown, A. R.; Marks, R. N.; Mackay, K.; Friend, R. H.; Burns, P. L.; Holmes, A. B. *Nature* **1990,** 347, (6293), 539-541.
7. Grimsdale, Andrew C.; Leok Chan, Khai; Martin, Rainer E.; Jokisz, Pawel G.; Holmes, Andrew B. *Chem. Rev.* **2009,** 109, (3), 897-1091.
8. Kraft, Arno; Grimsdale, Andrew C.; Holmes, Andrew B. *Angew. Chem., Int. Ed.* **1998,** 37, (4), 402-428.
9. Tseng, S. R.; Chen, Y. S.; Meng, H. F.; Lai, H. C.; Yeh, C. H.; Horng, S. F.; Liao, H. H.; Hsu, C. S. *Synth. Met.* **2009,** 159, (1-2), 137-141.
10. Jenekhe, Samson A.; de Paor, Liam R.; Chen, X. Linda; Tarkka, Richard M. *Chem. Mater.* **1996,** 8, (10), 2401-2404.
11. Jabbour, G. E.; Kawabe, Y.; Shaheen, S. E.; Wang, J. F.; Morrell, M. M.; Kippelen, B.; Peyghambarian, N. *Appl. Phys. Lett.* **1997,** 71, (13), 1762-1764.
12. Tonzola, C. J; Kulkarni, A. P; Gifford, A. P; Kaminsky, W.; Jenekhe, S. A. *Adv. Funct. Mater.* **2007,** 17, (6), 863-874.
13. Haiying, Chen; Junwu, Chen; Chengfeng, Qiu; Tang, B. Z.; Man, Wong; Hoi-Sing, Kwok. *IEEE J. Sel. Top. Quantum Electron.* **2004,** 10, (1), 10-15.
14. Zhang, Lianjie; Hu, Sujun; Chen, Junwu; Chen, Zhenhui; Wu, Hongbin; Peng, Junbiao; Cao, Yong. *Adv. Funct. Mater.* **2011,** 21, (19), 3760-3769.
15. Shu, Ching-Fong; Dodda, Rajasekhar; Wu, Fang-Iy; Liu, Michelle S.; Jen, Alex K. Y. *Macromolecules* **2003,** 36, (18), 6698-6703.

16. Ahmed, Eilaf; Kim, Felix S.; Xin, Hao; Jenekhe, Samson A. *Macromolecules* **2009,** 42, (22), 8615-8618.

17. Mikroyannidis, John A.; Gibbons, Katherine M.; Kulkarni, Abhishek P.; Jenekhe, Samson A. *Macromolecules* **2007,** 41, (3), 663-674.

18. Alam, Maksudul M.; Jenekhe, Samson A. *Chem. Mater.* **2002,** 14, (11), 4775-4780.

19. Babel, A.; Jenekhe, S. A. *Adv. Mater.* **2002,** 14, (5), 371-374.

20. Babel, Amit; Jenekhe, Samson A. *J. Phys. Chem. B* **2002,** 106, (24), 6129-6132.

21. Chen, Yan; Wang, Shanfeng; Zhuang, Qixin; Li, Xinxin; Wu, Pingping; Han, Zhewen. *Macromolecules* **2005,** 38, (23), 9873-9877.

22. Feng, Dongdong; Wang, Shanfeng; Zhuang, Qixin; Wu, Pingping; Han, Zhewen. *Polymer* **2004,** 45, (26), 8871-8879.

23. Wolfe, James F.; Arnold, F. E. *Macromolecules* **1981,** 14, (4), 909-915.

24. Wolfe, James F.; Loo, Bock H.; Arnold, F. E. *Macromolecules* **1981,** 14, (4), 915-920.

25. Intemann, Jeremy J.; Mike, Jared F.; Cai, Min; Bose, Sayantan; Xiao, Teng; Mauldin, Timothy C.; Roggers, Robert A.; Shinar, Joseph; Shinar, Ruth; Jeffries-El, Malika. *Macromolecules* **2010,** 44, (2), 248-255.

26. Mike, Jared F.; Intemann, Jeremy J.; Cai, Min; Xiao, Teng; Shinar, Ruth; Shinar, Joseph; Jeffries-El, Malika. *Polym. Chem.* **2011,** 2, (10), 2299-2305.

27. Mike, Jared F.; Makowski, Andrew J.; Jeffries-El, Malika. *Org. Lett.* **2008,** 10, (21), 4915-4918.

28. Mike, Jared F.; Inteman, Jeremy J.; Ellern, Arkady; Jeffries-El, Malika. *J. Org. Chem.* **2009,** 75, (2), 495-497.

29. Bhuwalka, Achala; Mike, Jared F.; He, Meng; Intemann, Jeremy J.; Nelson, Toby; Ewan, Monique D.; Roggers, Robert A.; Lin, Zhiqun; Jeffries-El, Malika. *Macromolecules* **2011**.

30. Tonzola, Christopher J.; Alam, Maksudul M.; Jenekhe, Samson A. *Macromolecules* **2005,** 38, (23), 9539-9547.

31. Miyamae, T.; Yoshimura, D.; Ishii, H.; Ouchi, Y.; Miyazaki, T.; Koike, T.; Yamamoto, T.; Muramatsu, Y.; Etori, H.; Maruyama, T.; Seki, K. *Synth. Met.* **1997,** 84, (1-3), 939-940.

32. Cardona, Claudia M.; Li, Wei; Kaifer, Angel E.; Stockdale, David; Bazan, Guillermo C. *Adv. Mater.* **2011,** 23, (20), 2367-2371.

33. Jenekhe, Samson A.; Osaheni, John A. *Science* **1994,** 265, (5173), 765-768.

34. Cheon, K. O.; Shinar, J. *Appl. Phys. Lett.* **2004,** 84, (7), 1201-1203.

35. Cai, Min; Xiao, Teng; Hellerich, Emily; Chen, Ying; Shinar, Ruth; Shinar, Joseph. *Adv. Mater.* **2011,** 23, (31), 3590-3596.

36. Choulis, Stelios A.; Choong, Vi-En; Mathai, Mathew K.; So, Franky. *Appl. Phys. Lett.* **2005,** 87, (11), 113503.

37. Chan, M. Y.; Lee, C. S.; Lai, S. L.; Fung, M. K.; Wong, F. L.; Sun, H. Y.; Lau, K. M.; Lee, S. T. *J. Appl. Phys.* **2006,** 100, (9), 094506.

38. Baldo, M. A.; Thompson, M. E.; Forrest, S. R. *Pure Appl. Chem.* **1999,** 71, (11), 2095-2106.

39. Pope, Martin; Swenberg, Charles E., *Electronic Processes in Organic Crystals*. Oxford University Press, Oxford: 1982.

40. Takihana, Yoshihiro; Shiotsuki, Masashi; Sanda, Fumio; Masuda, Toshio. *Macromolecules* **2004,** 37, (20), 7578-7583.

41. Moon, In Kyu; Kawamoto, Masuki; Wada, Tatsuo. *J. Polym. Sci., Part A: Polym. Chem.* **2009,** 47, (9), 2434-2442.

42. Maji, Modhu Sudan; Pfeifer, Thorben; Studer, Armido. *Chem.--Eur. J.* **2010,** 16, (20), 5872-5875.

43. Moroni, M.; Le Moigne, J.; Luzzati, S. *Macromolecules* **1994,** 27, (2), 562-571.

44. Dellsperger, Simon; Dötz, Florian; Smith, Paul; Weder, Christoph. *Macromol. Chem. Phys.* **2000,** 201, (2), 192-198.

45. Tlach, Brian C.; Tomlinson, Aimée L.; Bhuwalka, Achala; Jeffries-El, Malika. *J. Org. Chem.* **2011,** 76, (21), 8670-8681.

46. Kannan, Ramamurthi; He, Guang S.; Lin, Tzu-Chau; Prasad, Paras N.; Vaia, Richard A.; Tan, Loon-Seng. *Chem. Mater.* **2003,** 16, (1), 185-194.

47. Nad, Sanjukta; Kumbhakar, Manoj; Pal, Haridas. *J. Phys. Chem. A* **2003,** 107, (24), 4808-4816.

48. Zhou, Z.; Shinar, R.; Allison, A. J; Shinar, J. *Adv. Funct. Mater.* **2007,** 17, (17), 3530-3537.

# Chapter 5

## Changing the Conjugation Pathway in Benzobisoxazole-Containing Polymers: Effect on Physical and Electronic Properties

*Jeremy J. Intemann, Brian C. Tlach, Achala Bhuwalka, Robert A. Roggers, and Malika Jeffries-EL*[*]

Department of Chemistry, Iowa State University, Ames, IA 5001, United States

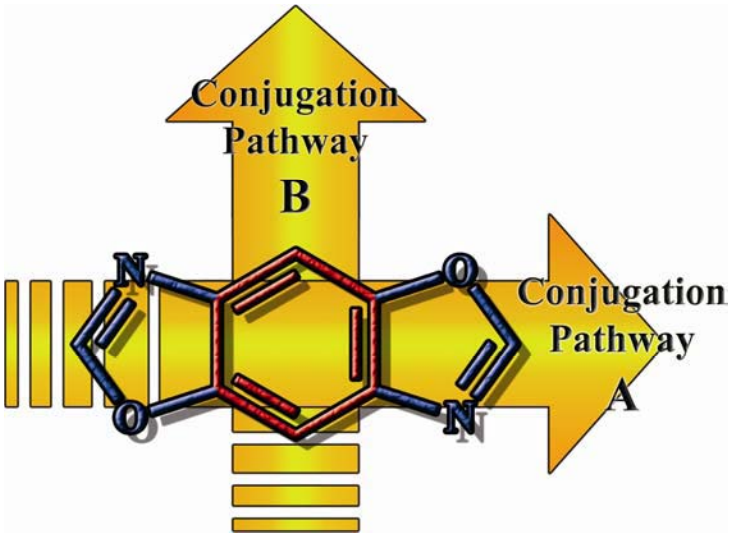

### 5.1 ABSTRACT

Recent developments in the synthesis of functional benzobisoxazoles have led to new benzobisoxazole-containing polymers that possess two possible conjugation pathways through the moiety. In one instance, the conjugation pathway is through the oxazole rings (pathway A) while the second conjugation pathway is directly through the central benzene ring (pathway B), leaving the oxazole rings perpendicular to the polymer backbone. In order to probe the structure-property relationships that exist between these different configurations, three polymers featuring conjugation pathway A were made, while three other structurally analogous polymers with conjugation pathway B were also synthesized. The changes in the physical and electronic properties were examined and it was found that the conjugation pathway resulted in improved

electron accepting strength and larger electron affinities in the polymers. Conversely, conjugation pathway B yields polymers with narrower bandgaps. The latter is due to the improved stabilization of the quinoid resonance forms of the polymers, which increases the effective conjugation length of the π-system. Polymers using conjugation pathway B also exhibited lower glass transition temperatures and produced the first benzobisoxazole-containing polymers that displayed melting points below their decomposition temperature. We attributed this to the increased number of alkyl side chains in these polymers compared to those that feature conjugation pathway A.

## 5.2 INTRODUCTION

As a result of their unique physical and electronic properties, conjugated polymers have found widespread interest as active materials in organic electronic applications such as photovoltaics (OPVs),[1-5] light-emitting diodes (OLEDs),[6-9] and field-effect transistors (OFETs).[10-13] These materials are attractive for semiconducting applications because their physical and optical properties can be synthetically tuned and devices can be fabricated from them using low-cost thin-film processing techniques such as spin-coating or inkjet printing[14-16]. A common strategy for designing semiconducting polymers is to synthesize donor-acceptor polymers by alternating electron-donating and electron-accepting moieties within a polymer backbone.[17-21] This approach has led to materials with narrow optical bandgaps and improved charge transport which has resulted in OPVs with power conversion efficiencies greater than 7% and OFETs with charge carrier mobilities exceeding 0.1 $cm^2$ $V^{-1}$ $s^{-1}$.[3, 22-26] However, the development of new acceptors is of particular interest as it has been shown that incorporating electron deficient moieties into emissive polymers improves electron injection and transport in OLEDs, providing better charge carrier balance.[27-29]

Benzobisazoles are an electron-deficient class of compounds that have shown a great deal of promise as acceptors in donor-acceptor copolymers. Polymers made from these materials are known to possess good electron transport,[29-31] high photoluminescence quantum yields,[32-34] and third-order nonlinear optical properties.[35-37] Within this class of compounds, the benzobisoxazole (BBO) isomer benzo[1,2-*d*;4,5-*d'*]bisoxazole (*trans*-BBO) has been by far the least developed. This is a result of the harsh reaction conditions traditionally used in the synthesis of polybenzobisoxazoles, which requires polyphosphoric acid at temperatures as high as 250 °C.[38]

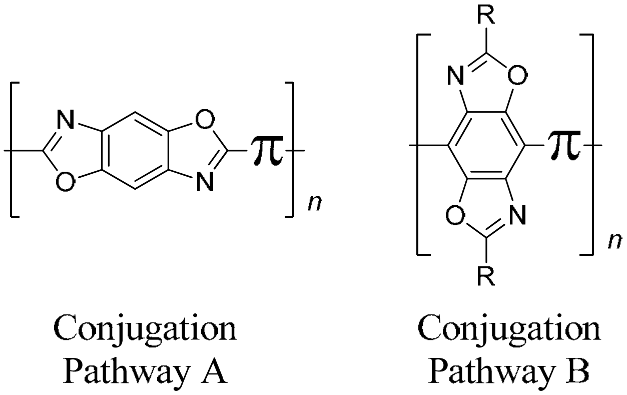

**Figure 5.1.** Polybenzobisoxazoles with the traditional 2,6-backbone connectivity (left) and the new 4,8-backbone connectivity (right).

Under these conditions, the required starting material, 1,4-diaminohydroquinone, is quickly oxidized to the quinone, preventing polymer growth. We recently reported a new method to prepare functional BBO monomers for conjugated polymers using orthoester condensations that has allowed for the first *trans*-BBO-containing semiconducting polymers.[39-41] To date, all BBO-containing polymers have had backbone connectivity at the 2 and 6-position of the BBO, resulting in a conjugation pathway through the oxazole rings (Figure 5.1). We recently reported several new *trans*-BBOs that have an extended π-conjugated system off of the central benzene ring.[42] We realized that this approach could be adapted to make *trans*-BBO-containing polymers that have backbone connectivity at the 4 and 8-position, giving the materials a novel conjugation pathway directly through the central benzene ring of the moiety (Figure 5.1). Such an approach potentially allows for further functionalization at the 2 and 6-position on the BBO, giving BBOs a level of versatility rarely demonstrated in monomers used to make organic semiconducting polymers.

Changing the conjugation pathway of these polymers has potentially significant implications on a wide range of their characteristics, such as thermal stability, electronic properties, solubility, film forming properties, and charge carrier mobilities. All of these characteristics could affect these materials performance in organic electronic devices. To better understand the structure-property relationships between the two different conjugation pathways, we prepared two functionalized BBO monomers. The first monomer (**M-A**) has a conjugation pathway through the oxazole rings (pathway A) while the second monomer (**M-B**) has a conjugation pathway directly through the central benzene ring (pathway B). We incorporated octyl chains into the 2 and 6-position of the **M-B** monomer, to improve the solubility of the polymers utilizing this monomer relative to polymers made from monomer **M-A**. The 2 and 6-position of BBO cannot be functionalized with halogens, boronic acids or tin groups, so in order to provide the monomers with a functional handle that could be used for polymerization, those positions were functionalized with 5-bromo-4-octylthiophenes, creating monomer **M-A**. To be consistent, monomer **M-B** was also functionalized with 5-bromo-4-octylthiophenes, but at the 4 and 8-positions. Alternating copolymers containing 9,9-dioctylfluorene, 3,3'-dioctyl-2,2'-bithiophene, or 4,4-dioctyldithieno[3,2-*b*:2',3'-*d*]silole were made with each of the BBO monomers and their physical and optical properties were investigated. The polymers with conjugation pathway B had smaller optical bandgaps resulting from improved stabilization of the quinoid resonance form of the polymers, while polymers with conjugation pathway A had higher electron affinities. The increased number of alkyl chains possessed by the polymers made from the **M-B** monomer, caused lower glass transition temperatures and produced the first benzobisoxazole polymers with melting points.

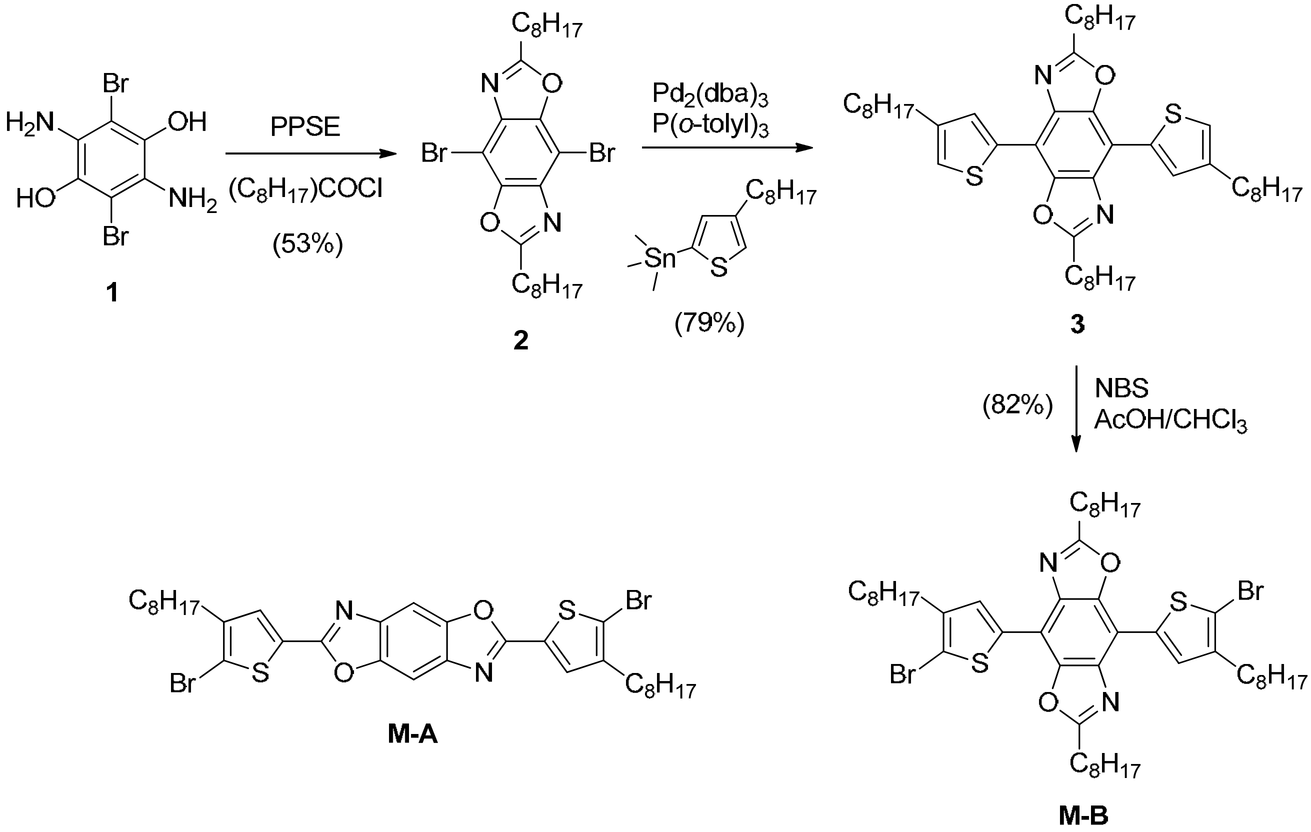

Br
H2N
OH
HO
NH2
Br
1
PPSE
(C8H17)COCl
(53%)
C8H17
N
O
Br
Br
O
N
C8H17
2
Pd2(dba)3
P(o-tolyl)3
Sn
S
C8H17
(79%)
C8H17
C8H17
S
N
O
S
C8H17
O
N
C8H17
3
(82%)
NBS
AcOH/CHCl3
C8H17
Br
S
N
O
O
N
S
Br
C8H17
M-A
C8H17
C8H17
S
Br
N
O
S
Br
C8H17
O
N
C8H17
M-B

**Scheme 5.1.** Synthesis of the benzobisoxazole monomers.

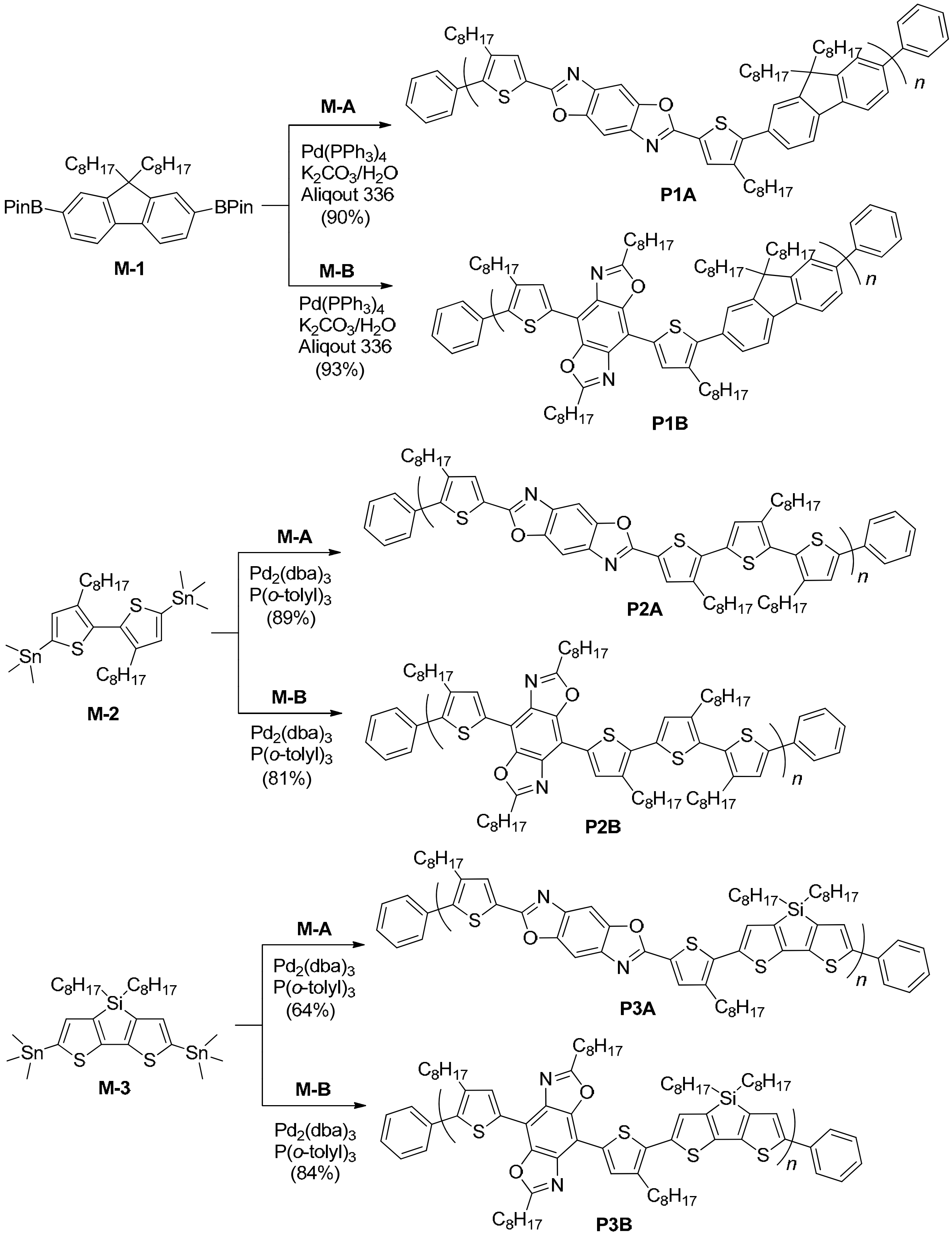
M-1
PinB
BPin
C8H17
M-A
Pd(PPh3)4
K2CO3/H2O
Aliqout 336
(90%)
P1A
M-B
Pd(PPh3)4
K2CO3/H2O
Aliqout 336
(93%)
P1B
M-2
Sn
S
M-A
Pd2(dba)3
P(o-tolyl)3
(89%)
P2A
M-B
Pd2(dba)3
P(o-tolyl)3
(81%)
P2B
M-3
Si
M-A
Pd2(dba)3
P(o-tolyl)3
(64%)
P3A
M-B
Pd2(dba)3
P(o-tolyl)3
(84%)
P3B
N
O
n

**Scheme 5.2.** Synthesis of benzobisoxazole polymers.

## 5.3 RESULTS AND DISCUSSION

**5.3.1 Synthesis.** Monomers **M-A**,[33] **M-1**,[43] **M-2**,[44] and **M-3**[45] were synthesized according to literature procedures. The synthetic route to monomer **M-B** is outlined in Scheme 5.1. 4,8-dibromo-2,6-dioctylbenzobisoxazole (**2**) was made via condensation of **1** with nonanoyl chloride in the presence of poly(trimethylsilyl phosphate) (PPSE). This was then used in a Stille cross-coupling reaction with 2-(trimethylstannyl)-4-octylthiophene using catalytic $Pd_2(dba)_3$ and $P(o\text{-}tolyl)_3$ to produce **3**. Bromination of **3** with NBS in acetic acid and chloroform yielded monomer **M-B** in good yields.

The syntheses of the six polymers are illustrated in Scheme 5.2. The fluorene-containing polymers **P1A** and **P1B** were made via Suzuki polymerizations between **M-1** and the corresponding BBO monomer using aqueous $NaCO_3$ and catalytic $Pd(PPh_3)_4$ in toluene followed by end-capping of the polymer chains with phenyl groups. This produced polymers in good yields with moderate molecular weights after removal of low molecular weight material. Polymer **P1A** is a material that we previously reported, but it was not end-capped.[33] Polymer **P1A** should exhibit better performance in devices as reactive end groups such as boronic acids can act as low energy charge traps and non-radiative recombination sites.[46-48] Polymers **P2A, P2B, P3A**, and **P3B** were synthesized via Stille polymerizations using **M-2** and the corresponding BBO monomer with catalytic $Pd_2(dba)_3$ and tri-o-tolylphosphine in toluene followed by end-capping of the polymer chains with phenyl groups. **P2A** is also a polymer that we previously reported,[44] although we were able to improve on its synthesis by running the polymerization at lower temperatures and changing the solvent from chlorobenzene to toluene. This resulted in a 43% increase in its molecular weight ($M_n$) accompanied by substantially improved yields. The polymer was also end-capped with phenyl groups, which was not previously done. All of the polymers had good solubility in common organic solvents such as chloroform, THF, *o*-dichlorobenzene, and toluene.

**5.3.2 Physical Properties.** The molecular weights of the polymers were determined by gel permeation chromatography (GPC) using polystyrene standards in THF, the results of which are listed in Table 5.1. Due to its poor solubility, the molecular weights for **P3A** are low. The poly dispersities (PDIs) of the polymers were all in line with step-growth polymerizations (~2).

Table 5.1. Physical Properties of Benzobisoxazole Polymers

| Polymer | $M_n$[a] (kDa) | $M_w$[a] (kDa) | PDI | DP[b] | $T_g$[c] (°C) | $T_m$[c] (°C) | $T_d$[d] (°C) |
|---|---|---|---|---|---|---|---|
| **P1A** | 16.1 | 29.8 | 1.8 | 17 | - | - | 327 |
| **P1B** | 20.2 | 44.6 | 2.2 | 17 | 142 | 202 | 356 |
| **P2A** | 11.7 | 29.1 | 2.5 | 13 | 198 | - | 388 |
| **P2B** | 11.3 | 23.6 | 2.1 | 10 | 104 | 180 | 365 |
| **P3A** | 4.5 | 20.0 | 4.4 | 5 | - | - | 315 |
| **P3B** | 10.2 | 47.4 | 4.6 | 9 | - | - | 342 |

[a] Determined by GPC in THF using polystyrene standards. [b] Degree polymerization calculated from the number averaged molecular weight. [c] Glass transition ($T_g$) and melting point ($T_m$) data from second scan reported, heating rate 20 °C/min under $N_2$. [d] 5% weight loss temperature by TGA in air.

The dithienosilole-containing polymers had much higher PDIs than the other polymers despite the similar reaction conditions of **P3A** and **P3B** with **P2A** and **P2B**.

The thermal properties of the polymers were studied using thermal gravimetric analysis (TGA) and differential scanning calorimetry (DSC), the results of which are summarized in Table 5.1. All of the polymers had high thermal stabilities with 5% weight loss occurring above 300 °C. The fluorene and dithienosilole-containing polymers show an improvement in thermal stability of 17-19 °C in the polymers featuring conjugation pathway B over the pathway A polymers. This is not a particularly large improvement and the trend does not exist in the bithiophene-containing polymers, which show a higher thermal stability in the polymer containing pathway A. Only three of the polymers, **P1B**, **P2A**, and **P2B**, showed endotherms corresponding to glass transition temperatures. Of those, **P1B** and **P2B** had melting points at 202 and 180 °C, respectively. This is interesting in that, to our knowledge, none of the previously reported benzobisoxazole-containing polymers have exhibited melting points below their decomposition temperature. Our previous report on **P2A** showed a $T_g$ of only 84.6 °C.[44] The increase in $T_g$ seen here is the result of the larger molecular weight of the polymer. Interestingly, our previous report on **P1A** showed a $T_g$ of 108 °C, yet there was no observable transition in the material reported here. The previous synthesis of this polymer featured boronic acid and bromine end groups that could have an impact on the solid state packing of the material, lowering its $T_g$ into an observable temperature range.

All of the polymers showed either $T_g$s or $T_d$s above typical operating temperatures of organic electronic devices and although there is a very limited selection from which to draw conclusions from, it appears the 4,8-BBO-containing polymers exhibit lower glass transition temperatures. In all likelihood, this is more of an effect of the introduction of flexible side chains to the 4,8-BBO and not necessarily a consequence of changing the conjugation pathway of the polymer. It is entirely possible, however, that pathway B causes twisting of the polymer's backbone to a greater extent than pathway A, reducing its ability to π-stack efficiently, lowering its $T_g$. If the latter is true, a large increase in the optical bandgap of the polymers utilizing pathway B would be seen, due to a reduced effective conjugation length. However, no such increase was observed.

**5.3.3 Optical Properties.** The optical properties of the polymers were examined using UV-Vis and fluorescence spectroscopy, the results of which are summarized in Table 5.2. The UV-Vis absorption spectra of the polymers in solution and as thin films are shown in figure 5.2. The fluorene-containing polymers **P1A** and **P1B** had the shortest wavelength absorption of the six polymers in solution. **P1B** had an absorption that was red-shifted 13 nm with respect to

**Table 5.2.** Optical Properties of the Benzobisoxazole Polymers in Solution and Film.

| | Solution[a] | | | Thin Film | | |
|---|---|---|---|---|---|---|
| **Polymer** | $\lambda_{max}$ (nm) | $\lambda_{em}$ (nm) | $\Phi_{rel}$[b] | $\lambda_{max}$ (nm) | $\lambda_{em}$ (nm) | $E_g^{opt}$ (eV)[c] |
| **P1A** | 420 | 472 | 0.43 | 438 | 524 | 2.55 |
| **P1B** | 433 | 492 | 0.37 | 465 | 548 | 2.46 |
| **P2A** | 438 | 553 | 0.20 | 514 | 601 | 2.07 |
| **P2B** | 455 | 569 | 0.22 | 494 | 720 | 1.94 |
| **P3A** | 499 | 577 | 0.15 | 535 | 649 | 2.01 |
| **P3B** | 480 | 600 | 0.09 | 534 | 652 | 1.91 |

[a] Solution measurements performed in chloroform. [b] Photoluminescence quantum yields measured in chloroform relative to Coumarin 152 in acetonitrile. [c] Optical bandgap measured from absorption onset.

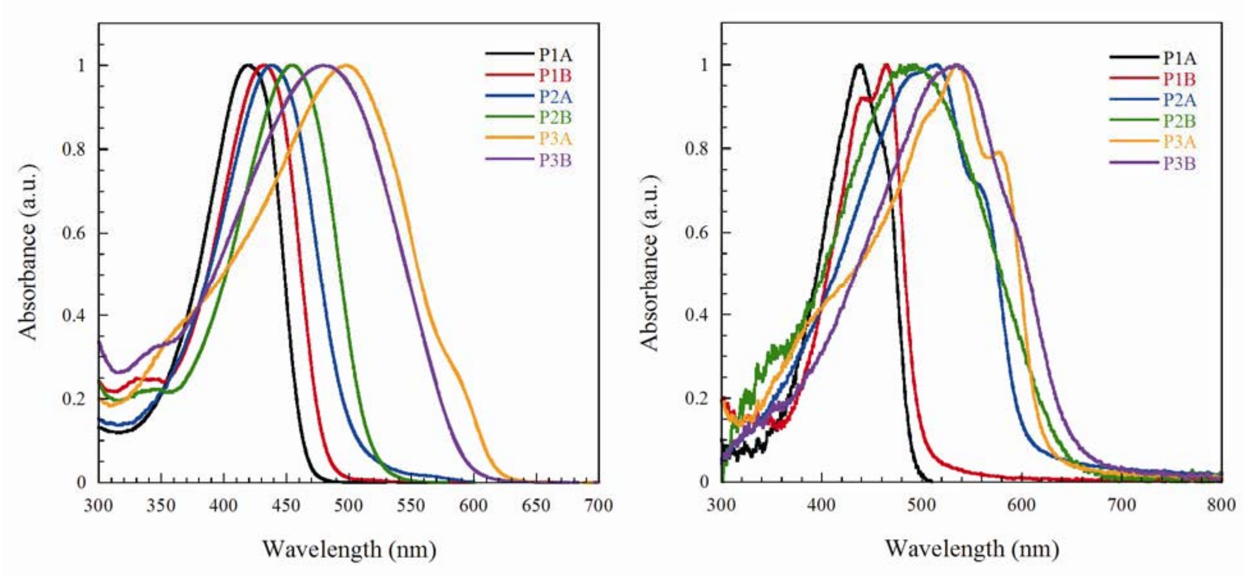

**Figure 5.2.** UV-Vis absorption spectra of polymers in solution (left) and as thin films (right).

**P1A**'s absorption. In films, these two polymers had maximum absorptions that were red-shifted 18 nm and 32 nm for **P1A** and **P1B**, respectively, compared to their solution absorption maxima. This difference appears to be the result of a change in the intensities of two electronic transitions in the polymers. In film, **P1A** has an absorption maximum at 438 nm and a shoulder at 460 nm, while **P1B** has an absorption maximum at 465 nm with a shoulder at 442 nm. This suggests that the overall spectrum of **P1A** and **P1B** is only separated by 4-5 nm, a slightly smaller difference than seen in solution.

Polymers **P2A** and **P2B** had absorptions in solution of 438 and 455 nm, respectively. They are red-shifted compared to the fluorene-containing polymers, which is the product of the increased donor strength of bithiophene relative to fluorene. In films, the absorption spectra of the two polymers are red-shifted to 514 nm (shifted 76 nm) and 494 nm (shifted 39 nm) compared to solution spectra. The increased red-shift of the absorptions of these polymers, compared to the fluorene-containing polymers, is the result of substituting the fluorene unit with the bithiophene. The C-9 carbon on the fluorene possesses $sp^3$ hybridization which causes the octyl chains on the fluorene to point out of the plane of the π-system, disrupting π-stacking and limiting intermolecular effects between polymer chains. This creates highly amorphous films which is evident from the x-ray diffraction analysis of the films (see Figure S5.5 in the supporting information) which shows no statistically meaningful periodicity in the **P1A** and **P1B** films. The bithiophene moiety has alkyl chains that are oriented in the plane of the π-system, leading to increased aggregation of the polymer chains and a red-shifted absorption. The larger red-shift of the **P2A** spectrum, relative to **P2B**, can be explained as increased aggregation in the films resulting from possessing fewer alkyl chains than **P2B**. Interestingly, the x-ray diffraction data of the **P2A** and **P2B** films shows no statistically meaningful periodicity in the **P2A** films, but does show periodicity in the **P2B** films, with a d-spacing of 19.6 Å. This distance correlates well with a side-by-side polymer chain configuration with the alkyl chains on adjacent polymer chains pointed towards each other. This suggests the alkyl chains on **P2B** helps assist in interdigitation of the alkyl chains, leading to greater order in the film. This is beneficial as increased film order is known to improve charge carrier mobilities in devices.[49] Though there is no periodicity in the **P1A** films, the reduced number of alkyl chains is likely causing increased formation of amorphous aggregates in the film, resulting in the increased red-shift of its absorption.

The dithienosilole containing polymers, **P3A** and **P3B**, have the longest wavelength of absorption in solution at 499 and 480 nm, consistent with the increased donor character of the dithienosilole compared to bithiophene and fluorene. Oddly, **P3A** has a longer wavelength of absorption relative to **P3B**. This goes against the trend seen in the fluorene and bithiophene-containing polymers where the polymers possessing pathway B have a longer wavelength of absorption. There is no obvious reason for this change in trend but one possibility could be that the much higher molecular weight of **P3B** has a much broader distribution of HOMO energy levels than **P3A**, causing increased absorption at shorter wavelengths. This conclusion is somewhat supported by the film measurements of the polymers as the dithienosilole-containing polymers have nearly identical absorption maxima. The fact that **P3B** has a smaller optical bandgap than **P3A**, yet has a similar absorption maximum in film, additionally supports the notion that **P3B** has a broader HOMO distribution. The x-ray diffraction data is not particularly helpful in this case, as it shows periodicity in both polymers with d-spacings of 53.2 and 43.1 Å for **P3A** and **P3B**, respectively. These values are too large to correspond to co-facially stacked polymer chains or interdigitation distances of the polymers and are more likely the result of periodicity between amorphous aggregates within the film.

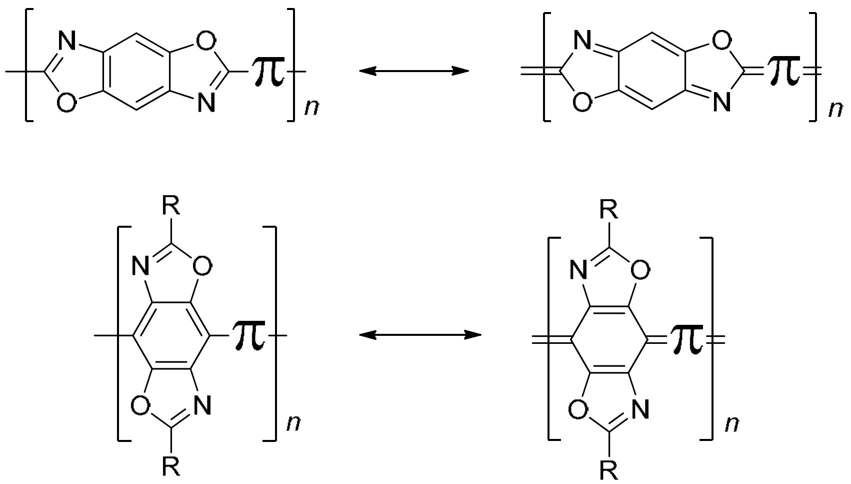

**Figure 5.3.** Benzoid and quinoid resonance structures of benzobisoxazole polymers.

One trend in the optical data that stands out is that the optical bandgaps of the polymers featuring the B pathway are all around 0.1 eV smaller than the polymers containing the A pathway, without exception. The likely reason for this trend is the improved stabilization of the quinoid resonance form from pathway B. Figure 5.3 illustrates how when the BBO is connected at the 2 and 6-positions, both the oxazole and benzene rings of the BBO lose their aromaticity, causing a large difference in the energy between the benzoid and quinoid resonance forms. But when the BBO is connected through the 4 and 8-positions, the oxazole rings remain aromatic in the quinoid form, lowering its energy and resulting in increased quinoid character of the polymer in the ground state. This is known to increase the HOMO energy levels while decreasing the LUMO of the polymer by extending the effective conjugation length of the π-system, narrowing the bandgap.[50]

The photoluminescence (PL) spectra of the polymers in solution and as thin films are shown in Figure 5.4. The fluorene-containing polymers exhibited the shortest wavelength of emission at 472 and 492 nm for **P1A** and **P1B**, respectively. In films, the emission of the polymers red-shifts to 524 and 548 nm, shifts of 52 and 56 nm for **P1A** and **P1B**, respectively, likely due to exciplex formation between polymers within the film. The bithiophene-containing polymers, **P2A** and **P2B**, show a similar trend in solution with **P2B** having a longer wavelength of emission at 569 nm than **P2A** (553 nm). In films, however, **P2B** has a much more drastic red-shift than **P2A**, which exhibits a 48 nm shift, while **P2B** red-shifts 151 nm to 720 nm. The extremely large red-shift seen in the **P2B** films is surprising and it must be noted that **P2B** films

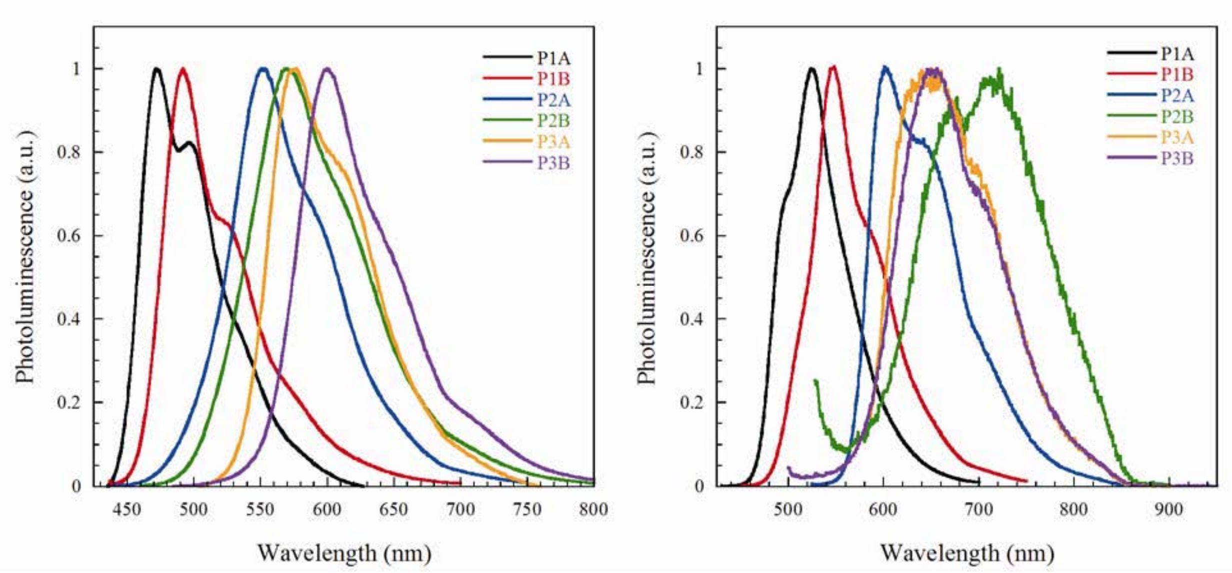

**Figure 5.4.** Photoluminescence spectra of polymers in chloroform solutions (left) and as thin films (right).

(as well as **P3A** and **P3B** films) was extremely weakly fluorescent, with the noise in the PL spectra being a consequence of this fact. As seen in the previously mentioned polymers, the pathway B-containing **P3B** shows a longer wavelength of emission than the pathway A-containing **P3A**, with emission maxima of 577 and 600 nm for **P3A** and **P3B**, respectively. The photoluminescence of the polymers red-shifts to 649 and 652 nm in films, corresponding to shifts of 72 and 52 nm, respectively. The larger red-shift in the pathway A-containing **P3A** is not consistent with the fluorene and bithiophene-containing polymers and the data as a whole suggests that how the two BBO moieties effect intermolecular interactions is highly dependent on the donor-acceptor system.

Photoluminescence quantum yield measurements of the polymers were taken in dilute chloroform solutions relative to coumarin 152 in acetonitrile and the results are summarized in Table 5.2. The quantum yields of the polymers decreased with increased acceptor strength and there was no significant change in the quantum yields between the two different conjugation pathways. Of the six polymers, only **P1A** and **P1B** were reasonably efficient fluorophores in solution. This suggests these two polymers are candidates as active materials in OLEDs.

**Table 5.3.** Electrochemical Properties of Benzobisoxazole Polymers[a]

| **Polymer** | **$E^{ox}_{onset}$ (V)** | **HOMO[b] (eV)** | **$E^{red}_{onset}$ (V)** | **LUMO[c] (eV)** |
|---|---|---|---|---|
| **P1A** | 0.87 | -5.67 | -2.19 | -3.12, -2.61[d] |
| **P1B** | 0.64 | -5.44 | - | -2.98 |
| **P2A** | 0.82 | -5.62 | - | -3.55 |
| **P2B** | 0.43 | -5.23 | - | -3.29 |
| **P3A** | 0.37 | -5.17 | - | -3.16 |
| **P3B** | 0.39 | -5.19 | - | -3.28 |

[a]Differential pulse voltammetry performed using a three-electrode cell with a Ag/AgNO$_3$ reference electrode, a platinum wire counter electrode, and a platinum button working electrode cast with a polymer film. Measurements performed in a 0.1M Bu$_4$NPF$_6$ acetonitrile solution as the electrolyte and then referenced to Fc/Fc$^+$. [b]Ionization potentials calculated using IP = -4.8 – ($E^{ox}_{onset}$). [c]Electron affinities calculated from the optical bandgap using EA = IP - $E_g^{opt}$. [d]Electron affinity calculated from EA = -4.8 – ($E^{red}_{onset}$).

**5.3.4 Electrochemical Properties.** Electrochemical analysis of the polymers was performed using differential pulse voltammetry (DPV), with the resulting data summarized in Table 5.3. Of the six polymers, only **P1A** showed a reduction wave. We know from ultraviolet photoelectron spectroscopy measurements of this polymer in our previous report, that DPV gives an accurate measurement of the ionization potential of the polymer but largely underestimates the electron affinity. This is why the measured electrochemical bandgap of **P1A** (3.06 eV) is so much larger than the optical bandgap of 2.55 eV. This fact, coupled with the need to use the optical bandgaps to calculate the electron affinities of the other polymers, suggests a better approach to comparing frontier orbital energy levels of the polymers is to use electron affinity values obtained from subtracting the optical bandgap from the IP for each polymer. This gives **P1A** an EA of -3.12 eV, instead of the measured -2.61 eV.

The polymers show a general trend of higher HOMO energy levels for the pathway B-containing polymers. This is consistent with the notion that pathway B leads to increased quinoid character, simultaneously increasing the HOMO energy level and decreasing the LUMO energy level. The LUMO energies for the polymers are generally lower for the pathway A-containing polymers, though. This indicates that when the conjugation pathway of the polymer goes directly through the oxazole rings, the BBO acts as a stronger acceptor, resulting in lower lying LUMOs.

These trends are not as well defined in the dithienosilole polymers. **P3A** and **P3B** have virtually identical HOMO energy levels while the LUMO of **P3B** is much deeper than **P3A**. This may be the result of differences in donor-acceptor orbital mixing in these polymers due to contributions from the electron deficient silole ring in the dithienosilole. It may be that the silole is a better acceptor than one or both of the BBO moieties. If this is the case it will have a heavy influence over the HOMO and LUMO energy levels[51] that doesn't exist in the fluorene and bithiophene-containing polymers.

## 5.4 CONCLUSIONS

Two different benzobisoxazole systems were examined, one with a conjugation pathway through the oxazole rings and the other with a conjugation pathway through the central benzene ring of the moiety. The structure-property relationships of the two systems were examined by making six donor-acceptor polymers and studying the changes in the physical and electronic properties caused by the difference in conjugation pathway. It was found that polymers with a conjugation pathway through the oxazole rings had higher ionization potentials, suggesting this configuration led to increased electron accepting strength of the moiety. Polymers featuring a conjugation pathway through the central benzene ring had narrower bandgaps due to improved stabilization of the polymer's quinoid resonance form. This configuration also allowed for alkyl functionalization on the benzobisoxazole which resulted in lower glass transition temperatures and melting points for these polymers. Further work is currently underway to fabricate OLEDs and OPVs out of these materials to study how the change in conjugation pathway affects the performance in organic electronic devices.

## 5.5 EXPERIMENTAL METHODS

**5.5.1 Materials.** 3,6-Diamino-2,5-dibromo-1,4-hydroquinone (1),[42] 2-trimethylstannyl-4-octylthiophene,[52] 2,6-bis(2-bromo-3-dodecyl-thiophene-5-yl)benzo[1,2-*d*;4,5-*d*']bisoxazole (**M-A**)[33], 2,7-bis(4,4,5,5-tetramethyl-1,3,2-dioxaborolan-2-yl)-9,9-dioctylfluorene (**M-1**),[43] 5,5'-bis(trimethylstannyl)-3,3'-dioctyl-2,2'-bithiophene (**M-2**),[44] and 4,4-dioctyl-2,6-bis(trimethylstannyl)dithieno[3,2-*b*:2',3'-*d*]silole (**M-3**)[45] were made according to literature procedures. Toluene was dried using an Innovative Technologies solvent purification system. Tetrakis(triphenylphosphine)palladium(0) was purchased from Strem Chemicals. Spectral grade coumarin-152 was purchased from Exciton. Poly(3,4-ethylenedioxy thiophene):poly(4-styrenesulfonate) (PEDOT:PSS) was purchased from H. C. Stark. All other chemicals were purchased from Sigma Aldrich and used without further purification.

**4,8-dibromo-2,6-dioctylbenzo[1,2-*d*;4,5-*d'*]bisoxazole (2).** A dry 2-neck 250 mL flask was purged with argon and poly(trimethylsilyl phosphate) (18.0 g, 118 mmol) was added followed by *o*-DCB (65 mL). The solution was then degassed by bubbling argon through it for 30 minutes. Freshly prepared 3,6-diamino-2,5-dibromo-1,4-hydroquinone (6.55 g, 23.0 mmol) and nonanoyl chloride (9.72 g, 55.0 mmol) were then added and the mixture was heated to 90 °C under an argon atmosphere for 72 hrs. The solution is concentrated by vacuum distillation of the *o*-DCB and the remaining liquid precipitated into methanol (200 mL). The precipitated product was filtered and washed with methanol. The product was then dissolved in hot hexanes, hot gravity filtered, and then allowed to recrystallize to yield white needles (6.35 g, 53%): mp 96-98 °C; $^1$H NMR (400 MHz, $CDCl_3$) δ: 0.88 (t, J=8 Hz, 6H), 1.27-1.36 (m, 16H) 1.45 (m, 4H), 1.93 (q, J=8 Hz, 4H), 3.01 (t, J=8 Hz, 4H); 13C NMR (100 MHz, $CDCl_3$) δ: 14.3, 22.8, 27.2, 29.21, 29.28, 29.3, 29.4, 32.0, 91.4, 138.6, 146.7, 169.4; HRMS (ESI, m/z): [M+H]+ Calcd for $C_{24}H_{35}N_2O_2Br_2$, 541.1060; found 541.1062.

**4,8-Bis(4-octylthien-2-yl)-2,6-dioctylbenzo[1,2-*d*;4,5-*d'*]bisoxazole (3).** To a dry 250 mL round-bottom flask was added compound **2** (2.71 g, 5 mmol), 2-(trimethylstannyl)-4-octylthiophene (3.95 g, 11 mmol), tri-*o*-tolylphosphine (122 mg, 8 mol%), and toluene (100 mL). The mixture was deoxygenated by bubbling argon through it for 30 minutes. Tris(dibenzylideneacetone)dipalladium(0) (137 mg, 3 mol%) was then added and the reaction was refluxed under argon for 24 hours. After cooling the mixture to room temperature, it was passed through a silica gel plug using an eluent of 9:1 hexanes: ethylacetate. The solvent was evaporated and the residue was recrystallized from hexanes to yield a yellow solid (3.04 g, 79% yield). Mp 95-96 °C; $^1$H NMR ($CDCl_3$) δ: 0.89 (t, *J* = 6.8 Hz, 12H), 1.30 (br m, 36H), 1.53 (m, *J* = 7.6 Hz, 4H), 1.72 (m, *J* = 7.6 Hz, 4H), 2.00 (m, *J* = 7.6 Hz, 4H), 2.73 (t, *J* = 8 Hz, 4H), 3.09 (t, *J* = 7.6 Hz, 4H), 7.10 (s, 2H), 8.15 (s, 2H); $^{13}$C NMR ($CDCl_3$) δ: 14.10, 14.11, 22.66, 22.68, 26.87, 29.02, 29.17, 29.25, 29.26, 29.31, 29.39, 29.50, 30.55, 31.84, 31.91, 107.69, 122.06, 130.02, 133.86, 135.38, 143.59, 144.35, 167.59; HRMS (ESI, *m/z*): $[M+H]^+$ Calcd for $C_{48}H_{73}N_2O_2S_2$, 773.5108; found 773.5113.

**4,8-Bis(5-bromo-4-octylthien-2-yl)-2,6-dioctylbenzo[1,2-*d*;4,5-*d'*]bisoxazole (M-B).** Compound **3** (1.16 g, 1.5 mmol), glacial acetic acid (12.5 mL), and chloroform (50 mL) were added to a round-bottom flask and stirred while gently heating the mixture until all solid was dissolved. The mixture was then cooled to room temperature before adding N-bromosuccinimide (547.3 mg, 3.075 mmol) as a single portion. The solution was stirred in the dark for 48 hours and then poured into water (100 mL). The mixture was diluted with chloroform (75 mL) and separated from the aqueous layer. It was then washed with 1M aqueous potassium hydroxide solution (120 mL) and brine before drying over magnesium sulfate. After evaporation of the solvent, the crude residue was purified via silica gel column chromatography using an eluent of 4:1 hexanes: toluene. Evaporation of the solvent gave the product as a yellow solid (1.15 g, 82% yield). Mp=74-75 °C; $^1H$ NMR ($CDCl_3$) δ: 0.88 (m, 12H), 1.29-1.42 (br m, 32H), 1.53 (m, *J* = 8 Hz, 4H), 1.69 (m, *J* = 7.6 Hz, 4H), 1.99 (m, *J* = 7.6 Hz, 4H), 2.67 (t, *J* = 8 Hz, 4H), 3.07 (t, J = 7.6 Hz, 4H), 7.96 (s, 2H); $^{13}C$ NMR ($CDCl_3$) δ: 14.01, 14.11, 22.66, 22.68, 26.83, 28.94, 29.18, 29.22, 29.25, 29.28, 29.29, 29.44, 29.58, 29.82, 31.84, 31.90, 107.06, 112.06, 129.40, 133.84, 135.24, 142.32, 143.95, 167.70; HRMS (ESI, *m/z*): $[M+H]^+$ Calcd for $C_{48}H_{71}Br_2N_2O_2S_2$, 929.3318; found 929.3305.

**P1A.** Monomers **M-1** (321.4 mg, 0.5 mmol) and **M-A** (353.2 mg, 0.5 mmol) were added to a Schlenk flask and placed under an argon atmosphere. 2M aqueous sodium carbonate (5 mL), toluene (7.5 mL), and 2 drops of Aliquat 336 were then added and the mixture was deoxygenated by bubbling argon through it for 30 minutes. Tetrakis(triphenylphosphine)palladium(0) (11.6 mg, 2 mol%) was then added and the mixture was refluxed under argon for 4 days. A drop of 4,4,5,5-tetramethyl-2-phenyl-1,3,2-dioxaborolane was then added and the reaction was refluxed for another 2 hours. Two drops of iodobenzene was then added and the mixture was refluxed overnight. The polymer was then precipitated twice in methanol (100 mL) and then washed sequentially with methanol, acetone, and chloroform in a Soxhlet extractor. The chloroform extract was evaporated to yield the polymer as a yellow solid (420 mg, 90% yield). $^1H$ NMR ($CDCl_3$) δ: 0.81-0.91 (16H), 1.10-1.43 (40H), 1.73 (4H), 2.05 (4H), 2.79 (4H), 7.52 (4H), 7.82 (2H), 7.86 (4H).

**P1B.** Polymer was made using the same procedure as **P1A** using monomer **M-B** (465.5 mg, 0.5 mmol) in place of **M-A**. The reaction yielded the polymer as a yellow solid (540 mg, 93% yield). $^1$H NMR ($CDCl_3$) δ: 0.84-0.90 (22H), 1.14-1.43 (56H), 1.59 (4H), 1.78 (4H), 2.06 (8H), 2.85 (4H), 3.14 (4H), 7.57 (4H), 7.80 (2H), 8.25 (2H).

**P2A.** Monomers **M-2** (358.2 mg, 0.5 mmol) and **M-A** (465.5 mg, 0.5 mmol) were added to a flame-dried Schlenk flask and placed under an argon atmosphere. Tri-o-tolylphosphine (12.2 mg, 8 mol%) and toluene (10 mL) were added and the mixture was deoxygenated by bubbling argon through it for 30 minutes. Tris(dibenzylideneacetone)dipalladium(0) (9.2 mg, 2 mol%) was then added and the mixture was reflux for 3 days under argon. A drop of trimethylphenyltin was then added and the reaction was refluxed an additional 2 hours. Two drops of iodobenzene was then added and the reaction was refluxed overnight. The polymer was then precipitated twice in methanol and then washed sequentially in methanol, acetone, and chloroform in a Soxhlet extractor. The chloroform extract was then evaporated to yield the polymer as a red solid (417 mg, 89% yield). $^1$H NMR ($CDCl_3$) δ: 0.89 (12H), 1.28 (38H), 1.64 (6H), 1.75 (4H), 2.61 (4H), 2.86 (4H), 7.12 (2H), 7.80 (4H).

**P2B.** Polymer was made using the same procedure as **P2A** using monomer **M-B** (465.5 mg, 0.5 mmol) in place of **M-A**. The reaction yielded the polymer as a red solid (470 mg, 81% yield). $^1$H NMR ($CDCl_3$) δ: 0.89 (18H), 1.31-1.47 (56H), 1.59 (4H), 1.68 (4H), 1.81 (4H), 2.05 (4H), 2.65 (4H), 2.94 (4H), 3.14 (4H), 7.17 (2H), 8.20 (2H).

**P3A.** Monomers **M-3** (372.2 mg, 0.5 mmol) and **M-A** (353.3 mg, 0.5 mmol) were added to a flame-dried Schlenk flask. Tri-o-tolylphosphine (12.2 mg, 8 mol%) and toluene (10 mL) were then added and the mixture was deoxygenated by bubbling argon through it for 30 minutes. Tris(dibenzylideneacetone)dipalladium(0) (9.2 mg, 2 mol%) was then added and the reaction was refluxed for 24 hours under argon. A drop of trimethylphenyltin was added to the reaction and then refluxed an additional 2 hours. Two drops of iodobenzene was then added and the reaction was then refluxed overnight. The reaction was cooled to room temperature and the polymer was precipitated twice in methanol. It was then washed sequentially with methanol, acetone, and chloroform in a Soxhlet extractor. The chloroform extract was evaporated to yield the polymer as a purple solid (310 mg, 64% yield). $^1$H NMR ($CDCl_3$) δ: 0.89-1.01 (22H), 1.27 (34H), 1.63 (4H), 1.76 (4H), 2.87 (4H), 7.80 (4H).

**P3B.** Polymer was made using the same procedure as **P3A** using monomer **M-B** (465.5 mg, 0.5 mmol) in place of **M-A**. The reaction yielded the polymer as a purple solid (503 mg, 84% yield). $^1$H NMR ($CDCl_3$) δ: 0.88 (18H), 1.02 (4H), 1.31 (64H), 1.80 (4H), 2.03 (4H), 2.94 (4H), 3.11 (4H), 8.19 (4H).

**5.5.2 Characterization.** NMR spectra were obtained on a Varian MR-400 at 400 MHz using $CDCl_3$ as the solvent and all samples were referenced to their internal protonated solvent. High-resolution mass spectra were recorded on a double focusing magnetic sector mass spectrometer using EI at 70 eV. Gel permeation chromatography (GPC) measurements were performed on a Viscotek GPC Max 280 separation module equipped with three 5µm I-gel columns connected in a series (guard, HMW, MMW and LMW) with a refractive index and UV-Vis detector. Analyses were performed at 35 °C using THF as the eluent with the flow rate at 1.0 mL/min. Calibration was based on polystyrene standards. Fluorescence spectroscopy and UV-Visible spectroscopy were obtained using polymer solutions in chloroform, and thin films. The films were made by spin-coating 25x25x1mm glass slides, using a solution of 10 mg of polymer per 1 mL *o*-dichlorobenzene at a spin rate of 1000 rpms on a Spin-Coater. Thermal gravimetric analysis measurements were made within the temperature interval of 30 ºC - 850 ºC, with a heating rate of 20 ºC/minute, under ambient atmosphere. Differential scanning calorimetry was performed with a first scan at a heating rate of 15 ºC/min to erase thermal history and a second scan to measure transitions from 0 °C to 250 °C under nitrogen. Transitions were also measured with cooling at 15 ºC/min. Differential pulse voltammetry was performed on an eDaq e-corder 410 potentiostat using a three-electrode cell (electrolyte: 0.1M $nBu_4NPF_6$ in acetonitrile) with an Ag/Ag+ reference electrode, a platinum auxiliary electrode, and a platinum button electrode as the working electrode. Polymer films were made by drop coating a 2.5 mg/mL solution of the polymers in 3:1 chloroform: *o*-dichlorobenzene on to the working electrode. All films were dried at 120 ºC for 2 hours in a vacuum oven prior to use. All differential pulse voltammetry experiments were carried out under argon atmosphere and were recorded at a scan rate of 125 mV/s, a pulse height of 100 mV, a pulse width of 25 ms, a ramp width of 50 ms, and a sampling period of 10 ms. Photoluminescence quantum yields were measured in dilute chloroform solutions relative to coumarin 152 in acetonitrile.[53] X-ray data was collected using a Rigaku Ultima IV X-ray Diffractometer equipped with a cross-beam optics and a point focus Cu x-ray tube emitting Kα radiation (1.541 Å). X-rays were generated under a 2.2 kW total load (40kV and 44 mA). Powder diffraction studies were performed with parallel beam geometry and a θ/2θ goniometer. Samples were first aligned with the beam using a moveable sample stage (MPA-U4 Eulerian cradle) in order to prevent collection of diffraction data from the sample plate. The incident angle of the beam was varied between 0.02° and 0.1° at increments of 0.02° in order to minimize internal reflectance; samples were then scanned from 1°-10° 2θ.

## 5.6 ACKNOWLEDGEMENTS

We thank the National Science Foundation (DMR-0846607) for generous financial support of this work. We would also like to thank Dr. Kamel Harrata and the Mass Spectrometry Laboratory of Iowa State University (ISU) for compound analysis, Brandon Kobilka (ISU) for assistance in the synthesis of monomer **M-3**, and Benjamin Hale (ISU) for helpful discussions of this research.

## 5.7 SUPPORTING INFORMATION

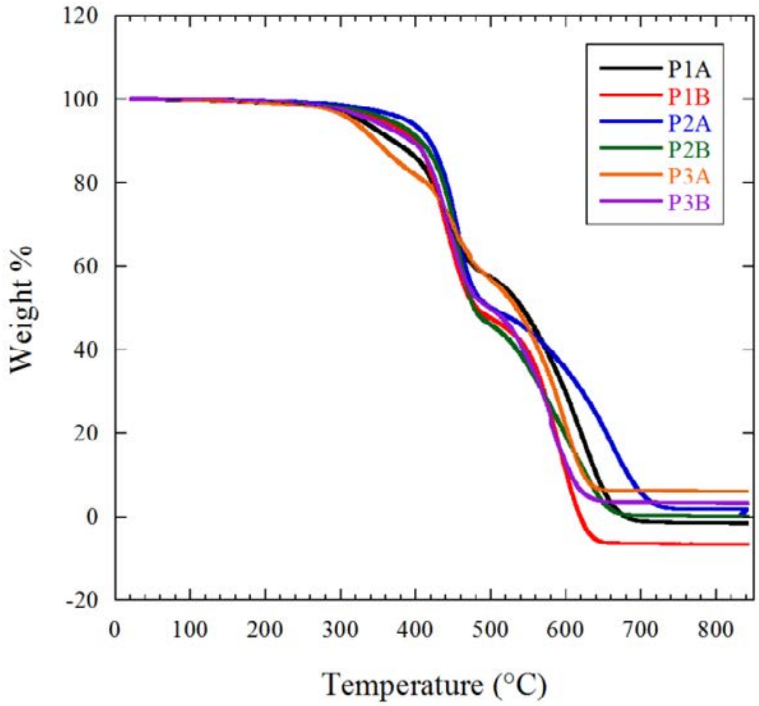

**Figure S5.1.** Thermal gravimetric analysis of benzobisoxazole polymers

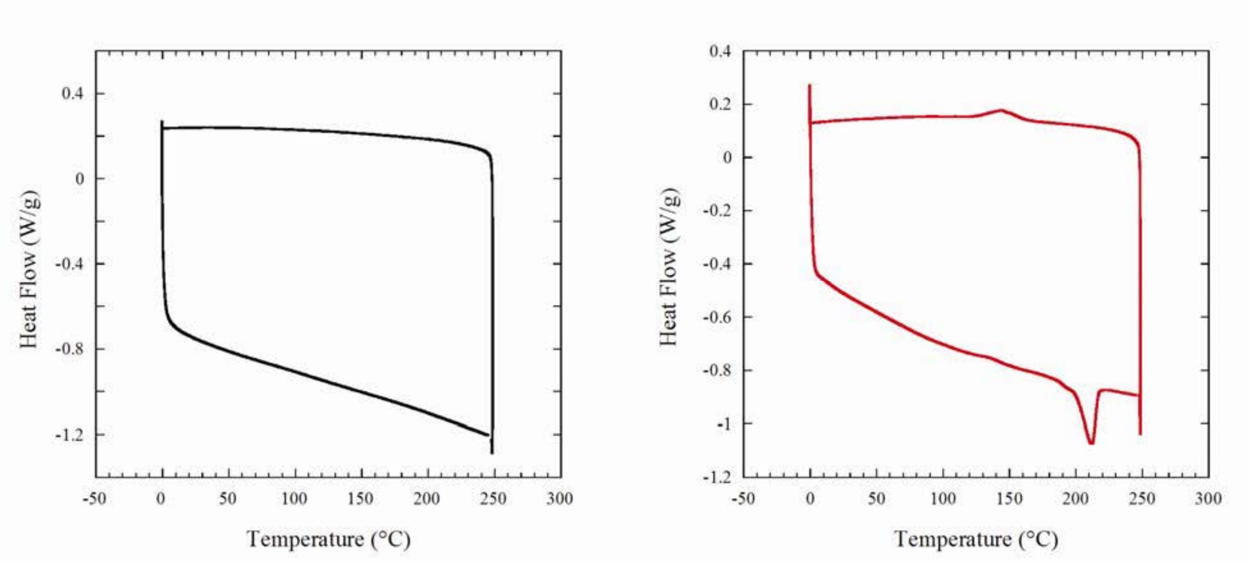

**Figure S5.2.** Differential scanning calorimetry plots for **P1A** (left) and **P1B** (right).

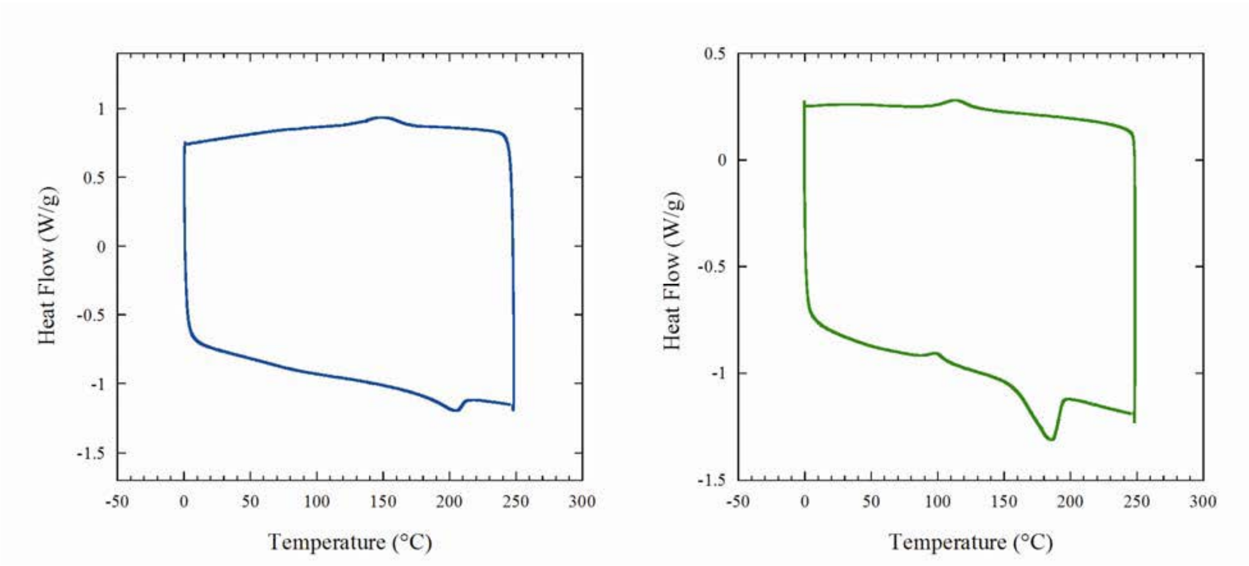

**Figure S5.3.** Differential scanning calorimetry plots for **P2A** (left) and **P2B** (right).

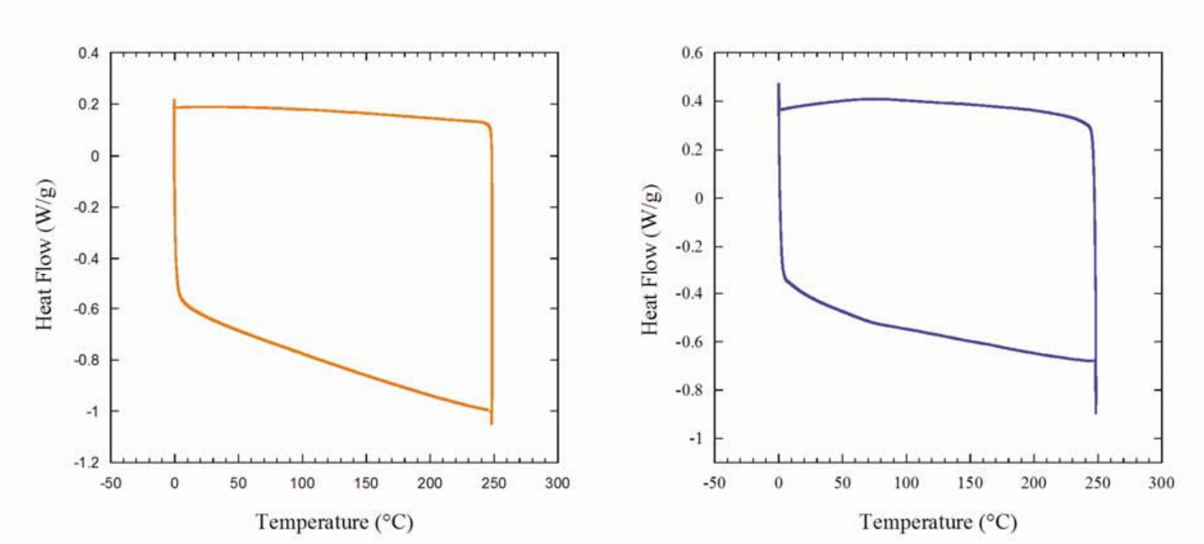

**Figure S5.4.** Differential scanning calorimetry plots for **P3A** (left) and **P3B** (right).

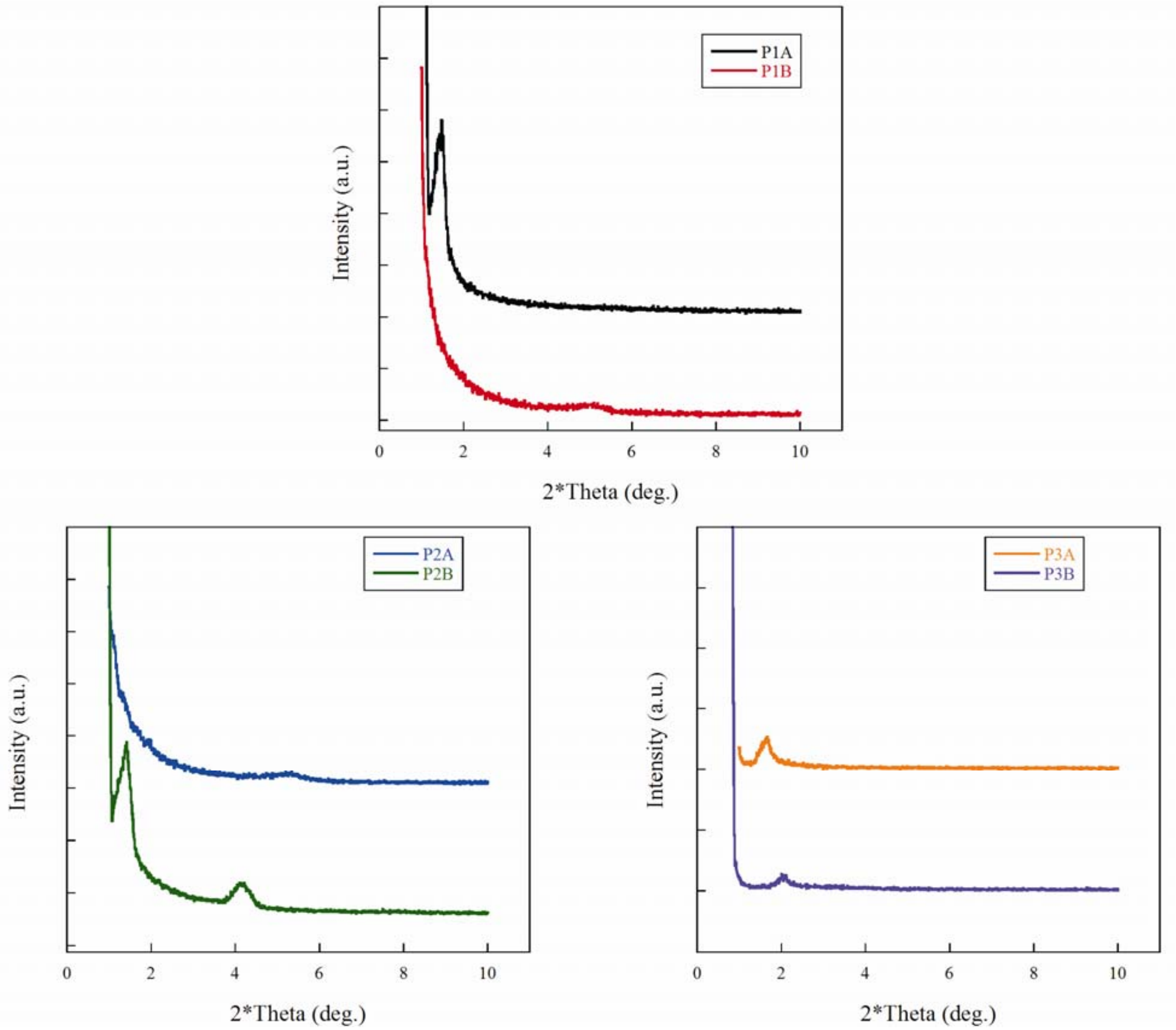

**Figure S5.5.** X-ray diffraction plots of benzobisoxazole polymers.

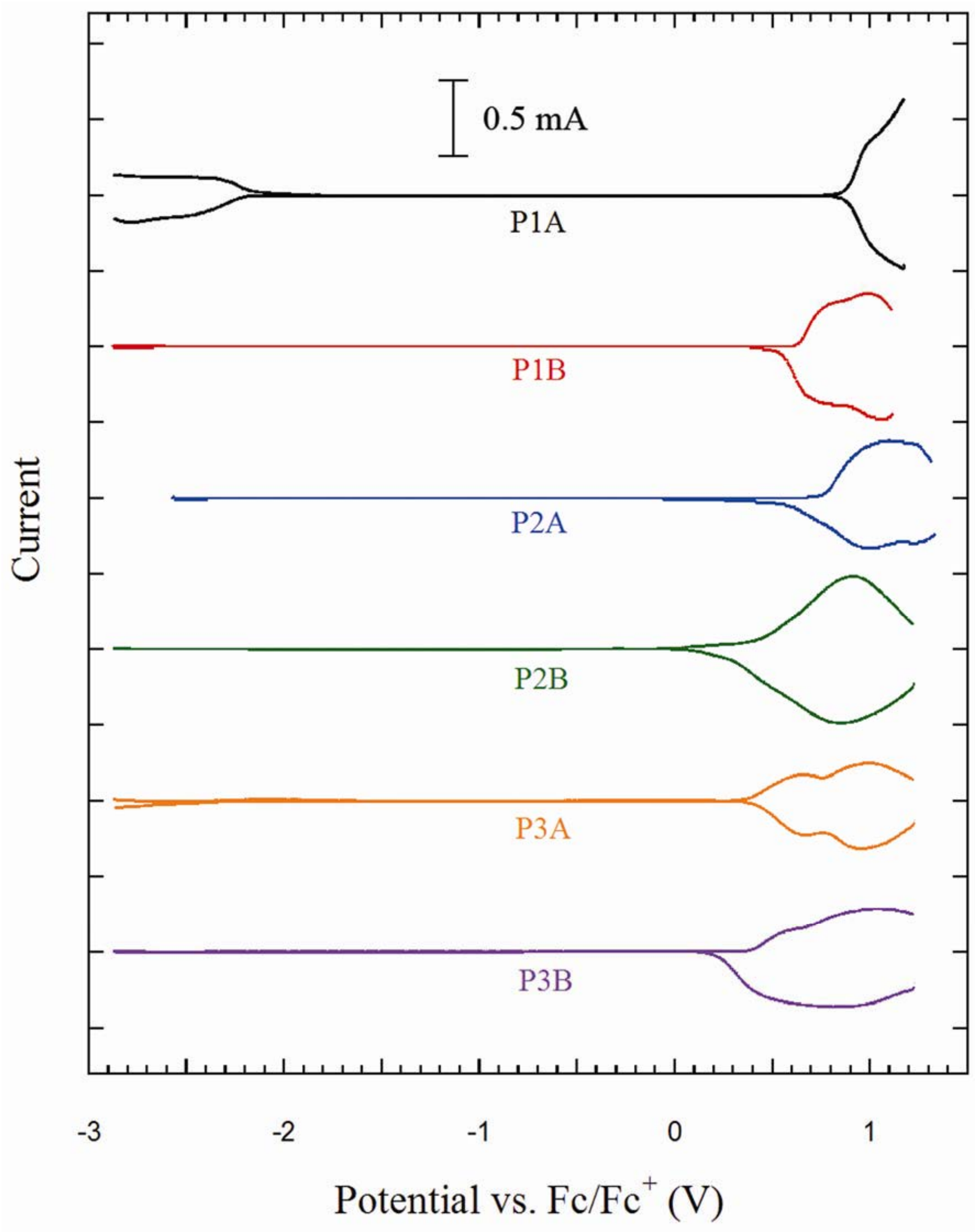

**Figure S5.6.** Differential pulse voltammetry plots of benzobisoxazole polymers

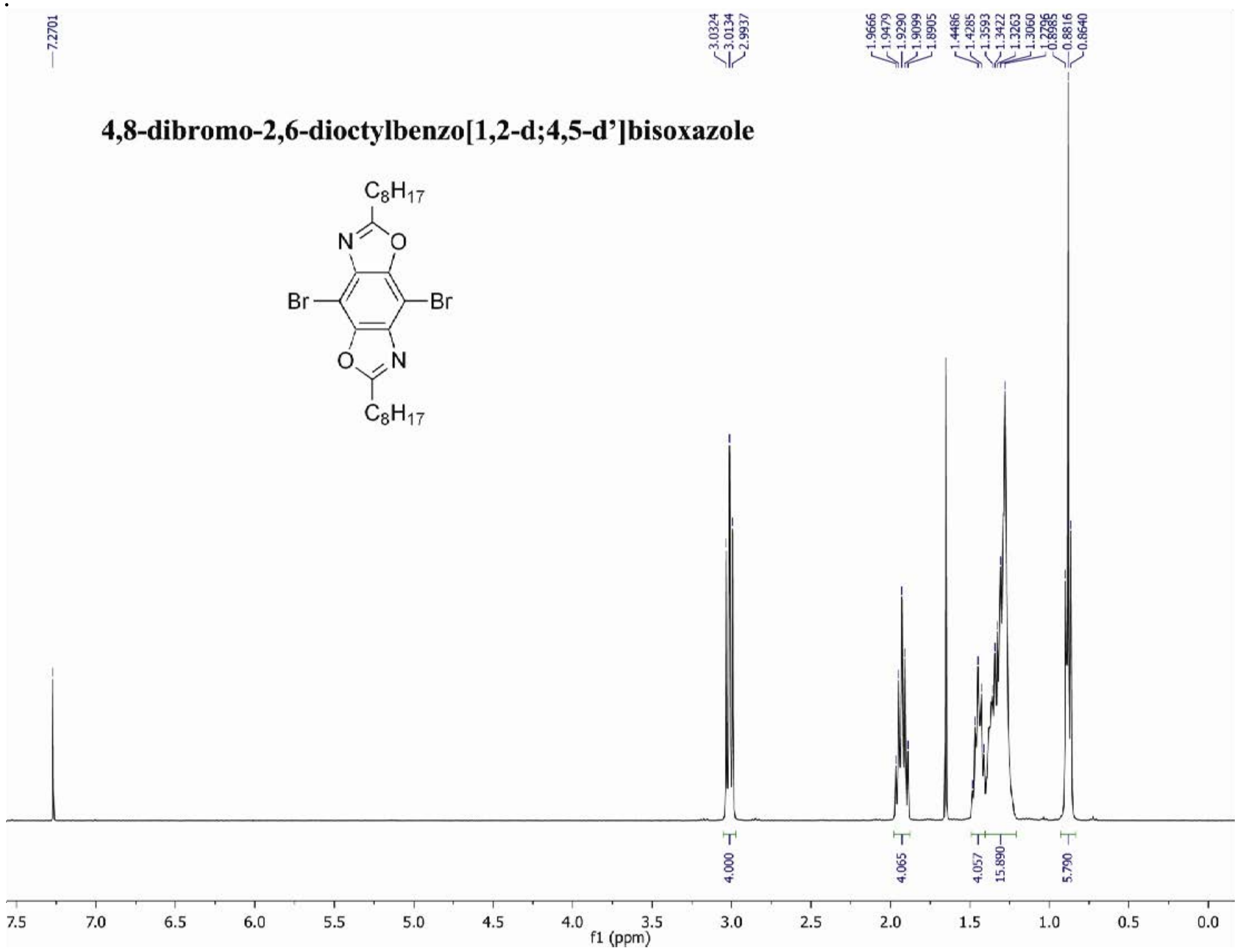

**Figure S5.7.** $^1$H NMR of 4,8-dibromo-2,6-dioctylbenzo[1,2-*d*;4,5-*d'*]bisoxazole.

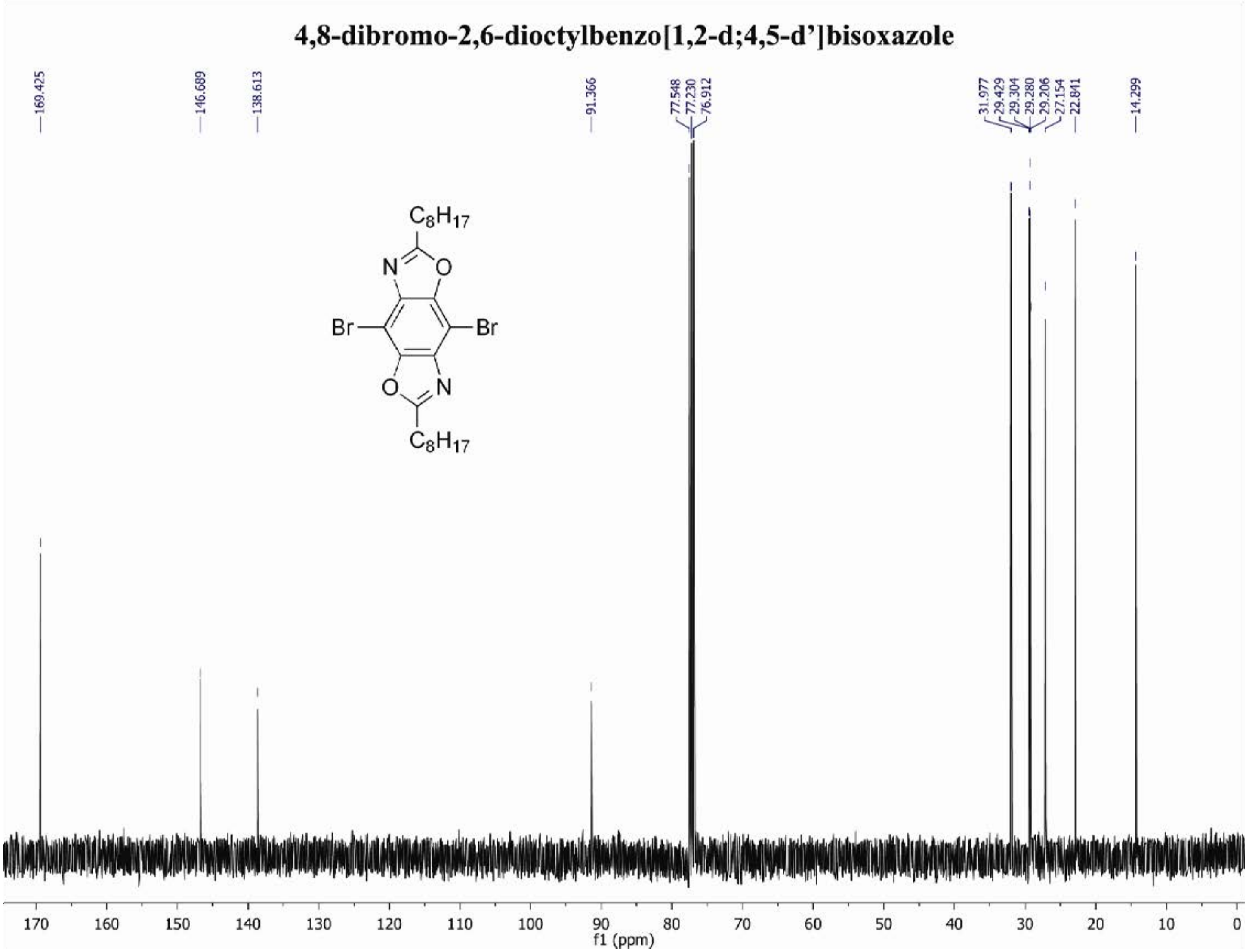

**Figure S5.8.** $^{13}$C NMR of 4,8-dibromo-2,6-dioctylbenzo[1,2-*d*;4,5-*d’*]bisoxazole.

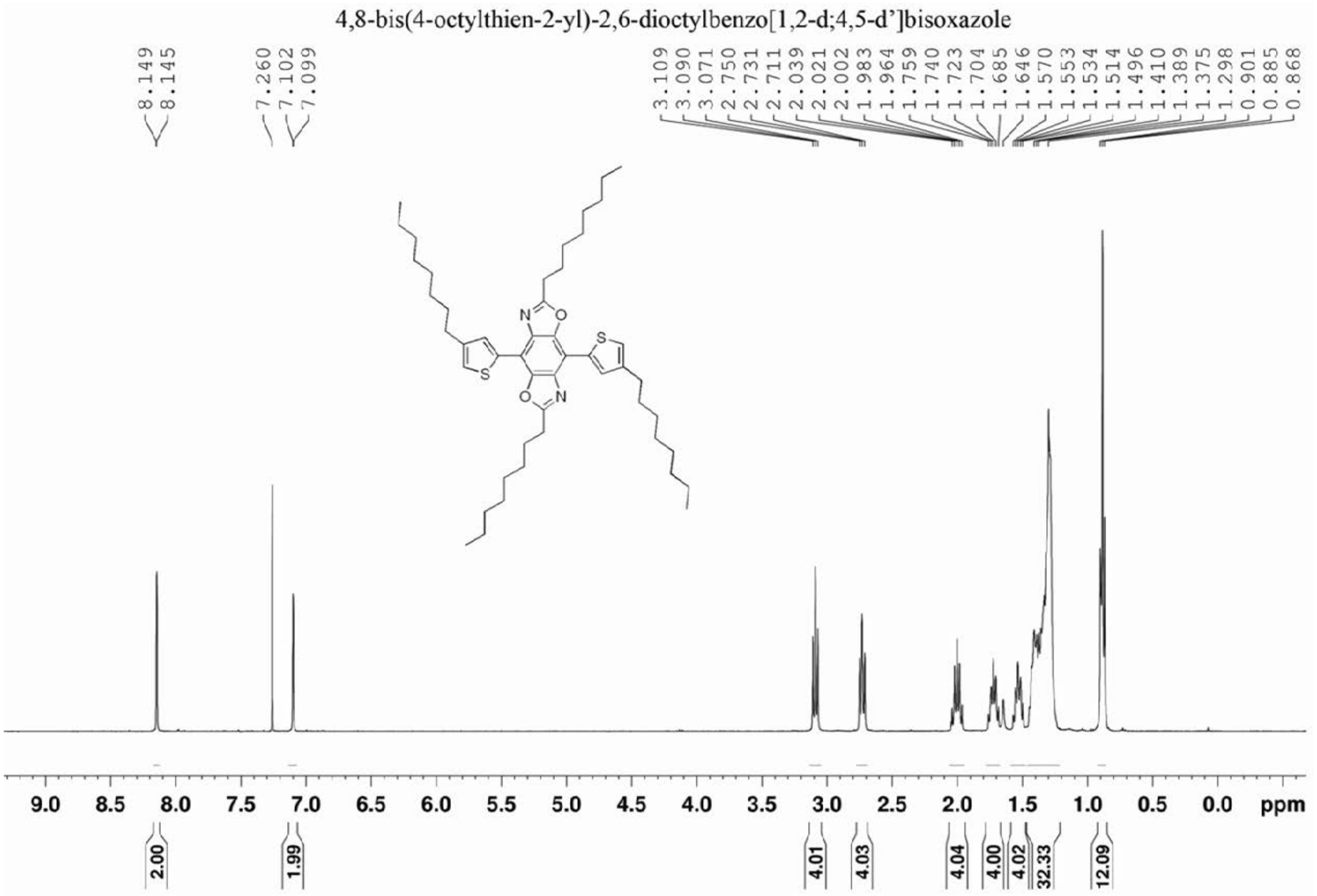

**Figure S5.9.** $^{1}$H NMR of 2,6-dioctyl-4,8-bis(4-octylthien-2-yl)benzo[1,2-*d*;4,5-*d'*]bisoxazole.

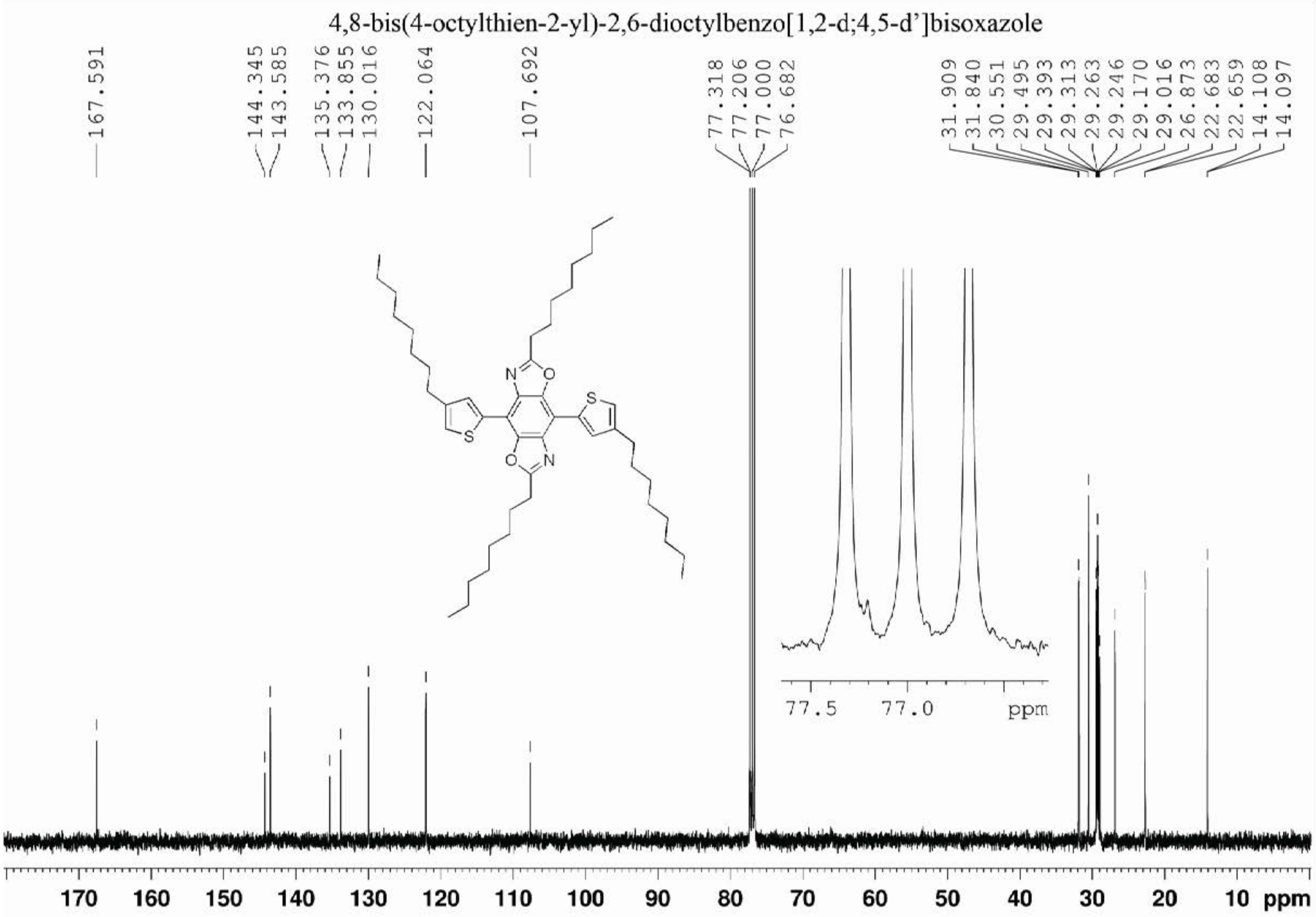

**Figure S5.10.** $^{13}$C NMR of 2,6-dioctyl-4,8-bis(4-octylthien-2-yl)benzo[1,2-*d*;4,5-*d'*]bisoxazole.

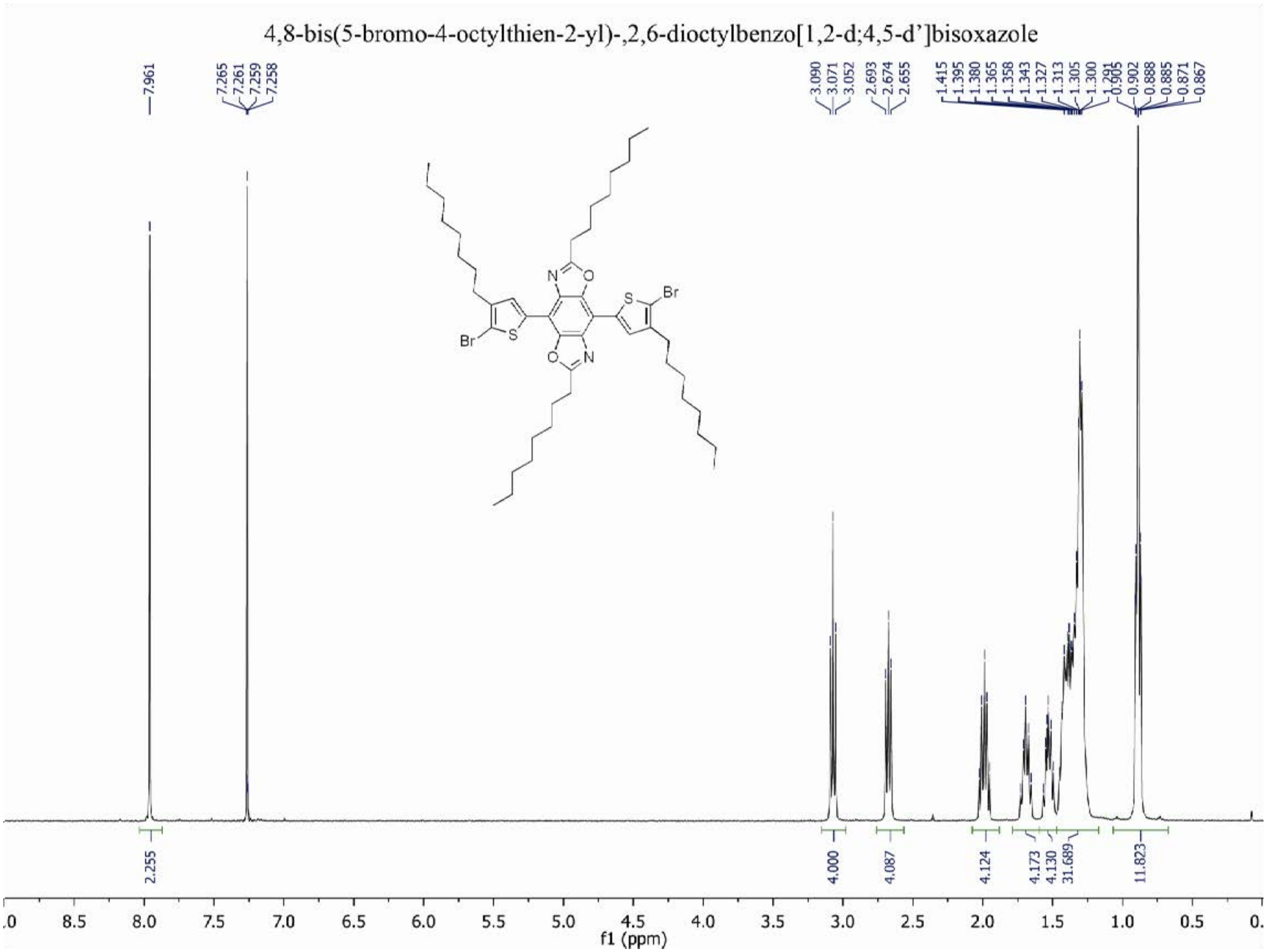

**Figure S5.11.** $^1$H NMR of 4,8-bis(5-bromo-4-octylthien-2-yl)-2,6-dioctylbenzo[1,2-*d*;4,5-*d'*]bisoxazole.

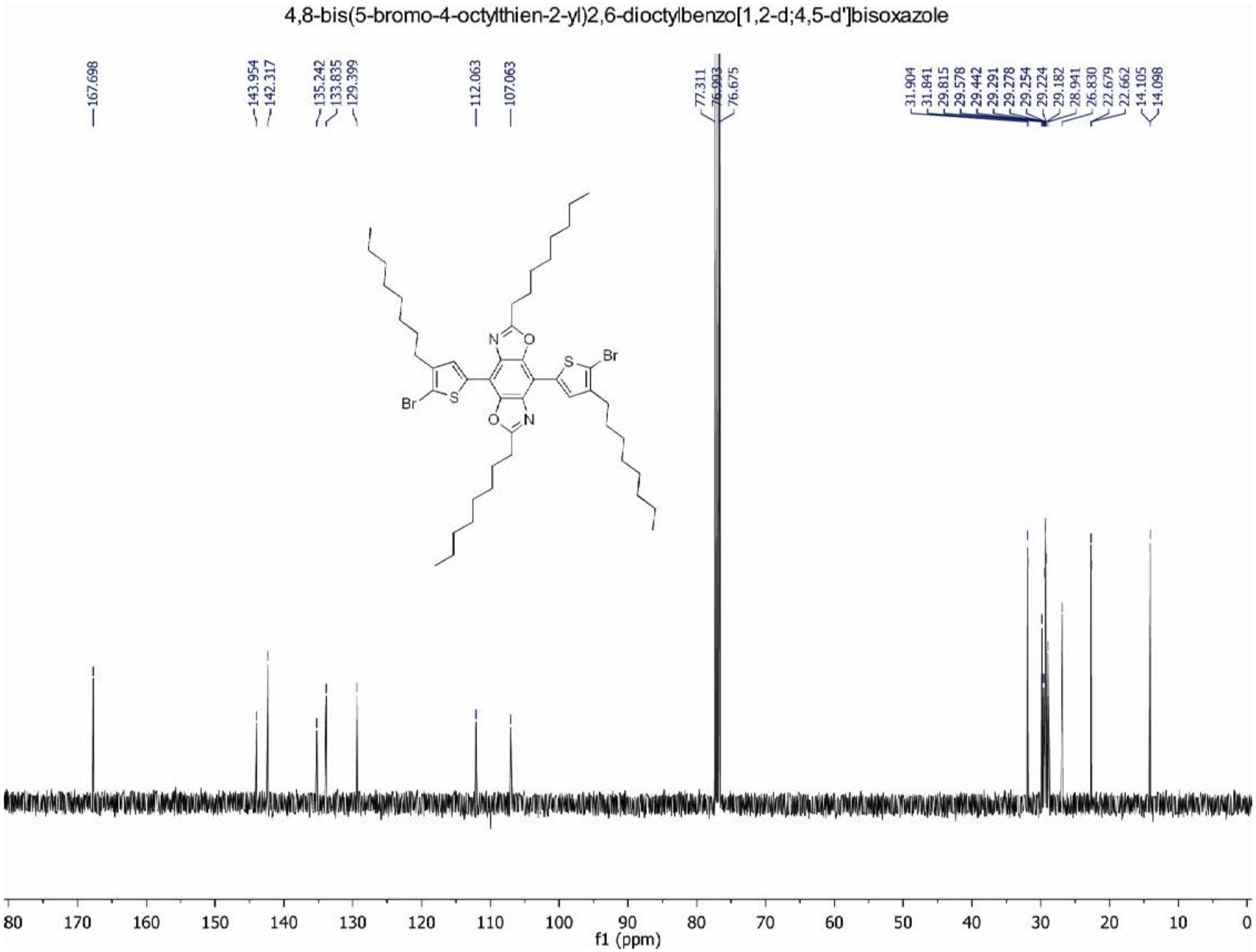

**Figure S5.12.** $^{13}$C NMR of 4,8-bis(5-bromo-4-octylthien-2-yl)-2,6-dioctylbenzo[1,2-*d*;4,5-*d'*]bisoxazole.

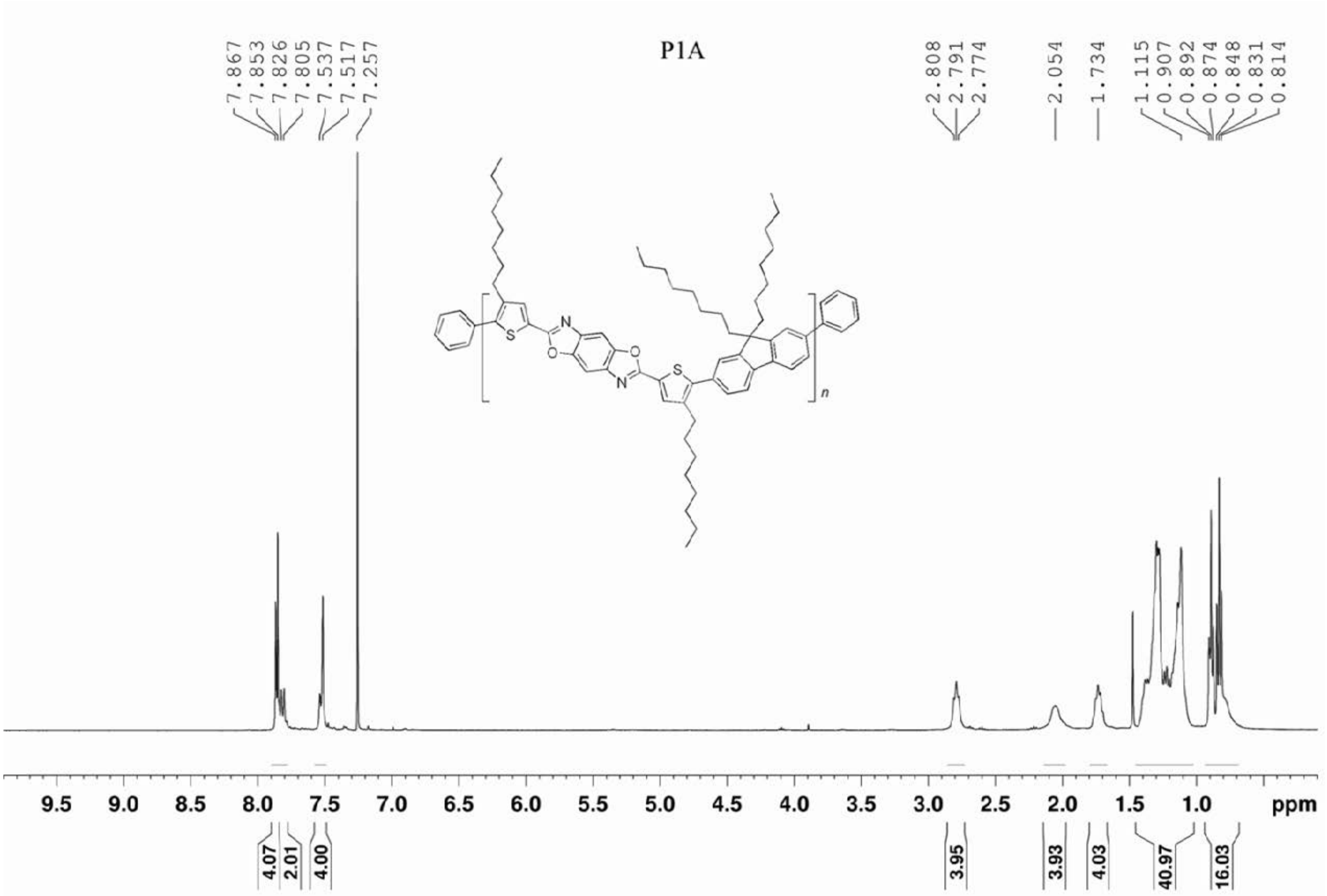

**Figure S5.13.** $^{1}$H NMR of **P1A**.

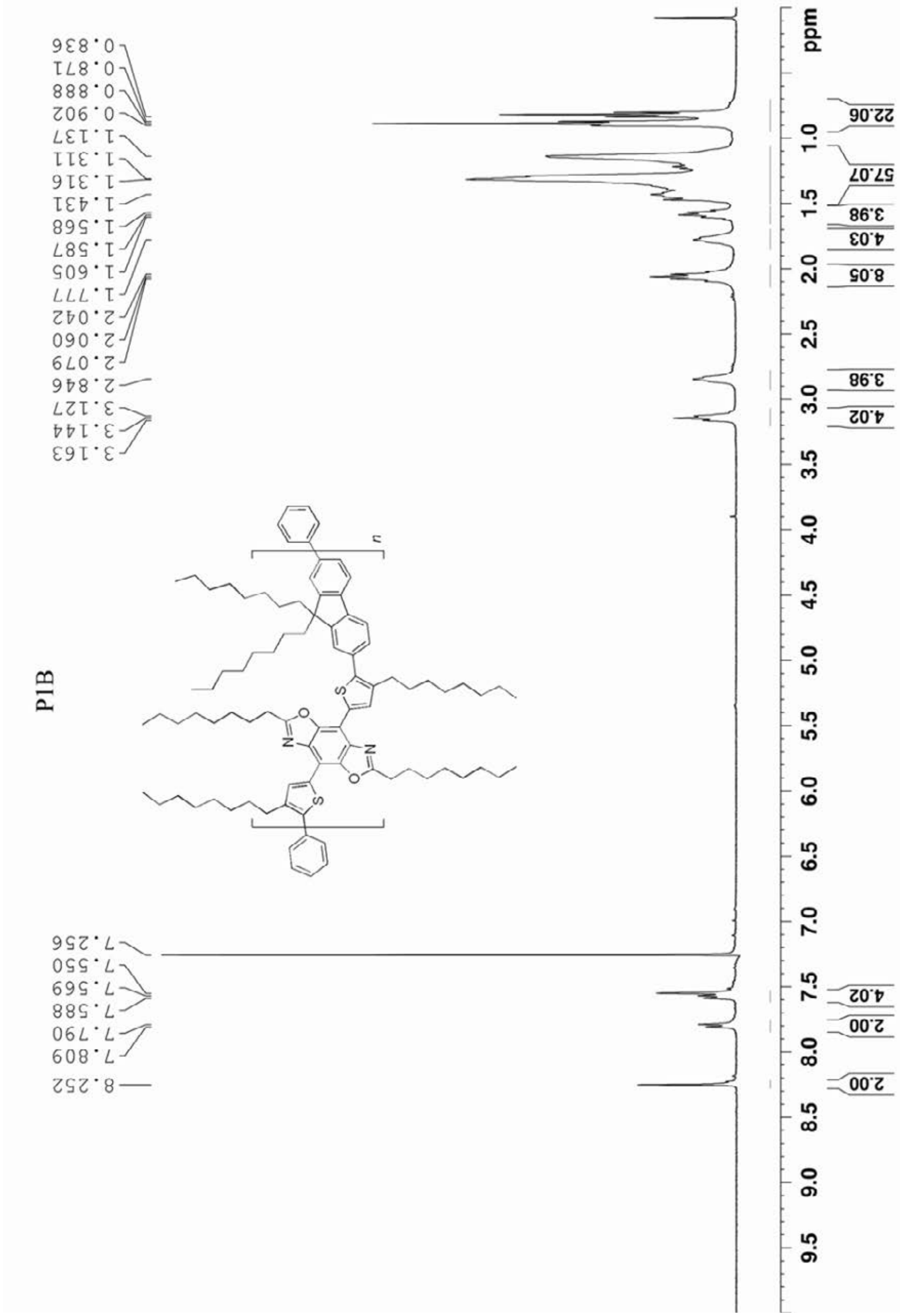

**Figure S5.14.** $^1$H NMR of **P1B**.

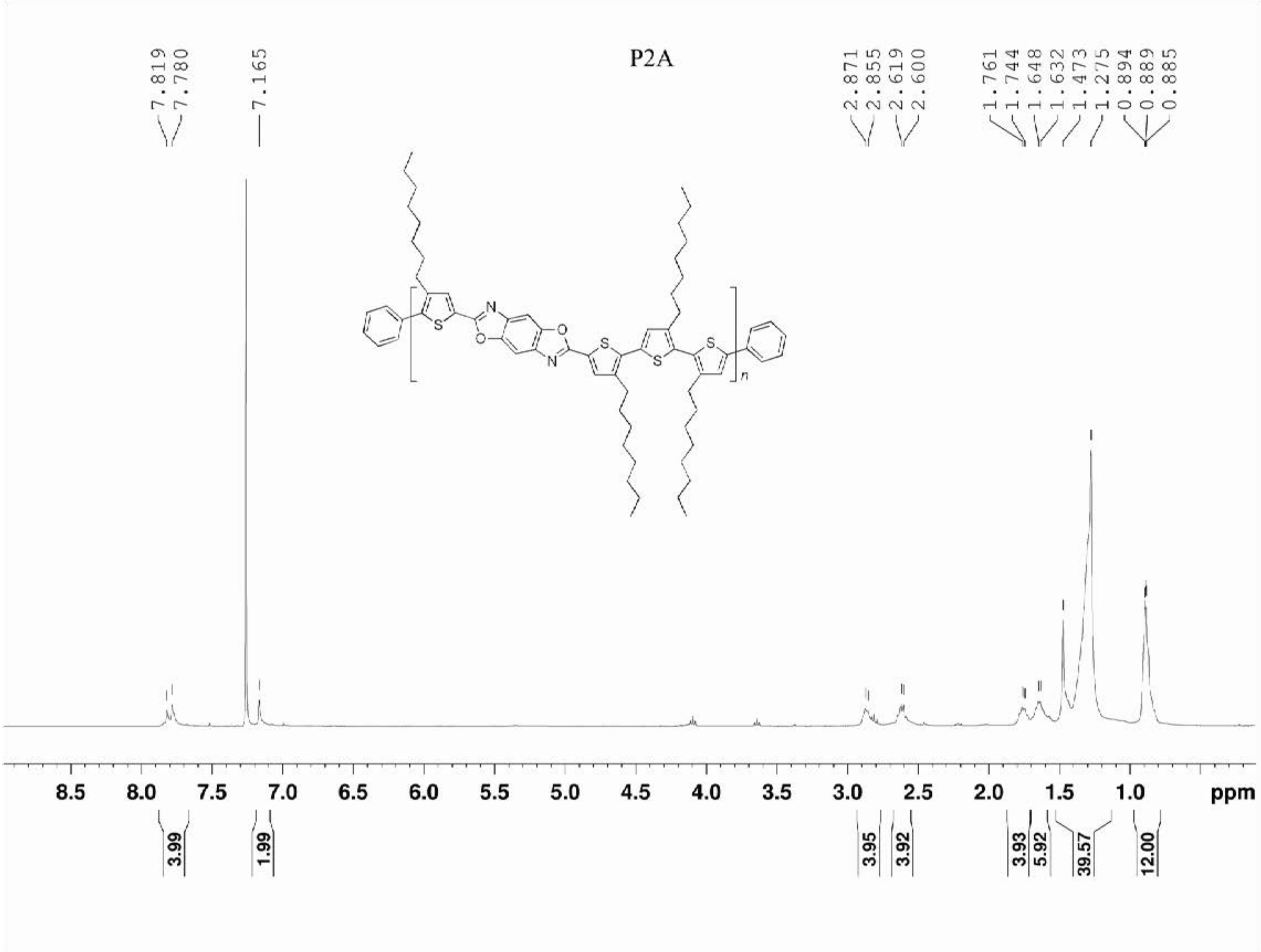

**Figure S5.15.** $^{1}$H NMR of **P2A**.

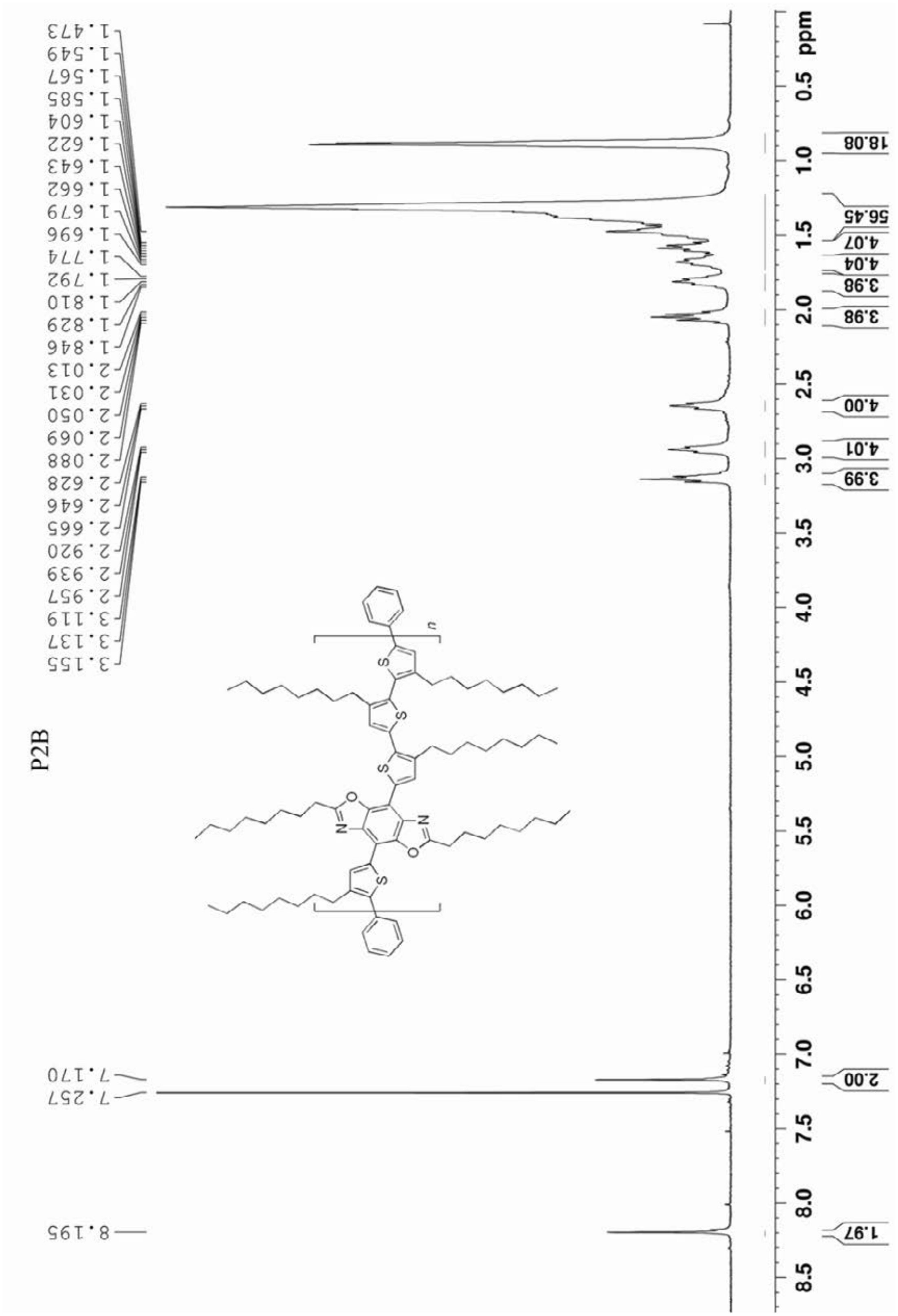

**Figure S5.16.** $^1$H NMR of **P2B**.

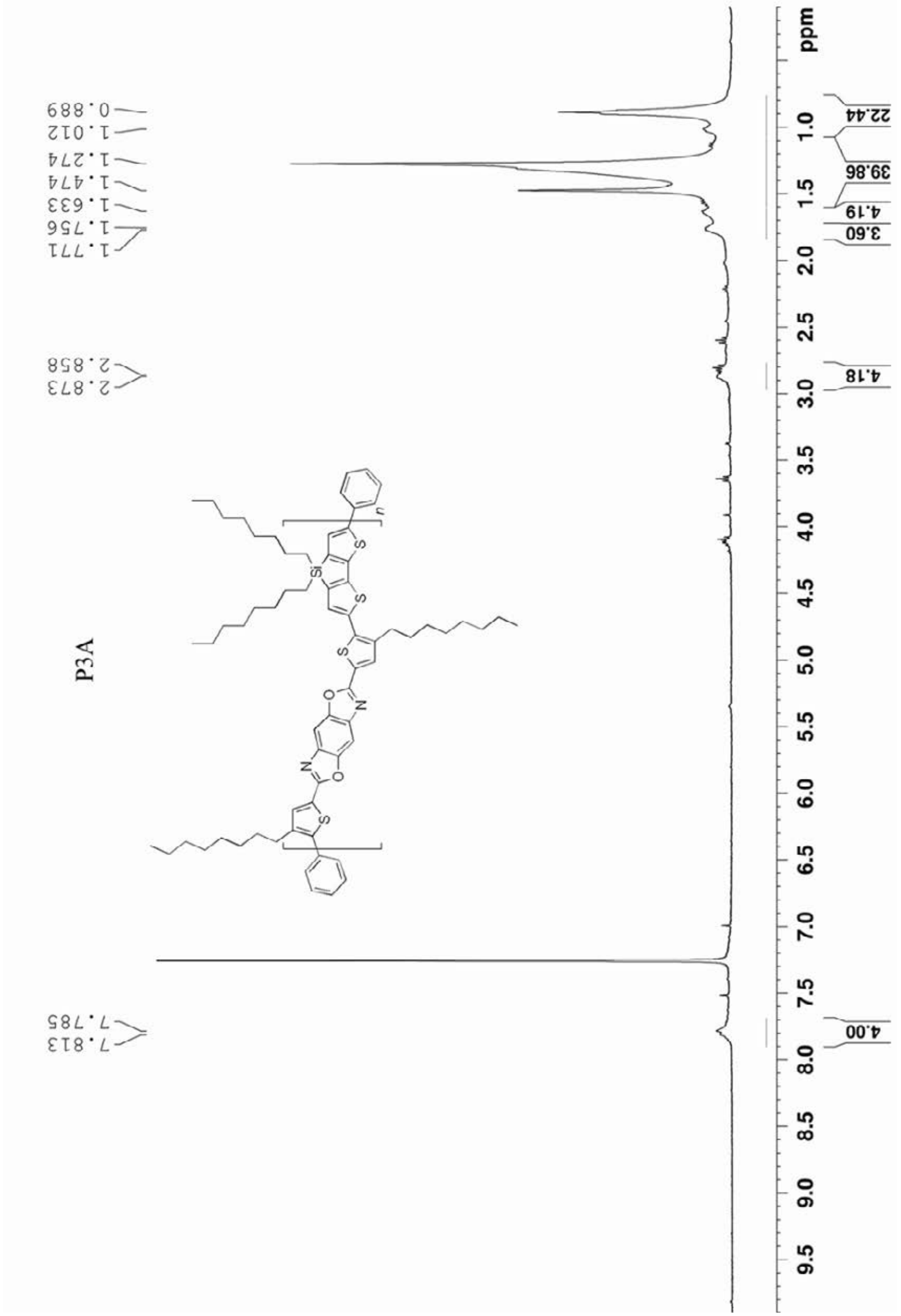

**Figure S5.17.** $^1$H NMR of **P3A**.

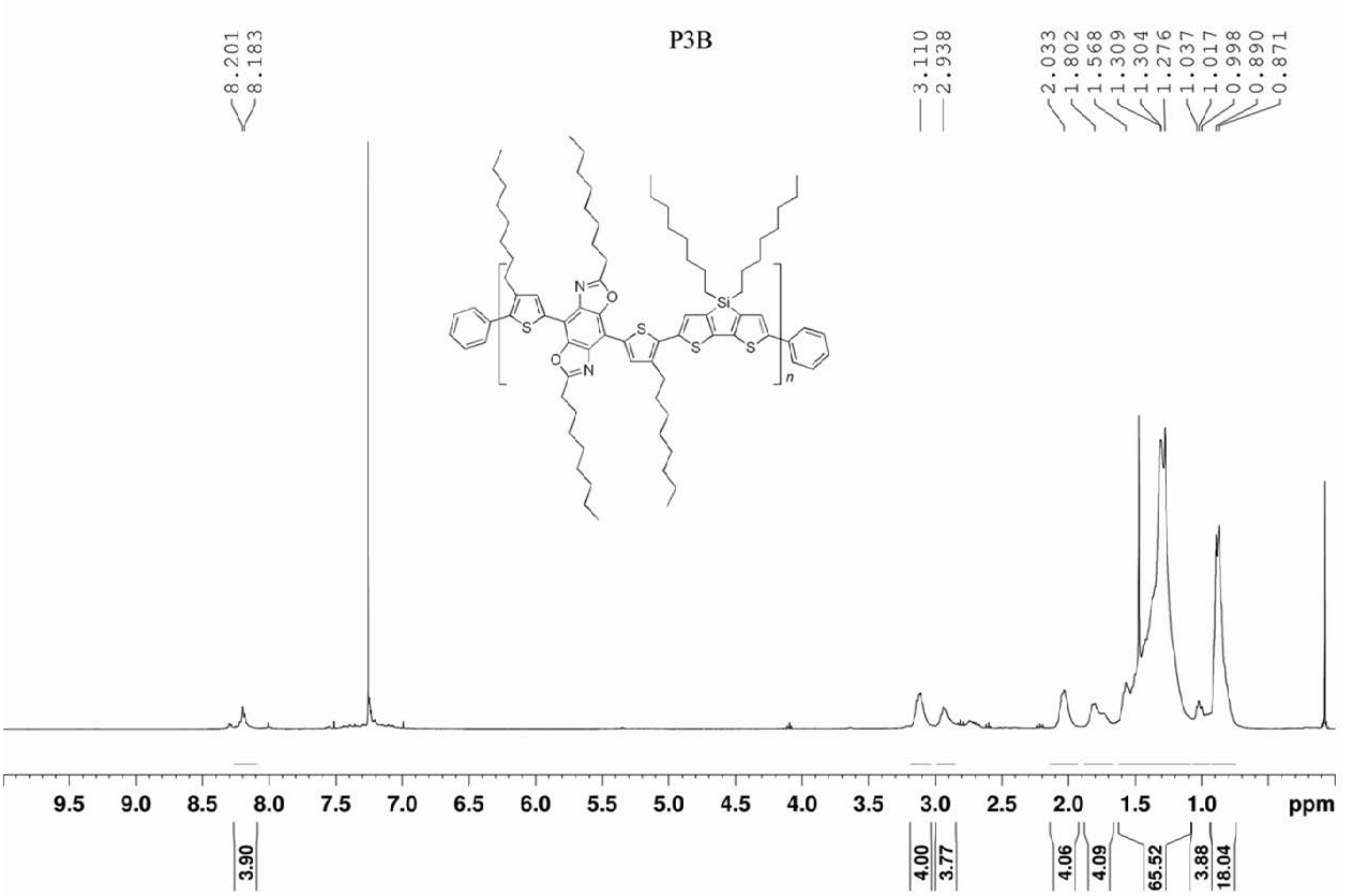

**Figure S4.18.** $^1$H NMR of **P3B**.

## 5.8 REFERENCES

1. Jenekhe, Samson A.; Yi, Shujian. *Appl. Phys. Lett.* **2000,** 77, (17), 2635-2637.
2. Jenny, Nelson. *Curr. Opin. Solid State Mater. Sci.* **2002,** 6, (1), 87-95.
3. Liang, Yongye; Xu, Zheng; Xia, Jiangbin; Tsai, Szu-Ting; Wu, Yue; Li, Gang; Ray, Claire; Yu, Luping. *Adv. Mater.* **2010,** 22, (20), E135-E138.
4. Thompson, Barry C; Fréchet, Jean M J. *Angew. Chem., Int. Ed.* **2008,** 47, (1), 58-77.
5. Scharber, M. C; Mühlbacher, D.; Koppe, M.; Denk, P.; Waldauf, C.; Heeger, A. J; Brabec, C. J. *Adv. Mater.* **2006,** 18, (6), 789-794.
6. Mitschke, Ullrich; Bauerle, Peter. *J. Mater. Chem.* **2000,** 10, (7), 1471-1507.
7. Tang, C. W.; Vanslyke, S. A. *Appl. Phys. Lett.* **1987,** 51, 913-915.
8. Becker, H.; Spreitzer, H.; Kreuder, W.; Kluge, E.; Vestweber, H.; Schenk, H.; Treacher, K. *Synth. Met.* **2001,** 122, (1), 105-110.
9. Zhang, Lianjie; Hu, Sujun; Chen, Junwu; Chen, Zhenhui; Wu, Hongbin; Peng, Junbiao; Cao, Yong. *Adv. Funct. Mater.* **2011,** 21, (19), 3760-3769.
10. Bronstein, Hugo; Chen, Zhuoying; Ashraf, Raja Shahid; Zhang, Weimin; Du, Junping; Durrant, James R.; Shakya Tuladhar, Pabitra; Song, Kigook; Watkins, Scott E.; Geerts, Yves; Wienk, Martijn M.; Janssen, Rene A. J.; Anthopoulos, Thomas; Sirringhaus, Henning; Heeney, Martin; McCulloch, Iain. *J. Am. Chem. Soc.* **2011,** 133, (10), 3272-3275.
11. Katz, H. E.; Bao, Z. *J. Phys. Chem. B* **1999,** 104, (4), 671-678.
12. Zaumseil, Jana; Sirringhaus, Henning. *Chem. Rev.* **2007,** 107, (4), 1296-1323.
13. Muccini, Michele. *Nat. Mater.* **2006,** 5, (8), 605-613.
14. Hoth, Claudia N.; Schilinsky, Pavel; Choulis, Stelios A.; Brabec, Christoph J. *Nano Lett.* **2008,** 8, (9), 2806-2813.
15. Hebner, T. R.; Wu, C. C.; Marcy, D.; Lu, M. H.; Sturm, J. C. *Appl. Phys. Lett.* **1998,** 72, (5), 519-521.
16. Ling, Mang Mang; Bao, Zhenan. *Chem. Mater.* **2004,** 16, (23), 4824-4840.
17. Chen, Hsiang-Yu; Hou, Jianhui; Zhang, Shaoqing; Liang, Yongye; Yang, Guanwen; Yang, Yang; Yu, Luping; Wu, Yue; Li, Gang. *Nat. Photonics* **2009,** 3, (11), 649-653.
18. Günes, Serap; Neugebauer, Helmut; Sariciftci, Niyazi Serdar. *Chem. Rev.* **2007,** 107, (4), 1324-1338.

19. Jo, Jang; Gendron, David; Najari, Ahmed; Moon, Ji Sun; Cho, Shinuk; Leclerc, Mario; Heeger, Alan J. *Appl. Phys. Lett.* **2010,** 97, (20), 203303-203303.

20. Yamamoto, Takakazu; Zhou, Zhen-hua; Kanbara, Takaki; Shimura, Masaki; Kizu, Kenichi; Maruyama, Tsukasa; Nakamura, Yoshiyuki; Fukuda, Takashi; Lee, Bang-Lin; Ooba, Naoki; Tomaru, Satoru; Kurihara, Takashi; Kaino, Toshikuni; Kubota, Kenji; Sasaki, Shintaro. *J. Am. Chem. Soc.* **1996,** 118, (43), 10389-10399.

21. Liao, Liang; Dai, Liming; Smith, Adam; Durstock, Michael; Lu, Jianping; Ding, Jianfu; Tao, Ye. *Macromolecules* **2007,** 40, (26), 9406-9412.

22. Zou, Yingping; Najari, Ahmed; Berrouard, Philippe; Beaupré, Serge; Réda Ai ch, Badrou; Tao, Ye; Leclerc, Mario. *J. Am. Chem. Soc.* **2010,** 132, (15), 5330-5331.

23. Liang, Yongye; Feng, Danqin; Wu, Yue; Tsai, Szu-Ting; Li, Gang; Ray, Claire; Yu, Luping. *J. Am. Chem. Soc.* **2009,** 131, (22), 7792-7799.

24. Piliego, Claudia; Holcombe, Thomas W.; Douglas, Jessica D.; Woo, Claire H.; Beaujuge, Pierre M.; Fréchet, Jean M. J. *J. Am. Chem. Soc.* **2010,** 132, (22), 7595-7597.

25. Price, Samuel C.; Stuart, Andrew C.; Yang, Liqiang; Zhou, Huaxing; You, Wei. *J. Am. Chem. Soc.* **2011,** 133, (12), 4625-4631.

26. Tsao, Hoi Nok; Cho, Don M.; Park, Insun; Hansen, Michael Ryan; Mavrinskiy, Alexey; Yoon, Do Y.; Graf, Robert; Pisula, Wojciech; Spiess, Hans Wolfgang; Mu llen, Klaus. *J. Am. Chem. Soc.* **2011,** 133, (8), 2605-2612.

27. Peng, Qiang; Huang, Yan; Lu, Zhi-Yun; Qin, Sheng-Ying; Xie, Ming-Gui; Gao, Wei-Xian; Peng, Jun-Biao; Cao, Yong. *Chin. J. Chem.* **2004,** 22, (6), 599-604.

28. Aubouy, Laurent; Huby, Nolwenn; Hirsch, Lionel; van der Lee, Arie; Gerbier, Philippe. *New J. Chem.* **2009,** 33, (6).

29. Alam, Maksudul M.; Jenekhe, Samson A. *Chem. Mater.* **2002,** 14, (11), 4775-4780.

30. Mike, Jared F.; Nalwa, Kanwar; Makowski, Andrew J.; Putnam, Daniel; Tomlinson, Aimee L.; Chaudhary, Sumit; Jeffries-El, Malika. *Phys. Chem. Chem. Phys.* **2011,** 13, (4), 1338-1344.

31. Babel, Amit; Jenekhe, Samson A. *J. Phys. Chem. B* **2002,** 106, (24), 6129-6132.

32. Intemann, Jeremy J.; Mike, Jared F.; Cai, Min; Bose, Sayantan; Xiao, Teng; Mauldin, Timothy C.; Roggers, Robert A.; Shinar, Joseph; Shinar, Ruth; Jeffries-El, Malika. *Macromolecules* **2010,** 44, (2), 248-255.

33. Mike, Jared F.; Intemann, Jeremy J.; Cai, Min; Xiao, Teng; Shinar, Ruth; Shinar, Joseph; Jeffries-El, Malika. *Polym. Chem.* **2011,** 2, (10), 2299-2305.

34. Jenekhe, Samson A.; Osaheni, John A. *Chem. Mater.* **1994,** 6, (11), 1906-1909.

35. Jenekhe, Samson A.; Osaheni, John A.; Meth, Jeffrey S.; Vanherzeele, Herman. *Chem. Mater.* **1992,** 4, (3), 683-687.

36. Osaheni, John A.; Jenekhe, Samson A. *Chem. Mater.* **1992,** 4, (6), 1282-1290.

37. Reinhardt, Bruce A.; Unroe, Marilyn R.; Evers, Robert C.; Zhao, Mingtang; Samoc, Marek; Prasad, Paras N.; Sinsky, Mark. *Chem. Mater.* **1991,** 3, (5), 864-871.

38. Wolfe, James F.; Arnold, F. E. *Macromolecules* **1981,** 14, (4), 909-915.

39. Mike, Jared F.; Makowski, Andrew J.; Jeffries-El, Malika. *Org. Lett.* **2008,** 10, (21), 4915-4918.

40. Mike, Jared F.; Inteman, Jeremy J.; Ellern, Arkady; Jeffries-El, Malika. *J. Org. Chem.* **2009,** 75, (2), 495-497.

41. Mike, Jared F.; Makowski, Andrew J.; Mauldin, Timothy C.; Jeffries-El, Malika. *J. Polym. Sci., Part A: Polym. Chem.* **2010,** 48, (6), 1456-1460.

42. Tlach, Brian C.; Tomlinson, Aimée L.; Bhuwalka, Achala; Jeffries-El, Malika. *J. Org. Chem.* **2011,** 76, (21), 8670-8681.

43. Zoombelt, Arjan P.; Mathijssen, Simon G. J.; Turbiez, Mathieu G. R.; Wienk, Martijn M.; Janssen, Rene A. J. *J. Mater. Chem.* **2010,** 20, (11).

44. Bhuwalka, Achala; Mike, Jared F.; He, Meng; Intemann, Jeremy J.; Nelson, Toby; Ewan, Monique D.; Roggers, Robert A.; Lin, Zhiqun; Jeffries-El, Malika. *Macromolecules* **2011**.

45. Stalder, Romain; Grand, Caroline; Subbiah, Jegadesan; So, Franky; Reynolds, John R. *Polym. Chem.* **2012,** 3, (1), 89-92.

46. Hou, Qiong; Xu, Yishe; Yang, Wei; Yuan, Min; Peng, Junbiao; Cao, Yong. *J. Mater. Chem.* **2002,** 12, (10).

47. Park, Jin Kuen; Jo, Jang; Seo, Jung Hwa; Moon, Ji Sun; Park, Yeong Don; Lee, Kwanghee; Heeger, Alan J.; Bazan, Guillermo C. *Adv. Mater.* **2011,** 23, (21), 2430-2435.

48. Nesterov, Evgueni E.; Zhu, Zhengguo; Swager, Timothy M. *J. Am. Chem. Soc.* **2005,** 127, (28), 10083-10088.

49. Zhan, Xiaowei; Zhu, Daoben. *Polym. Chem.* **2010,** 1, (4).

50. Cheng, Yen-Ju; Yang, Sheng-Hsiung; Hsu, Chain-Shu. *Chem. Rev.* **2009,** 109, (11), 5868-5923.

51. Yuen, J. D.; Fan, J.; Seifter, J.; Lim, B.; Hufschmid, R.; Heeger, A. J.; Wudl, F. *J Am Chem Soc* **2011,** 133, (51), 20799-20807.

52. Leclerc, N.; Michaud, A.; Sirois, K.; Morin, J. F.; Leclerc, M. *Adv. Funct. Mater.* **2006,** 16, (13), 1694-1704.

53. Nad, Sanjukta; Kumbhakar, Manoj; Pal, Haridas. *J. Phys. Chem. A* **2003,** 107, (24), 4808-4816.

# Chapter 6

## General Conclusions

### 6.1 FUTURE RESEARCH

We have shown that the ability to functionalize benzobisoxazoles at the 4 and 8-positions can be used to create benzobisoxazole-containing polymers with a new conjugation pathway, resulting in unique physical and electronic properties. This has also opened the door for making benzobisoxazole monomers with extended π-systems (Figure 6.1) at either the 4 and 8-position

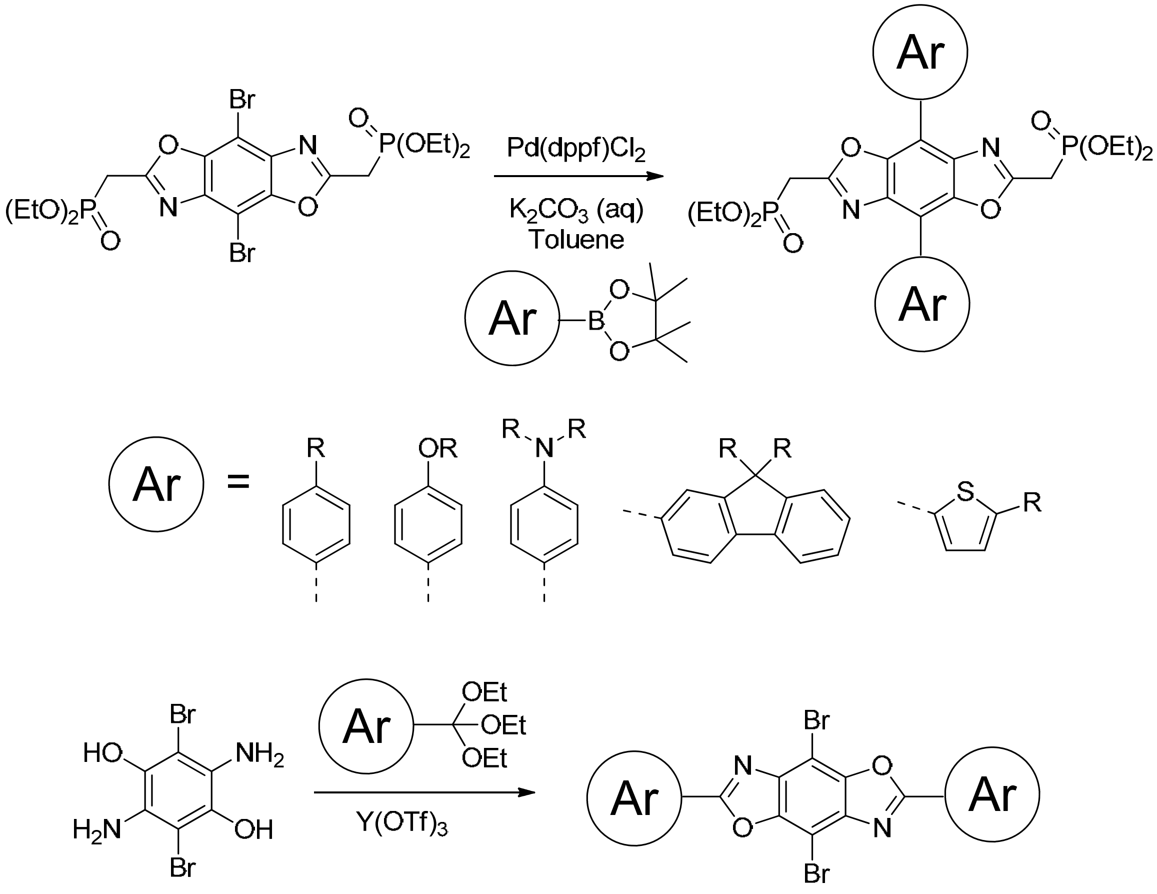
Br
(EtO)2P
P(OEt)2
Pd(dppf)Cl2
K2CO3 (aq)
Toluene
Ar
B
O
N
Ar =
R
OR
R N R
S
HO
NH2
H2N
OH
OEt
Y(OTf)3

**Scheme 6.1** Some examples of Benzobisoxazoles with extended two-dimensional π-systems.

or the 2 and 6-position. These would result in polymers with a two-dimensional π-system. By changing the aromatic pendant groups on the polymer, the physical and electronic properties of the polymers can be synthetically tuned in order to achieve the best possible material for a given application. Preliminary work to develop 4,8-π-functionalized benzobisoxazoles is already underway in our group with encouraging results.

π-Functionalization of the 2 and 6-position is much more challenging synthetically, however. Our most successful approach to functionalizing the 2 and 6-position has been through the use of orthoester condensations. This would require the use of aromatic orthoesters, and although we have had some success making thiophene-based orthoesters,[1, 2] attempts at making other aromatic or conjugated orthoesters have failed. These orthoesters are generally made by metalation of an aryl bromide with magnesium followed by reaction with tetraethyl orthocarbonate. Problems arise when the desired aryl halide won't undergo metalation or complications with the purification of the product. Because orthoesters are extremely acid sensitive, silica gel columns cause the product to decompose to the ester, even when treated with a base such as triethylamine. Orthoesters are usually oils, preventing recrystallization techniques making the best strategy for purifying orthoesters vacuum distillation. Unfortunately, only smaller aromatic orthoesters such as thiophenes are volatile enough to use this method on and even they generally distill off at over 200 °C at 0.3 mbar. In order to make more versatile orthoesters our group has been developing a new synthetic approach that converts aldehydes into orthoesters using a two pot synthesis. In this method (Scheme 6.2), the aldehyde is converted to the dithiane with propanedithiol which can then be deprotonated with n-butyllithium and reacted with dimethyldisulfide to make the thioorthoester. Finally, conversion to the orthoester is

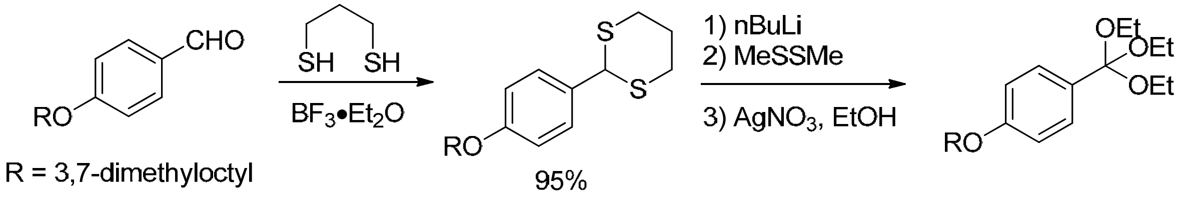

**Scheme 6.2.** Alternate orthoester synthesis.

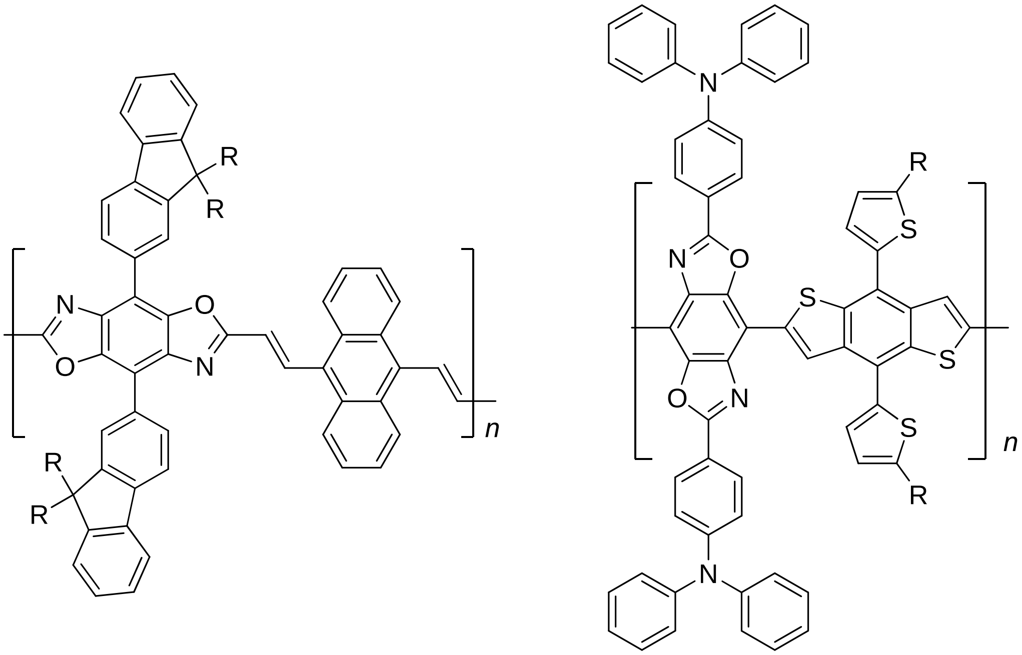

**Figure 6.1.** Examples of benzobisoxazole-containing polymers featuring two-dimensional conjugated systems.

achieved by reacting the thioorthoester with ethanol and silver nitrate. The final step of the synthesis yields clean product without the need for column chromatography. This route has been performed on a handful of aromatic systems by our group with mixed, though encouraging results. The use of aryl acid halides, like the method used to alkylate the benzobisoxazoles in Chapters 4 and 5, could potentially be used instead of orthoesters, though attempts have not been made as of yet to explore this option.

With these new benzobisoxazole monomers in hand, we could make new polymers with two-dimensional π-systems (Figure 6.1). This could potentially open a new area of research in organic semiconductors as conjugated polymers with large multi-dimensional π-systems have not been well studied. Most conjugated monomers are not versatile enough and do not readily lend themselves to making such materials the way benzobisoxazoles do. One interesting system that has recently been developed for such an approach is benzodithiophene (BDT), where Huo and coworkers were able to attached thiophene units off of the benzene core.[3] Their approach, while synthetically challenging with low yields (the reaction to attach pendant thiophene groups

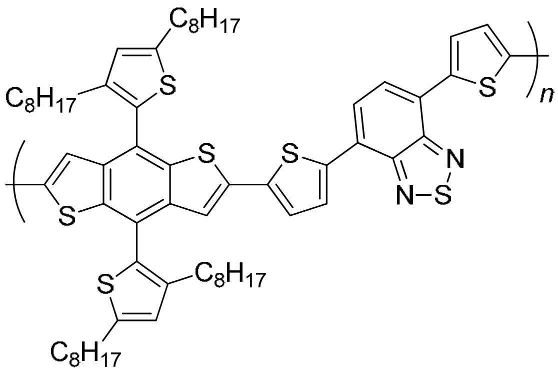

**Figure 6.2.** Illustration of benzodithiophene-dithienylbenzothiadiazole copolymer with thiophene pendant groups on the benzodithiophene.

provides a yield of 44%), showed that the new material, when copolymerized with dithienylbenzothiadiazole (Figure 6.2), had improved mobilities and power conversion efficiencies in solar cells over BDT-containing polymers that do not have an extended two-dimensional π-system.

## 6.2 DISSERTATION CONCLUSIONS

In the last six years the development of benzobisazoles for semiconducting polymers has come a long way. Originally developed as high performance materials for the military, benzobisazole polymer development stagnated after the 1970s due to an inability to functionalize them and the poor solubility in common organic solvents. We have since made solution processable benzobisazoles-based polymers a reality and demonstrated their utility beyond the role of high performance materials through their incorporation into organic electronic devices. We have transformed benzobisoxazoles (BBOs) into one of the most versatile conjugated moieties known by utilizing multiple conjugation pathways in a wide array of copolymers.

The promise these materials have shown in organic light-emitting diodes (OLEDs) has been very encouraging and we were able to show cis-benzobisoxazoles performed better than the trans-isomer when polymerized at the 2 and 6-position, but were plagued by inefficient energy transfer in guest-host OLEDs. We found that by polymerizing the BBOs at the 4 and 8-position materials were obtained that overcame the problems with energy transfer in OLEDs. Through studying the structure-property relationships between the two different conjugation pathways, we were able to determine the 4,8-polymers exhibited a narrower bandgap than polymers with a conjugation pathway through the 2 and 6-position on the BBO, due to stabilization of the quinoid resonance form of the polymer. We also demonstrated that BBOs polymerization through the 2 and 6-position provided greater acceptor strength as evidenced by higher electron affinities. A decrease in the optical bandgap of benzobisazoles has also been observed in the order of *cis*-BBO, *trans*-BBO, and Benzobisthiazole when polymerized through the 2 and 6-position on the moiety. Although OLEDs utilizing benzobisazole-based emitters still lag behind other systems in efficiency and brightness, we have shown a steady improvement in performance as the evolution of the materials has taken place. This demonstrates the potential these materials still have and the need for further research to produce improved materials.

## 6.3 ACKNOWLEDGEMENTS

I would like to thank my wife Robbyn for all the love and support she has given me throughout my time as a graduate student and my dog Bailey for always making me smile. To my parents, I want you to know I appreciate the love and support you have given me throughout my life. Most of all I want to thank my advisor, Dr. Malika Jeffries-EL, who instilled in me a great passion for research and whom has made me the chemist that I am today. I would like to mention my appreciation for the other members of my research group, past and present, Brandon Kobilka, Ben Hale, Achala Bhuwalka, Monique Ewan, Brian Tlach, Dana Drochner, Dr. Jared Mike, Robyn Laskowski, Drew Makowski, and Mike Mitchell. All of whom made my research possible and from whom I have learned so much. I would like to acknowledge my collaborators Drs. Ruth and Joe Shinar, Dr. Min Cai, and in particular, Emily Hellerich who helped to realize the full potential of my research and from whom I learned a great deal. I would also like to thank Michael Zenner for taking some truly amazing photos of the OLEDs we made, although, seriously, get rid of the Hawaiian shirts already. It was fun at first but then it just became sad after a while. I would also like to acknowledge Dr. Diane Hinkens who demonstrated the dangers of organotin reagents and the importance of good chemical hygiene by poisoning our entire lab. My research and this dissertation were made possible due to the sustenance provided by the

wonderful people at Topped Doughnuts and their amazing maple bacon doughnuts. Last but certainly not least, I would like to thank the hard working individuals at New Glarus Brewing Company, for without their tasty beverages, I doubt this thesis would have been possible.

## 6.4 REFERENCES

1. Mike, J. F.; Intemann, J. J.; Cai, M.; Xiao, T.; Shinar, R.; Shinar, J.; Jeffries-El, M. *Polymer Chemistry* **2011,** 2, (10), 2299-2305.
2. Bhuwalka, A.; Mike, J. F.; He, M.; Intemann, J. J.; Nelson, T.; Ewan, M. D.; Roggers, R. A.; Lin, Z.; Jeffries-El, M. *Macromolecules* **2011**.
3. Huo, L.; Hou, J.; Zhang, S.; Chen, H.-Y.; Yang, Y. *Angewandte Chemie International Edition* **2010,** 49, (8), 1500-1503.

# Appendix

## List of Acronyms and Descriptions

| Acronym | Description |
|---|---|
| BBO | Benzobisoxazole |
| BHJ | Bulk Heterojunction |
| BPhen | 4,7-Diphenyl-1,10-phenanthroline |
| CBP | 4,4’-Bis(N-carbazolyl)-1,1’-biphenyl |
| CIE | Commission internationale de l'éclairage |
| CV | Cyclic Voltammetry |
| DP | Degree of Polymerization |
| DPV | Differential Pulse Voltammetry |
| DSC | Differential Scanning Calorimetry |
| EA | Electron Affinitiy |
| $E_g^{opt}$ | Optical Band Gap Energy |
| EI | Electron Ionization |
| EL | Electroluminescence |
| EQE | External Quantum Efficiency |
| ESI | Electrospray Ionization |
| FRET | Förster Resonance Energy Transfer |
| FWHM | Full Width at Half Maximum |
| GPC | Gel Permeation Chromatography |
| HIL | Hole Injection Layer |
| HMW | High Molecular Weight |
| HOMO | Highest Occupied Molecular Orbital |
| HRMS | High Resolution Mass Spectrometry |
| HWE | Horner-Wadsworth-Emmons |
| IP | Ionization Potential |
| ITO | Indium Tinoxide |

| **Acronym** | **Description** |
|---|---|
| LCD | Liquid Crystal Display |
| LED | Light-Emitting Diode |
| LMW | Low Molecular Weight |
| LUMO | Lowest Unoccupied Molecular Orbital |
| MCP | Microchannel Plate |
| MMW | Medium Molecular Weight |
| $M_n$ | Number Averaged Molecular Weight |
| $M_w$ | Weight Averaged Molecular Weight |
| NMR | Nuclear Magnetic Resonance |
| *o*-DCB | o-dichlorobenzene |
| OFET | Organic Field-Effect Transistor |
| OLED | Organic Light-Emitting Diodes |
| OPV | Organic Photovoltaic |
| PAV | Polyarylene vinylene |
| PBO | Polybenzobisoxazole |
| PCBM | [6,6]-Phenyl C61 butyric acid methyl ester |
| PDAF | Polydialkylfluorene |
| PDI | Poly Dispersity Index |
| PEDOT:PSS | Poly(3,4-ethylenedioxythiophene) poly(styrenesulfonate) |
| PL | Photoluminescence |
| PLED | Polymer Light-Emitting Diode |
| PPA | Polyphosphoric Acid |
| PPSE | poly(trimethylsilylphosphate) |
| PPV | Polyphenylene vinylene |
| PVK | Poly(N-vinylcarbazole) |
| SCE | Standard Calomel Electrode |
| $T_d$ | Decomposition Temperature |
| $T_g$ | Glass Transition Temperature |

| **Acronym** | **Description** |
|---|---|
| TGA | Thermal Gravimetric Analysis |
| THF | Tetrahydrofuran |
| UPS | Ultraviolet Photoelectron Spectroscopy |
| Wt% | Wegith Percent |
| XRD | X-Ray Diffraction |